Modeling Gas-Grain Chemistry in Dark Cloud Conditions

Dissertation

zur

Erlangung des Doktorgrades (Dr. rer. nat.)

der

Mathematisch-Naturwissenschaftlichen Fakultät

der

Rheinischen Friedrich-Wilhelms-Universität Bonn

vorgelegt von

Fujun Du

aus

Chongqing, China

Bonn 2012

Angefertigt mit Genehmigung der Mathematisch-Naturwissenschaftlichen Fakultät der
Rheinischen Friedrich-Wilhelms-Universität Bonn

1. Gutachter: Prof. Dr. Karl M. Menten

2. Gutachter: Prof. Dr. Pavel Kroupa

Tag der Promotion: August 20, 2012

Erscheinungsjahr: 2012

Diese Dissertation ist auf dem Hochschulschriftenserver der ULB Bonn unter
`http://hss.ulb.uni-bonn.de/diss_online` elektronisch publiziert.

Abstract

I first wrote a gas phase chemical code, which solves for the gas phase composition of an interstellar cloud as a function of time. We used this code to study the abundance ratios between the H_3^+ isotopologues, since in this case the interaction between processes in the gas phase and on the dust grain surface can be treated in a simplified way.

Grain chemistry is necessary to explain the formation of many interstellar molecules. My first investigation on grain chemistry is from the mathematical side, by looking deep into the difficulties posed by its stochasticity and discreteness. After writing a Monte Carlo code to serve as a benchmark, I developed a new method called "hybrid moment equation" (HME) approach, which gives results that are more accurate than those obtained with the usual rate equation approach, and it runs much faster than the Monte Carlo method for a medium-to-large-sized reaction network. Improvements in this HME approach are needed if a very large surface network is to be used.

Following the recent detection of hydrogen peroxide (H_2O_2) in the ρ Ophiuchus A cloud core, I modeled its formation with a gas-grain network. Its observed abundance, together with the abundances of other species detected in the same source can be reproduced in our model. These molecules are mainly driven into the gas phase from the dust grain surface by the heat released in chemical reactions. Our model predicted the presence of O_2H molecule in the gas phase, which has indeed been detected recently. Further investigations are needed to answer whether H_2O_2 is widespread in the interstellar medium.

I then studied the chemistry involving species containing one or more deuterium atoms with a gas-grain-mantle three-phase model, which takes into account recent experimental results on the key reactions. The observed fractionated deuterium enhancement in water, methanol, and formaldehyde is reproduced in our models. I demonstrated that the existence of abstraction reactions for methanol and formaldehyde is the main reason for these species to be more prone to deuterium enhancement than water. The observed low $[D_2O/H_2O]$ ratio suggests that water is mainly formed through $H_2 + OH \longrightarrow H_2O + H$ on the dust grain surface. Our model also gives a range of ice mantle compositions for the dust grains that agree with the observations in different sources.

Contents

Chapter 1

Introduction

— Chemistry in astronomical environments

Since ancient times, the formation of complex structures from simple components has always been one of the central themes in natural science. The very existence of a vast number of different molecules on Earth, when contrasted with the primordial "hot soup" state of the early Universe, where nothing except for elementary particles (such as protons, neutrons, and electrons, depending on which specific stage we are talking about) existed, indicates that formation processes of these molecules must have occurred in the past. The discovery of more than one hundred different molecules (including ions and radicals) in interstellar space suggests that such processes have started in the interstellar environment, where the physical conditions are completely different from those we are familiar with here on Earth.

1.1 Interstellar environments

By the terrestrial standards, interstellar space is essentially empty. The average density of visible matter in our Milky Way galaxy—even if the stars are counted in—is merely about 100 protons cm^{-3}, which may be compared with the air density of our atmosphere at sea level, being approximately 7×10^{20} protons cm^{-3}. But in our Galaxy, the stars are the major mass component of the visible mass[1], and the total mass of the interstellar medium (ISM) is only about 5% of the total stellar mass (Lequeux et al. 2005), so the actual average density of interstellar space, not counting the stars, is much lower, about a few protons cm^{-3}; this is somewhat similar to the density of interplanetary space (Prölss 2004). The typically low density of the ISM does not mean that nothing interesting can occur; rather it only suggests that the relevant time scales may be much longer than what we are used to on Earth. These time scales are literally "astronomical"! On the other hand, the low density of the ISM makes the existence of non-negligible amounts of reactive radical and charged species possible, because the rates to destruct them through two-body chemical reactions are low.

In fact, the interstellar space is highly inhomogeneous, both in physical condition

[1] For the Galaxy as a whole, most of the mass is generally believed to be in the form of the so-called "dark matter", whose nature is still a mystery.

and in material composition, and an average description is not quite helpful for our understanding. The ISM can be divided into three phases: cold neutral medium, warm neutral/ionized medium, and hot ionized medium. According to Snow & McCall (2006), the cold neutral medium itself can be classified into four types, from diffuse atomic clouds (number density of hydrogen nuclei n=10–100 cm^{-3}, temperature T=30–100 K), to diffuse molecular clouds (n=100–500 cm^{-3}, T=30–100 K), translucent clouds (n=500–5000 cm^{-3}, T=15–50 K), and dense molecular clouds ($n > 10^4$ cm^{-3}, T=10–50 K). Such a classification is only qualitative, and there is no clear separation from one type to another. The general trend is that an increase in density is accompanied by a decrease in temperature. Multiplying the typical density by the typical temperature for each class of medium shows that these different phases are in approximate pressure equilibrium.

Not all of the ISM is in such an equilibrium state. For example, very high density and temperature condition may be created in shocks, which may be generated by supernova explosion, or by outflows and winds in the course of star formation. Stars at their late evolution stages can also lose mass and develop outflowing circumstellar envelope that replenish the ISM with metals. These (more or less) violent processes "activate" the host galaxy from time to time, and their effects are not limited to enhancements in density and temperature. The intense radiation fields and/or high energy particles, as well as the ejected material, can actually determine the evolution track and fate of a galaxy.

The elemental composition of the ISM is generally close to the solar composition. Namely, the dominant elements are hydrogen and helium, with a mass ratio of approximately 3 : 1. The heavier elements, which are referred to as "metals" in astronomy, including C, N, O, Na, Mg, Si, P, S, Cl, Fe, comprise about 2% of the total mass.

A large variety can be seen in the material composition of different types of clouds, which is already indicated in their names. The hot and warm ionized medium is completely or partly ionized, where the radiation field is dominated by free-free, free-bound emissions, as well as recombination and forbidden lines. In the neutral atomic gas, hydrogen is in atomic form, which can be observed by the famous 21 cm line, but other heavy elements can still be partially ionized, and their fine-structure lines are the main cooling mechanism of the gas.

In this thesis we are mainly concerned with the conditions relevant to cold dark clouds where star formation takes place. They have a relatively high density and low temperature with respect to the general ISM. The higher density and lower temperature allow them to develop and harbor a chemical repository that is much richer than in other classes of clouds, which will be described in the next section.

1.2 From molecular clouds to stars

The cold dark clouds are mainly composed of molecular hydrogen, hence they are also called molecular clouds. They are places where many different kinds of molecules exist, and the birthplaces of stars.

When a diffuse cloud gradually becomes denser and denser, the atoms and ions have a higher probability to meet each other, at the same time they can shield themselves

better from external radiation fields[2]. This provides a shelter for the molecules to be produced. Observationally, it has been shown that the molecular H_2 becomes more and more dominant over atomic H as the visual extinction grows.

Observational studies on the molecules in the cold ISM are mostly based on their emission lines. Molecular line emission can be divided into three types: electronic emission, which is due to transition between different electronic states; vibrational emission, due to transition between different vibration states; and rotational emission due to transition between different rotation states. The typical energy released in each type (hence their typical frequency) decreases by a factor of roughly[3] $\sqrt{m_\mathrm{p}/m_\mathrm{e}}\sim 40$, the square root of the mass ratio between proton and electron, from one type to another in the above sequence. Thus the electronic transitions usually fall in the UV or optical band, the vibrational transitions fall in the infrared band, and the rotational transitions fall in the radio band.

Only a few simple molecules have their electronic transitions in the optical band, and many molecules detected in this type have their transitions in the UV band (Lequeux et al. 2005), which is not readily available from the ground due to atmosphere absorption. More importantly, in cold dark clouds, the temperature is generally too low to excite the vibration levels (a temperature of 10 K corresponds to a wavelength of 1 mm), let alone electronic levels. Hence the detection of molecules relies predominantly on radio observations of the rotational lines. For the H_2 molecule, due to its small size and small mass, even the non-ground rotation energy levels[4] are too high to populate in cold conditions, and its column density (particles per cm^2) is usually traced by other molecules (such as CO), or dust emission/absorption.

Up to now, around 165 molecules have been detected in space[5]; some of them (such as the fullerenes C_{60} and C_{70}) are detected in circumstellar envelopes only. These molecules are listed in Table (1.1). Among them, besides H_2, the most common one is CO, which takes up almost all the carbon atoms, with an abundance relative to H_2 about 10^{-4}. Molecules with more than three atoms are mostly organic[6] in nature. One fact is that not all the observed spectral lines (e.g. the diffuse interstellar bands, mainly in the optical) have been attributed to a specific molecule.

As the cloud gets richer in molecular species, the cooling efficiency rises because more radiation modes are possible, and the temperature can decrease in the condensation process of clouds. As a consequence the gravitational force becomes more and more dominant over the thermal pressure. If this process is not interrupted by external forces, then most

[2] The degree of extinction (the astronomical term for attenuation of radiation fields by gas or dust) is proportional to the optical depth, and the optical depth is proportional to the column density, namely, the integral of density over a straight line along which the intruding photon propagates.

[3] This separation in energy scale comes from the Born-Oppenheimer approximation in quantum mechanics. Heuristically we may understand it as follows. Imagine the heavy nuclei and light electrons move in the same harmonic potential, then their vibrational frequency differ by a factor of $\sqrt{m_\mathrm{p}/m_\mathrm{e}}$ (note that the vibration frequency of a harmonic oscillator is $\frac{1}{2\pi}\sqrt{\frac{k}{m}}$, where k is Hooke's constant and m is the mass of the oscillating body). This "explains" the separation between electronic and vibrational energies. The rotation energy is related to the overall size of the molecule (see the next footnote). Such a size can be estimated to be the vibration amplitude of the nucleus for which the vibration energy and electronic energy are comparable. This gives another factor $\sqrt{m_\mathrm{p}/m_\mathrm{e}}$.

[4] The rotation energy is quantized into $j(j+1)\hbar^2/2I$ (j=0, 1, ...), where I is the moment of inertia.

[5] `http://www.astro.uni-koeln.de/cdms/molecules`

[6] There is no rigorous definition of "organic"; generally if a species contains a C−H bond, then it might be considered "organic"; see `http://en.wikipedia.org/wiki/Organic_compound`.

2 atoms (total: 36) H_2, AlF, AlCl, C_2, CH, CH^+, CN, CO, CO^+, CP, SiC, HCl, KCl, NH, NO, NS, NaCl, OH, PN, SO, SO^+, SiN, SiO, SiS, CS, HF, HD, FeO, O_2, CF^+, SiH, PO, AlO, OH^+, CN^-, SH^+
3 atoms (total: 38) C_3, C_2H, C_2O, C_2S, CH_2, HCN, HCO, HCO^+, HCS^+, HOC^+, H_2O, H_2S, HNC, HNO, MgCN, MgNC, N_2H^+, N_2O, NaCN, OCS, SO_2, c-SiC_2, CO_2, NH_2, H_3^+, H_2D^+, HD_2^+, SiCN, AlNC, SiNC, HCP, CCP, AlOH, H_2O^+, H_2Cl^+, KCN, FeCN, O_2H
4 atoms (total: 24) c-C_3H, l-C_3H, C_3N, C_3O, C_3S, C_2H_2, NH_3, HCCN, $HCNH^+$, HNCO, HNCS, $HOCO^+$, H_2CO, H_2CN, H_2CS, H_3O^+, c-SiC_3, CH_3, C_3N^-, PH_3, HCNO, HOCN, HSCN, H_2O_2
5 atoms (total: 18) C_5, C_4H, C_4Si, l-C_3H_2, c-C_3H_2, H_2CCN, CH_4, HC_3N, HC_2NC, HCOOH, H_2CNH, H_2C_2O, H_2NCN, HNC_3, SiH_4, H_2COH^+, C_4H^-, HC(O)CN
6 atoms (total: 16) C_5H, l-H_2C_4, C_2H_4, CH_3CN, CH_3NC, CH_3OH, CH_3SH, HC_3NH^+, HC_2CHO, NH_2CHO, C_5N, l-HC_4H, l-HC_4N, c-H_2C_3O, H_2CCNH, C_5N^-
7 atoms (total: 10) C_6H, CH_2CHCN, CH_3C_2H, HC_5N, CH_3CHO, CH_3NH_2, c-C_2H_4O, H_2CCHOH, C_6H^-, NH_2CH_2CN
8 atoms (total: 9) CH_3C_3N, $HC(O)OCH_3$, CH_3COOH, C_7H, H_2C_6, CH_2OHCHO, l-HC_6H, CH_2CHCHO, CH_2CCHCN
9 atoms (total: 9) CH_3C_4H, CH_3CH_2CN, $(CH_3)_2O$, CH_3CH_2OH, HC_7N, C_8H, $CH_3C(O)NH_2$, C_8H^-, C_3H_6
10 atoms (total: 4) CH_3C_5N, $(CH_3)_2CO$, $(CH_2OH)_2$, CH_3CH_2CHO
11 atoms (total: 3) HC_9N, CH_3C_6H, C_2H_5OCHO
12 atoms (total: 3) C_6H_6, $C_2H_5OCH_3$, n-C_3H_7CN
$>$ 12 atoms (total: 3) $HC_{11}N$, C_{60}, C_{70}

Table 1.1: Molecules detected in space. Taken from the CDMS database (as of 01/2012; `http://www.astro.uni-koeln.de/cdms/molecules`) at Cologne university, except for O_2H, which is very recently detected by Parise et al. (2012b). Isotopic species are not included except for the case of H_2D^+ and HD_2^+, since they are detected with a different method as H_3^+. A similar table can also be found in the Wikipedia page `http://en.wikipedia.org/wiki/List_of_interstellar_and_circumstellar_molecules`.

likely at a certain stage the gravitation instability will set in, and the cloud will collapse. Depending on the initial configuration, a central protostar and a surrounding accretion disk can be formed. The central star gains mass through accretion and becomes more luminous over time. Its radiation field and wind act in the reverse direction of gravity, blowing out the surrounding material. Finally, the environment becomes clear of gas and dust, and a newly born star is visible to distant observers. As a bonus, a planet system (like our solar system) may have also formed (and may still be evolving) in the accretion disk. This is an important bonus, since we are residing in such a system.

The above a picture is an oversimplification. Many details of these processes are not known for sure, or are yet to be discovered. For example, what actually triggers the conversion from the diffuse phase to dense phase for interstellar clouds? How do these processes determine the statistical distribution of the resulting stellar masses? How is the prestellar material transported to the final planetary system? Many such questions can be asked. However, they are not the topic of this thesis.

1.3 The role of modeling in astrochemistry

Any modeling study in astronomy is based on the rationale that the physical laws (including chemistry) at the place of the celestial objects, no matter how far away they are, are the same as in any laboratory on Earth. Thus the goal of any modeling effort is trying to understand the interstellar processes in terms of our local understanding of physics (as well as chemistry and mathematics).

Studies on the chemistry of interstellar molecules started almost 70 years ago. For example, Swings (1942) discussed the production and destruction of the optically detected species CH and CH^+, Ter Haar (1944) studied the problem of dust ("smoke particle") formation, Bates (1951) worked on molecule formation through radiative association, and Bates & Spitzer (1951) also studied the formation of CH and CH^+. These works are largely analytical. These early studies usually focused on CH and CH^+ (and CN possibly) because they were the only molecules discovered in the ISM at that time.

Then, in the 1960s, the fast development in radio astronomy led to the discovery of a dozen of new molecules (as noted in Stief et al. 1972; see also Menten & Wyrowski 2011). This triggered new systematic studies. The modeling effort in astrochemistry seems to have started in the end of 1960s. A non-exhaustive search into the literature shows some of the earliest works: Williams (1968) on adsorption to dust grains, Duley (1970) on grain chemistry, Hollenbach & Salpeter (1970) on surface adsorption, Hollenbach & Salpeter (1971) on surface H_2 formation, de Jong (1972) on H_2 formation through surface reaction and H^-, Solomon & Klemperer (1972) with a large network, focused on CH, CH^+, and CN, Stief et al. (1972) on photochemistry, Watson & Salpeter (1972) on grain chemistry, Dalgarno et al. (1973) on chemical ionization, Dalgarno & McCray (1973) on negative-ion-assisted molecule formation, Herbst & Klemperer (1973) with a large network, Solomon & Woolf (1973) on deuterium fractionation, Millar & Williams (1975) on the formation of large molecules. The importance of cosmic-rays in triggering the ion-neutral reactions, and the role played by dust grains have been identified. A comprehensive review of these studies can be found in Watson (1976). Basically, these pioneering studies set the stage for the field of astrochemistry.

Later studies generally follow the lines of research of these early works, and stimulated

by interaction between several fields, have proliferated into more branches focusing on different types of objects, such as dark clouds (Millar & Nejad 1985), hot cores and corinos (Hassel et al. 2008), proto-planetary disks (Aikawa et al. 1997), photon-dominated regions (Tielens & Hollenbach 1985), shocks (Gusdorf et al. 2008), circumstellar envelopes around evolved stars and planetary nebulae (Glassgold 1996), etc. Among them, a specific topic of interest to us is the phenomenon of deuterium fractionation, in which the observed [D/H] ratios in certain species appear much higher (Parise et al. 2002, 2004; Bergman et al. 2011a) than the cosmic value of $\sim 10^{-5}$, and the degree of [D/H] enhancement can differ for different species. This topic has been investigated since the early times and continues to be an intriguing phenomenon to study (Millar et al. 1989; Roberts & Millar 2000b). One chapter of this thesis is devoted to it, emphasizing the role of surface processes on deuterium fractionation.

As more and more molecules are discovered observationally, more questions arise regarding their formation mechanism. For many of the detected molecules in Table (1.1), it is not completely clear[7] how they are produced, especially for the complex ones; the formation channels that are proposed for a species cannot always account for its observed abundance (though it is not always possible to get an accurate abundance observationally either). Sometimes, when the gas phase processes are unable to explain the abundances of certain species, grain chemistry is resorted to. Though once being ironically described as "the last refuge of the scoundrel" (Charnley et al. 1992), grain chemistry is commonly agreed to be essential for astrochemistry, and besides its role in explaining existent observations, it also has a predictive power in some sense. This is discussed in this thesis.

Besides gas phase species, many molecules have also been detected in solid form in the ice mantles of dust grains (van Dishoeck 2004). The most abundant is water ice, followed typically by CO, CO_2, CH_3OH, H_2CO, and NH_3, etc. These ice species may have formed *in situ* on the dust grains or they are first formed in the gas phase and then accreted to the grain mantle. It is one of the major goals of astrochemistry to explain their absolute and relative abundances, and how they mix together (which can be inferred from their spectral features; Tielens et al. 1991). The formation of grain ice mantles is touched upon in this thesis.

Observers who are interested in the dynamics of the ISM and star formation (either on the cloud scale or on the galactic scale) care about molecular tracers, which are indicative of the local physical conditions. The performance of a tracer is related to its chemistry and radiative transfer properties. Ideally the abundance of a tracer should be constant. It is not always straightforward for chemical modelers to determine which molecules are good tracers, since chemistry is intrinsically complex[8], and the trend seems to be that it will not get simpler in the future. Besides this complexity, the uncertainties in the models (initial condition, reaction rates, physical parameters, and evolution history) often make the interpretation of the modeling results ambiguous. But such a situation has to be accepted and faced up, since nature is complex by itself, especially when we talk about fields such as chemistry (and biology, economics, etc.). Nevertheless the advances in our understanding of the chemical processes—mainly gained from experimental/theoretical studies, and

[7] Hence Einstein's famous quote "it is the theory which decides what can be observed" does not apparently apply here.

[8] Note that a chemical system is a nonlinear dynamical system containing hundreds of variables, while those dynamical systems studied by mathematicians usually contain only a few variables.

partly from observations and innovative thinking, together with improvements in computation and analysis power enable us to extract insights from a complicated chemical network, as will be shown in the latter half of this thesis.

1.4 Beyond simple molecules?

Table (1.1) shows that some of the detected molecules are quite complex, such as ethyl formate (C_2H_5OCHO) and *n*-propyl cynanide (C_3H_7CN), both of which were detected in Sagittarius B2 (close to the Galactic center) by Belloche et al. (2009). Another molecule, amino acetonitrile (NH_2CH_2CN), which is likely a direct precursor of glycine (NH_2CH_2COOH, the simplest amino acid), has also been detected in the same source by Belloche et al. (2008). It is clear that a lot of effort and patience is required for identifying the spectral lines of these and even more complex species—such as amino acids and nucleobases—since their structures are so complex that many internal motions are possible, which produce exceedingly rich spectra.

Grain chemistry is believed to be pivotal in producing the observed abundances of many complex molecules. In cold conditions, most species except for the lightest ones (such as H, D, H_2) on the grains are immobile, and complex organic molecules with more than three heavy atoms cannot form effectively under such conditions. However, as will be shown in the latter part of this thesis, precursors to the complex molecules, such as formaldehyde (H_2CO) and methanol (CH_3OH), can indeed accumulate to a high amount on the grain even at very low temperature. They can be broken into fragments by the cosmic-ray induced photons, and when the cloud core gets warmed up, these fragments can combine with each other and form complex species, either in the gas phase, or on the grain surface (Garrod et al. 2008). The protonation of these precursor molecules after desorption in the warm-up phase also leads to the formation of complex molecules (Charnley et al. 1992). However, the formation of complex species is not a topic of the present thesis.

1.5 Outline of this thesis

Chapter 2 contains an overview of the gas phase reactions and their rate parameters, followed by a description of the methods and our code to solve the rate equations governing the evolution of a gas phase system. An application of this code to study deuterated H_3^+ is briefly discussed.

Chapter 3 begins with a description of a few general facts about interstellar dust grains, followed by a brief discussion of the necessity of grain chemistry for astrochemical study. Then the rates of various processes related to grain chemistry are shown in detail. Finally the mathematical framework, specifically the master equation and the Monte Carlo approach for gas-grain chemistry are presented.

Chapter 4 is about the hybrid moment equation approach we developed for calculating the gas-grain chemical evolution, aimed at a faster speed than the Monte Carlo method, while the stochastic and discrete nature of grain surface chemistry are still properly accounted for. Its relation with previous approaches is discussed. It has been benchmarked with the Monte Carlo method.

Chapter 5 contains a gas-grain chemical study for the formation of the interstellar H_2O_2 molecule. The observed abundance of H_2O_2 in ρ Ophiuchus A can be reproduced at a certain stage of the chemical evolution. Desorption of surface species by the heat released in surface chemical reactions plays a vital role in producing gas phase H_2O_2. The abundances of other gas phase species, such as O_2, H_2O, and O_2H from our model are also presented.
Chapter 6 is about a gas-grain-mantle chemical model with deuterium included. It is the longest chapter. The special role of deuterium in the general physics context and in astrochemistry is discussed, followed by a description of the procedures by which we compile our network. Some technical issues regarding extracting information from experimental results on surface chemistry are included. The way we implement the three-phase model is described in detail. The ice mantle composition and the deuterium fractionation in various species are finally presented.
Chapter 7 includes a summary and a discussion on possible extensions of my work.
Appendix A contains a comparison of different methods for calculating the surface formation rate of H_2.
Appendix B contains a mathematical discussion on the formal solution of the chemical master equation.

Chapter 2

Gas phase chemistry

Contents

About 99% of the mass of the ISM is in gas phase, so gas phase processes deserve first consideration in any study on interstellar chemistry. Although in this thesis we emphasize processes on dust grains, the coupling between gas phase chemistry and grain surface chemistry is important for a consistent model, hence we cannot neglect gas phase chemistry. There are also cases in which the two regimes can be taken as decoupled, which allows adopting a simple gas phase model; one such example is the deuterium fractionation in the H_3^+ isotopologues, which will be discussed in the last section of this chapter. Historically, gas phase processes received more consideration, partly due to the dominance of gas over dust in mass, partly due to the relative mathematical simplicity of gas phase models, and partly due to the fact that the rate parameters of gas phase reactions seem to be easier to obtain experimentally or theoretically[1]. In addition, the actual physical constitution of dust grains, in particular of their surface is poorly constrained and adds uncertainty. In the following, an overview of gas phase chemistry is first given in the context of ISM, then our code for gas phase chemistry is described, followed by an application of this code.

2.1 Gas phase reactions

2.1.1 Gas phase reaction networks

A chemical system contains more than one species. These species are related to each other through reactions, forming a network structure. The details of these reactions are usually stored in a chemical network file, which is usually a plain text file containing a

[1] By "theoretically" we mean to calculate the rate parameters using quantum chemical methods (by the chemists). The modeling work we have done in this thesis sometimes may also be regarded as "theoretical", but the meaning is different, since we don't calculate the rate parameters by ourselves, instead we make use of these parameters taken from various sources and see how the whole system evolves.

list of reactions and their rate parameters, together with possibly other descriptive tags (reaction type, reference, etc.) for each reaction. A chemical network is the starting point of any chemical modeling. Here I give a brief non-exhaustive description of several chemical networks for astrochemical study compiled (and maintained) by different groups in the world.

The OSU network

This network is maintained by the astrochemistry group lead by Eric Herbst at Ohio State University[2]. One of its latest version (OSU09)[3] contains 6046 (6039 after removing duplicate entries) reactions and 468 species.

One feature of this network is the inclusion of a rich anion chemistry (Walsh et al. 2009). The anions included are of the form C_n^- (n=3–10), C_nH^- (n=4–10), and C_nN^- (n=3, 5). They are mainly formed by combining of C_n with an electron (the C_n itself is formed from $C + C_{n-1}H$), accompanied by emission of a photon, and they are mainly destroyed by reacting with other atoms or cations. The work of Walsh et al. (2009) showed that the anions do not have a dramatic effect on the chemistry of other species: the species mostly affected are the carbon-chain molecules. The reason to include anions is because they have been detected in space, e.g., in the carbon star IRC+10216 (McCarthy et al. 2006; Cernicharo et al. 2007), the Taurus molecular cloud (McCarthy et al. 2006), and the low mass star forming region L1527 (Agúndez et al. 2008). The possible existence of anions in the ISM had been theoretically predicted by Herbst (1981).

Another recent network provided by the OSU group is described in Harada et al. (2010) [4], which is mainly targeted at conditions with higher temperatures up to 800 K, AGN (active galactic nucleus) accretion disk for example. They approximate the X-ray ionization by modifying the cosmic-ray ionization rates. More accurate treatment would involve using different ionization cross sections for each species in X-ray ionization than in cosmic-ray ionization.

The UMIST RATE06 network

This network has several predecessors. The oldest one seems to be RATE90 (Millar et al. 1991), followed by RATE95 (Millar et al. 1997), RATE99 (Le Teuff et al. 2000), and RATE06[5] (Woodall et al. 2007). The most recent one, RATE06, contains 420 species[6] and 4606 reactions. Species with up to ten carbon atoms are included.

One feature of the RATE06 network is that each reaction is assigned a temperature range in which the rate parameters work best, together with a quality mark indicating to what extent the parameters are accurate. The same reaction may have multiple entries,

[2] Now Prof. Herbst has moved to the University of Virginia

[3] The reaction file can be downloaded at `http://www.physics.ohio-state.edu/~eric/research_files/osu_01_2009`, and the species included in this network can be downloaded at `http://www.physics.ohio-state.edu/~eric/research_files/List_species_01_2009.dat`.

[4] Downloadable at `http://www.physics.ohio-state.edu/~eric/research_files/osu_09_2010_ht`

[5] Downloadable at `http://www.udfa.net/`.

[6] They have made alterations to the chemical formulae of some species with respect to their previous versions. There is a table in the paper of Woodall et al. (2007) which lists the new and old chemical formulas of these species. However, in the downloaded reaction file, old formulae are still used for some species, for example, C_7H_4 (it should be CH_3C_6H).

each has its own temperature range[7], with different rate parameters. This is due to the fact that at different temperatures the rates of some reactions are best described by different parameters, and the maintainers of this network intend to make the network applicable for a wider temperature range (cold clouds and shocked gas). Care must be taken to use the correct one when calculating the rates. The temperatures at which the rate parameters change are usually quite high (∼300 K) by the standard of cold dark cloud conditions, so those redundant reactions that are applicable at higher temperatures are unimportant for our purpose.

Another feature of the RATE06 network is that reactions have negative activation barriers. This is because in certain temperature ranges the experimentally measured rates are best fit with a negative barrier. These experiments are usually done at relatively high temperatures ($\gtrsim$100 K), so that assuming negative barriers are likely inappropriate for lower temperatures, and indeed they can cause a big problem if blindly used. For the study of cold interstellar environments, these reactions are usually discarded.

The RATE06 network has two versions: one is the non-dipole case, another is dipole-enhanced. The difference between the two is, a temperature dependence $T^{-1/2}$ is included for ion-neutral reactions in which the neutral has a large dipole moment in the dipole case, but not in the non-dipole case.

The H_2 formation reaction $H + H \longrightarrow H_2$ on dust grains is not included in the file, so it needs to be added manually. The sample run presented in the accompanying papers of the UMIST network seems to have used a formation rate of $9.5\times10^{-18} nn(H)$ cm^{-3} s^{-1} (explicitly stated in Millar et al. 1991, but not in Woodall et al. 2007).

KIDA

KIDA (KInetic Database for Astrochemistry) is a relatively new database, mainted by V. Wakelam at the University of Bordeaux. It has a more "modern" web interface[8] than the previous two. Chemists are invited to submit new data to this database, which are then checked by the experts.

The KIDA database is planned to contain reactions for the study of ISM for a temperature range of 10–300 K, as well as for planetary atmospheres and circumstellar envelopes.

Other miscellaneous networks

- The NIST (National Institute of Standards and Technology) Chemistry WebBook[9] is a general-purpose database, which contains chemical kinetic and thermal chemistry data (and many other types of data) for many species. However, not all these data have been carefully scrutinized by experts. Another chemical database hosted by NIST is the CCCBDB database[10], which stands for Computational Chemistry Comparison and Benchmark Database. Its focus is on thermochemical data (formation enthalpies, entropies, etc.), instead of chemical kinetic data.

[7] It has been tried to ensure that the temperature ranges of the same reaction do not overlap; but in practice several reactions do have overlapping temperature ranges.

[8] `http://kida.obs.u-bordeaux1.fr/`

[9] `http://webbook.nist.gov/`

[10] `http://cccbdb.nist.gov/`

- The network provided by the Meudon PDR code group [11] (Le Petit et al. 2006) is relatively simple one; species containing a single deuterium atom are also included. Their code, aimed at modeling photon dominated regions, deals with a stationary plane-parallel slab of gas and dust, taking into account the illumination by the interstellar radiation field. Radiative transfer, as well as heating and cooling processes, are included.

- Various relatively small networks have been used in the past to study a special class of problems. For example, the completely depleted network by Walmsley et al. (2004) and Flower et al. (2004) contains no elements heavier than He; its smallness leaves room for multiply deuterated species, and for the ortho/para/meta discrimination of the H_3^+ and H_2 isotopologues.

2.1.2 Calculating the reaction rates

Denote the density of species X by $n(\mathrm{X})$. Its abundance [X] is usually defined to be relative to the total hydrogen nuclei density,

$$[\mathrm{X}] \equiv n(\mathrm{X})/n_{\mathrm{H}},$$

where n_{H} is the total hydrogen nuclei density, which is approximated by

$$n_{\mathrm{H}} = n(\mathrm{H}) + 2n(\mathrm{H_2}).$$

Note that sometimes the abundance is defined to be relative to the H_2 density, which may cause confusion when making comparison between different studies.

The rate of a reaction describes how frequently a reaction can occur, either expressed in terms of density, or in terms of abundance, of the species that are involved in this reaction.

The chemical reactions of interest in astrochemistry are mainly one-body or two-body reactions. Three body reactions are rarely included, due to the low density of the interstellar environment. In the following the mathematical form for the contribution to the evolution rate of a species from one- and two-body reactions are described.

Reaction rates

- For an one-body reaction, suppose A is the only reactant, we have

$$\partial_t n(\mathrm{A}) = -k n(\mathrm{A}). \tag{2.1}$$

  The rate coefficient k has the dimension of the inverse of time, and is usually provided with the unit of s^{-1}. It sets the time scale for the consumption of A. Dividing both sides by the total hydrogen density n_{H}, the equation becomes

$$\partial_t [\mathrm{A}] = -k[\mathrm{A}]. \tag{2.2}$$

  Thus for one-body reactions, the evolution equation for the density of a species is the same as the equation for the relative abundance. The abundances of all the products get increased by the same amount.

[11] `http://pdr.obspm.fr/PDRCode/Chemistry/Drcnosd.chi`

- For a two-body reaction, suppose A and B are the two reactants, we have

$$\partial_t n(\mathrm{A}) = -kn(\mathrm{A})n(\mathrm{B}). \tag{2.3}$$

  k is usually provided in the unit $\mathrm{cm}^3\ \mathrm{s}^{-1}$. Dividing both sides by the total hydrogen density n_{H}, the equation becomes

$$\partial_t [\mathrm{A}] = -kn_{\mathrm{H}} \cdot [\mathrm{A}][\mathrm{B}]. \tag{2.4}$$

  Now kn_{H} has the unit of s^{-1}. The abundances of all the products get increased by the same amount.

- The reaction $\mathrm{H} + \mathrm{H} \rightarrow \mathrm{H_2}$ for the formation of $\mathrm{H_2}$ on dust grains is a bit special. Although it appears to be a two-body reaction, however, in gas phase models, which do not consider the surface processes in detail, usually it is treated in a very simplified way, by assuming the formation rate of $\mathrm{H_2}$ takes the form

$$\partial_t n(\mathrm{H_2}) = kn_{\mathrm{H}} n(\mathrm{H}); \tag{2.5}$$

  thus

$$\partial_t [\mathrm{H_2}] = kn_{\mathrm{H}} [\mathrm{H}], \tag{2.6}$$

  which is similar to the expression for one-body reactions. The underlying assumption is that all (or a fixed fraction of) the hydrogen atoms hitting a dust grain are quickly converted into $\mathrm{H_2}$ molecules. So the formation rate of $\mathrm{H_2}$ is essentially half (a fixed fraction of) the adsorption rate of H.

  However, if deuterium is included in the chemistry, then the above simplified expressions cannot be directly extended to calculate the formation rate of HD and $\mathrm{D_2}$, because one cannot assume all the H and D atoms are converted into $\mathrm{H_2}$ or $\mathrm{D_2}$ anymore, and one has to find a way to arrange the adsorbing H and D atoms into different possible products.

Arrhenius equation for rate coefficient

The rate coefficient k as a function of temperature T is usually conveniently expressed in a form with three parameters

$$k = \alpha \left(\frac{T}{300\ \mathrm{K}} \right)^{\beta} \exp\left[-\gamma / T \right]. \tag{2.7}$$

This is called modified Arrhenius equation, while the original form does not contain the power-law part. That the temperature is scaled by 300 K seems to come from the fact that reaction rates are commonly measured at room temperature. γ has the physical meaning of an activation barrier that has to be crossed in the reaction path.

Not all the rate coefficients of reactions of any type can be expressed in the Arrhenius form, and sometimes more than three parameters are needed. In the RATE06 network, as described in Woodall et al. (2007), the γ parameters they give do not always correspond to activation energy, but can also mean the efficiency for the dissociation by cosmic-ray induced photons, or a parameter to correct for the dust extinction at ultraviolet wavelengths based on the visual extinction A_{V}; see the description of different types of reactions in the next section.

2.1.3 Different types of reactions, and their properties

Chemical reactions can be classified into different types, depending on the reaction mechanism and the character of the reaction participants. In the following, a summary of the reaction types commonly encountered in astrochemical studies are listed. The name of various reaction types are taken from Table 7 of Woodall et al. (2007), and the example reactions are taken from their RATE06 network.

`Type 1:` **Neutral-Neutral**

Example	Description
$H + CH \longrightarrow C + H_2$ $H + HCO \longrightarrow CO + H_2$ $C + OH \longrightarrow CO + H$ $O + OH \longrightarrow O_2 + H$ $N + OH \longrightarrow NO + H$	• 549 in RATE06, 275 measured • α range: 10^{-13}–10^{-9} cm^3 s^{-1} • β range: (-2)–(8), mostly zero • Many of them have a high barrier

`Type 2:` **Ion-Neutral**

Example	Description
$H_2^+ + H_2 \longrightarrow H_3^+ + H$ $H_2^+ + O_2 \longrightarrow O_2H^+ + H$ $H_3^+ + O \longrightarrow H_2O^+ + H$ $H_3^+ + CO \longrightarrow HCO^+ + H_2$ $C^+ + H_2O \longrightarrow HCO^+ + H$ $C^+ + O_2 \longrightarrow CO + O^+$ $He^+ + CO \longrightarrow O + C^+ + He$	• 2387 in RATE06, 956 measured • α range: 10^{-19}–10^{-7} cm^3 s^{-1}, mostly 10^{-11}–10^{-9} cm^3 s^{-1} • β: 0 or 0.5 • Mostly barrierless • It is the most dominant reaction type in interstellar conditions.

Notes: Caveat—this note is two-pages long. You may skip it and continue to read on Page 16.

The Langevin rate coefficient for ion-neutral reactions without a barrier when the neutral is non-polar (i.e. has no permanent dipole) is (Woon & Herbst 2009)

$$k_{\rm L} = 2\pi e(\alpha_{\rm pol}/m_{\rm red})^{1/2},$$

where e is the elementary charge, $\alpha_{\rm pol}$ is the polarizability of the neutral, and $m_{\rm red}$ is the reduced mass.

This rate is derived from a r^{-4} potential[12]. It may be instructive to see how the rate coefficient is derived. Consider the general case, where the potential function is $V(r)$. The total energy of the incoming particle can be expressed as

$$E_{\rm T} = \frac{1}{2}mv_{\rm r}^2 + \frac{L^2}{2mr^2} + V(r), \tag{2.8}$$

where $v_{\rm r}$ is the radial velocity, and L is the (conserved) angular momentum, which can be expressed as $L{=}mbv_0$, where b is the impact parameter, and v_0 is the velocity when the two particles are far apart. Usually people define an effective potential, which is

$$V_{\rm eff} = \frac{L^2}{2mr^2} + V(r).$$

[12] The induced dipole is proportional to the Coulomb force, hence to r^{-2}, and the potential of a dipole in a static electric field is also proportional to r^{-2}, which makes up the r^{-4} potential. When the neutral has a permanent dipole, the potential becomes proportional to r^{-2}.

Note that L is related to the kinetic energy of the incoming particle at infinity, by $E_0{=}L^2/(2mb^2)$.

A chemical reaction occurs if the incoming particle is captured. What does "capture" mean? Since the total energy is positive and conserved, we should not expect the two-particle system to become bound by acquiring a negative total energy unless certain energy release processes are explicitly accounted for (and for chemical reactions such an expectation is wrong, simply due to the fact that endothermic reactions exist). However, these complications are unnecessary (at least in the present rudimentary discussion). The key is explained in the following.

The effective potential varies as one particle moves from far away towards another particle. If the $V_{\rm eff}$ decreases indefinitely as r decreases, then there will be no obstacle for the two particles to come close to each other and merge (react). In reality $V_{\rm eff}$ may have a local maximum at certain radius, or may increase with decreasing r when r is smaller than a certain value.

Let's only consider the case in which $V_{\rm eff}$ has a local maximum at radius $r_{\rm p}$. The effective potential at this point is $V_{\rm eff}(r_{\rm p})$. If $V_{\rm eff}(r_{\rm p}){>}E_0$, then the particle won't be able to reach this peak point, which means that the inter-molecular distance has no chance to become smaller than $r_{\rm p}$, and the reaction cannot occur. In contrast, when $V_{\rm eff}(r_{\rm p}){<}E_0$, the radial velocity $v_{\rm r}$ at $r_{\rm p}$ is still nonzero, and must still be pointed towards the center (i.e. $\mathrm{d}r/\mathrm{d}t{<}0$), because for $r{>}r_{\rm p}$ the corresponding $|v_{\rm r}|$ must be larger (due to the conservation of energy and the fact that $r_{\rm p}$ is the peak position of $V_{\rm eff}$), hence $v_{\rm r}$ can never be zero or positive since initially $v_{\rm r}{<}0$.

So we have arrived at a criterion for a capture event to occur (for simplicity we may assume a capture event always leads to a chemical reaction, though this may not be true):

$$V_{\rm eff}|_{r=r_{\rm p}} < E_0, \tag{2.9}$$

where $r_{\rm p}$ is defined so that $\partial_r V_{\rm eff}|_{r=r_{\rm p}}{=}0$. Note that the left side is a function of both the impact parameter b and initial kinetic energy E_0. The critical impact parameter $b_{\rm c}$ is defined such that both sides of Eq. (2.9) are equal.

Assuming a power-law attractive potential $V(r){=}-\kappa r^{-n}$, we have

$$V_{\rm eff} = \frac{L^2}{2mr^2} - \kappa r^{-n},$$

$$r_{\rm p} = \left(\frac{nm\kappa}{L^2}\right)^{1/(n-2)},$$

and

$$V_{\rm eff}|_{r=r_{\rm p}} = \frac{n-2}{2}\kappa^{-2/(n-2)}\left(\frac{L^2}{nm}\right)^{n/(n-2)}. \tag{2.10}$$

The critical impact parameter for capture can thus be solved for. It is

$$b_{\rm c} = \left(\frac{\kappa}{E_0}\right)^{1/n}\cdot\left(\frac{n}{n-2}\right)^{1/2}\left(\frac{n-2}{2}\right)^{1/n}. \tag{2.11}$$

For the ion-neutral reaction involving a non-polar neutral, $n{=}4$, $\kappa{=}\alpha_{\rm pol}e^2/2$, hence

$$b_{\rm c}{=}(2\alpha_{\rm pol}e^2/E_0)^{1/4},$$

and the rate coefficient is

$$k = \pi b_c^2 v = 2\pi e \left(\frac{\alpha_{\rm pol}}{m}\right)^{1/2}$$
$$= 2.3 \times 10^{-9}\ {\rm cm^3\ s^{-1}}\ \left(\frac{\alpha_{\rm pol}}{10^{-24}\ {\rm cm^3}}\right)^{1/2} \left(\frac{m}{m_{\rm H}}\right)^{-1/2},$$

which is called Langevin rate. A typical value for $\alpha_{\rm pol}$ can be found in Duley & Williams (1984). k has no temperature dependence, so that extrapolating experimental results obtained usually at room temperature to low temperatures becomes a simple task.

When the neutral species does possess a significant dipole moment, the potential may be approximated by a power-law with n=2, hence $b_c \propto E_0^{-1/2} \propto v^{-1}$, and $k = \pi b_c^2 v \propto v^{-1} \propto T^{-1/2}$. The real situation is more complex since the barrier also depends on the direction of the dipole (Woon & Herbst 2009).

As a side note, we may see from Eq. (2.10) that for n=1 (Coulomb potential), $V_{\rm eff}|_{r=r_{\rm p}} < 0$. This does not mean that a Coulomb potential always leads to a capture (which is obviously wrong), but the inequality holds simply because in this case $r_{\rm p}$ is not a local maximum, but a local minimum! Actually, $\partial_r^2 V_{\rm eff}|_{r=r_{\rm p}} = n(2-n)\kappa r_{\rm p}^{-(n+2)}$, which is positive for $n < 2$.

Type 3: Charge Exchange

Example	Description
$H + H_2^+ \longrightarrow H_2 + H^+$ $H + CO^+ \longrightarrow CO + H^+$ $CH_2 + O^+ \longrightarrow O + CH_2^+$ $OH^+ + HCO \longrightarrow HCO^+ + OH$	• 552 in RATE06, 201 measured • α range: 10^{-16}–10^{-8} cm^3 s^{-1}, mostly 10^{-11}–10^{-9} cm^3 s^{-1} • Mostly barrierless

Type 4: Atomic Ion-Ion Neutralization

Example	Description
$H^+ + H^- \longrightarrow H + H$ $H^- + H_2^+ \longrightarrow H_2 + H$ $He^+ + C^- \longrightarrow C + He$ $C^- + O^+ \longrightarrow O + C$	• 31 in RATE06, none of them is measured • α=2.3×10^{-7} cm^3 s^{-1} • β= − 0.5 • Barrierless

Type 5: Dissociative Recombination

Example	Description
$H_2^+ + E^- \longrightarrow H + H$ $H_3^+ + E^- \longrightarrow H + H + H$ $H_3^+ + E^- \longrightarrow H_2 + H$ $H_3O^+ + E^- \longrightarrow OH + H + H$ $H_3O^+ + E^- \longrightarrow H_2O + H$ $CH_3OH_2^+ + E^- \longrightarrow CH_3OH + H$ $CH_3OH_2^+ + E^- \longrightarrow H_2CO + H_2 + H$	• 486 in RATE06, 95 measured • The name means recombination between an ion and an electron (denoted by E$^-$), producing neutral fragment species. • α range: 10^{-9}–10^{-4} cm^3 s^{-1}, mostly 10^{-8}–10^{-6} cm^3 s^{-1} • β range: (−3)–(−0.3); typically −0.3 or −0.5 • Barrierless

`Type 6:` **Radiative Recombination**

Example	Description
$H + E^- \longrightarrow H^- + Photon$ $H^+ + E^- \longrightarrow H + Photon$ $C + E^- \longrightarrow C^- + Photon$ $C^+ + E^- \longrightarrow C + Photon$ $CH_3^+ + E^- \longrightarrow CH_3 + Photon$	• 25 in RATE06, none of them is measured • α range: 10^{-17}–10^{-9} cm^3 s^{-1} • β range: (= 1.4)–(2.5); no obvious pattern • Mostly barrierless

`Type 7:` **Associative Detachment**

Example	Description
$H^- + H \longrightarrow H_2 + E^-$ $H^- + C \longrightarrow CH + E^-$ $H^- + CH_3 \longrightarrow CH_4 + E^-$ $H_2 + C^- \longrightarrow CH_2 + E^-$ $CH + OH^- \longrightarrow H_2CO + E^-$ $C^- + O_2 \longrightarrow CO_2 + E^-$	• 47 In RATE06, 1 measured • α range: 10^{-13}–10^{-9} cm^3 s^{-1}, mostly 10^{-10}–10^{-9} cm^3 s^{-1} • β=0, except for one reaction ($O^- + NO \longrightarrow NO_2 + E^-$) • Barrierless

`Type 8:` **Radiative association**

Example	Description
$H^+ + H \longrightarrow H_2^+ + Photon$ $H + C \longrightarrow CH + Photon$ $C^+ + C \longrightarrow C_2^+ + Photon$ $C + N \longrightarrow CN + Photon$ $C + O \longrightarrow CO + Photon$ $O + O \longrightarrow O_2 + Photon$	• 91 in RATE06, 17 measured • α range: 10^{-23}–10^{-9} cm^3 s^{-1} • β range: (−5)–(2) • Mostly barrierless

`Type 9:` **Photoprocess**

Example	Description
$H^- + Photon \longrightarrow H + E^-$ $H_2^+ + Photon \longrightarrow H^+ + H$ $C + Photon \longrightarrow C^+ + E^-$ $CO + Photon \longrightarrow C + O$ $H_2CO + Photon \longrightarrow CO + H_2$	• 216 in RATE06, none of them is measured • α range: 10^{-15}–10^{-7} s^{-1}, mostly 10^{-11}–10^{-9} s^{-1} • No temperature dependence • $k = \alpha \exp(-\gamma A_V)$ s^{-1}, where A_V is the visual extinction. • γ range: (0.5)–(5)

Notes: The photo-dissociation of CO and H_2 is mainly through line absorption, and self-shielding can be important (Millar et al. 1997), hence a depth-dependent model is needed. These effects cannot be included in the rate file. But for dark cloud interior the photo-processes are unimportant.

`Type 10`: **Cosmic-Ray Proton (CRP)**

Example	Description
$H_2 + CRP \longrightarrow H^+ + E^-$ $H_2 + CRP \longrightarrow H_2^+ + E^-$ $C + CRP \longrightarrow C^+ + E^-$ $N + CRP \longrightarrow N^+ + E^-$ $O + CRP \longrightarrow O^+ + E^-$ $CO + CRP \longrightarrow C + O$	• 11 in RATE06, none of them is measured • α range: 10^{-21}–10^{-17} s^{-1}, normalized to a total H_2 ionization rate of 1.36×10^{-17} s^{-1}, and can be rescaled. • No temperature dependence

Notes: The canonical value used by Woodall et al. (2007) for the total cosmic-ray ionization rate of H_2 is

$$\zeta_0 = 1.36 \times 10^{-17} \text{ s}^{-1}.$$

So the corresponding time scale is

$$\tau_{\text{cosmic-ray}} = 2.3 \times 10^9 \text{ yr}.$$

However, the value of ζ_0 is very uncertain. For example, using H_3^+ observations, Indriolo & McCall (2012) obtained ζ_0 (denoted by ζ_2 in their paper) in the range $(1.7 \pm 1.3)\times10^{-16}$ to $(10.6 \pm 8.2)\times10^{-16}$ s^{-1} for diffuse clouds, without any apparent pattern in the sky. They also speculate that local enhancement by acceleration sites for cosmic-rays such as supernova remnant might be important. Their value is one-to-two orders of magnitudes higher than rates adopted earlier (see, e.g., Herbst & Klemperer 1973). The cosmic-ray ionization rate depends on the spectrum of the penetrating cosmic rays, and suffers from attenuation due to energy loss and deflection by magnetic fields (Padovani et al. 2009; Rimmer et al. 2012). Studies on the origin, propagation, spatial distribution, and energy spectrum of the cosmic rays are themselves fascinating, and chemical modeling and observations together can help to constrain the parameters for some of them (van Dishoeck & Black 1986).

`Type 11`: **Cosmic-Ray induced Photon (CRPhoton)**

Example	Description
$C + CRPhoton \longrightarrow C^+ + E^-$ $CH + CRPhoton \longrightarrow C + H$ $CO + CRPhoton \longrightarrow C + O$ $H_2O + CRPhoton \longrightarrow OH + H$ $OH + CRPhoton \longrightarrow O + H$ $O_2 + CRPhoton \longrightarrow O + O$ $H_2O_2 + CRPhoton \longrightarrow OH + OH$	• 156 in RATE06, none of them is measured • α=1.3×10^{-17} s^{-1} • $k = \alpha(T/(300\text{ K})^{\beta}\gamma/(1-\omega)$ s^{-1}, where ω is the dust grain albedo in the far ultraviolet, usually taken to be 0.5 or 0.6. • β=1.17 for CO + CRPhoton $\longrightarrow$ C + O, otherwise β=0. • γ range: (8.5)–(5000), mostly of the order 1000.

Notes: The ultraviolet photons are created in the dense cloud interiors when H_2 molecules are excited by the secondary electrons generated by cosmic-ray ionization (Gredel et al. 1989). This is the so called Prasad-Tarafdar mechanism (Prasad & Tarafdar 1983), which yields a UV photon flux of $\sim$1000 cm^{-2} s^{-1}.

The cosmic-ray induced photons are mainly absorbed by dust. Suppose the flux of

these photons is F_γ, we have

$$F_\gamma \sigma_G n_G (1-\omega) = 0.15 \zeta_0 n_H,$$

which gives

$$F_\gamma = \frac{0.15\zeta_0 n_H}{\sigma_G n_G (1-\omega)} = \frac{0.15\zeta_0}{\tilde{\sigma}_G (1-\omega)},$$

where $\tilde{\sigma}_G \simeq 2\times10^{-21}$ cm^2 is the absorption cross section of the dust grains per hydrogen nucleus (Sternberg et al. 1987), and n_G is the dust density. This gives $F_\gamma \simeq 1700$ cm^{-2} s^{-1}. The factor 0.15 comes from the impact excitation efficiency of H_2 by an electron with energy 30 eV.

Note that the γ value for these reactions are a factor of two smaller than those calculated by Gredel et al. (1989), due to a difference in whether it is scaled to the total cosmic ionization rate of H_2 or H.

`Type 12:` **Collisional Dissociation**

Example	Description
$H + H_2 \longrightarrow H + H + H$ $H + CH \longrightarrow C + H + H$ $H + OH \longrightarrow O + H + H$ $H + H_2O \longrightarrow OH + H + H$ $H + O_2 \longrightarrow O + O + H$ $H_2 + O_2 \longrightarrow O + O + H_2$	• 16 in RATE06, 2 measured • α range: 10^{-15}–10^{-7} cm^3 s^{-1} • β range: -1, 0, 0.35, or 4.5; mostly 0

Notes: Most of them have very high barriers (>1 eV), except for five of them; they are (neglecting duplicates) $H^+ + HNC \longrightarrow HCN + H^+$, $H + HNC \longrightarrow HCN + H$, $H_2 + HOC^+ \longrightarrow HCO^+ + H_2$, $C_2H_2 + H_2C_3H^+ \longrightarrow C_3H_3^+ + C_2H_2$, which are all isomerization reactions.

Their rate coefficients may depend on both temperature and density, hence they cannot be accurately described by the Arrhenius equation (Millar et al. 1997).

`Type 13:` **Chemical Ionization**

Example	Description
$CH + O \longrightarrow HCO^+ + E^-$	• Only one in RATE06; not measured • α=2×10^{-11} cm^3 s^{-1}, β=0.44, γ=0

`Type 14:` **Ion-Molecular Ion Neutralization**

Example	Description
$H^- + H_3^+ \longrightarrow H_2 + H_2$ $H^- + NH_4^+ \longrightarrow NH_3 + H_2$ $H^- + H_3O^+ \longrightarrow OH + H_2 + H$ $H^- + H_3O^+ \longrightarrow H_2O + H_2$ $H^- + HCO^+ \longrightarrow CO + H_2$	• Only five in RATE06, none of them is measured • α=2.3×10^{-7} cm^3 s^{-1} • β=-0.5, γ=0

`Type 15:` **Collider**

Example	Description
$CO + M \longrightarrow O + C$ $CO + HOC^+ + M \longrightarrow HCO^+ + CO$ $H + O + M \longrightarrow OH$ $H + OH + M \longrightarrow H_2O$ $H + CO + M \longrightarrow HCO$ $H + HCO + M \longrightarrow H_2CO$	• 32 in RATE06, 11 measured • α range: 3×10^{-3} for $CO + M \longrightarrow O + C$, otherwise 10^{-10}–10^{-33}. The unit may be either $cm^3\ s^{-1}$ or $cm^6\ s^{-1}$. • β range: (-7)–(0) • γ: 10 eV for $CO + M \longrightarrow O + C$, otherwise zero or large negative or positive values

Notes: These include ternary (three-body) reactions, where M can be viewed as a catalyst. They are somewhat similar to grain surface reactions, although such a simplistic format cannot capture the details of the latter. They are only important at densities higher than 10^{10} cm^{-3} (Le Teuff et al. 2000). Hence this type of reactions are usually excluded from astrochemical modeling.

2.2 The chemical rate equation

In Section 2.1.2 the general form for the rate of each individual reaction has been written down. In a reaction network, a single species can take part in many reactions, and can be produced by many channels. To describe the evolution of its abundance, the contributions from all those reactions need to be added together; since the rate of each of these reactions depends on the abundances of other species, which are themselves unknown, we actually need an equation for every species. Hence we get a set of coupled ordinary differential equations (ODE), called the chemical rate equation(s), which is nonlinear in general.

Suppose the abundance of species i is x_i, we have

$$\begin{aligned}\partial_t x_i = &-x_i \sum_r k_r - x_i \sum_s k_s x_{s(1)} \\ &+ \sum_p k_p x_{p(1)} + \sum_q k_q x_{q(1)} x_{q(2)},\end{aligned} \tag{2.12}$$

where the sums are over reactions related to species i; specifically, the index r refers to all the one-body destruction reactions (such as cosmic-ray ionization) of i, s refers to all the reactions between i and other species, and p and q refer to all the one- and two-body reactions that produce i; $s(1)$ means the reactant of the reaction s other than i; similar for $p(1)$, $q(1)$, and $q(2)$. Since at most two-body reactions are considered, the right hand side of Eq. (2.12) contains nonlinear terms to at most the second degree.

Usually, the production (positive) terms in the above equation do not contain x_i, although exceptions do exist; e.g., $H + H_2 \longrightarrow 3\,H$ or $H + CH \longrightarrow C + 2\,H$, both of which are of the type collisional dissociation, and have a huge barrier.

If all the rate coefficients are independent of the physical conditions, or the physical conditions (density, temperature, optical depth, etc.) can be treated as a constant, then the differential equation system Eq. (2.12) is autonomous. Usually, we assume that this condition holds, although we also investigate the effect of variable physical conditions.

Since different spatial points may have different chemical composition, the most general form of the evolution equation should contain partial derivatives over the spatial coordinate, to take into account the convection and diffusion effects. In cold dark clouds the diffusion through thermal motions should be very slow. Turbulent mixing might be important, but it works only locally, where the gradient in chemical composition is small. Hence we may neglect the convection effect, and put the explicit form of the physical parameters as a function of time into Eq. (2.12) through the rate coefficients.

In a completely self-consistent model, the chemical rate equations should be coupled with the dynamical equations. This means that not only the evolution in the density and temperature can affect the chemical evolution, but that the compositional variations caused by the chemical processes can also affect the dynamical evolution by changing the heating and cooling rates (Neufeld et al. 1995) or by changing the interaction between matter and magnetic fields through the degree of ionization (see, e.g. Tassis et al. 2011). However, in models of this class, the chemistry considered is usually relatively simple, where only the key species (such as the major coolants) are included. Since our goal is not to give a comprehensive chemical-dynamical model of cloud evolution, we don't take the coupling and feedback effect into account; namely, our emphasis is on the chemical part, isolated from complications from the dynamics.

The solutions to Eq. (2.12) can be divided into two types. The first type is to solve only the steady-state equations, which means to solve a set of algebraic equations by setting $\partial_t x_i = 0$, for all i. This is usually done with a Newton-Raphson scheme (Le Bourlot 1991), and is adopted for studies on chemical bi-stability[13] (Le Bourlot et al. 1993; Charnley & Markwick 2003). Another type is the time-dependent solution, in which the evolution of the abundances of all the species are calculated as a function of time from a given initial condition. Sometimes this type of solution is called pseudo-time-dependent, since the physical conditions are kept constant. Note that the second type of solution can indeed be viewed as an iterative way to obtain the steady-state solution, though this may not be as efficient as the Newton-Raphson method for this kind of problem.

In our work we always obtain the time-dependent solution of Eq. (2.12). In the following I give a description of the problems encountered in solving the chemical rate equation and the way to deal with them. Then I describe a code I wrote for obtaining the solutions, based on a general-purpose solver.

2.2.1 Solving a stiff system of equations

The chemical rate equation is a stiff system[14], meaning that a large range of time scales are involved. For example, the cosmic-ray dissociation time scale is of the order 10^9 yr, while the time scale for the dissociative recombination reactions can be as short as several years. Since we are usually interested in time scales that are not too short, the existence

[13] The chemical bi-stability is a phenomenon in which there are two (maybe more in the general case) stable solutions for the steady state, for certain physical conditions. It is related to the bifurcation phenomenon, in which the continuous variation of one controlling parameter (density for example) can lead to the appearance or disappearance of one of the two steady states. Whether this theoretically discovered behavior has any observational significance seems to be unanswered (Charnley & Markwick 2003; Boger & Sternberg 2006).

[14] The word "stiff" in the name seems to be related to the motion of spring systems with large spring constants.

of a large range of time scales means that we have to deal with those very fast processes occurring in time intervals much shorter than the time scales we care about.

This stiffness causes problems when trying to solve the equations numerically with an explicit method. For example, if the following equation

$$y' = -cy \qquad (c > 0) \tag{2.13}$$

is solved using the explicit forward Euler scheme

$$y_{n+1} = y_n + hy'_n = (1 - ch)y_n = (1 - ch)^n y_1, \tag{2.14}$$

where h is the time step, then its long-time behavior (i.e. when n is large) is correct only if $|1-ch| < 1$, which requires $h < 2/c$. This is because if h is so large that $(1-ch) < -1$, the solution Eq. (2.14) will be oscillating between positive and negative values. So when c is large, a very small time step is needed for the numerical solution to converge to zero, although the exact analytical solution vanishes exponentially. A similar problem appears in the general case of a nonlinear set of equations (rather than only one equation), where the right hand side can be linearized and analyzed similarly.

For these stiff equations, it is impractical to avoid the instability problem by adopting very small integration intervals, since—if such an approach is taken—extremely small interval (in comparison to the time scales we are interested in) will be necessary, leading to a huge number of integration steps.

The solution to this stiffness problem is to use implicit methods. The form in Eq. (2.14) is explicit, as its right hand side involves only quantities at step n, and the calculation involved is straightforward. In contrast, in the implicit approach the right hand side of an integration step contains quantities that need to be solved for. For example, one may simply replace Eq. (2.14) by

$$y_{n+1} = y_n + hy'_{n+1} = y_n - chy_{n+1}, \tag{2.14$'$}$$

which gives

$$y_{n+1} = \frac{y_n}{1 + ch} = \frac{y_1}{(1 + ch)^n}. \tag{2.15}$$

Since both c and h are positive, the above form is always stable; no oscillatory behavior will appear.

The fact that unknown quantities appear in both sides of each integration step in the implicit method requires solution of a set of (nonlinear) algebraic equations, similar to what we did to get Eq. (2.15) from Eq. (2.14$'$).

The method used in solving these algebraic equations are usually based on Newton's method, i.e., by linearizing these equations and iterating until the solution has converged. The linearization step may be done by numerical differencing, or, probably more efficiently, by making use of the Jacobian matrix.

For a set of differential equations with the form

$$\partial_t x_i = f_i(x_1, x_2, \ldots, x_n; t), \tag{2.16}$$

each element of the associated Jacobian matrix at each time is defined to be

$$J_{ij} = \frac{\partial f_i}{\partial x_j}, \tag{2.17}$$

which is easy to evaluate based on the rate equations Eq. (2.12).

For a large chemical network, the Jacobian matrix is most likely very sparse, meaning that most of its elements are zero at all time. For example, when species j does not react with species i, and does not participate in any reactions producing i, then $J_{ij} = 0$. This property should be utilized in the solver.

The ODE solver we use

We did not write an ODE solver by ourselves, rather we use the 2003 version of the `DLSODES` solver of the *ODEPACK* package[15] (Hindmarsh 1983; Radhakrishnan & Hindmarsh 1993), which is written in FORTRAN77. The name of the solver means "the double precision version of the Livermore Solver for Ordinary Differential Equations with general Sparse Jacobian matrix". The *ODEPACK* package contain 9 solvers, each of which suits different class of problems. The one we use is best suited for stiff and sparse problems; it supersedes and improves upon the older *GEARS* package.

2.2.2 The gas phase chemical code

The code for a pure gas phase chemical model is relatively simple. The basic form of the whole code is no more than 1200 lines long. A flowchart for our code is shown in Fig. (2.1). It is written in FORTRAN90, although the solver we use is written in FORTRAN77. The merit of FORTRAN90 is that it has more functionalities (such as support of longer variable name, free layout, dynamic memory allocation, string processing, etc.), and code written in it is much easier to understand and maintain than FORTRAN77. We use the GNU `gfortran` compiler[16].

Here we may note that some authors implement the differential equations Eq. (2.12) directly into the code (Leung et al. 1984; Millar et al. 1991). Namely, in addition to the code for chemical evolution, they have another code that imports all the reactions, calculates their rates, and then write all the rate equations in Eq. (2.12) with the coefficients assigned pre-calculated numeric values into a code, which will be compiled and called by the solver in the solution step.

Such a procedure is not necessary, and our code does not work like this. In each iteration step the solver will ask for the values of $\partial_t x_i$, namely, the right hand side of Eq. (2.12), and also for the values of one column of the Jacobian matrix (if the related option is turned on). This can be done by simply looping over all the reactions and adding (or subtracting in case of consumption) the contribution from each reaction to the evolution rates of the species that take part in the corresponding reaction.

Performance of the code

With the OSU09 network The physical parameters we used are $n(\mathrm{H_2}) = 10^4$ cm^{-3}, $T = 10$ K, $A_\mathrm{V} = 10$. Using this network (containing 468 species and 6046 reactions), and running on a normal desktop computer[17], the program takes 1–3 seconds for all the preparation work before the solver really starts iterating, and the solver takes 18–25

[15] `http://www.netlib.org/odepack/`
[16] `http://gcc.gnu.org/wiki/GFortran`
[17] Intel(R) Core(TM)2 Duo CPU E8400@3GHz, 4 GB Memory; Ubuntu 10.04.

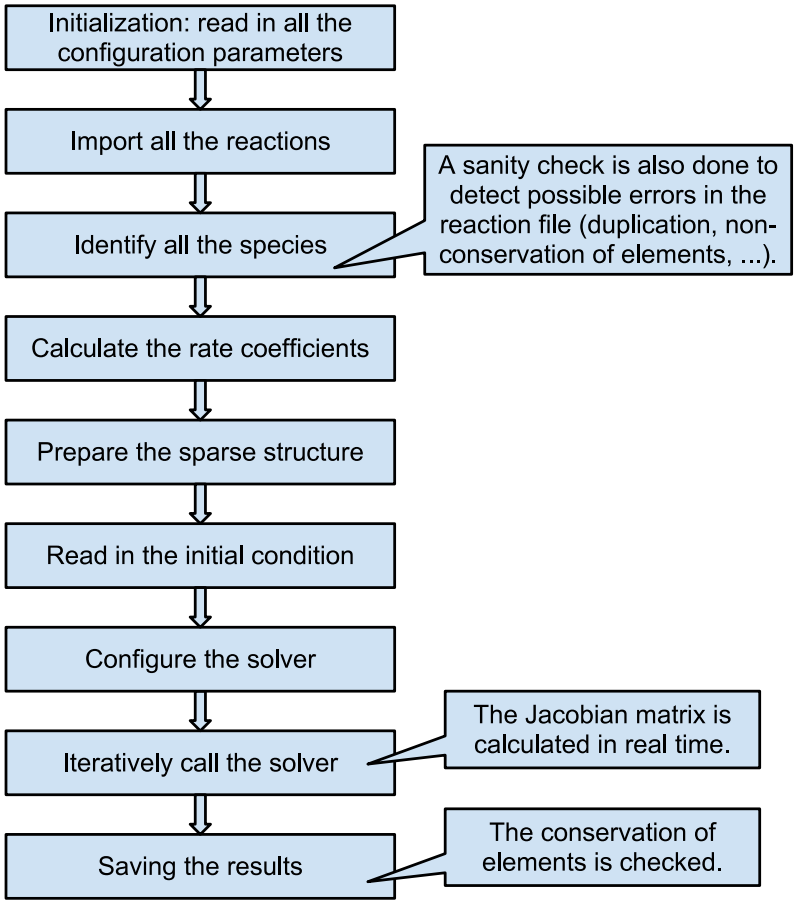

Figure 2.1: A flowchart for the gas phase chemical code.

seconds to reach 1.2×10^8 years, with an absolute tolerance of 10^{-50}, a relative tolerance[18] of 10^{-6}, and a user-provided iteration number 710 (which is the number of output data points, not the number of internal iteration steps of the solver). About one second is needed to save the results. The total abundance of each element varies by no more than a factor of 10^{-10} between the initial and final states, which means at least in this sense the code is working fine.

With the UMIST RATE06 network As this network is smaller than the OSU09 network, containing 420 species and 4605 reactions, the program takes ∼9 seconds to reach 10^8 years, with a relative tolerance of 10^{-6}, and an absolute tolerance of 10^{-50}.

Since the RATE06 network is accompanied by a paper (Woodall et al. 2007), which contains a benchmark model, we compared the results from our model with theirs (Table 9 in Woodall et al. 2007). The agreement is generally good, with relative differences of the order 1% (the values in their Table 9 contains only three digits). The differences may originate from different treatment of some of the reactions with negative energy barriers, or maybe slightly different physical conditions have been used.

With the depleted network This network is based on the completely depleted network of Walmsley et al. (2004) and Flower et al. (2004), which contains no elements heavier than He, supplemented by Pagani et al. (2009) and Hugo et al. (2009), compiled by B. Parise. With 28 species, 389 reactions, and with relative tolerance set to 10^{-6}, absolute tolerance set to 10^{-90}, the run time needed to reach 10^8 years is about 0.1 second. If the relative tolerance is set to 10^{-2}, then the time needed becomes 0.04 second, with essentially no change in the results.

2.2.3 Application of the gas phase code to study H_2D^+ and D_2H^+

In Parise et al. (2011) a spatially extended distribution of D_2H^+ was for the first time firmly detected in the H-MM1 prestellar core in the L1688 cloud. The exact temperature and density of this source has not been derived, but the temperature is constrained to be <13 K based on the velocity width. Together with data on H_2D^+, the ratio between para-D_2H^+ and ortho-H_2D^+ is constrained to be ∼1–10, depending on the assumed density and kinetic temperature of the source that are needed for the non-LTE[19] radiative transfer modeling.

The ortho- and para- (and possibly meta-) designations are used to distinguish different nuclear spin states of a molecule that contain two or more equivalent H or D atoms. The fact that the H nucleus is a fermion while the D nucleus is a boson exerts requirements on the symmetry of possible spatial wave functions of the molecule, specifically the rotation states, which determine the rotation energy levels. The transition between different nuclear spin states is forbidden, hence two molecules with the same chemical structure

[18] The absolute tolerance and relative tolerance are setup parameters for the solver, which set the maximum allowable absolute and relative errors for the abundances. A very small absolute tolerance is used merely to let the solver proceed, since, if the absolute tolerance is set to zero, then for a species with very low abundance, the allowed error determined from the relative tolerance may be too small to achieve.

[19] LTE: Local thermodynamic equilibrium. For non-LTE conditions, in which the gas density is not high enough to thermalize the distribution of the occupation number in each energy level of a molecule because the radiative cascade is relatively fast, the kinetic temperature of the gas (which describes the thermal velocity of a molecule) and the Boltzmann equation cannot be used to describe the energy level population.

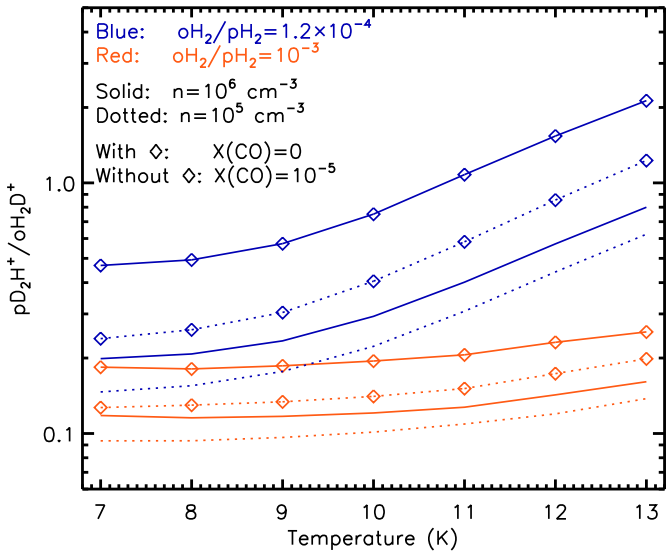

Figure 2.2: The ratio between the abundances of para-D_2H^+ and ortho-H_2D^+ as a function of temperature, for different ortho/para ratios of H_2, different densities, and different degree of depletion of CO.

but with different nuclear spin states are taken to be different species. The conservation of nuclear spin symmetries, together with other conservation laws (for mass, energy, and rotational angular momentum) put strong restrictions on the possible reactions that can occur, which has been studied by Hugo et al. (2009).

The goal of our modeling is to see whether the ratio between the abundances of ortho-H_2D^+ and para-D_2H^+ can be reproduced with a reasonable density, temperature, and a depletion degree of CO and N_2. For this purpose, the coupling between gas phase chemistry and dust grain surface processes are not important, since we are not concerned about the abundances of species that are created on the dust grains. Only the depletion of CO and N_2 onto the dust grains and formation of the H_2 isotopologues need to be considered, which can be easily handled in a gas phase chemical model.

CO and N_2 are important for our purpose here because they are the major consumer of the H_3^+ isotopologues. When CO and N_2 are depleted, the abundances of the H_3^+ isotopologues will rise accordingly.

Fig. (2.2) shows the abundance ratio between para-D_2H^+ and ortho-H_2D^+ as a function of temperature for $n_{\rm H} = 10^5$ and 10^6 cm^{-3} and for two different CO abundances, at a time when the ortho-to-para ratio of H_2 is 10^{-3} and 1.2×10^{-4}. Clearly, to get a $[pD_2H^+/oH_2D^+]$ ratio higher than one, the $[oH_2/pH_2]$ ratio has to be much smaller than 10^{-3}, and CO has to be heavily depleted. Considering that pD_2H^+ is detected in a region extended over 40", a high depletion of CO in such a large area seems unlikely, which poses a challenge to the model.

A more detailed discussion on the observation, radiative transfer, and chemical modeling can be seen in Parise et al. (2011). The related study is still ongoing, both in observation and in modeling.

Chapter 3

Grain chemistry

Contents

In the previous chapter, the gas phase chemical reactions and the networks that are relevant for interstellar clouds, together with their mathematical formulation, have been described. The vast majority of the interstellar mass resides in the gas phase; only around one percent of the mass is in mesoscopic solid form, which we call dust grains. Though being tiny, this dust material has an impact on astronomy that cannot be overestimated. Dust affects the dynamical evolution of the ISM in many aspects. From a chemical point of view, it can act as a reservoir of gas phase molecules, a factory and catalyst for producing molecules, and, can enrich the gas phase composition by partially or completely being fragmented.

In this chapter I first give a brief review of the general aspects of dust properties, then state the reasons why do we need to study grain chemistry, followed by an investigation of the basic processes involved in grain chemistry. A mathematical formalism that is needed to model these processes is then presented. Finally, one method (Monte Carlo simulation) to model the grain chemistry is described. Another method (hybrid moment equation method) that is developed by us will be presented in the next chapter.

3.1 General facts about interstellar dust grains

The existence of dust in the interstellar space is not a trivial fact even when viewed in retrospect. In the early times astronomers noticed dark regions in the sky in which the number of stars is much lower than their neighborhood (mentioned in Greenberg 1963 and Bergin & Tafalla 2007); that these dark regions are not really empty but rather contain a lot of gas and dust is unveiled by observations in the optical and infrared band. Light rays passing through these clouds are absorbed and scattered by the dust grains. This so-called extinction demonstrates the existence of opaque material between the observer and

the stars, and can be used to quantitatively study the physical properties (composition, size, morphology, etc.) of the dust grains.

Most of our knowledge about interstellar dust comes from its interaction with electromagnetic fields. The degree of extinction as a function of wavelength can be used to constrain the size and material composition of the dust grains, and the polarized light from the dust indicates their non-spherical shape, the existence of a magnetic field (with a strength greater than a few μG), via the alignment of the dust grains with respect to the magnetic field (Davis & Greenstein 1951). Besides absorption features, the emission spectra from dust provide independent and complementary information on the dust composition, leading to the discovery of PAH (Polycyclic Aromatic Hydrocarbon) molecules in the interstellar space (Li & Draine 2001; Tielens 2008).

The infrared light scattered by the interstellar dust (leading to the so-called "cloudshine" and "coreshine") can also be used as a proxy to study the dust grain sizes and the host cloud cores (Pagani et al. 2010). This is somewhat similar to the case in our solar system, where the presence of zodiacal light indicates the condensation of dust particles towards the ecliptic plane.

The interstellar dust grains contain a core, usually composed of refractory materials, such as carbonaceous compounds (graphite, PAH, etc.) and silicates (containing Si, O, Fe, and Mg) (Draine 2003). The core may also be chemically differentiated due to its formation process. In cold conditions the grain core will be covered with an ice mantle, mainly composed of solid water, CO, CO_2, CH_3OH, and some other species. The size of a dust grain can be described by the famous MRN power-law distribution (Mathis et al. 1977), $\mathrm{d}n/\mathrm{d}r \propto r^{-3.5}$, for 0.005 μm$<r<$1 μm. It gives a mean radius of about 0.008 μm. Grain chemistry models typically adopt a larger radius of 0.1 μm, considering the growth of dust in cold dense conditions.

Dust particles in the interplanetary space close to Earth can be directly captured by balloons or airplanes flying in the stratosphere[1], or by satellites (such as *MIDAS* on board *Rosetta*, the aerogel collector of *Stardust*, and *VBSDC* on board *New Horizons*). The dust grains that have been captured and directly imaged by scanning electron microscope(Bradley et al. 1992) usually appear as a porous and heterogeneous mixture of particles with different compositions (refractory or organic). Dust fallen onto the Earth in the pristine continent of Antarctica (where contamination from terrestrial sources are reduced as much as possible) can also be collected (Hodge 1981). They are visually classified into several types, such as opaque or transparent spherules, and irregular particles; chemically they are rich in iron or silicon (Schmidt & Keil 1966). The isotopic ratio in these particles can be used to confirm their extraterrestrial origin. Most of the interplanetary dust are fragments of comets or ejecta produced in asteroid collisions, and only a minor part may come from the interstellar space.

The interstellar dust grains have their origins in the ejecta of old stars or in supernova explosions. It is not clear which contributes more by now. The detailed mechanism for the formation of dust particles from atoms and molecules (e.g., how the atomic silicon can combine with other elements such as oxygen, magnesium, ..., to form clusters) in these conditions is still under active investigation (see, e.g., Goumans & Bromley 2012). In their journey from the circumstellar envelopes to the diffuse ISM, to the dense dark clouds, and

[1] See, e.g., `http://www.spaceref.com/news/viewpr.html?pid=28009`

then finally to newly formed stars and planets (and other cometary and asteroid bodies), the dust grains must have been heavily altered by radiation field and particle encounters. A dust particle can gain material by accumulating gas phase molecules, or by merging with other dust particles upon close encounter. But if the collision with an incoming particle is too fierce, it may lose mass by sputtering (Draine & Salpeter 1979; Draine 1979; Tielens et al. 1994), or it may get reshaped. If the collision is energetic enough, the dust particle may be hot enough to restructure itself (crystallization or glassification). Energetic photons or cosmic rays can also change the dust composition by evaporating surface molecules (Purcell 1976) or by initiating chemical reactions.

Among the researches on interstellar dust, the work of Hoyle & Wickramasinghe seems to be a heresy (Wickramasinghe 2011). Although their early work (Hoyle & Wickramasinghe 1962) is in the mainstream, which studied the extinction caused by dust grains made of graphite (graphite flake), and their polarizing effect, later these authors conjectured the presence of prebiotic or even biotic materials on the dust grains (Hoyle & Wickramasinghe 1977, 1979) based on the extinction features and the presence of amino acids in carbonaceous chondrites. It is not our objective to defend or dispute such a radical viewpoint here, but the formation and accumulation of a vast variety of organic materials (see, e.g. Garrod et al. 2008) on the dust grains does make the idea about the existence of biotic material in the interstellar space not too far-fetched.

3.2 Why do we study grain chemistry

The reason grain chemistry was introduced to astrochemical study may be two-folds. First, certain species that are observed to be abundant cannot be accounted for by gas phase chemistry. The most important species of this kind is molecular hydrogen (H_2). Simple addition of two gas-phase H atoms does not work because the excess energy cannot be released through radiation efficiently since the H−H system has zero dipole moment; the H−H system can indeed stabilize through electronic or vibrational transition, but as estimated by Duley & Williams (1984), the rates are too low, being about 10^{-31}–10^{-29} cm^3 s^{-1}. Another possible route is

$$\begin{aligned} \mathrm{H} + \mathrm{H}^+ &\longrightarrow \mathrm{H}_2^+ + \mathrm{Photon}, \\ \mathrm{H}_2^+ + \mathrm{H} &\longrightarrow \mathrm{H}_2 + \mathrm{H}^+. \end{aligned}$$

The H_2 formation rate from this route is about $10^{-18} n(\mathrm{H}) n(\mathrm{H}^+)$, hence it is too low. Yet another possibility is to form H_2 through the anion H^-,

$$\mathrm{H} + \mathrm{H}^- \longrightarrow \mathrm{H}_2 + \mathrm{E}\text{-},$$

with rate coefficient 1.3×10^{-9} cm^3 s^{-1}. This route requires a high H^- abundance, which may indeed be satisfied at a relatively high temperature (Duley & Williams 1984). In general, grain chemistry is the most efficient way to produce H_2.

Another molecule that cannot be efficiently produced in the gas phase is methanol (CH_3OH), which was proposed to form through (Bates 1983)

$$\mathrm{CH}_3^+ + \mathrm{H}_2\mathrm{O} \longrightarrow \mathrm{CH}_3\mathrm{OH}_2^+ + \mathrm{Photon},$$

followed by (Millar et al. 1988)

$$CH_3OH_2^+ + E^- \longrightarrow CH_3OH + H.$$

However, this latter dissociative recombination reaction has other branches, such as $CH_3 + OH + H$ and $CH_2 + H + H_2O$, which are measured to be dominant over the one producing CH_3OH (Geppert et al. 2006), hence the amount of CH_3OH that can be produced in the gas phase is very low, at most 10^{-11} relative to H_2 (Garrod et al. 2006), even lower than the typically detected abundance of 10^{-9} in cold regions (Friberg et al. 1988; Gómez et al. 2011), and much lower than 10^{-6} in warm regions (Menten et al. 1986). The inability of gas phase chemistry to reproduce the observed abundance of CH_3OH points to grain chemistry.

The reasons why dust grains can enhance the production of some molecules can be heuristically understood as follows: (i) They can act as a third body, absorbing excess energies of the intermediate reaction complex. (ii) They can alter the reaction barrier of certain reactions. (iii) They can prolong the time for two reactants to stay together, by confining them on the surface, or even in the same site on the surface.

Finally, we may argue that grain chemistry is important not just because it helps to solve some of the problems encountered in pure gas phase chemistry, but rather because we believe important processes are occurring on dust grain surfaces, which deserve to be studied. The observed grain mantle composition requires an explanation. Reactions between the mantle species, when they become mobile and reactive in the warm-up phase, may lead to the formation of molecules with much higher complexity, some of which are even prebiotic. However, only the fundamentals of grain chemistry will be discussed in this chapter.

3.3 Rates of processes in grain chemistry

At least four basic processes are encountered in grain chemistry. Namely, accretion[2] of gas phase species onto the grain surface, desorption of surface species from the grain surface, migration of surface species on the grain surface, and reaction between two species upon meeting. In the following the rates of these processes will be discussed.

3.3.1 Adsorption rates

Strictly speaking, the adsorption process is not a surface process, but rather an interaction between the surface and gas phase. When a gas phase molecule encounters a dust grain, it has a probability to be captured by the latter. Such a process is called adsorption. The particle being adsorbed is called an adsorbate, and the surface material is called an adsorbent. Adsorption is different from absorption, in that the word "adsorption" emphasizes the incoming particles are captured and stored on a surface, while in the latter process the incoming particles are dissolved into bulk material.

The theory of adsorption, pioneered by Langmuir (Langmuir 1918), is based on several assumptions (Moore 1972):

[2] We use the words "accretion" and "adsorption" interchangeably in this thesis. Also the words "evaporation" and "desorption" are equivalent for our purpose.

> (i) The surface contains a fixed number of adsorption sites. (ii) Each site can hold one and only one molecule, (iii) All the sites have a binding energy, which does not depend on the surface coverage. (iv) The molecule residing in one site does not affect molecules in other sites.

Furthermore, it was also assumed by Langmuir that, when a molecule attacks a surface site already occupied, it will be rejected, and the molecule in that site is not affected. This is called Langmuir rejection. However, this rejection mechanism will not be included in our model, since the interaction (in contrast to rejection) between the dust grain material and the incoming particles is essential for the grain chemistry.

Two types of adsorption are generally considered: chemisorption and physisorption. In chemisorption the adsorbate is attached to the adsorbent through covalent bonds, while in physisorption the adsorbate is attracted to the surface by the van der Waals force. The binding energy $E_{\rm bind}/k$ (k is the Boltzmann constant) due to chemisorption can be more than 10^4 K, which is much stronger than physisorption, whose binding energy is typically $\sim$1000 K. Some species can also form hydrogen bond with the surface, the strength of which is roughly $\lesssim$5000 K, stronger than physisorption but weaker than chemisorption.

The accretion rate for species X can be written as

$$k_{\rm acc}({\rm X}) = \eta n({\rm X}) v({\rm X}) \sigma, \tag{3.1}$$

where n(X) is the gas phase density of X, v(X) is its thermal velocity, η is the sticking coefficient, usually taken to be unity (or a fractional value of order unity), and σ is the cross section area of a dust grain. $k_{\rm acc}$(X) is the number of X particles that are accreted onto a single dust grain in unit time. Note that usually v(X) is taken to be the average velocity of a Maxwell distribution,

$$v({\rm X}) = \sqrt{\frac{8kT}{\pi m_{\rm X}}}, \tag{3.2}$$

and σ should be taken to be the cross section area πr^2, *not* the total surface area $4\pi r^2$, where r is the dust grain radius.

Numerically, we have

$$\begin{aligned} k_{\rm acc}({\rm X}) = {} & 1.44 \times 10^{-5}\ {\rm s}^{-1} \quad \left[\simeq 1.24\ {\rm day}^{-1} \simeq 454\ {\rm yr}^{-1}\right] \\ & \times \left(\frac{\eta}{1}\right) \left(\frac{n({\rm X})}{1\ {\rm cm}^{-3}}\right) \left(\frac{T}{10\ {\rm K}}\right)^{1/2} \left(\frac{m_{\rm H}}{m_{\rm X}}\right)^{1/2} \left(\frac{r}{0.1\ \mu{\rm m}}\right)^2 . \end{aligned} \tag{3.3}$$

Thus we see that for the typical physical parameters written in the parentheses, approximately one X particle is adsorbed onto a dust grain per day.

The decreasing rate of the gas phase density of species X is

$$\partial_t n({\rm X}) = -k_{\rm acc}({\rm X})/V \tag{3.4}$$

where V is the average gas phase volume containing a single dust grain:

$$V = \frac{1}{n_{\rm H} R_{\rm G,n}}, \tag{3.5}$$

where $n_{\rm H}$ is the total number density of hydrogen nuclei, which is essentially $2n({\rm H}_2)$ since most of the hydrogen nuclei are in molecular form; $R_{\rm G,n}$ is the dust-to-gas number ratio, which can be calculated from the dust-to-gas mass ratio:

$$R_{\rm G,n} = R_{\rm G,m} \frac{m_{\rm p}\mu_{\rm mol}}{\frac{4\pi}{3} r^3 \rho_{\rm G}}, \tag{3.6}$$

where $R_{\rm G,m}$ is the dust-to-grain mass ratio, usually taken to be 0.01; $m_{\rm p}$ is the proton mass, and $\mu_{\rm mol}$ is the mean molecular weight of the interstellar gas, usually taken to be 1.4. $\rho_{\rm G}$ is the mass density of the dust material, usually taken to be 2–3 g cm^{-1}.

Hence we have

$$\begin{aligned} \partial_t n({\rm X}) &= -n({\rm X}) \times \eta n_{\rm H} v({\rm X}) R_{\rm G,m} \frac{m_{\rm p}\mu_{\rm mol}}{\frac{4r}{3}\rho_{\rm G}} \\ &\simeq -n({\rm X}) \times 1.3 \times 10^{-4}\ {\rm yr}^{-1} \\ &\quad \times \left(\frac{\eta}{1}\right) \left(\frac{n_{\rm H}}{10^5\ {\rm cm}^{-3}}\right) \left(\frac{T}{10\ {\rm K}}\right)^{1/2} \left(\frac{m_{\rm H}}{m_{\rm X}}\right)^{1/2} \\ &\quad \left(\frac{0.1\ \mu{\rm m}}{r}\right) \left(\frac{R_{\rm G,m}}{0.01}\right) \left(\frac{2\ {\rm g\ cm}^{-3}}{\rho_{\rm G}}\right). \end{aligned} \tag{3.7}$$

So the time scale for depleting the gas phase molecules is of the order 10^4–10^5 yr for typical dark cloud densities. This may be compared with the free-fall time scale of a uniform cloud,

$$t_{\rm ff} = \left(\frac{3\pi}{32 G\rho}\right) \simeq 10^5\ {\rm yr} \left(\frac{n_{\rm H}}{10^5\ {\rm cm}^{-3}}\right)^{-1/2}, \tag{3.8}$$

where ρ is the cloud mass density. Hence for molecules such as CO, when the gas density is higher than $\sim 10^5$ cm^{-3}, the depletion time scale will be shorter than the free-fall time scale, and a shortage of gaseous CO should be observable (see, e.g., Kramer et al. 1999; Bacmann et al. 2002; Caselli et al. 1999).

3.3.2 Evaporation rates

The thermal evaporation rate of species X is simply

$$k_{\rm eva}({\rm X}) = \nu_{\rm X} \exp\left[-E_{\rm bind}({\rm X})/T\right], \tag{3.9}$$

where $\nu_{\rm X}$ is a frequency characteristic of the vibrational motion of the species in a direction perpendicular to the dust surface. Usually it is taken to be the same as the characteristic frequency in the plane of the surface, and calculated through the following formula (Hasegawa et al. 1992)

$$\begin{aligned} \nu_{\rm X} =& (2\rho_{\rm S} E_{\rm bind}/\pi^2 m_{\rm X})^{1/2} \\ =& 2.4 \times 10^{12}\ {\rm Hz} \left(\frac{\rho_{\rm S}}{10^{15}\ {\rm cm}^{-2}}\right)^{1/2} \left(\frac{E_{\rm bind}}{350\ {\rm K}}\right)^{1/2} \left(\frac{m_{\rm X}}{m_{\rm H}}\right)^{-1/2}, \end{aligned} \tag{3.10}$$

where $\rho_{\rm S}$ is the number density of surface sites, typically taken to be around 10^{15} cm^{-2}. It is not clear which is the original source for the above formula. It seems to be related

to the Debye frequency[3] of a crystal, and resembles the frequency characteristic for the collision within a repulsive potential as shown in equation (11) of Hollenbach & Salpeter (1970).

The binding energy $E_{\rm bind}$ depends on the type of the bond between the adsorbate and adsorbent, and is usually taken to be ∼400 K for species such as H, D, HD, H_2, ∼800 K for C, N, O atoms, ∼1200 K for CO, O_2, and CH_4, and to be of a much higher value ∼5000 K for H_2O and CH_3OH on water ice. These values are all based on the assumption that these species are physisorbed or confined by hydrogen bonds, not by chemical bond.

Each species has a zero-point vibrational energy, which should in principle be added to the (negative) potential barrier. A higher zero-point energy makes it easier for a species to evaporate. Different species have different zero-point energies, which can be a source of the differences in their evaporation rates. But such an effect is of secondary importance, given that the binding energies of most species are poorly constrained experimentally. However, in Chapter 6 we consider this effect for the atomic and molecular hydrogen isotopologues (H, D, H_2, HD, and D_2).

Cosmic-ray desorption of surface species

Under dark cloud conditions, photo-desorption can be neglected because UV radiation is heavily attenuated. But cosmic-rays can still penetrate deep into the cloud and may contribute to the desorption of surface species. Hasegawa & Herbst (1993a) assumed that each time a cosmic-ray particle hits a dust grain, the temperature of the grain immediately rises to 70 K[4], and cools down in a short time by evaporating the dominant mantle species (CO for example). Thus the contribution of cosmic-rays to the desorption rate is

$$k_{\rm eva,cosmic}({\rm X}) = \zeta(70\ {\rm K}) \cdot \nu_{\rm X} \exp\left[-E_{\rm bind}({\rm X})/(70\ {\rm K})\right], \tag{3.11}$$

where ζ(70 K) is the "duty cycle" fraction of the cosmic rays, which is the ratio between the time for the dust grain to stay at around 70 K after being hit by a cosmic-ray particle, and the time interval between two successive cosmic-ray collisions (∼10^6 yr). Hasegawa & Herbst (1993a) estimated the time for a dust grain to stay at around 70 K to be the evaporation time of CO ice at such a temperature, which can be calculated to be $1/\left[(10^{12}\ {\rm s}^{-1})\exp(-1210/70)\right] \simeq 3.2\times10^{-5}$ s, where 1210 (K) is the binding energy of CO. Hence $\zeta(70\ {\rm K}) \simeq 10^{-18}$. The value used by Hasegawa & Herbst (1993a) is 3.16×10^{-19}.

Hence, in the case of CO, the evaporation rate due to cosmic-rays is roughly

$$k_{\rm eva,cosmic}({\rm CO}) = 3\times10^{-14}\ {\rm s}^{-1} = 10^{-6}\ {\rm yr}^{-1}. \tag{3.12}$$

This means the time scale of cosmic-ray desorption is 10^6 yr. But we have to note that the derivation of this number involves quite some uncertainties. For example, in such a

[3] The Debye frequency is

$$\nu_{\rm Debye} = v_{\rm s}\left(\frac{3\rho_{\rm n}}{4\pi}\right)^{1/3},$$

where $v_{\rm s}$ is the sound speed of the crystal, and $\rho_{\rm n}$ is the crystal number volume density.

[4] They assume that a relativistic Fe nucleus with energy in the range 20–70 MeV deposits 0.4 MeV to each dust grain. Then the temperature of the mantle will rise by an amount that can be estimated to be ∼46 K $\left(\frac{10^8}{N_{\rm m}}\right)$, where $N_{\rm m}$ is the number of mantle species that are promptly heated by the cosmic-ray particle. The number 10^8 corresponds to 100 mantle layers, each layer containing 10^6 particles. This may be an overestimate of the number of layers affected by the cosmic-ray particle.

treatment the effect of each cosmic-ray particle, which takes action for a very brief time ($\sim 10^{-5}$ s^{-1}) only, is smoothed out over a time scale as long as 10^6 yr. This seems to be inequivalent to a scenario in which dust particles are striped off the ice mantle (assuming that a cosmic-ray particle can destroy the whole mantle) randomly (namely, treated as a Poisson process with average time interval $\sim 10^6$ yr), episodically driving the newly-made ice mantle species into the gas phase and enriching the gas phase chemistry.

Equilibrium between adsorption and evaporation when Langmuir rejection is included

Although we will not consider Langmuir rejection in our modeling, this process has one simple but interesting application in astrochemistry that will be described below.

Consider a very simple system with only a single species that can be adsorbed onto a surface and can evaporate from it, with rate coefficients $k_{\rm acc}$ and $k_{\rm eva}$, respectively. Denote its surface coverage by θ (the fraction of surface area that is covered by the species being considered), and assume no surface recombination reaction. We have

$$\partial_t \theta = k_{\rm acc}(1-\theta) - k_{\rm eva}\theta, \tag{3.13}$$

where the $(1-\theta)$ term accounts for the Langmuir rejection. For the steady state, we get the so-called Langmuir isotherm

$$\theta = \frac{k_{\rm acc}}{k_{\rm eva}+k_{\rm acc}}. \tag{3.14}$$

Now inserting the expression for $k_{\rm eva}$ (Eq. (3.9)) yields

$$\theta = \frac{1}{1+k_{\rm eva}/k_{\rm acc}} = \frac{1}{1+\nu/k_{\rm acc}e^{-E_{\rm bind}/T}}, \tag{3.15}$$

which mimics the Fermi-Dirac distribution in quantum statistics, where the average occupation number of a non-degenerate state is written as

$$\frac{1}{1+e^{(E-\mu)/T}}, \tag{3.16}$$

where μ is the chemical potential. Note that the potential energy of a molecule confined to the surface should be considered as negative when making the analogy. We also see that the chemical potential $\mu = -T\ln[\nu/k_{\rm acc}]$.

Is this resemblance merely a coincidence? Maybe not. The Langmuir rejection principle explicitly requires that each surface site can accommodate at most one molecule at each time. This is similar to the Pauli exclusion principle, saying that identical fermions cannot be in the same quantum state at the same time, which is fundamental to the Fermi-Dirac distribution. The surface coverage θ can be interpreted as the probability that a randomly-picked surface site is occupied, which closely resembles the probability that a single quantum state is occupied in the Fermi-Dirac statistics. The Pauli exclusion principle is a very deep result of theoretical physics, which seems to have no intuitive explanation, while the Langmuir rejection mechanism is understandable by practically everyone, nevertheless the two have a very similar mathematical form when applied to statistics.

Amiaud et al. (2006) and Kristensen et al. (2011) have used such a formulation in studying the surface binding of H_2 and its isotopologues. They assume the binding energy of different surface sites can take different values, described by a power-law distribution of the form $(E_0 - E_{\rm bind})^b$. For each site, they assume the probability that it is occupied takes the form of Eq. (3.16). At first sight it may be surprising that quantum statistics is involved in this apparently "classical" problem (meaning that the adsorption and desorption processes can be understood easily in a classical picture; whereas calculating the rates require quantum mechanics; see Section 3.3.3.), but as discussed before, this merely reflects the fact that the Langmuir rejection mechanism is being incorporated.

3.3.3 Surface migration rates

In principle, because of the low temperature and small scales involved, the surface migration of a molecule should be studied using quantum random walk theory. Hollenbach & Salpeter (1970) used a model based on the spreading-out of wave packet on a zero-temperature perfect lattice surface to derive that the time scale for a particle to diffuse n steps away is nt_0, where $t_0 \simeq 4\hbar/\Delta E_{\rm bind}$, $\Delta E_{\rm bind}$ being the width of the ground energy band. However, that the particle diffuses n steps away does not necessarily mean that it has covered a surface area of the order n^2. How does this result make itself into the reaction rate equation is not clear.

The problem with quantum random walk is that dust grain surfaces cannot be expected to be of perfect crystalline configuration; rather they should be quite amorphous or fractal. The surface imperfections make the quantum wave function incoherent, and the migration of a particle should behave classically.

In classical random walk theory, a theorem in Dvoretzky & Erdős (1951) claims that the average number of different points visited by a particle during n steps in a two-dimensional random walk is $N \simeq \pi n/\ln n$, from which we get $n \sim N \ln N/\pi$, which approximates the average number of steps required to cover N different points. Note that the lattice structure is square. A different configuration may lead to a different numeric factor (Montroll 1969).

However, rigorously speaking, the question about the number of steps needed to cover a given finite region with N points is not exactly the inverse problem of finding the number of different points visited in an infinite lattice after n steps. Nemirovsky et al. (1990) gave semi-empirical formulae for the number of jumps required to cover a D-dimensional torus, and in the 2-D case it is $\sim 0.33N\,(\ln N)^2$, while for 3-D or higher dimensions it is $AN\ln N$, where A is a constant of order one.

Thus the time needed to cover the whole surface containing $N_{\rm S}$ sites is of the order $N_{\rm S}\ln^2(N_{\rm S})t_0/3$. The time interval t_0 between successive steps can be determined either classically or quantum-mechanically.

It might be meaningful to consider the fact that interstellar dust grains are likely fractal in nature, which is determined by the slow growth process by accretion (although heating of the dust grains may restructure and crystallize them.). Rammal (1984) summarized some results regarding random walk on fractal structure, and it seems no radical modifications have to be made to our usual understanding in the 2-dimensional case. Furthermore, the dust grain surface in reality is not only fractal in shape, the physical properties of the binding sites can also vary from one to another, which may have a larger

impact on chemistry than the morphology.

Thermal hopping rate and quantum tunneling rate

Classically, the time needed to jump to a neighboring site is

$$t_{0,\mathrm{C}} = \nu^{-1} \exp(E_{\mathrm{diff}}/T), \tag{3.17}$$

where E_{diff} is the barrier against surface migration, usually taken to be a fixed fraction (0.3–0.8) of E_{bind}, and ν is the characteristic frequency, which is usually fixed to a value of the order 10^{12} s^{-1} or calculated with Eq. (3.10). We can interpret ν^{-1} as the time scale for a particle with kinetic energy E_{bind} to travel a distance $1/\sqrt{\rho_{\mathrm{S}}}$, where ρ_{S} is the number of surface sites per unit surface area.

For the quantum-mechanical version of t_0, there are several different formulae. One is the t_0 parameter in Hollenbach & Salpeter (1970) as already mentioned before,

$$t_{0,1} = 4\hbar/\Delta E_{\mathrm{bind}} = 3 \times 10^{-12} \text{ s } \left(\frac{10 \text{ K}}{\Delta E_{\mathrm{bind}}}\right). \tag{3.18}$$

According to Hollenbach & Salpeter (1970), ΔE_{bind}=5 K for H_2 molecules on H_2O ice, and 20 K for H atoms on H_2O ice. Another quantum tunneling time scale is (Hasegawa et al. 1992)

$$\begin{aligned} t_{0,2} =& \nu^{-1} \exp[\frac{2a}{\hbar}\sqrt{2mE_{\mathrm{diff}}}] \\ =& \nu^{-1} \exp\left[4\left(\frac{a}{1 \text{ Å}}\right)\left(\frac{m}{m_{\mathrm{H}}}\right)^{1/2}\left(\frac{E_{\mathrm{diff}}}{100 \text{ K}}\right)^{1/2}\right], \end{aligned} \tag{3.19}$$

with no temperature dependence. This form is derived from the WKB (Wentzel-Kramers-Brillouin) approximation (Gould & Salpeter 1963; Watson 1976). A third form is (Le Petit et al. 2009)

$$\begin{aligned} t_{0,3} =& \nu^{-1}\left[1 + \frac{E_{\mathrm{diff}}^2}{4E(E_{\mathrm{diff}} - E)}\sinh^2(a/\lambda_{\mathrm{DB}})\right] \\ \simeq& \nu^{-1}\left[1 + \frac{E_{\mathrm{diff}}}{16E}\exp(2a/\lambda_{\mathrm{DB}})\right], \end{aligned} \tag{3.20}$$

where in the last step it is assumed that $E \ll E_{\mathrm{diff}}$ and $a \gtrsim \lambda_{\mathrm{DB}}$, with E being the kinetic energy of the tunneling particle and a being the barrier width. The de Broglie wavelength λ_{DB} is

$$\lambda_{\mathrm{DB}} = \hbar/\sqrt{2m(E_{\mathrm{diff}} - E)} \simeq 0.5 \text{ Å } \left(\frac{m_{\mathrm{H}}}{m}\right)^{1/2}\left(\frac{100 \text{ K}}{E_{\mathrm{diff}}}\right)^{1/2}, \tag{3.21}$$

where it has been assumed that $E \ll E_{\mathrm{diff}}$. The term in the bracket of equation (3.20) is the inverse of the transmission coefficient of a particle with total energy E across a rectangular potential barrier E_{diff} ($E_{\mathrm{diff}} > E$) with width a (Eisberg 1961). A fourth form[5] is due to

[5] This form was cited by Dash to be also from the quantum-mechanical treatment of a particle crossing a rectangular barrier, just as the form of $t_{0,3}$. The author referred to pages 94, 95 of Schiff (1949). However, pages 94, 95 of Schiff (1949) apparently do not lead to the form of $t_{0,4}$. On the other hand, $t_{0,3}$ is a consequence of equation (17.7) on page 95 of Schiff (1949).

Dash (1968)

$$\begin{aligned} t_{0,4} =& \frac{\tau_0}{2} \exp\left[\frac{a}{\hbar}\sqrt{2m(E_{\rm diff}-E)}\right] \\ \simeq& 1.3\times10^{-10}\ {\rm s}\ \left(\frac{m}{m_{\rm H}}\right)\left(\frac{a}{1\ {\rm \AA}}\right)^2 \exp\left[a/\lambda_{\rm DB}\right], \end{aligned} \tag{3.22}$$

where $\tau_0 \simeq ma^2/h$. Dash (1968) also gives the criteria for tunneling to be important, namely, the temperature should be below $\sim\hbar/(kt_{0,4})$.

Equation (3.19) is not a special form of (3.20), and in general the two gives different results, but the difference should not be much more than one order of magnitude. For $t_{0,1}$–$t_{0,4}$, roughly we may have

$$t_{0,1} \lesssim t_{0,2} \sim t_{0,3} \lesssim t_{0,4}. \tag{3.23}$$

In literature most frequently the form of $t_{0,2}$ (equation 3.19) is used for quantum tunneling. For a given $E_{\rm diff}$, the temperature at which $t_{0,\rm C}$=$t_{0,2}$ is

$$T_0 = \frac{\hbar}{2a}\left(\frac{E_{\rm diff}}{2m}\right)^{1/2} = 24.6\ ({\rm K})\ \left(\frac{1\ {\rm \AA}}{a}\right)\left(\frac{E_{\rm diff}}{100\ {\rm K}}\right)^{1/2}\left(\frac{m_{\rm H}}{m}\right)^{1/2}. \tag{3.24}$$

Below this temperature, the quantum tunneling rate is dominant over the thermal hopping rate. However, if the criterion of Dash (1968) is used, then quantum tunneling is unimportant at any practical temperature of astrochemistry.

The surface migration rate of species X is defined to be the rate at which an X jumps from one surface site to another, hence

$$k_{\rm mig,X} = 1/t_0, \tag{3.25}$$

where the time interval t_0 between successive jumps can be calculated with the thermal hopping time scale $t_{0,\rm C}$ or each of the quantum tunneling time scales $t_{0,1}$–$t_{0,4}$. We take either $t_{0,\rm C}$ or $t_{0,2}$, depending on which one leads to a higher $k_{\rm mig,X}$.

3.3.4 Two-body reaction rates on the surface

For a surface reaction $\rm A + B \longrightarrow C + D + \cdots$, the rate at which A is consumed is

$$\partial_t N({\rm A}) = -(k_{\rm mig,A} + k_{\rm mig,B}) p_{\rm A,B} \frac{N({\rm A})N({\rm B})}{N_{\rm S}}, \tag{3.26}$$

where N(A) is the number of species A on the surface of a dust grain, and $p_{\rm A,B}$ is the probability for A and B to cross over the reaction barrier upon meeting at the same site; it also accounts for the fact that the reaction may have several exit channels. The migration rates $k_{\rm mig,A}$ and $k_{\rm mig,B}$ controls how frequently the two reactants meet each other. $N_{\rm S}$ is the number of surface sites, $N_{\rm S}$=$\rho_{\rm S}\times\sigma$, where σ is the surface area of a dust grain, and $\rho_{\rm S}$ is the density of surface sites (see Eq. (3.10) on page 32). $N({\rm B})/N_{\rm S}$ is the probability for a randomly chosen site to contain a B molecule in it.

The reaction probability $p_{\rm A,B}$ can be determined either by the thermal rate using the Boltzmann formula, or by the quantum tunneling efficiency

$$p_{\rm tun} = \exp\left[-\frac{2a}{\hbar}\sqrt{2m_{\rm tun}E_{\rm a}}\right], \tag{3.27}$$

which is similar to Eq. (3.19), except that the factor before the exponential function is dropped. The barrier width a, tunneling mass $m_{\rm tun}$, and the activation barrier $E_{\rm a}$ are specific to each reaction.

In the quantum tunneling case $p_{\rm A,B}$ does not depend on the temperature. Thus if one can get the $p_{\rm A,B}$ parameter for a specific temperature, it can be applied to other temperatures within a certain range. In the case of thermal crossing-over, $p_{\rm A,B}$ does have a temperature dependence, but it does not depend on the barrier width, thus only one parameter is needed, namely, the barrier height, which is obtainable from theoretical calculation. In summary, for calculating the rate of a surface two-body reaction, all we need are: (1) The surface migration rate of A and B; (2) the branching ratios for the exit channels; (3) the barrier height and width.

Garrod & Pauly (2011) and Chang et al. (2007) enhanced the reaction rates by replacing Eq. (3.26) with

$$\partial_t N({\rm A}) = -(k_{\rm mig,A} + k_{\rm mig,B}) \frac{\nu p_{\rm A,B}}{\nu p_{\rm A,B} + k_{\rm mig,A} + k_{\rm mig,B}} \frac{N({\rm A}) N({\rm B})}{N_{\rm S}}, \tag{3.28}$$

based on the competition between reaction and migration of surface species, where ν is the vibrational frequency of either A or B. The idea behind the above expression is that the two reactants of a reaction mediated by a barrier—even if they do not react immediately—can stay in the same surface site for a long time, hence can make many reaction attempts before they depart through migration. We may also understand this by imaging that an intermediate complex AB* is formed when A and B meet. AB* may proceed to the product channel to yield C + D + $\cdots$, or it may be destructed due to the migration (or evaporation, which is less important here) of A or B. The steady-state solution to the corresponding rate equations will give Eq. (3.28). We note that the validity of such a formalism really depends on the microscopic picture of how surface reaction proceeds, and choose not to include it at the moment.

3.4 Mathematical framework for surface chemistry

3.4.1 Why the rate equation may fail for surface chemistry

In the previous section we have discussed various chemical processes of surface chemistry. In the present section a general mathematical framework describing the kinetics of grain chemistry will be developed.

Why does grain chemistry need a special mathematical framework? Why not use the same rate equation approach as gas phase chemistry? There can be two reasons, and the framework described in the following copes with only one of them.

The first reason for the possible failure of the rate equation approach is related to the smallness of interstellar dust grains. For a small grain size, the number of reactants of a specific reaction on the surface at any time can be very small—if averaged over time (or over an ensemble of grains), this number can be much smaller than one, which means most of the time no reactants are present on the surface. The smallness itself does not cause a problem; however, it causes the chemical reactions to have strong correlations between under-abundant species. This invalidates the rate equation, because the latter is based on the assumption that the concentrations of the reactants are uncorrelated.

Take the formation of H_2 molecules as an example (see also Appendix A). As discussed in Section 3.3.1–3.3.3, roughly one hydrogen atom hits a dust grain per day, which can walk through all the surface sites in ∼0.001 second, and may evaporate within about 10 minutes. Thus if there is no reaction partner on the grain, a newly adsorbed hydrogen atom will be evaporated. This gives an average abundance of (10 min)/(1 day)=0.007 for surface hydrogen atoms. But if one hydrogen atom is already on the surface, and before its desorption another hydrogen atom arrives, then they will most likely recombine to form a H_2 molecule (the reaction $H + H \longrightarrow H_2$ is barrierless hence the reaction efficiency is 100%). What is the formation rate of H_2? The rate equation would give[6]

$$R_{\rm RE}(H_2) = 0.007^2/(0.001\ {\rm s}) = 0.05\ {\rm s}^{-1}.$$

However, since approximately one hydrogen atom arrives on the grain each day, and the probability that another hydrogen atom is waiting there is 0.007, the formation rate of H_2 should be[7]

$$R(H_2) = 0.007/(1\ {\rm day}) = 8{\times}10^{-8}\ {\rm s}^{-1}.$$

It is much smaller than the evaporation rate $0.007/(10\ {\rm min}){\simeq}10^{-5}\ {\rm s}^{-1}$. Hence we have seen that the rate equation severely over-predicts the H_2 formation rate.

How could the rate equation result be so far-off? When considering two body reactions such as $H + H \longrightarrow H_2$, the important quantity is the probability that two reactants are present at the same time; denote this probability by $p(HH)$. If there is no such two-body reaction, then it is utterly true that $p(HH) = p(H)^2$. However, since two hydrogen atoms recombine very quickly when they are on a dust grain at the same time, the actual time they both stay on the grain before reaction is the time scale for migrating the full surface, namely, ∼0.001 s. Hence the formation rate of H_2 can also be calculated as

$$R'(H_2) = \frac{1}{0.001\ {\rm s}} \times 0.007^2 \times \frac{0.001\ {\rm s}}{10\ {\rm min}} = 8 \times 10^{-8}\ {\rm s}^{-1}.$$

The factor $\frac{0.001\ {\rm s}}{10\ {\rm min}}$ accounts for the reduction in the time a hydrogen atom can stay on the surface due to the two-body reaction. Thus it is clear that the joint probability $p(HH)$ is reduced from the value $p(H)^2$ by the two-body reaction, which significantly reduces the time that the two reactants can stay together.

Using the rate equation for the under-abundant species not only affects the species that are directly involved (H and H_2 in the present case), in a chemical network the abundances of other species can also be affected. To see why, we still take the $H + H \longrightarrow H_2$ reaction as an example. Assuming the incoming flux of H atoms is constant, then, as estimated before, the correct average number of H atoms on a dust grain is $N_{\rm corr}(H) \simeq 0.007$. With the rate equation, we have the following equation for the evolution rate of this average number

$$\partial_t N({\rm H}) = \frac{1}{1\ {\rm day}} - \frac{1}{10\ {\rm min}} N({\rm H}) - 2\frac{1}{0.001\ {\rm sec}} N({\rm H})^2. \tag{3.29}$$

A quasi-steady state can quickly be established, so by letting $\partial_t N(H_2){=}0$ we get $N_{\rm RE}(H) \simeq 8{\times}10^{-5}$, which is much smaller than the correct value. This is because by overestimating

[6] Note that this calculation is not consistent with itself, since with such a high consumption rate of H by recombination, the average H population based merely on evaporation is not valid anymore. See the discussion around Eq. (3.29).

[7] This type of argument is one basis of the modified rate equation of Garrod (2008); see Chapter 4.

the production rate of H_2, the rate equation converts H into H_2 quicker than it should. The conversion rate in the rate equation is $\left(8\times10^{-5}\right)^2/0.001\simeq6\times10^{-6}$ s^{-1}, much larger than the evaporation rate $8\times10^{-5}/(10\text{ min})\simeq10^{-7}$ s^{-1}, which is opposite to the correct result. The aftermath is, less H atoms will be available for other hydrogenation reactions, thus affecting the behavior of other parts of the chemical system.

The second reason for the rate equation approach to not describe the surface processes correctly is that structures may form on the grain surface. Different species on the grain can form an onion-like mantle structure, or islands where certain species are concentrated. The rate equation is based on the uniform distribution of species on the dust grain, so such small-scale structures are smoothed out. But these structures may affect the chemistry since they may alter the energy barriers of various processes. Astrochemical models aimed at addressing this aspect (and the first aspect is in principle simultaneously solved in this approach) have been developed by, e.g., Chang et al. (2005) and Cuppen & Herbst (2007). The drawback of this class of models is the heavy computational burden involved, so that only a small chemical network can be simulated; the parameters about the structure and energetics of the grain ice mantle are usually not well constrained either.

The master equation prescription can solve the first problem met by the rate equation. It can be considered the "master" of the mathematical description of a stochastic system, since essentially all the quantities of practical interest, such as the average and standard deviation of a certain physical parameter, are derivable from it. The Monte Carlo simulation should also be based on it. The commonly-used rate equation can be viewed as an approximation to the master equation, in the limit where stochastic fluctuations are not important. In the next section I discuss the mathematical form and properties of the master equation.

3.4.2 The chemical master equation

A chemical system at a given time t can be described by a state vector $\mathbf{x}$ which is a function of time, with its jth component x_j being the number of the jth species in this system. As chemical reaction proceeds, $\mathbf{x}$ changes. Due to the intrinsic stochastic nature of chemical reactions at the microscopic scale, the way in which $\mathbf{x}$ evolves is subject to uncertainties, so $\mathbf{x}$ should be viewed as a random variable, even if at the initial instant $\mathbf{x}$ is known for sure. The probability distribution function for $\mathbf{x}$ is denoted by $P(\mathbf{x},t)$, which describes the probability to find the system in $\mathbf{x}$ at time t. The equation governing the evolution of $P(\mathbf{x},t)$ is called the master equation, which has the following form (Gillespie 2007)

$$\partial_t P(\mathbf{x},t)=\sum_{i=1}^{M}\left[a_i(\mathbf{x}-\nu_i)P(\mathbf{x}-\nu_i,t)-a_i(\mathbf{x})P(\mathbf{x},t)\right]. \tag{3.30}$$

Here $a_i(\mathbf{x})$ is called the propensity function, with $a_i(\mathbf{x})\Delta t$ being the probability that, given a current state vector $\mathbf{x}$, an ith reaction will happen in the next infinitesimal time interval $[t,\, t+\Delta t)$. ν_i is the stoichiometry vector of the ith reaction, namely, the jth component of ν_i is the number of the jth species being produced (a negative value means consumption) in the ith reaction. The sum is over all the reactions, and M is the total number of reactions.

Since the ith component of $\mathbf{x}$ records the number of the ith species in the system, x_i

must be an integer. Denote the set of state vectors reachable from all the possible initial states by Ω, and denote the collection of all the states reachable from a given initial state vector $\mathbf{x}_0$ by $\Omega(\mathbf{x}_0)$. We have $\Omega(\mathbf{x}_0)\subseteq\Omega$, and in general $\Omega(\mathbf{x}_0)\neq\Omega$. The evolution of the system can be viewed as a random walk in Ω according to certain rules defined by the chemical reactions. Ω is a finite and irregular subset of the n-dimensional space $\mathbb{N}^n$, where n is the number of species in the system, and $\mathbb{N}$ denotes the set of nonnegative numbers. Ω is finite simply because of the conservation of elements and that the number of an element in a chemical species cannot be negative; it is irregular because the state vector $\mathbf{x}$ reachable from $\mathbf{x}_0$ is determined by the set of chemical reactions, or more specifically, by the stoichiometry vector of the chemical reactions, which is irregular; not all the states allowed by conservation of elements are reachable by chemical reactions. $\Omega(\mathbf{x}_0)$ does not depend on time, since it is the states reachable "in principle", and not limited to any finite time interval.

Under the above specifications, the evolution of a chemical system can be viewed as a (continuous time) Markov chain, since which reaction will occur in the next infinitesimal time step only depends on the current status of the system, not (explicitly) on its past history. The transition probabilities do not depend on time if the physical conditions of the system are kept constant, in this case it is a time-homogeneous Markov chain. But in general the system is affected by external conditions (radiation and pressure), and it is not time-homogeneous.

The probability distribution function $P(\mathbf{x},t)$ itself can also be viewed as a time-dependent vector:

$$\mathbf{p}(t) = (p_{\mathbf{x}_1}, p_{\mathbf{x}_2}, \ldots)\,, \tag{3.31}$$

where $p_{\mathbf{x}} \equiv P(\mathbf{x},t)$. In this case, the subscript of the vector $\mathbf{p}$ is not a single integer anymore, but rather the state vector $\mathbf{x}$ themselves (although one may define a rule to label the states by a series of integers). Note that $\mathbf{p}$ is still a finite-dimensional vector, since the number of possible states of the chemical system (=the cardinality of Ω) is finite. The $\mathbf{x}$th component $p_{\mathbf{x}}$ is the probability for the system to be in state $\mathbf{x}$ (at time t), thus $0\leq p_{\mathbf{x}}\leq 1$, $\sum_{\mathbf{x}} p_{\mathbf{x}}=1$ must be satisfied at any time t. The master equation can be rewritten as

$$\partial_t p_{\mathbf{x}} = \sum_{i=1}^{M} \left[a_i(\mathbf{x}-\nu_i)p_{\mathbf{x}-\nu_i} - a_i(\mathbf{x})p_{\mathbf{x}}\right].$$

Or, in a more abstract matrix form,

$$\partial_t \mathbf{p} = \mathsf{T}\mathbf{p}. \tag{3.32}$$

Since $\partial_t p_i = \sum_j T_{ij}p_j$, T_{ij} is the transition probability from state j to state i when $i\neq j$. T_{ii} is the rate at which the probability of the system to be at state i decays, hence $T_{ii}\leq 0$. The merit of Eq. (3.32) is that it has an apparently simple form.

The matrix T does not seem to have a standard name (it is called $\mathbb{W}$-matrix in van Kampen 2007, page 101). It is related to the probability transition matrix (also called stochastic matrix). T is a finite, albeit very large matrix. It has several important properties (van Kampen 2007). For example, $T_{ij}\geq 0$ for $i\neq j$, because the transfer rate from state j to state i is never a negative number; and $\sum_i T_{ij}=0$ for each j, which simply says that the rate at which the probability for the system to be in state j decays equals the total transfer rate from state j to all others. This latter property tells that T has a

left eigenvector with eigenvalue 0: $\sum_i v_i T_{ij}=0$ for $v_i=(1,1,\ldots,1)$. Since eigenvalue does not distinguish between left or right, we conclude that T also has a right eigenvector with eigenvalue 0; namely, there exists a vector $\mathbf{u}$ such that $\sum_j T_{ij}u_j=0$. Using Eq. (3.32), we have $\partial_t \mathbf{u} = 0$, which means $\mathbf{u}$ is the steady-state distribution of the system[8].

The master equation is generally unsolvable analytically, or even numerically. But it is still tempting to see what the solution would look like if it were obtainable "in principle", given its deceptively simple form. The formal solution to the master equation is discussed in Appendix B.

3.4.3 Monte Carlo method

There is not a unique Monte Carlo method. It may be based on an intuitive physical picture of the microscopic processes, without a rigorous mathematical formulation, or, it can be based on the master equation. In the latter case, it can be viewed as a faithful "realization" of the master equation, and in this sense (and only in this sense) it is the most exact. In this section I only discuss the latter type. Application of the stochastic method to chemical study was pioneered by Gillespie (1976, 1977) (see also the review by Gillespie 2007). Recently Vasyunin et al. (2009) applied it to a big gas-grain network.

The name of the method to be discussed here is subject to debate. Some prefer to call it "stochastic simulation", as they think the Monte Carlo method is only a probabilistic approach to solve certain deterministic and difficult mathematical problems, such as multi-dimensional integrals, while "simulation" is to translate an intrinsically stochastic process into a set of operations in a computer (Kalos & Whitlock 2008), where random numbers are used to mimic the uncertainties in reality. One classic example for the application of Monte Carlo method (though not using a computer) is Buffon's needle experiment, which can be used to "measure" the value of π. As said in Kalos & Whitlock (2008), since an intrinsically random physical system can be described by a set of deterministic equations (e.g., the master equation for a chemical system, and the radiative transfer equation for a radiation problem), such a stochastic simulation of the system can also be viewed as a Monte Carlo approach to solve the set of equations. Hence we don't consider the nomenclature issue a big problem, and don't intentionally distinguish between the two names.

Besides being "exact" in the aforementioned sense, another big merit of the Monte Carlo method is that it is very easy to implement, and suffers no instability issues. The price to pay is that it is very slow (especially for a large system), because it has to follow every single event, which means in a chemical system the occurrence of every single reaction has to be recorded. As an extreme example, if the adsorption of H_2 molecule is allowed, then approximately for each second one H_2 will hit the grain (at a density of 10^5 cm^{-3}). Then if one is interested in an "astronomical" time scale of 10^6 yr, one has to follow $\sim 3\times 10^{13}$ H_2 adsorption events. For a typical desktop computer this can take $\sim$8 hr or more (depending on how much time is needed for each simulation step). Note that other processes have not been included. Apparently for an even higher density and longer time of interest the computation time needed will render this method impractical.

[8] Of course, to be a distribution function, each component of $\mathbf{u}$ has to be non-negative. It can be proved that all the components of the steady-state solution of Eq. (3.32) are either completely non-negative or non-positive. The steady-state solution is also unique. See page 104–107 of van Kampen (2007).

Basic ingredients of the Monte Carlo approach

First of all, we need to have a time-dependent state vector $\mathbf{x}(t)$, to record the population (i.e. number) of each species in a system, each component of which can only take non-negative integer values. Then we need a rule to update this vector. In Gillespie (2007), a quantity $p(\tau, j|\mathbf{x}, t)$ is introduced. $p(\tau, j|\mathbf{x}, t)\mathrm{d}\tau$ is the probability that the next reaction will occur in an infinitesimal time interval between $t+\tau$ and $t+\tau+\mathrm{d}\tau$ (thus no reaction occurs between t and $t+\tau$), and this reaction is the jth one of the reaction set.

To calculate $p(\tau, j|\mathbf{x}, t)\mathrm{d}\tau$, we need the master equation, which is rewritten below

$$\partial_t P(\mathbf{x}, t) = \sum_{i=1}^{M} \left[a_i(\mathbf{x} - \nu_i)P(\mathbf{x} - \nu_i, t) - a_i(\mathbf{x})P(\mathbf{x}, t)\right], \tag{3.30}$$

where the summation is over all the reactions. Since at each instant of the simulation the state of the system is known for sure, the probability distribution function $P(\mathbf{x}, t)$ takes the value 1 for $\mathbf{x}(t)$, and 0 for all the others. Thus the first term in the bracket of the above equation is zero, and we have

$$\partial_t P\left(\mathbf{x}(t), t\right) = -\left(\sum_{i=1}^{M} a_i(\mathbf{x}(t))\right) P(\mathbf{x}(t), t). \tag{3.33}$$

At time $t + \tau$, the probability that the system state is still $\mathbf{x}(t)$ is thus

$$\exp\left(-\alpha\tau\right). \tag{3.34}$$

where we have abbreviated $\sum_{i=1}^{M} a_i(\mathbf{x}(t))$ by α. By definition, the probability that the jth reaction occurs in a small time interval $\mathrm{d}\tau$ is $a_j(\mathbf{x})\mathrm{d}\tau$. So we get

$$p(\tau, j|\mathbf{x}, t) = a_j(\mathbf{x}) \exp\left(-\alpha\tau\right). \tag{3.35}$$

The probability that no reaction occurs between t and $t+\tau$ and exactly one reaction occurs in $t+\tau$ to $t+\tau+\mathrm{d}\tau$ is thus $\alpha \exp(-\alpha\tau)\mathrm{d}\tau$, which means τ is a random variable described by a exponential distribution with mean value $1/\alpha$. The probability that the reaction occurred in this short time interval is the jth reaction is $a_j(\mathbf{x})/\alpha$.

Now the simulation procedure is clear: given a state vector $\mathbf{x}$ at time t, we first calculate the propensity function $a_i(\mathbf{x})$ for all the reactions, from which we calculate their sum α. With this α a random number τ can be generated based on the distribution function $\alpha \exp(-\alpha\tau)$; now the system time will be updated to $t + \tau$; a reaction j will be selected to occur with a probability $a_j(\mathbf{x})/\alpha$; finally, the state vector is updated to a new value $\mathbf{x}(t+\tau)=\mathbf{x}(t)+\nu_j$, where ν_j is the stoichiometry vector of the selected jth reaction. These procedures are repeated until the system time has reached a certain value, or no reaction can happen anymore, which is possible when all the $a_i(\mathbf{x})$ are zero. A flowchart for the whole process is shown in Fig. (3.1).

The random number generators of common math libraries usually give numbers uniformly distributed in $[0, 1]$. To convert such a number y into a number obeying the exponential distribution

$$p(t)=\alpha e^{-\alpha t},$$

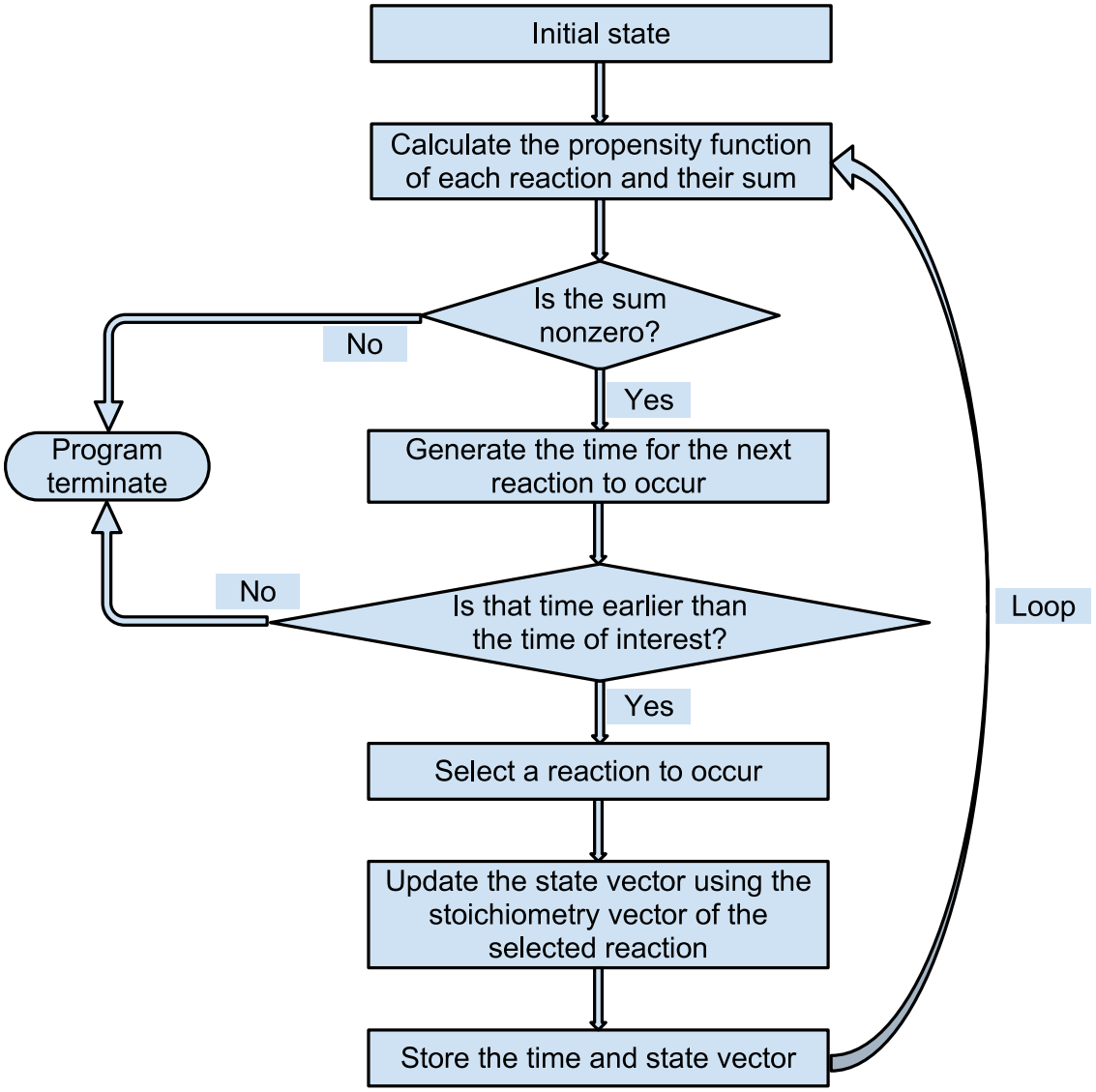

Figure 3.1: A flowchart for the Monte Carlo simulation of a chemical system.

simply letting $t = -\ln y/\alpha$ would suffice.

To select a reaction to occur, we generate another random number z from the uniform distribution on $[0, 1]$, then search for an integer j such that

$$\frac{1}{\alpha}\sum_{i=1}^{j-1} a_j \leq z, \text{ and } \frac{1}{\alpha}\sum_{i=1}^{j} a_j > z,$$

and the jth reaction is thus selected out. Note that the reactions do not have to be ordered in any sense. This is schematically shown in Fig. (3.2).

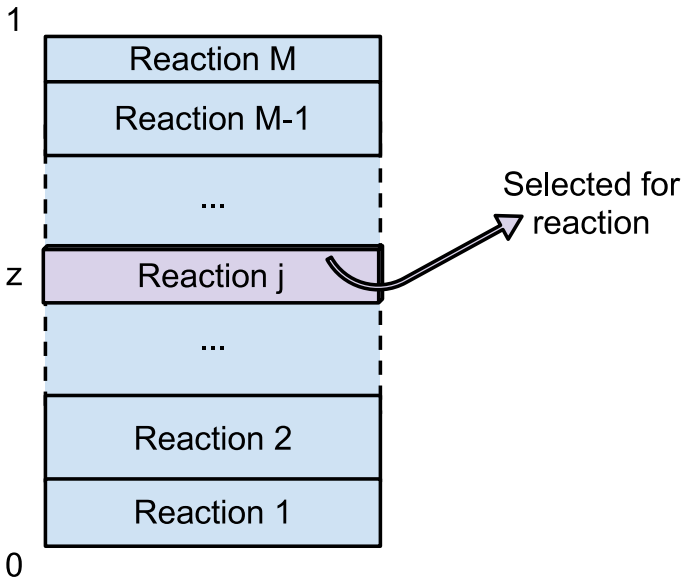

Figure 3.2: A schematic demonstration of how a reaction is selected to occur. z is a random number uniformly distributed in $[0, 1]$. The size of the block of each reaction represents its propensity (i.e. the tendency for a reaction to occur; can be simply understood as the rate of a reaction).

For a typical gas-grain chemical system, usually the number of steps required to reach a time of the order 10^6 yr can be $\sim 10^9$ or more[9]. It is not practical to store all the intermediate population data for all these steps, because a lot of disk space (hundreds of gigabytes) would be used. One possibility is to store one record every n steps, where $n > 1$. This way the stored population of each species take only integer values, and the increment in the population between two saved records may be high, since $n-1$ intermediate steps have been omitted; this will make the evolution curve appear noisy with large fluctuations. Furthermore, the computation used in these intermediate steps seems to be wasted, since

[9] Here the adsorption and desorption of H_2 is not considered. The number of steps is set by the number of reactions that occur in a time range, which is itself roughly set by the number of available reactants. The total abundance of the three elements, C, N, O, which are the constituents of most of the interesting species, is $\sim 5\times10^{-4}$ with respect to hydrogen nuclei. With a dust-to-gas number ratio of $\sim 2\times10^{-12}$, the total number of C, N, O elements in a volume containing one dust grain is $\sim 2\times10^{8}$, which basically determines the number of reaction events to reach the equilibrium state. Of course, the real situation is more complicated, since elements can be transferred back and forth, and species can break up and recombine.

their data are discarded. A better way of storing the data is to take the average population of n successive steps and store it; now the average population will not take integer value anymore. The time stamp associated with each average population should also be the average occurring time of these n steps. In this way the fluctuations can be greatly reduced, resulting a much smoother evolution curve.

Another issue with the Monte Carlo approach is that, to get the average behavior of a system, in principle many instances of simulations have to be carried out. The reason is the following. Let's assume the average population of a species (called A) is a constant, for example, 0.1. Then we may expect that if we look at the system at ten different time intervals, A will show up in one of them. However, it can also be that if we look at ten different realizations of the same system, A will always show up in one of them at any time, but never show up in all the others. This is the case in which a time-average is not equivalent to an ensemble average. The real situation may be a mixture of the two. It is not straightforward to determine whether a system has such a behavior before running the simulations.

In our work, the Monte Carlo approach is not used as a major tool, because it is too slow in the general case; rather it is utilized to set a benchmark (see Chapter 4), and the results of other methods should comply with it. So here I only show, in Fig. (3.3), a sample Monte Carlo calculation (ten realizations with identical condition) for the H_2 formation on dust grains, using typical parameters as discussed in Section 3.4.1. It can be seen that the surface population of H atoms and the production rate of H_2 agree quite well with the values estimated there.

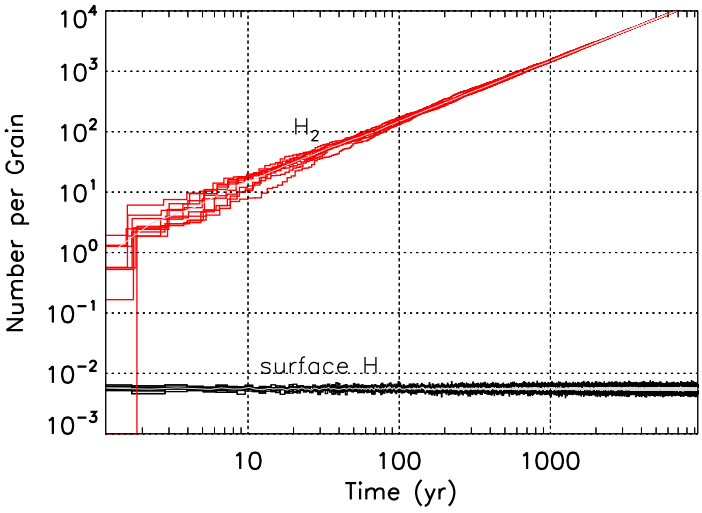

Figure 3.3: Monte Carlo simulation of the $H + H \longrightarrow H_2$ problem. Ten realizations are plotted.

Other methods have also been proposed to solve the gas-grain chemical problem, including one developed by us, which is the topic of the next chapter, where a brief review on those previous methods is also included.

Chapter 4

The hybrid moment equation (HME) approach

The content of this chapter is based on:
Du, F., & Parise, B. 2011, A&A, 530, A131+

Contents

In addition to gas phase reactions, the chemical processes on the surfaces of interstellar dust grains are important for the energy and material budget of the ISM. The stochasticity of these processes requires special care in modeling. Previously methods based on the modified rate equation, the master equation, the moment equation, and Monte Carlo simulations have been used.

In this chapter, a systematic and efficient way is developed to model the gas-grain chemistry with a large reaction network as accurately as possible. We name our method "hybrid moment equation approach". It is a general and automatic method where the generating function is used to generate the moment equations. For large reaction networks, the moment equation is cut off at the second order, and a switch scheme is used when the average population of certain species reaches 1. For small networks, the third order moments can also be utilized to achieve a higher accuracy.

For physical conditions in which the surface reactions are important, our method provides a major improvement over the rate equation approach, when both are benchmarked against the rigorous Monte Carlo results. For either very low or very high temperatures, or large grain radii, results from the rate equation are similar to those from our new

approach. Our method is faster than the Monte Carlo approach, but slower than the rate equation approach.

The hybrid moment equation approach with a cutoff and switch scheme is potentially a powerful way to solve gas-grain chemistry. It is applicable to medium-to-large gas-grain networks, and is demonstrated to have a degree of accuracy high enough to be used for astrochemistry studies. Further work should be done to investigate how to cut off the hybrid moment equation selectively to make the computation faster, more accurate, and more stable, how to make the switch to rate equation more mathematically sound, and how to make the errors controllable. The layered structure of the grain mantle could also be incorporated into this approach, although a full implementation of the grain microphysics appears to be difficult.

4.1 Introduction

The chemistry of the ISM can be roughly divided into two types: gas phase chemistry and grain surface chemistry. The two types of chemistry are coupled by the adsorption and desorption processes. Species adsorbed on the grain surface migrate in a random walk manner, and they may react with each other upon encounter at the same site (a local potential minimum). The products can be released back to the gas phase through certain desorption mechanisms. In addition to the gas phase chemistry, grain chemistry is important for the material and energy budget of the ISM. For example, besides H_2, molecules such as methanol are believed to be formed on the grain surfaces (Garrod et al. 2007), because its relatively high abundance (see, e.g., Menten et al. 1988) cannot be reproduced by gas phase chemistry.

Several methods have been used to model the gas-grain chemistry. In the rate equation (RE) approach (see, e.g., Hasegawa et al. 1992), the surface processes are treated the same way as the gas phase processes. This works fine when the number of reactants on a single grain is large (under the assumption that the system is well stirred; see Gillespie (2007)), but might not be accurate enough when the average populations[1] of some reactants on a single grain is small. This failure of the rate equation is related to the treatment of two-body reaction. For the REs to be applicable, the probability of one reactant being present should be independent of that of another being present. This is not always true, especially when the average populations of both reactants are low, in which case they might be highly correlated. The flaws in employing the RE for grain-surface chemistry were pointed out by Charnley et al. (1997) and Tielens & Charnley (1997).

To remedy this problem, modification schemes based on some empirical, heuristic, and/or physical reasoning have been applied to the RE approach (Caselli et al. 1998; Stantcheva et al. 2001), and are called modified rate equation (MRE) approach. The validity of this method has been questioned (Rae et al. 2003). A modification scheme developed by Garrod (2008) uses different functional forms for different surface populations, taking various competition processes and refinements into account. It has been shown to work very well, even for very large reaction networks (Garrod et al. 2009).

[1] Here by "population" we mean the number of a species in a volume of interest, and by "average" we mean an ensemble average (i.e. average over many different realizations of the same system setup). Hence "population" can only take non-negative integer values, while "average population" is a non-negative real number.

Mathematically, the gas-grain system should be viewed as a stochastic chemical system (see, e.g., McQuarrie 1967; Gillespie 1976; Charnley 1998), being described by a probability distribution $P(\mathbf{x}, t)$, which is the probability that the system has a population vector $\mathbf{x}$ at time t, with x_i being the number of the ith species in the system. The evolution equation of $P(\mathbf{x}, t)$ is the so-called master equation, whose form is determined by the reaction network.

Many sophisticated methods have been proposed (mainly outside the astro-chemical community; see, e.g., the operator method described in Mattis & Glasser (1998), or the variational approach used by Ohkubo (2008)) to solve the master equation. However, these methods work fine only when either the chemical network is small or some special assumptions are made in the derivation, thus their validity in the general case should be questioned. It is unclear whether these methods can be generalized to large complex networks.

The numerical solution of the master equation has also been performed (Biham et al. 2001; Stantcheva et al. 2002; Stantcheva & Herbst 2004). To limit the number of variables in the set of differential equations and to separate the deterministic and stochastic species, usually *a priori* knowledge of the system is required in these studies. The steady state solution of the master equation can also be obtained analytically in some very simple cases, such as the formation of H_2 molecules on the grain surface (Green et al. 2001; Biham & Lipshtat 2002).

On the other hand, the master equation prescription can be "realized" through a stochastic simulation algorithm (SSA), proposed by Gillespie (1976) (see also Gillespie (1977) and Gillespie (2007)). In this approach, the waiting time for the next reaction to occur, as well as which specific reaction will occur are random variables that are completely determined by the master equation, so this approach should be considered the most accurate. In principle, multiple runs are needed to average out the random fluctuations, but in practice this is unnecessary if one only cares about the abundant species. This approach has been applied successfully to astrochemical problems (Charnley 1998, 2001; Vasyunin et al. 2009), even in the case of very large networks (Vasyunin et al. 2009). Besides providing results that are accurate, this approach is very easy to implement. However, it requires a very long run time for large networks if a long evolution track is to be followed, although some approximate accelerated methods do exist (e.g. Gillespie 2000).

The SSA described above is somewhat different from a Monte Carlo (MC) approach which has also been applied to astrochemistry (e.g. Tielens & Hagen 1982); however, this approach is not rigorously consistent with the master equation (see the comment by Charnley 2005), and can lead to a reaction probability higher than 1 (Awad et al. 2005) in certain cases. The nomenclature of these two approaches is not always consistent in the astrochemical literature[2]. For example, the SSA used by Vasyunin et al. (2009) is called the Monte Carlo approach in their paper. Hereafter, we use the term "Monte Carlo" when referring to the rigorous stochastic simulation approach of Gillespie.

By taking various moments of the master equation, the so-called moment equation (ME) is obtained (Lipshtat & Biham 2003; Barzel & Biham 2007a,b). This set of equations describes the evolution of both the average population of each species and the average

[2]For a discussion about the relations and differences between "stochastic simulation" and "Monte Carlo", see Kalos & Whitlock (2008) and Ripley (2008).

value of the products of the population of a group of species, usually cut off at the second order moments. Its formulation is similar to that of the RE, so it is relatively easy to implement. Furthermore, in this approach the gas phase chemistry and grain surface chemistry can be coupled together naturally. It has been tested on small surface networks.

In the present paper, we propose yet another approach to modeling gas-grain chemistry, named the hybrid moment equation (HME) approach. The goal is to find a systematic, automatic, and fast way to modeling gas-grain chemistry as accurately as possible. Our method is based on the ME approach. Different approximations are applied to the MEs at different time depending on the overall populations at that specific time. It is hybrid in the sense that the RE and the ME are combined together. The basic modification and competition scheme presented in Garrod (2008) can be viewed as a semi-steady-state approximation to our approach (by assuming that the time derivatives of certain second order moments are equal to zero), while our approach can also be viewed as a combination of the ME approach of Barzel & Biham (2007a) and the RE. In our approach, the MEs are generated automatically with the generating function technique, and in principle MEs up to any order can be obtained this way. We benchmark our approach against the exact MC approach (i.e. the SSA of Gillespie).

The remaining part of this paper is organized as follows. In section 4.2, we review the chemical master equation and ME, then describe the main steps of the HME approach. In section 4.3, we benchmark the HME approach with a cutoff at the second order and the RE approach against the MC approach with a large gas-grain network; we also tested the HME approach with a cutoff at the third order with a small network. In section 4.4, we discuss the performance of the HME, and its relation with previous approaches, as well as possibilities for additional improvements. Our way of generating the MEs is described in Appendix 4.A. A surface chemical network we used for benchmark is listed in Appendix 4.B.

4.2 Description of the hybrid moment equation (HME) approach

In this section, we first review both the chemical master and moment equations. Although this content can be found in many other papers (e.g., Charnley 1998; Gillespie 2007), we present them here as they are the basis of our HME approach. We then describe the MEs and REs for a simple set of reactions as an example, to demonstrate how the HME approach naturally arise as a combination of ME and RE. Finally we show the main steps of the HME approach.

4.2.1 The chemical master equation and the moment equation (ME)

A chemical system at a given time t can be described by a state vector $\mathbf{x}$ which changes with time, with its jth component x_j being the number of the jth species in this system. As a chemical system is usually stochastic, $\mathbf{x}$ should be viewed as a random variable, whose probability distribution function $P(\mathbf{x}, t)$ evolves with time according to the master equation, which has been discussed in Chapter 3 (see Eq. (3.32)), and will be repeated

here:

$$\partial_t P(\mathbf{x},t) = \sum_{i=1}^{M} [a_i(\mathbf{x}-\nu_i)P(\mathbf{x}-\nu_i,t) - a_i(\mathbf{x})P(\mathbf{x})], \tag{4.1}$$

where $a_i(\mathbf{x})$ is called the propensity function, $a_i(\mathbf{x})\Delta t$ is the probability that given a current state vector $\mathbf{x}$ an ith reaction will happen in the next infinitesimal time interval Δt, and ν_i is the stoichiometry vector of the ith reaction. The sum is over all the reactions, and M is the total number of reactions.

The ME is derived by taking moments of the master equation. For example, for the *first order* moment $\langle x_j \rangle$, which is simply the average number of species j, $\langle x_j \rangle \equiv \sum_{\mathbf{x}} P(\mathbf{x},t)x_j$, its evolution is determined by (Gillespie 2007)

$$\begin{aligned}
\partial_t \langle x_j \rangle &= \sum_{\mathbf{x}} \partial_t [P(\mathbf{x},t)] x_j \\
&= \sum_{i}^{M} \sum_{\mathbf{x}} x_j [a_i(\mathbf{x}-\nu_i)P(\mathbf{x}-\nu_i,t) - a_i(\mathbf{x})P(\mathbf{x})] \\
&= \sum_{i}^{M} \sum_{\mathbf{x}} [(x_j+\nu_{ij})a_i(\mathbf{x})P(\mathbf{x},t) - x_j a_i(\mathbf{x})P(\mathbf{x})] \\
&= \sum_{i}^{M} \sum_{\mathbf{x}} \nu_{ij} a_i(\mathbf{x})P(\mathbf{x},t) = \sum_{i}^{M} \nu_{ij} \langle a_i(\mathbf{x}) \rangle,
\end{aligned} \tag{4.2}$$

where ν_{ij} is the jth component of the stoichiometry vector of the ith reaction, i.e. the number of jth species produced (negative when being consumed) by the ith reaction. For higher order moments, their corresponding evolution equations can be similarly derived, although the final form will be more complex. In Appendix 4.A, we present another method based on the generating function technique to derive the MEs, which is more suitable for programming.

For the simplest network, in which all the reactions are single-body reactions, $a_i(\mathbf{x})$ is a linear function of $\mathbf{x}$. In this case the ME is closed and can easily be solved. However, when two-body reactions are present, this is no longer true, as $\langle a_i(\mathbf{x}) \rangle$ might be of a form $\langle x_k(x_k-1) \rangle$ or $\langle x_k x_l \rangle$, which is of order two and cannot be determined in general by the lower order moments. Hence additional equations governing their evolution should be included, i.e., they should be taken to be independent variables. The evolution equation of these second order moments may also involve moments of order three, and this process continues without an end, thus the ME is actually an infinite set of coupled equations (although in principle they are not completely independent if the chemical system being considered is finite, which leads to a finite-dimensional space of state vectors). The equation cannot be solved without a compromise, e.g., a cutoff procedure, except for the simplest cases in which an analytical solution is obtainable in the steady state. Such a situation is common in many other fields which deals with objects with a certain degree of stochastic nature, and the problem is called a "moment closure" problem in general. Thus our work can be viewed as an option for moment closure.

4.2.2 The MEs and REs for a set of reactions

We take the following symbolic reactions as an illustrative example

$$\text{Adsorption:} \quad a \xrightarrow{k_{\text{ad}}} A, \tag{4.3}$$

$$\text{Evaporation:} \quad A \xrightarrow{k_{\text{evap}}} a, \tag{4.4}$$

$$\text{Surface reaction:} \quad A + B \xrightarrow{k_{\text{AB}}} C + D, \tag{4.5}$$

$$\text{Surface reaction:} \quad A + A \xrightarrow{k_{\text{AA}}} E, \tag{4.6}$$

where the ks are the reaction rates of each reaction, A – E are assumed to be surface species that are distinct from each other, and "a" is the gas phase counterpart of A.

In the following we first write down the MEs and REs for this system, then discuss the relations and differences between them, as well as the relation between a cutoff of MEs and a cutoff of master equations in previous studies. These discussions will be essential to developing our HME approach.

The MEs for this system

The propensity functions for the above four reactions are $k_{\text{ad}}a$, $k_{\text{evap}}A$, $k_{\text{AB}}AB$, and $k_{\text{AA}}A(A-1)$, respectively. Here for convenience we use the letter "A" to represent both the name of a species and the population of the corresponding species.

For the first order moments, we have

$$\partial_t\langle A\rangle = k_{\text{ad}}\langle a\rangle - k_{\text{evap}}\langle A\rangle - k_{\text{AB}}\langle AB\rangle - 2k_{\text{AA}}\langle A(A-1)\rangle, \tag{4.7}$$

$$\partial_t\langle C\rangle = k_{\text{AB}}\langle AB\rangle, \tag{4.8}$$

$$\partial_t\langle E\rangle = k_{\text{AA}}\langle A(A-1)\rangle. \tag{4.9}$$

Other similar equations are omitted. The symbol $\langle *\rangle$ is used to represent the average population of "*" in the system; the average should be understood as an ensemble average. The second order moments $\langle AB\rangle$ and $\langle A(A-1)\rangle$ have their own evolution equations, which are

$$\begin{aligned}\partial_t\langle AB\rangle =& k_{\text{ad}}\langle aB\rangle - k_{\text{evap}}\langle AB\rangle \\ &- k_{\text{AB}}[\langle A(A-1)B\rangle + \langle AB(B-1)\rangle + \langle AB\rangle] \\ &- 2k_{\text{AA}}\langle A(A-1)B\rangle,\end{aligned} \tag{4.10}$$

$$\begin{aligned}\partial_t\langle A(A-1)\rangle =& 2k_{\text{ad}}\langle aA\rangle - 2k_{\text{evap}}\langle A(A-1)\rangle \\ &- 2k_{\text{AB}}\langle A(A-1)B\rangle \\ &- 2k_{\text{AA}}[2\langle A(A-1)(A-2)\rangle + \langle A(A-1)\rangle].\end{aligned} \tag{4.11}$$

For this simple example set of reactions (equation (4.3 – 4.6)), the above equations can be easily obtained from the master equation (see, e.g., Lipshtat & Biham 2003, page 8). In the general case (e.g., when A – E are not completely distinct from each other), an automatic way of obtaining the MEs is described in Appendix 4.A. The method described

there is also applicable to moments with any order, and to all the common reaction types in astrochemistry.

In general, the third order moments in the above equations cannot be expressed as a function of the lower order moments, so they need their own differential equations. In the case of a cutoff at the second order, the chain of equations, however, stops here. We describe the method required to evaluate them in section 4.2.3.

The REs for this system

When using REs, equations (4.7 – 4.11) are replaced by

$$\partial_t\langle A\rangle = k_{\mathrm{ad}}\langle a\rangle - k_{\mathrm{evap}}\langle A\rangle - k_{\mathrm{AB}}\langle A\rangle\langle B\rangle - 2k_{\mathrm{AA}}\langle A\rangle^2, \tag{4.7′}$$

$$\partial_t\langle C\rangle = k_{\mathrm{AB}}\langle A\rangle\langle B\rangle, \tag{4.8′}$$

$$\partial_t\langle E\rangle = k_{\mathrm{AA}}\langle A\rangle^2. \tag{4.9′}$$

$$\begin{aligned}\partial_t[\langle A\rangle\langle B\rangle] = {} & k_{\mathrm{ad}}\langle a\rangle\langle B\rangle - k_{\mathrm{evap}}\langle A\rangle\langle B\rangle \\ & - k_{\mathrm{AB}}[\langle A\rangle^2\langle B\rangle + \langle A\rangle\langle B\rangle^2] \\ & - 2k_{\mathrm{AA}}\langle A\rangle^2\langle B\rangle,\end{aligned} \tag{4.10′}$$

$$\begin{aligned}\partial_t[\langle A\rangle^2] = {} & 2k_{\mathrm{ad}}\langle a\rangle\langle A\rangle - 2k_{\mathrm{evap}}\langle A\rangle^2 \\ & - 2k_{\mathrm{AB}}\langle A\rangle^2\langle B\rangle - 4k_{\mathrm{AA}}\langle A\rangle^3.\end{aligned} \tag{4.11′}$$

The equations for $\langle A\rangle\langle B\rangle$ and $\langle A\rangle^2$ are of course not needed in the RE approach but are simply derived from equation (4.7′) (and an omitted similar equation for $\langle B\rangle$) using the chain rule of calculus.

The relation between MEs and REs

The differences between the MEs (equation 4.7 – 4.11) and the REs (equation 4.7′ – 4.11′) in the present case are as follows: All the $\langle AB\rangle$ are replaced by $\langle A\rangle\langle B\rangle$, all the $\langle A(A-1)\rangle$ are replaced by $\langle A\rangle^2$, all the $\langle A(A-1)B\rangle$ are replaced by $\langle A\rangle^2\langle B\rangle$, the $\langle AB(B-1)\rangle$ is replaced by $\langle A\rangle\langle B\rangle^2$, and the $\langle A(A-1)(A-2)\rangle$ is replaced by $\langle A\rangle^3$. Furthermore, the term $k_{\mathrm{AB}}\langle AB\rangle$ in equation (4.10) and the term $k_{\mathrm{AA}}\langle A(A-1)\rangle$ in equation (4.11) disappear in the RE (4.10′) and (4.11′).

These differences make clear why the REs are accurate when the involved species are abundant (namely when $\langle A\rangle \gg 1$ and $\langle B\rangle \gg 1$). This is because, in this case, $\langle AB\rangle$ can be approximated well by[3] $\langle A\rangle\langle B\rangle$, and $\langle A(A-1)\rangle$ can be approximated well by $\langle A\rangle^2$.

The RE approach will be erroneous when $\langle A\rangle$ or $\langle B\rangle$ are smaller than 1 because, in this case, the correlation between A and B might cause $\langle AB\rangle$ to differ considerably from $\langle A\rangle\langle B\rangle$, and the fluctuation in A might cause $\langle A(A-1)\rangle$ to differ considerably from $\langle A\rangle^2$. It can also be viewed like this: in equation (4.10′) and equation (4.11′) that govern the evolution of second order moments, the omitted term $k_{\mathrm{AB}}\langle AB\rangle$ might be much larger

[3] Assuming Poisson statistics, we have

$$\frac{|\langle AB\rangle - \langle A\rangle\langle B\rangle|}{\langle A\rangle\langle B\rangle} \lesssim \sqrt{\frac{1}{\langle A\rangle} + \frac{1}{\langle B\rangle}} \ll 1.$$

than the retained terms such as $\langle A\rangle^2\langle B\rangle$ or $\langle A\rangle\langle B\rangle^2$, and the omitted term $k_{\mathrm{AA}}\langle A(A-1)\rangle$ might be much larger than the retained term $\langle A\rangle^3$.

The relation between a cutoff of MEs and a cutoff of possible states in previous master equation approaches

In Eqs. (4.7 – 4.11) we do not write terms such as $\langle A(A-1)\rangle$ in the split form $\langle A^2\rangle - \langle A\rangle$. We keep terms such as $\langle A(A-1)B\rangle$ and $\langle A(A-1)(A-2)\rangle$ in their present forms intentionally. One reason for this is that terms such as $\langle A(A-1)\rangle$ look more succinct and follow naturally from our way of deriving them (see Appendix 4.A). When $\langle A\rangle \gg 1$, $\langle A(A-1)\rangle$ and $\langle AB\rangle$ can be directly replaced by $\langle A\rangle^2$ and $\langle A\rangle\langle B\rangle$, respectively, to obtain the RE formulation.

More importantly, this formulation can be directly connected to the cutoff schemes in the previous master equation approaches (e.g., Biham et al. 2001; Stantcheva et al. 2002). For example, in a scheme in which no more than two particles of A are expected to be present on a single grain at the same time, we have $P(A{>}2) = 0$. In this case, $\langle A(A-1)(A-2)\rangle = \sum_{A=3}^{\infty} P(A)A(A-1)(A-2) = 0$. Thus we see that a cutoff at a population of two in the master equation approach corresponds naturally to assigning a zero value to moments containing A more than twice, as far as the moments are defined in the form presented above.

4.2.3 The HME approach

The HME approach is a combination of the ME and RE approaches. The basic idea is that, for deterministic (average population >1) species, the REs are used, while for stochastic (average population <1) species, the stochastic effects are taken into account by including higher order moments in the equations. Since a deterministic species may become stochastic as time goes by, and vice versa, the set of ODEs governing the evolution of the system also changes with time, and is determined dynamically. A flow chart of our HME code is shown in Fig. 4.1.

We first set up all potentially needed MEs (using the procedure described in Appendix 4.A), with a cutoff of moments at a prescribed order (usually two). After this and some other initialization work, the program enters the main loop.

Since the system of MEs is a set of ordinary differential equations (ODEs), the main loop contains an ODE solver, for which we use the one from the *ODEPACK* package[4].

Not all MEs and moments are used at all times; which ones are used is determined dynamically. In each iteration of the main loop, we verify whether some surface species have changed from stochastic to deterministic, or from deterministic to stochastic. The gas phase species are always treated as deterministic, regardless of how small their average populations are. In either of these two cases, we re-examine all the moments, and determine the way to treat them. There are four cases:

1. All the first order moments are treated as independent variables.

2. If a moment consists of only stochastic species, and its order is no larger than the prescribed highest allowed order, it will be treated as an independent variable, and

[4] Downloaded from www.netlib.org

the corresponding moment equation will be included and solved. For the sake of numerical stability, its value should be no larger than its deterministic counterpart. For example, if the ODE solver yields a value of $\langle AB\rangle > \langle A\rangle\langle B\rangle$, then the latter value will be assigned to $\langle AB\rangle$.

3. If a moment consists of only stochastic species, and its order is larger than the prescribed highest allowed order, its value will be set to zero, and of course, its moment equation will not be solved. For example, if $\langle A\rangle<1$ and $\langle B\rangle<1$, then, with a highest allowed order set to two, moments such as $\langle A(A-1)(A-2)\rangle$ and $\langle A(A-1)B\rangle$ will be set to zero. This follows from the discussion in section 4.2.2.

4. If a moment contains at least one deterministic species, it will not be treated as an independent variable, and its moment equation will not be solved. It can be evaluated in the following way: assuming that the moment under consideration has a form $\langle AB(B-1)\rangle$, and that A is deterministic (i.e. $\langle A\rangle>1$), then the value of $\langle AB(B-1)\rangle$ is set to be $\langle A\rangle\langle B(B-1)\rangle$. If B is also deterministic, then it will be evaluated as $\langle A\rangle\langle B\rangle^2$. This follows from the discussion in section 4.2.2.

From these procedures, we see that the number of equations, as well as the form of these equations will change when a transition between stochastic and deterministic state of certain species occurs. Each time the ODE system is updated, the ODE solver must therefore be re-initialized.

It seems possible to replace the sharp transition between the stochastic and deterministic state of a species (based on whether its average population is smaller than 1) with a smooth transition, e.g., using a weight function similar to that in Garrod (2008). However, it is not mathematically clear which weight function we should choose, and an arbitrary one might cause some artificial effects, so we prefer not to use this formulation.

4.3 Benchmark with the Monte Carlo approach

We compare the results of our HME approach with those from the exact stochastic simulation (Gillespie 2007; Charnley 1998, 2001; Vasyunin et al. 2009). The RE results are also compared for reference. As in previous studies (Charnley 2001; Vasyunin et al. 2009), we consider a closed chemical system in a volume containing exactly one grain particle. The number of each species in this volume is called a "population", which can be translated into an abundance relative to H nuclei by multiplying it by the dust-to-gas ratio, which is $2.8 \times 10^{-12}(0.1\ \mu\mathrm{m}/r)^3$, where r is the grain radius, assuming an average molecular weight of 1.4, a dust-to-gas mass ratio 0.01, and a density of grain material of 2 g cm^{-3}.

In the MC approach, the number of each species in this volume at any time is an integer. Owing to the large amount of time steps ($>10^9$), it is impractical to store all intermediate steps, so we average the population of each species in time, weighted by the time intervals (remember that the lengths of time intervals between reactions are also random in MC). Because of this weighted average (rather than merely saving the state vector at certain instants), the MC approach can resolve average populations much smaller than one, although the fluctuations that are intrinsic to the MC approach can be larger than the average populations when the latter is small.

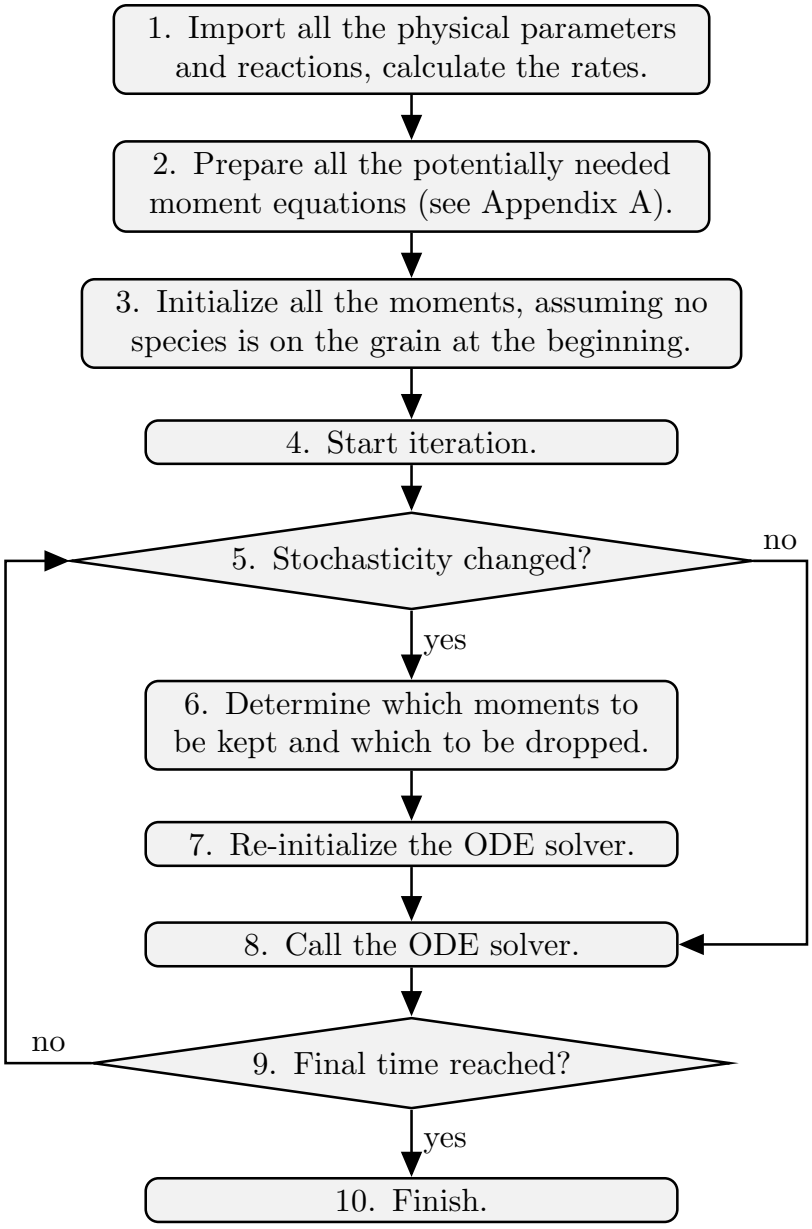

Figure 4.1: A flow chart of the main components of our HME code. Steps 2, 5, 6, and 8 are described in detail in the text.

We first demonstrate how our method works for a large gas-grain network. We then show that for a small surface network, third order moments can also be included to improve the accuracy.

4.3.1 Test of the HME approach truncated at the second order on a large gas-grain network

We use the "dipole-enhanced" version of the RATE06 gas phase reaction network[5] (Woodall et al. 2007), coupled with a surface network of Keane (1997) (see Appendix 4.B). The surface network contains 44 reactions between 43 species, which is basically a reduced and slightly revised version of the network of Tielens & Hagen (1982), containing the formation routes of the most common grain mantle species, such as H_2O, CH_3OH, CH_4, NH_3, etc. This surface network is not really large in comparison with some of the previous works, such as that used by Garrod et al. (2009). However, it is already essential for the most important species. The energy barriers for thermal desorption and diffusion are taken from Stantcheva & Herbst (2004). Diffusion of H atoms on the surface through quantum tunneling is included. Desorption by cosmic rays is taken into account following the approach of Hasegawa & Herbst (1993a). The rate coefficients of the gas phase reactions are calculated according to Woodall et al. (2007), while the rate coefficients of the surface reactions are calculated following Hasegawa et al. (1992). The initial condition is the same as in Stantcheva & Herbst (2004).

We assumed a dust-to-gas mass ratio of 0.01. The grain mass density is taken to be 2 g cm^{-3}, with a site density 5×10^{13} cm^{-2}. Two grain sizes have been used: 0.1 μm and 0.02 μm. A cosmic ray ionization rate of 1.3×10^{-17} s^{-1} is adopted. Four different temperatures (10, 20, 30, 50 K) and three different densities (10^3, 10^4, 10^5 cm^{-3}) have been used. In total, the comparison has been made for 24 different sets of physical parameters. These conditions are commonly seen in translucent clouds and cold dark clouds.

As in Garrod et al. (2009), we make a global comparison between the results of MC, HME, and RE. For each set of physical parameters, the comparisons are made at a time of 10^3, 10^4, and 10^5 years. We calculate the percentage of species for which the agreement between MC and HME/RE is within a factor of 2 or 10. Only species with a population (either from MC or from HME/RE) larger than 10 are included for comparison. This is because for species with smaller populations, the intrinsic fluctuation in the MC results can be significant. For several different sets of physical parameters, we repeated the MC several times to get a feeling for how large the fluctuation magnitude would be, although this is impractical for all the cases.

The comparison results are shown in Table 4.1 (grain radius = 0.1 μm) and Table 4.2 (grain radius = 0.02 μm). The HME approach always has a better global agreement (or the same for several cases) than the RE approach in the cases we tested. The typical time evolution of certain species is shown in Fig. 4.2. In each panel of the figure, the species with a name preceded with a "g" means it is a surface species.

The poorest agreement of HME (Fig. 4.3) is at $t = 10^3$ year for T=20 K, $n_H = 10^5$ cm^{-3}, and grain radius = 0.02 μm. This is mostly because at the time of comparison the populations of certain species were changing very rapidly, so a slight mismatch in time leads to a large discrepancy. This mismatch is probably caused by the truncation

[5] http://www.udfa.net/

of higher-order terms in the HME (see section 4.3.2). For gN_2 in Fig. 4.3, its population seems to be systematically smaller in HME than in MC during the early period, although the HME result matches the one from MC at a later stage (after 3×10^3 years).

The RE is as effective as the HME in several cases, when the temperature is either relatively low ($\sim$10 K) or high ($\sim$ 50 K) (see also Vasyunin et al. 2009), and generally works better for a grain radius of 0.1 μm than of 0.02 μm. When the temperature is very low, many surface reactions with barriers cannot happen (at least in the considered timescales). On the other hand, when the temperature is high, the surface species evaporate very quickly and the surface reactions are also unable to occur. In these two extreme cases, the surface processes are inactive, and the RE works fine.

The RE becomes problematic in the intermediate cases, when the temperature is high enough for many surface reactions to occur, but not too high to evaporate all the surface species; in these cases the HME represents a major improvement over the RE. For a smaller grain radius, the population of each species in a volume containing one grain will be smaller, thus the stochastic effect will play a more important role, and the RE will tend to fail.

We note that, in the HME approach, there is no elemental leakage except those caused by the finite precision of the computer. In all the models that we have run, all the elements (including electric charge) are conserved with a relative error smaller than 5×10^{-14}. The reason why elemental conservation is always guaranteed is that either the rate equations or the moment equations for the first order moments conserve the elements exactly.

Table 4.1: Percentage of agreement between the results from MC and those from HME/RE. The comparison is only made between those species with populations (from MC or HME/RE) larger than 10. The two numbers in each table entry means the percentage of agreement within a factor of 2 or 10, respectively. The grain radius is taken to be 0.1 μm.

	$n_H = 2 \times 10^3$ cm^{-3}			$n_H = 2 \times 10^4$ cm^{-3}			$n_H = 2 \times 10^5$ cm^{-3}		
t	10^3 yr	10^4 yr	10^5 yr	10^3 yr	10^4 yr	10^5 yr	10^3 yr	10^4 yr	10^5 yr
hybrid moment equation									
T = 10 K	100, 100	100, 100	100, 100	100, 100	100, 100	97.6, 99.2	99.0, 100	100, 100	100, 100
T = 20 K	100, 100	100, 100	100, 100	97.7, 98.9	98.2, 100	100, 100	100, 100	100, 100	100, 100
T = 30 K	100, 100	100, 100	100, 100	98.8, 100	100, 100	99.2, 100	100, 100	100, 100	100, 100
T = 50 K	100, 100	100, 100	100, 100	100, 100	100, 100	100, 100	100, 100	100, 100	97.9, 100
rate equation									
T = 10 K	100, 100	100, 100	94.1, 98.8	100, 100	100, 100	93.7, 98.4	99.0, 100	100, 100	95.8, 99.3
T = 20 K	90.2, 93.4	85.3, 90.7	83.6, 93.2	95.5, 95.5	91.2, 95.6	92.3, 96.2	95.3, 96.2	95.0, 95.8	93.9, 96.6
T = 30 K	96.6, 96.6	95.5, 95.5	95.5, 97.0	94.3, 96.6	98.1, 98.1	96.9, 97.7	94.9, 96.9	92.9, 97.4	40.0, 75.0
T = 50 K	100, 100	100, 100	100, 100	100, 100	100, 100	100, 100	100, 100	100, 100	97.9, 100

Table 4.2: Same as Table 4.1 except a smaller grain radius of 0.02 μm is taken.

	$n_H = 2 \times 10^3$ cm^{-3}			$n_H = 2 \times 10^4$ cm^{-3}			$n_H = 2 \times 10^5$ cm^{-3}		
t	10^3 yr	10^4 yr	10^5 yr	10^3 yr	10^4 yr	10^5 yr	10^3 yr	10^4 yr	10^5 yr
hybrid moment equation									
T = 10 K	100, 100	100, 100	100, 100	100, 100	100, 100	100, 100	100, 100	100, 100	100, 100
T = 20 K	95.5, 100	100, 100	97.1, 100	100, 100	100, 100	94.4, 100	73.0, 83.8	97.7, 100	98.3, 100
T = 30 K	100, 100	100, 100	100, 100	100, 100	100, 100	100, 100	100, 100	100, 100	97.0, 100
T = 50 K	100, 100	100, 100	100, 100	100, 100	100, 100	100, 100	100, 100	100, 100	100, 100
rate equation									
T = 10 K	100, 100	100, 100	82.1, 94.9	100, 100	100, 100	87.1, 95.2	100, 100	100, 100	94.8, 98.3
T = 20 K	87.0, 91.3	76.7, 83.3	71.4, 82.9	74.3, 88.6	68.3, 87.8	28.6, 60.0	61.8, 82.4	42.3, 82.7	59.4, 92.2
T = 30 K	100, 100	95.7, 95.7	92.3, 92.3	89.3, 92.9	90.9, 93.9	87.8, 90.2	82.1, 89.3	45.2, 90.3	24.3, 62.2
T = 50 K	100, 100	100, 100	100, 100	100, 100	100, 100	100, 100	100, 100	100, 100	93.3, 93.3

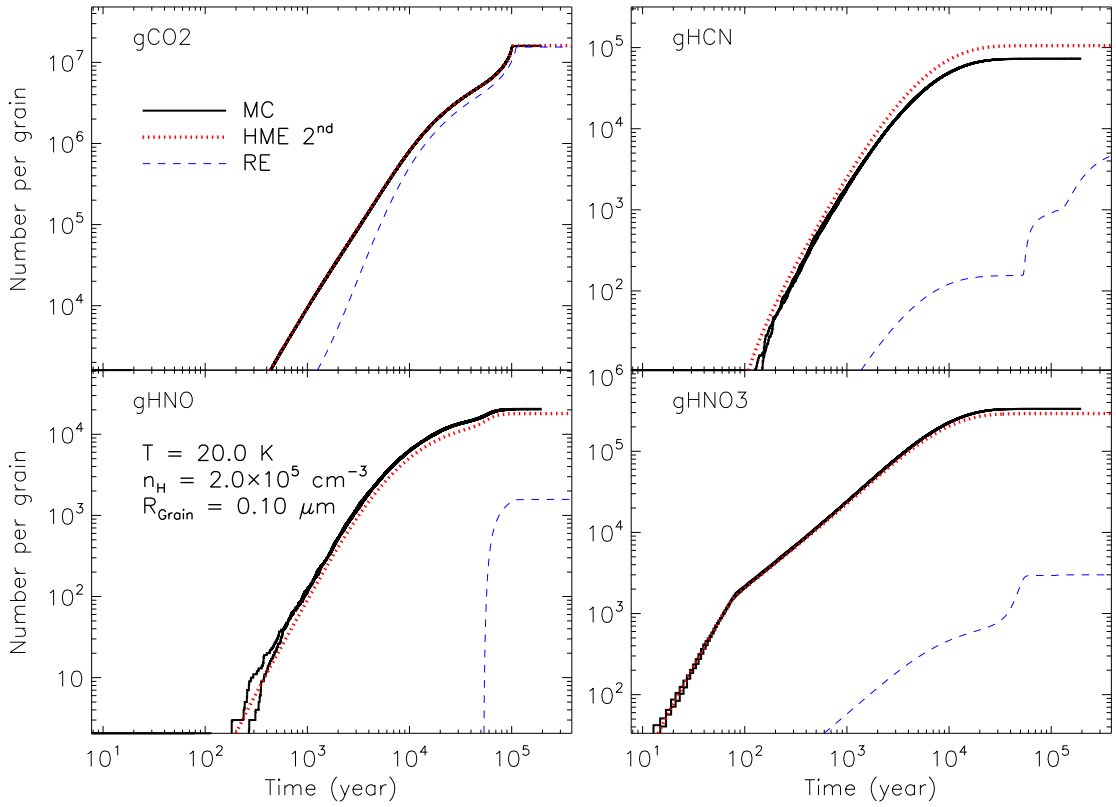

Figure 4.2: Typical time evolution of the average populations of certain species from MC (solid lines), HME to the 2nd order (dotted lines), and RE (dashed lines). Note that the Monte Carlo has been repeated twice. The y-axis is the number of each species in a volume containing exactly one grain. To translate it into abundance relative to H nuclei, it should be multiplied by 2.8×10^{-12}. Physical parameters used: $T = 20$ K, $n = 2 \times 10^5$ cm^{-3}, grain radius = 0.1 μm.

When comparing the results from the HME approach with those from MC simulation, it is important to see how the intrinsic fluctuation in MC behaves. If we assume the probability distribution of the population of a species, say A, is Poissonian, then the variance of A is $\sigma^2(A) = \langle A \rangle$. Hence if $\langle A \rangle$ is small, the relative fluctuation of the MC result can be quite large. This fluctuation might be smoothed out by means of a weighted average in time, but this procedure does not always work. This is why we choose to only compare species with a population higher than 10, corresponding to an abundance relative to H nuclei of 2.8×10^{-11} (for grain radius = 0.1 μm) or 3.5×10^{-9} (for grain radius = 0.02 μm). For a real reaction network, it is usually difficult to predict the intrinsic fluctuation in a MC simulation, unless it is repeated many times. These fluctuations will not have any observational effects, because along a line of sight there are always a large number of a certain species (as far as it is detectable) and the fluctuations are averaged out.

We note that the gas phase processes are not treated identically in our HME approach and MC simulation. In the MC approach, the gas phase processes are always treated as being stochastic (see, e.g., Charnley 1998; Vasyunin et al. 2009), in the same way as the surface processes. However, in our HME approach, the gas phase species are treated in

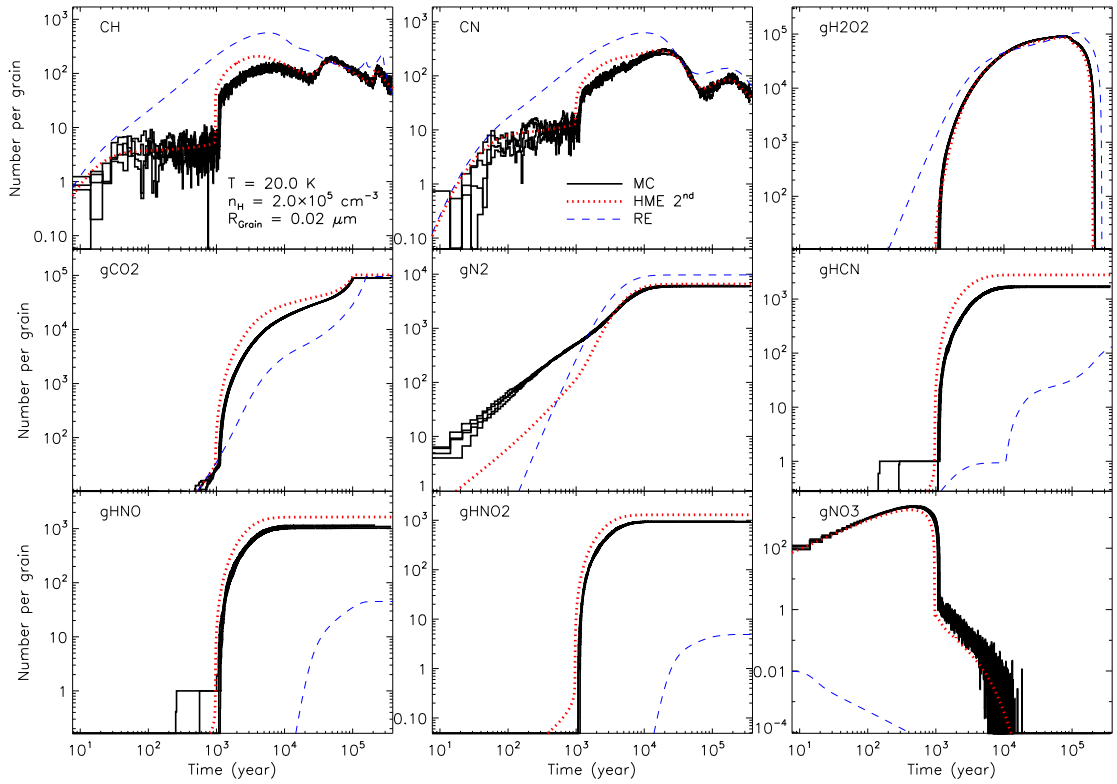

Figure 4.3: Cases in which the agreement between the results of MC and those of HME are not so good, especially at t = 10^3 year. The y-axis is the number of each species in a volume containing exactly one grain. To translate it into abundance relative to H nuclei, it should be multiplied by 3.5×10^{-10}. Physical parameters used: $T = 20$ K, $n = 2 \times 10^5$ cm^{-3}, grain radius = 0.02 μm.

a deterministic way, i.e., REs are always applied to them. This means that even if two reacting gas phase species A and B both have average populations much smaller than one, we still assume that $\langle AB \rangle = \langle A \rangle \langle B \rangle$. This is physically quite reasonable, because the presence of large amounts of reacting partners in the gas phase (if not limited to a volume containing only one dust grain; see, e.g., Charnley (1998)) ensures that the RE is applicable. However, although it might sound a bit pedantic, mathematically this is not equivalent to the MC approach, and some discrepancies caused by this are expected. For a large network, it is impractical to treat the gas phase processes in the same way as the surface processes in the HME approach, because in that case the number of independent variables in the ODE system will be quite large (at least no less than the number of two-body reactions), and the performance of the ODE solver will be degraded.

4.3.2 Test of the HME approach truncated at the third order on a small surface network

To test the improvement in accuracy when the cutoff is made at a higher order, we compare the results of the HME approach with a cutoff at the second order to those obtained from the same approach with a cutoff at the third order. We use a small surface reaction network of Stantcheva & Herbst (2004), containing 17 surface reactions between 21 species, producing H_2O, CH_3OH, CH_4, NH_3, and CO_2. No gas phase reactions are included, except adsorption and desorption processes. The initial gas phase abundances of the relevant species are obtained from the steady state solution of the RATE06 network under the corresponding physical conditions.

As before, we run the HME, RE, and the MC code for different sets of physical parameters. Although by transferring from the RE to the second order HME a major improvement in accuracy can be obtained, the inclusion of the third order moments to the HME usually only improves slightly over the second order case. In Fig. 4.4, we show an example (T = 10 K, $n_{\rm H} = 2 \times 10^5$ cm^{-3}, grain radius=0.02 μm), in which the distinctions between the results from the second and third order HME are relatively large.

For several species, we note that the third order HME is still unable to match the MC results perfectly, and for gHCO (Fig. 4.4) the third order HME even produces an artificial spike in the time evolution curve. The results from the third order HME are otherwise of greater accuracy than the second order one, the abundances of gH_2CO and gCH_3OH in particular being in almost perfect agreement with those from the MC approach. In the case of gHCO, the timescale mismatch between HME and MC is alleviated by including the third order moments.

It might be useful to see the difference between the second order HME and the third order HME in a computational sense. For the current reaction network with physical parameters described above, the number of variables (same as the number of equations, which changes with time) is 145 initially in the second order case, and this number becomes 705 for the third order case. To reach a time span of $\sim 10^6$ year, the second order HME takes about 3 seconds, while the third order one takes about 220 seconds on a standard desktop computer (a CPU @ 3.00 GHz with double cores, 4 GBytes memory). The number of variables depends on the network structure, and it is not straightforward to derive a formula to calculate it. Qualitatively, this number (as a function of the number of reactions or the number of species) seems to increase with the cutoff order less quickly

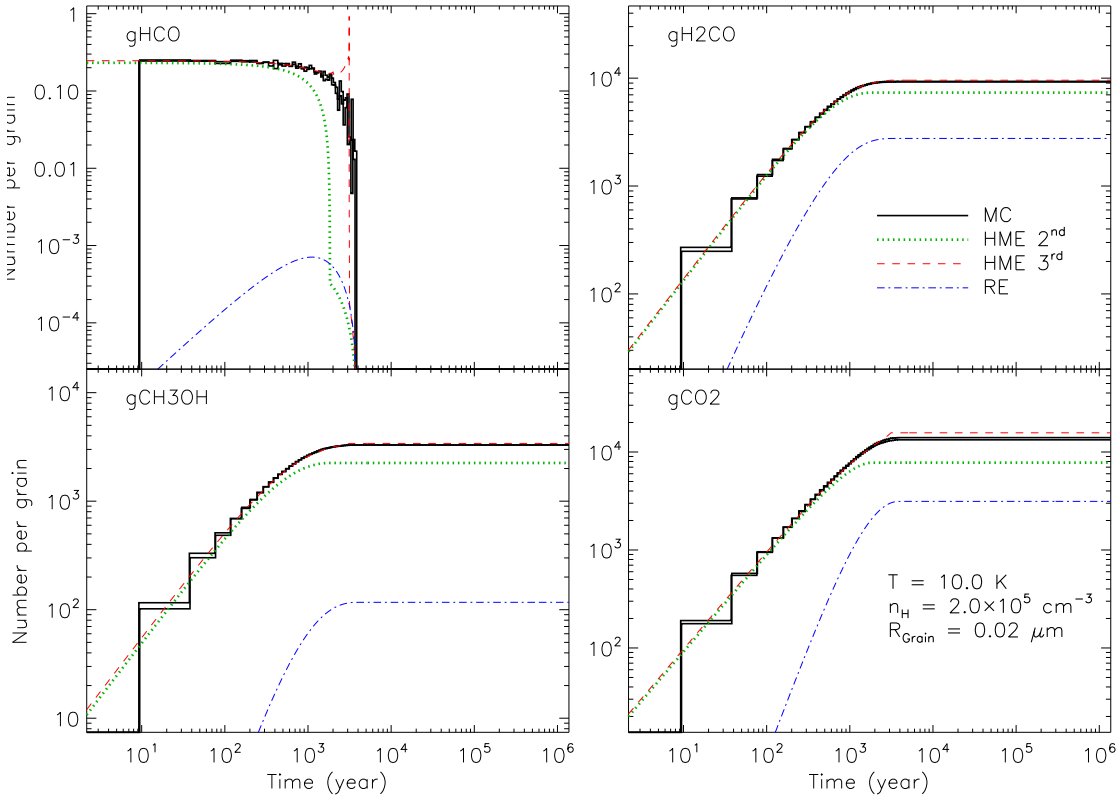

Figure 4.4: Comparison of the results from MC, HME to the 2$^{\text{nd}}$ order, HME to the 3$^{\text{rd}}$ order, and RE. The y-axis is the number of each species in a volume containing exactly one grain. To translate it into abundance relative to H nuclei, it should be multiplied by 3.5×10^{-10}. Physical parameters used when running these models include $T = 10$ K, $n_{\text{H}} = 2 \times 10^5$ cm^{-3}, grain radius = 0.02 μm.

than exponential growth. However, such a "mild" increase affects the behavior of the ODE solver quite significantly. This is partly because the solver contains operations (such as matrix inversion) that become slower as the number of variables become larger. An increase in the number of variables might also increase the stiffness of the problem, let alone the memory limitation of the computer. For the larger reaction network described in the previous section, the third order HME would involve about 5000 variables and has not been tested successfully.

4.4 Discussion

In our HME approach, we have used a general and automatic way to derive the MEs. For large gas-grain networks, the MEs are cut off at the second order. For small networks, a cutoff at the third order is possible and higher accuracy can be obtained. We incorporate a switching scheme between the ME and RE when the average population of a species reaches 1.

The results from HME are more accurate than those from the RE in the cases we have tested, when benchmarked against the exact MC results. The abundances of almost all the abundant species ($\gtrsim 2.8\times10^{-11}$ for a grain radius of 0.1 μm and $\gtrsim 3.5\times10^{-9}$ for a grain radius of 0.02 μm) from HME are accurate to within a factor of two, especially at later stages of the chemical evolution, while in some cases nearly 40% of the results from RE are incorrect by a factor of at least ten.

In terms of computation time, our approach usually takes several tens of minutes to reach a evolution time span of 10^6 years, so it is slower than the RE, but faster than the MC approach (which usually takes from several hours to days). Our approach may also be slower than the MRE approach of Garrod (2008), because more variables (namely the moments with orders higher than one) are present in our method, and the ODE system in HME is usually stiffer. For example, for a moderate temperature many surface reactions can be much faster than any gas phase reactions, and yield a very large coefficient in some of the MEs. However, this is not the case in the stochastic regime of the MRE approach, because when a competition scheme is used in MRE, such a large coefficient does not appear. In this sense, we also advocate the MRE approach of Garrod (2008).

Mathematically, our approach is partially equivalent to the master equation approach of Stantcheva & Herbst (2004) in two respects. 1) They separated stochastic and deterministic species, which is similar to our adopting RE for the abundant species. 2) They set a cutoff for the possible states of the stochastic species. This is in essence equivalent to letting moments containing these species with order higher than a certain number equal to zero.

Our approach can also be viewed as a combination of some of the ideas of Garrod (2008) and Barzel & Biham (2007a). The basic modification and competition scheme in Garrod (2008) can be derived from the MEs, with a semi-steady state assumption for the second order moments. Barzel & Biham (2007a) used the MEs, but they did not include a switch scheme, and their way of deriving the MEs is different from the one in the present paper.

There are still many possibilities for improvement. Although in principle moments with any order can be included, the number of equations grows quite quickly with the cutoff order, which makes the system of equations intractable with a normal desktop

computer. It is unclear whether it is possible to include the moments selectively. It is unclear whether there are better, and more mathematically well founded strategies than the switch at an average population of 1. The present approach is usually stable numerically. However, this is not always guaranteed, especially if higher order moments are to be included. The behavior of the numerical solution also depends on other factors, such as the ODE solver being used and the tunable parameters for it, while the MC approach does not have such issues. In this sense, the MC approach is the most robust.

Even in the accurate MC approach described above, the detailed morphology of the grain surface and the detailed reaction mechanism is not taken into account. One step in this direction would be to take into account the layered structure of the grain mantle. This was done by Charnley (2001) (see also Charnley & Rodgers (2009)) by means of stochastic simulation. It could also be included in the HME approach, as far as the underlying physical mechanism could be described by a master equation.

However, a microscopic MC approach has also been used to study the grain chemistry (see, e.g., Chang et al. 2005; Cuppen & Herbst 2007). In this approach, the morphology of the grain mantle and the interaction between species are modeled in detail. As far as we know, this approach is only practical when the network is small. It remains unclear whether it is possible to incorporate these details into the current HME approach.

In some cases, errors caused by uncertainties in the reaction mechanism and rate parameters might be larger than those introduced by the modeling method (Vasyunin et al. 2008). Hence, further experimental study and a more sophisticated way of interpreting those results would be indispensable.

4.A A method to generate the moment equations based on the generating function

We describe our means of getting the MEs. Our method is automatic, and can be easily coded into a computer program. It is applicable to moments of any order and all the common astrochemical reactions. It makes use of the probability generating function. While preparing the present paper, we noted that Barzel & Biham (2011) also proposed a binomial formulation of ME, which in essence is partly equivalent to our approach presented here, although our way of deriving the MEs is quite different from theirs.

For a probability distribution $P(\mathbf{x}, t)$, the corresponding generating function is defined as (van Kampen 2007)

$$f(z_1, z_2, \ldots, t) = \sum_{\mathbf{x}} P(\mathbf{x}, t) z_1^{x_1} z_2^{x_2} \cdots . \tag{4.12}$$

Here all the z_is should be thought of as merely symbols without any physical meaning, and they have a one-to-one correspondence with the x_is.

It is obvious that $f(\mathbf{z} = \mathbf{1}, t) \equiv 1$, which is just the normalization condition for probability. It is also easy to see that the average population of the ith species is

$$\langle x_i \rangle = \partial_{z_i} f(z_1, z_2, \ldots, t)|_{\mathbf{z}=\mathbf{1}}. \tag{4.13}$$

The right hand side of the above equation means taking the partial derivative first, then assigning a value one to all the z_is.

For the second order moment between two distinct species i and j, we have

$$\langle x_i x_j \rangle = \partial_{z_i} \partial_{z_j} f(z_1, z_2, \ldots, t)|_{\mathbf{z}=\mathbf{1}}. \tag{4.14}$$

If i equals j in the above equation, then what we actually get is

$$\langle x_i(x_i - 1) \rangle = \partial_{z_i}^2 f(z_1, z_2, \ldots, t)|_{\mathbf{z}=\mathbf{1}}. \tag{4.15}$$

In general, we have

$$\langle x_i x_j x_k \cdots \rangle = \partial_{z_i} \partial_{z_j} \partial_{z_k} \cdots f(z_1, z_2, \ldots, t)|_{\mathbf{z}=\mathbf{1}}. \tag{4.16}$$

If several of the subscripts are the same in the left hand side of the above equation, say, $i = j = k$, then the second should be understood as $(x_j - 1)$, while the third should be understood as $(x_k - 2)$, and so on.

From the master equation in Eq. (4.1), it seems possible to get an equation for the evolution of $f(\mathbf{z}, t)$ in the general case. However, if the propensity functions $a_i(\mathbf{x})$ (see Eq. (4.1)) are allowed to take any functional form, then this is not straightforward. Fortunately, in practice $a_i(\mathbf{x})$ usually has a very simple form. On the other hand, we note that in the right hand side of the master equation in Eq. (4.1) the contributions from all the reactions are added linearly. Hence the contribution of each reaction to the evolution of generating function can be considered independently of each other.

We assume there is only one reaction in the network, which has a form

$$x_1 + x_2 + \cdots + x_n \xrightarrow{k} y_1 + y_2 + \cdots + y_m, \tag{4.17}$$

where the x_is and y_is represent the reactants and products, which do not have to be different from each other. We also use these symbols to represent the populations of the corresponding species. If, given a population of x_1, x_2, …, x_n, the probability that the above reaction will happen in a unit time is $kx_1x_2 \cdots x_n$ (namely, the propensity function $a(\mathbf{x}) = kx_1x_2 \cdots x_n$; the product should be understood as explained in the sentence following Eq. (4.16)), then the generating function[6] will evolve according to

$$\partial_t f = k(y_1y_2 \cdots y_m - x_1x_2 \cdots x_n)\partial_{x_1}\partial_{x_2} \cdots \partial_{x_n} f. \tag{4.18}$$

It is not difficult to derive the above equation from the master equation and the definition of generating equation and our assumption about the propensity function.

We note that equation (4.18) has a very simple pattern that is easy to remember: (a) The constant coefficient is the rate coefficient; (b) In the parenthesis, the *symbols* of all the products are multiplied together, with a coefficient +1, while the *symbols* of all the reactants are multiplied together, with a coefficient −1; (c) In the differential part, all the reactants are present as they are in the left hand side of equation (4.17), while none of the products appear.

We now attempt to derive the ME. We obtain the evolution equation of each moment (as defined in Eq. (4.16)) by simply differentiating both sides of equation (4.18) with respect to the relevant components in the moment, then setting all the symbols to a value of one.

[6] Instead of using z_is as symbols for the independent variables of the generating function f, we use x_is and y_is instead. This will not cause any confusion.

For example, for the reaction $A+B \xrightarrow{k} C+D$, the evolution equation of the generating function f is

$$\partial_t f = k(CD - AB)\partial_A \partial_B f.$$

For $\langle AB \rangle$, we differentiate both sides of the above equation by A and B. We obtain

$$\begin{aligned}\partial_t \partial_A \partial_B f =& k[(CD - AB)\partial_A^2 \partial_B^2 f \\ & - A\partial_A^2 \partial_B f - B\partial_A \partial_B^2 f - \partial_A \partial_B f].\end{aligned}$$

Next we assign a value of one to all the symbols (A – D) appearing in the resulting expressions, and "translate" the remaining terms into moments (recalling the remark about equation (4.16)), obtaining

$$\partial_t \langle AB \rangle = -k[\langle A(A-1)B \rangle + \langle AB(B-1) \rangle + \langle AB \rangle].$$

Although the above derivation involves differentiations, these operations can be easily translated into some combinatorial rules and written as a computer program. A recursive procedure is needed to generate all the potentially needed moments up to a given order.

4.B The surface reaction network we used to test our code

Table 4.3: The surface network used in Section 4.3.1 of this chapter. Note that the validity of the numerical method (namely the HME approach) presented in this paper does not depend on the specific test network that we used.

Number	Reactants		Products		E_{reac} (K)
1	H	H	H_2		0.0
2	H	O	OH		0.0
3	H	OH	H_2O		0.0
4	H	O_2	O_2H		1200.0
5	H	O_2H	H_2O_2		0.0
6	H	H_2O_2	H_2O	OH	1400.0
7	H	O_3	O_2	OH	450.0
8	H	CO	HCO		1000.0
9	H	HCO	H_2CO		0.0
10	H	H_2CO	CH_3O		1500.0
11	H	H_2CO	H_2COH		1500.0
12	H	CH_3O	CH_3OH		0.0
13	H	H_2COH	CH_3OH		0.0
14	H	HCOO	HCOOH		0.0
15	H	N	NH		0.0
16	H	NH	NH_2		0.0
17	H	NH_2	NH_3		0.0
18	H	C	CH		0.0
19	H	CH	CH_2		0.0
20	H	CH_2	CH_3		0.0
21	H	CH_3	CH_4		0.0
22	H	CN	HCN		0.0
23	H	NO	HNO		0.0
24	H	NO_2	HNO_2		0.0
25	H	NO_3	HNO_3		0.0
26	H	NHCO	NH_2CO		0.0
27	H	NH_2CO	NH_2CHO		0.0
28	H	N_2H	N_2H_2		0.0
29	H	N_2H_2	N_2H	H_2	650.0
30	O	O	O_2		0.0
31	O	O_2	O_3		1200.0
32	O	CO	CO_2		1000.0
33	O	HCO	HCOO		0.0
34	O	N	NO		0.0
35	O	NO	NO_2		0.0
36	O	NO_2	NO_3		0.0
37	O	CN	OCN		0.0

... continued on next page

Number	Reactants		Products		E_{reac} (K)
38	C	N	CN		0.0
39	N	N	N_2		0.0
40	N	NH	N_2H		0.0
41	N	HCO	NHCO		0.0
42	H_2	OH	H_2O	H	2600.0
43	O	HCO	CO_2	H	0.0
44	OH	CO	CO_2	H	80.0

References. Keane (1997) and Tielens & Hagen (1982).

Chapter 5

Production of interstellar hydrogen peroxide (H_2O_2) on the surface of dust grains

The content of this chapter is based on:
Du, F., Parise, B., & Bergman, P. 2012, A&A, 538, A91

Contents

The formation of water on the dust grains in the ISM may proceed with hydrogen peroxide (H_2O_2) as an intermediate. Recently gas-phase H_2O_2 has been detected in ρ Oph A with an abundance of $\sim 10^{-10}$ relative to H_2.

The study presented in this chapter is aimed at reproducing the observed abundance of H_2O_2 and other species detected in ρ Oph A quantitatively.

For this purpose, we make use of a chemical network that includes gas phase reactions, as well as processes on the grains. We also include the desorption mechanism triggered by the heat released in chemical reactions. We run the model for a range of physical parameters.

The modeling results show that the abundance of H_2O_2 can be best reproduced at $\sim 6\times10^5$ yr, which is close to the dynamical age of ρ Oph A. The abundances of other species detected in the same source such as H_2CO, CH_3OH, and O_2 can also be reasonably reproduced at this time. In the early time, the gas-phase abundance of H_2O_2 can be much higher than the currently detected value. We predict a gas phase abundance of O_2H at

the same order of magnitude as H_2O_2, and an abundance on the order of 10^{-8} for gas phase water in ρ Oph A. A few other species of interest are also discussed.

The main conclusion is, H_2O_2 can be produced on the dust grains and released into the gas phase through nonthermal desorption via surface exothermic reactions. The H_2O_2 molecule on the grain is an important intermediate in the formation of water. The fact that H_2O_2 is over-produced in the gas phase for a range of physical conditions suggests that its destruction channel in the current gas phase network may be incomplete.

5.1 Introduction

Oxygen is the most abundant "metal" element in the cosmos (Savage & Sembach 1996; Asplund et al. 2009). In the cold dense interstellar clouds, gas-phase chemical models predict that oxygen mainly resides in CO and O_2 molecules (Herbst & Leung 1989; Millar & Herbst 1990; Wakelam et al. 2006). However, although CO is ubiquitously distributed in the ISM, O_2 is not. The latter is only detected very recently in ρ Oph A at a low abundance (relative to molecular hydrogen) of 5×10^{-8} (Larsson et al. 2007), and in Orion at an abundance of $(0.3 - 7)\times10^{-6}$ (Goldsmith et al. 2011). On the other hand, the observed water (gas or ice) abundance can be as high as 10^{-4} (van Dishoeck 2004). Thus it seems that water, instead of O_2, is a main reservoir of oxygen in addition to CO. When only gas phase chemistry is included, the H_2O abundance can be on the order 10^{-7} at most (see, for example, Bergin et al. 2000; Roberts & Herbst 2002) for typical dark cloud conditions. That O_2 is overproduced and H_2O is underproduced in gas phase chemistry suggests that adsorption onto the grain surfaces and the reactions on the surfaces may play important roles.

On the grain surface, H_2O can form through successive additions of hydrogen atoms to an oxygen atom:

$$\mathrm{H + O \rightarrow OH}, \tag{5.1}$$

$$\mathrm{H + OH \rightarrow H_2O}, \tag{5.2}$$

both of which are barrierless (Allen & Robinson 1977). It can also form via hydrogen addition to molecular oxygen:

$$\mathrm{H + O_2 \rightarrow O_2H}, \tag{5.3}$$

$$\mathrm{H + O_2H \rightarrow H_2O_2}, \tag{5.4}$$

$$\mathrm{H + H_2O_2 \rightarrow H_2O + OH}. \tag{5.5}$$

Reaction (5.3) was assumed to have an activation barrier of 1200 K in Tielens & Hagen (1982). However, based on experimental results, Cuppen et al. (2010) have recently concluded that it is barrierless. Other possible formation pathways of water include the reaction between H_2 and OH and the route with O_3 as an intermediate (Tielens & Hagen 1982).

In the second route described above (Eqs. (5.3) – (5.5)), hydrogen peroxide (HOOH, also written as H_2O_2, which is adopted in this paper) appears as an intermediate product. Thus if this route is indeed important, a significant amount of H_2O_2 might form on the grain, and its gas phase counterpart could also be detectable if effective desorption mechanisms exist.

In the current mainstream gas phase reaction networks for astrochemistry, H_2O_2 is not efficiently formed in the gas phase. For example, in the 2009 version of the OSU network[1], the only two reactions leading to the formation of H_2O_2 are

$$H_2 + O_2H \rightarrow H_2O_2 + H,$$
$$OH + OH \rightarrow H_2O_2 + h\nu.$$

The first one has a large activation barrier of 10^4 K, rendering it inactive at low temperatures. H_2O_2 is mainly consumed by

$$H_2O_2 + h\nu \rightarrow OH + OH,$$
$$OH + H_2O_2 \rightarrow H_2O + O_2H,$$

the first of which is dissociation by cosmic-ray induced radiation. Other destruction channels by reacting with H and O are ineffective due to large activation barriers. At a temperature of 10 K and an H_2 density of 10^4 cm^{-3}, the steady-state abundance of H_2O_2 can be approximated by

$$X(H_2O_2) \simeq 10^3 X^2(OH) \simeq 5 \times 10^{-12}.$$

At a higher density, the abundance of H_2O_2 will be even less because OH is less abundant in this case. With the UMIST RATE06 network the abundance of H_2O_2 is essentially zero (Woodall et al. 2007). Thus if a substantial amount of H_2O_2 can be detected in the ISM, then it must have been synthesized on the dust grains, rather than in the gas phase. This would also provide information and constraints on the formation route of H_2O.

It has indeed recently been detected (for the first time) in the ρ Oph A cloud by Bergman et al. (2011b), at an abundance of $\sim 10^{-10}$, which is well above what would be predicted by the gas phase chemistry, indicating that chemical processes on the grains are responsible for this detection. Why this molecule has not been detected in the past seems to be a puzzle and will be discussed later. Previously Clancy et al. (2004) detected H_2O_2 in the atmosphere of Mars.

In the present work we aim at modeling the gas phase abundance of H_2O_2 at a physical condition relevant to ρ Oph A, to demonstrate whether the grain chemistry is able to explain its observed abundance. The model is also required to give consistent abundances for other species detected earlier in this region. Also, ice and gas-phase abundance predictions for previously undetected species are made.

The remaining part of this paper is organized as follows. In section 5.2 we describe the chemical model used in this work. In section 5.3 we present the results of our modeling. The conclusions are in section 5.4. Appendix 5.A contains an explanation to a spike-like feature in the evolution curves of some species. The surface reaction network we use is listed in Appendix 5.B, and the enthalpies of the surface species, which are needed in the chemical desorption mechanism (see section 5.2) are listed in Appendix 5.C.

5.2 Chemical model

For the gas phase chemistry, we use a subset of the UMIST RATE06 network[2] (Woodall et al. 2007). Species containing Fe, Na, Mg, and Cl are excluded. In total 284 gas phase

[1] http://www.physics.ohio-state.edu/~eric/research_files/osu_01_2009
[2] http://udfa.net

species and 3075 gas phase reactions are included. The cosmic-ray ionization rate is taken to be the canonical value of 1.36×10^{-17} s^{-1} (Woodall et al. 2007).

The surface chemical network is a combination of a selection of the reactions in Allen & Robinson (1977), Tielens & Hagen (1982), and Hasegawa et al. (1992), with the rates of a few reactions updated according to the recent experimental results and/or theoretical calculations. In total 56 surface species and 151 surface reactions are included (see appendix 5.B).

The binding energies of the surface species are either taken from Hasegawa & Herbst (1993a) or estimated from the value of a similar species as in Garrod et al. (2008). These values are applicable to bare grains, i.e., grains without an ice mantle. A grain will be covered by ice (typically water) as adsorption and reaction proceeds, thus these values are not always appropriate. Ideally, they should be varied according to the real-time composition of the grain. The water ice mantle mainly affects the binding energies of species with a hydrogen bond, such as OH and H_2O. The effect of this should be minor for our purpose, because most of the reactions involving a species with a hydrogen bond are primarily mediated by another reaction partner that does not have a hydrogen bond.

The barriers against surface diffusion are taken to be a fixed fraction of the binding energies. A range of values have been used for this fraction in the past, from 0.3 (Hasegawa et al. 1992) through 0.5 (Garrod et al. 2008) to 0.77 (Ruffle & Herbst 2000). We use a value of 0.77, based on the analysis of Katz et al. (1999). Because our model is mainly for a relatively high temperature (∼20 K) in comparison with most of the previous models (predominantly for a temperature of ∼10 K), a low diffusion barrier for the surface species would lead to an unrealistic ice mantle composition. The effect of changing this parameter is discussed later. We allow H and H_2 on a dust grain to migrate through quantum tunneling or thermal hopping, depending on which is faster. All the heavier species are only allowed to move by thermal hopping. The quantum tunneling and thermal hopping rates are calculated using the formulation of Hasegawa et al. (1992). For calculating of the quantum tunneling rates, we use a barrier width of 1 $\mathring{A}$. The exact value of this width depends on the composition and structure of the surface, which has not been fully quantified.

About the activation barrier of reaction (5.3), as there is a big discrepancy between the value adopted in the past and the value proposed recently based on experiments (Cuppen et al. 2010), we adopt an intermediate value of 600 K. However, the effect of varying this parameter is also tested during the modeling, and will be discussed later. Reaction (5.5) has a barrier of 1400 K in Tielens & Hagen (1982), while in Cuppen et al. (2010) this reaction is found to be about 20 times slower than reaction (5.4), suggesting a non-negligible barrier[3]. We adopt the latter result, which can be translated into a barrier height of ∼92 K for a barrier width of 1 Å; a more detailed discussion on this reaction is on page 127.

Surface reactions with an activation barrier are allowed to proceed thermally or through quantum tunneling, depending on whichever is faster. The formula used to calculate the rates is also the same as in Hasegawa et al. (1992), and the reaction barriers are assumed to have a width of 1 $\mathring{A}$, although different values are possible (Garrod & Pauly 2011).

[3] Our original publication Du et al. (2012) contains an error here, saying that reaction (5.5) is barrierless, though our conclusions are not affected.

The reaction rate of a two-body surface reaction

$$\mathrm{A} + \mathrm{B} \rightarrow \mathrm{C} + \cdots$$

is

$$[k_{\mathrm{diff}}(\mathrm{A}) + k_{\mathrm{diff}}(\mathrm{B})]N(\mathrm{A})N(\mathrm{B})/N_{\mathrm{S}},$$

if A $\neq$ B. Here N_{S} is the number of reaction sites of a grain, $k_{\mathrm{diff}}(\mathrm{A})$ and $k_{\mathrm{diff}}(B)$ are the diffusion rates of A and B, and $N(\mathrm{A})$ and $N(\mathrm{B})$ are the number of species A and B on a single grain. If A = B, then the reaction rate should be

$$k_{\mathrm{diff}}(A)N(\mathrm{A})(N(\mathrm{A}) - 1)/N_{\mathrm{S}}.$$

With a number density of reaction sites being 10^{15} cm^{-2}, a dust grain with radius 0.1 μm has an N_{S} of about 10^6.

As we are mainly concerned with the gas phase abundances of several species, their desorption mechanism must be treated carefully, especially if they are mainly produced on the grains. Besides the normal thermal desorption, species can also get evaporated episodically when a cosmic-ray hits a grain. This is treated in the same manner as in Hasegawa & Herbst (1993a). Furthermore, the nonthermal desorption mechanism via exothermic surface reactions (for brevity we call it "chemical desorption") proposed by Garrod et al. (2006; see also Watson & Salpeter 1972; Garrod et al. 2007; Cazaux et al. 2010) is also included. Here the products of the exothermic reactions on the grain have a probability of being directly ejected into the gas phase. The rate of such a desorption mechanism depends on the exoergicity of the reaction, as well as on the desorption energy of the products. A parameter characterizing the efficiency of this mechanism (the "a" parameter in Garrod et al. 2007) is introduced, which we take to be 0.1. The yield of chemical desorption is directly proportional to this "a" parameter, although it is not well constrained. The value we adopt here gives a good match to the observational results. See section 5.3.6 for further discussion. The exoergicities of these reactions are estimated from the enthalpies of the reactants and products in the same manner as in Allen & Robinson (1977) (their equations (3) and (4)), and the enthalpies of the species involved in these reactions are taken from Binnewies & Milke (1999), from the NIST chemistry web book[4], or from some other sporadic sources (see appendix 5.C).

However, the desorption mechanisms described above are not always sufficient to provide enough gas phase abundances for some species, especially at late times. Even if a large amount of a species is produced on the grain and released into the gas phase at early times, it would later be accreted back to the grain surface. If at this later time its production is no longer active (due to the exhaustion of the precursor species), its gas phase abundance cannot be maintained. Dust sputtering (Tielens et al. 1994) and photodesorption (Öberg et al. 2007) might help release them to the gas phase, both of which should not be very important in a quiet cold dark cloud. Another possible mechanism is that cosmic-ray induced radiation can dissociate the species on the grain, and when the fragments recombine, the products can possibly be ejected into the gas phase directly because of the energy release of the reaction, as described before. We implement this mechanism in the same way as in Ruffle & Herbst (2001a) and Garrod & Pauly (2011)

[4] http://webbook.nist.gov/chemistry/

(see also Cuppen & Herbst 2007), namely, the cosmic-ray induced photodissociation rates for the surface species are taken to be the same as in the gas phase. Several dissociation branches from Garrod et al. (2008) (their Table 1) are included.

In our model the numbers of all the species on a single grain are solved with the hybrid moment equation (HME) approach (Du & Parise 2011). It has been shown in Du & Parise (2011) that the rate equation method can be inaccurate in some cases, and the HME approach provides a major improvement over the rate equation method. Since the HME approach is relatively new, in several cases we also benchmarked our HME results with the exact Monte Carlo method (similar to the one of Vasyunin et al. 2009) as in Du & Parise (2011), and the agreement is satisfactory. It is impractical to run all the models with the Monte Carlo method because the run time would be too long.

At present the layered structure of the grain mantle is not incorporated into our model. Such a structure might be more realistic, and it is important for retaining some of the ice species. However, it is also possible that the interstellar dust grains may have an amorphous structure, which renders the layered structure an inaccurate description. On the other hand, particles landing on a grain are able to penetrate the interior by several to tens of layers, as demonstrated by experiments (see, e.g., Ioppolo et al. 2010), thus although a model neglecting the layered structure is not accurate, one that deactivates all the layers below the outermost surface does not reflect the whole reality either. In fact, for the H-addition reactions, whether the layered structure is taken into account only plays a minor role in determining the reaction rates in the accretion limit (i.e. when the accretion and evaporation processes are much slower than the reactions; Garrod 2008), because the species involved in these reactions never build up a full layer.

5.3 Results and discussions

5.3.1 Modeling ρ Oph A

We ran the chemical model for the physical parameters that are appropriate for ρ Oph A, where H_2O_2 has first been detected by Bergman et al. (2011b). In Fig. 5.1 we show the abundances of several species as a function of time. In this model, a temperature of 21 K and a hydrogen density of 6×10^5 cm^{-3} have been assumed, which are determined for ρ Oph A observationally by Bergman et al. (2011a,b). The dust temperature and gas temperature are assumed to be the same. A fixed value of 15 for the visual extinction A_V has been adopted. We assume a canonical grain size of 0.1 μm and a reaction site density of 10^{15} cm^{-2}. The dust-to-gas mass ratio is set to 0.01, and the dust grain material is assumed to have a mass density of 2 g cm^{-3}. We also assume that the ratio between the diffusion barrier and the binding energy is 0.77, which is at the higher end of the values used in the past, to give a reasonable ice composition. The initial condition is atomic except for H_2. The elemental abundances are the same as in Garrod & Pauly (2011).

The observed abundance of gas phase H_2O_2 is $\sim10^{-10}$ relative to H_2 (Bergman et al. 2011b). This value is best matched at a time of $\sim6\times10^5$ yr. In the early time, before about 2×10^5 years, the gas phase H_2O_2 abundance can be as high as $\sim5\times10^{-7}$. At late times, the H_2O_2 abundance decreases to a very low value, due to the exhaustion of O_2 on the grain and a full conversion of H_2O_2 into H_2O.

H_2O_2 is mainly formed through reaction (5.4) on the grain, followed by immediate

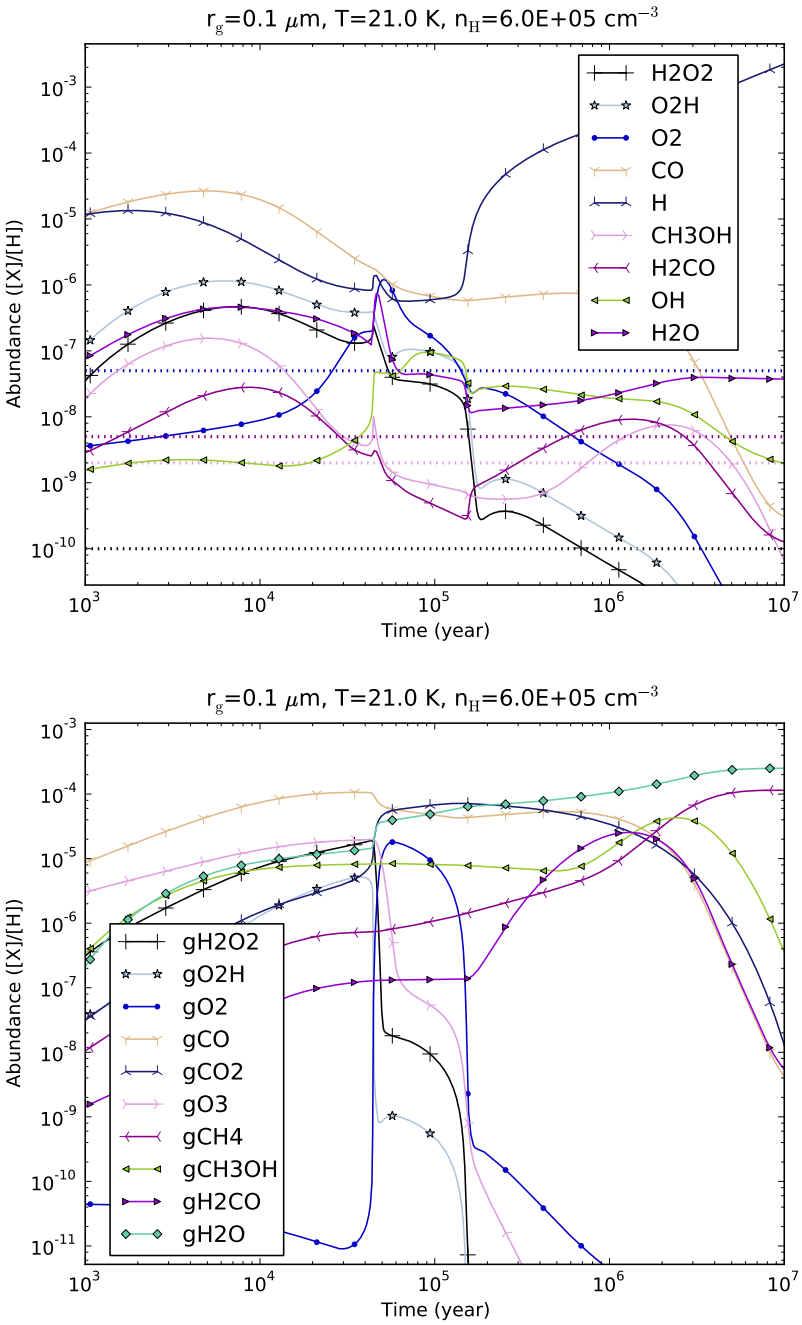

Figure 5.1: The time evolution of the abundances of selected species. A prefix "g" means a grain surface species (bottom panel), while a name without a prefix means a gas phase species (top panel). The dotted lines are the observed abundances (relative to H_2) of O_2 (blue), H_2CO (cyan), CH_3OH (magenta), and H_2O_2 (black), respectively, in the ρ Oph A source.

desorption of the product into the gas phase caused by the reaction heat. About 7% of the produced H_2O_2 is released this way. Its gas phase abundance is determined by the adsorption and chemical desorption processes. The dissociation of gas phase H_2O_2 by cosmic-ray-induced photons is unimportant in consuming it, compared to adsorption.

Ioppolo et al. (2008) modeled the abundance of H_2O_2 ice briefly, giving a value of 10^{-14} – 10^{-10} relative to molecular hydrogen, depending on which energy barriers of several relevant reactions were used. Our major goal is to model the gas phase H_2O_2 abundance, rather than the H_2O_2 ice. In our model results, the gas phase abundance of H_2O_2 is much higher than its ice counterpart. The H_2O_2 ice does not have a significant abundance in the later stage, being well below the upper limit (5.2% with respect to H_2O ice) given by Boudin et al. (1998), because it is constantly transformed into H_2O by reacting with the accreted H atoms. However, by irradiating thin water ice film with low energy ions, Gomis et al. (2004) found that it is possible to obtain an H_2O_2 to H_2O ratio in the solid phase up to a few percent. This direct processing of the grain mantle by cosmic rays is not included in our model. The production of H_2O_2 inside water ice in an O_2-rich environment triggered by UV radiation (Shi et al. 2011) should also be of little importance here. We notice in Fig. 5.1 (bottom panel) that in the early stage (before $\sim 5\times10^4$ yr) the H_2O_2 ice can achieve a rather high abundance, $\sim 5\times10^{-6}$ relative to H nucleus or $\sim$10% relative to H_2O. During this early period the water formation on the grain mainly proceeds through reaction (5.5) with H_2O_2 as an intermediate, which is responsible for about half of the final water ice repository on the grain mantle. In the later stage, reaction (5.2) takes over. In the results of Ioppolo et al. (2008) (their Fig. 4), we do not see a similar feature (i.e. a high abundance of H_2O_2 ice in the early stage). In our current model the layered structure of the grain mantle is not taken into account. It is possible that, if such a structure is considered, the inner layers with a relatively high H_2O_2 content might be maintained, which would give a value of a few percent for the H_2O_2-to-H_2O ratio in the solid phase.

Methanol (CH_3OH) and formaldehyde (H_2CO) are also detected in the ρ Oph A SM1 core (Bergman et al. 2011a), at an abundance of $\sim 2\times10^{-9}$ and $\sim 5\times10^{-9}$, respectively. Their abundances are also reproduced very well at a time of $\sim 6\times10^5$ yr in our model. At early times, both CH_3OH and H_2CO have a high abundance. Their abundances also have a peak in the period between 2×10^5 yr to 10^7 yr. In our current network, CH_3OH is mainly formed on the grains, and mainly through the addition of H atom to CH_2OH, while the latter is mainly produced from the reaction between C and OH to form HOC followed by successive H additions. Thus the abundance of CH_3OH decreases at very late times due to the depletion of atomic C (which is mainly in CH_4 ice in the late stage). The normal formation channel through successive hydrogenation of CO is important at around 5×10^5 – 2×10^6 yr. The gas phase H_2CO mainly forms in the gas phase in the early stage ($< 10^5$ yr), and mainly through the reaction $CH_3 + O \rightarrow H_2CO + H$. Later it is mainly formed through successive hydrogenation of CO on the grain surface followed by chemical desorption. The abundance of methanol and formaldehyde ice relative to water ice can be as high as $\sim$20% at their peaks at a time of $\sim 2\times10^6$ yr, but falls to a very low value in the late times. The late-time abundances are consistent with the upper limit derived for quiescent environment and low-mass young stellar objects in Gibb et al. (2004). However, in Pontoppidan et al. (2004) a much higher abundance of CH_3OH ice is observed along the line-of-sight of SVS4 (a dense cluster of pre-main sequence stars),

which is close to a class 0 protostar, and this is consistent with the peak abundances in our model.

From Fig. 5.1 (top panel) it can be seen that the abundance of gaseous O_2 at an intermediate time of 6×10^5 year is $\sim6\times10^{-9}$, which is within one order of magnitude of the observed abundances of 5×10^{-8} for O_2 (Larsson et al. 2007). The late-time abundance of O_2 drops to a very low value, while its observed abundance is best matched at a time of $\sim2\times10^5$ yr. We notice that during the period $\sim(0.6 - 2)\times10^5$ yr, the abundance of O_2 ice has a prominent bump, reaching a peak abundance of $\sim10^{-5}$ relative to H_2. At the same time, the gas phase O_2 also reaches an abundance of $\sim(1 - 5)\times10^{-7}$. These values can be compared with the recent detection of gas phase O_2 at an abundance of $(0.3 - 7)\times10^{-6}$ in Orion by Herschel (Goldsmith et al. 2011). Warm-up of the dust grain at this stage may release a large amount of O_2 molecule into the gas phase.

As a precursor of H_2O_2, O_2H mainly forms from the reaction between O and OH (which does not have a barrier according to Hasegawa et al. 1992) on the grain at an early stage ($<5\times10^4$ yr), and through reaction $H + O_2$ at a later stage. The ratio between the gas phase O_2H and H_2O_2 is almost constant throughout the evolution, being approximately 3. Thus in our current network, the gas phase O_2H also has a remarkable abundance, which might be detectable in the future[5].

Except at very early times, the grain mantle is mainly composed of water ice. The abundances of CO and CO_2 are comparable at an intermediate time of $(0.3–1)\times10^6$ yr, being about 40–60% of water ice. This is in rough agreement with the ice composition for intermediate-mass YSOs (Gibb et al. 2004) (see also Öberg et al. 2011), and is also in line with the suggestion of An et al. (2011) that CO_2 ice is mixed with CH_3OH ice (the latter is about 10% of the former in our model). Water ice mainly forms from reaction (5.5) in the early time, and from reaction (5.2) in the late time. The gas phase formation route of water only plays a minor role. In contrast, the CO ice mantle is mainly from accretion of CO molecules formed in the gas phase. For the CO_2 ice, it is mainly accreted from its gas phase counterpart in the early time, and its abundance is increased further through the reaction $OH + CO \rightarrow CO_2 + H$ in the late stage. At late times ($> 3\times10^6$ yr), most of the carbon resides in the form of CH_4 ice, with the latter about half of the water ice. However, as far as we know, such a high abundance of CH_4 ice (see also Garrod & Pauly 2011) has not been observed in the ISM.

The gas phase CO is heavily depleted, with an abundance $\sim10^{-6}$ relative to the H nucleus or $\sim1\%$ relative to its ice counterpart, at an intermediate time (10^5 – 10^6 yr). Its abundance is mainly determined by the balance between the adsorption and cosmic-ray induced evaporation processes. At late times the CO ice abundance drops to a very low value. This is because CO is continuously hydrogenated into H_2CO or CH_3OH, and the dissociation of CH_3OH by cosmic-ray induced photons produces CH_3, which quickly becomes CH_4 by hydrogenation. Taking the layered structure of grain mantle into account can retain a fair amount of CO ice.

The abundance of gas phase H_2O in the intermediate to late time is on the order 10^{-8}. At these times, its grain surface production route (5.2) followed by chemical desorption and the gas phase production route $H_3O^+ + e^- \rightarrow H_2O + H$ plays a similarly important role. H_3O^+ itself is mainly formed from successive protonation of atomic oxygen at this

[5] O_2H has been recently detected in the same source by Parise et al. (2012a), with an abundance of $\sim10^{-10}$, close to the prediction here.

stage.

The hydroxyl radical (OH) has an abundance $\sim 10^{-8}$ – 10^{-9} in the gas phase at the intermediate-to-late times. These values are comparable to the observed abundance of $\sim(0.5 - 1)\times10^{-8}$ in the envelope around the high-mass star-forming region W3 IRS 5 obtained with HIFI onboard *Herschel* (Wampfler et al. 2011). The physical condition in this source is different from ρ Oph A. However, since OH is readily produced and recycled in the gas phase by the reactions $H_3O^+ + e^- \rightarrow OH + 2H$ and $H_3^+ + OH \rightarrow H_2O^+ + H_2$, grain processes will not play a dominant role in determining its abundance, especially when the temperature is not too low. However, Goicoechea et al. (2006) detected a much higher abundance $(0.5 - 1)\times10^{-6}$ of OH in the Orion KL outflows, which seems to require other formation pathways (e.g. shock destruction of H_2O ice).

A relatively high abundance ($\sim 10^{-7}$ and $\sim 10^{-5}$) of gas phase and grain surface ozone (O_3) is also obtained for $t \lesssim 10^5$ yr. However, these values should be treated with caution, because the chemistry of O_3 is very incomplete in our current model: neither the OSU gas phase network nor the UMIST RATE06 network includes it. Possible gas phase destruction pathways involving atomic O and S (according to the NIST chemistry web book; see footnote [4]) may lower its gas phase abundance significantly, but its ice mantle abundance should not be severely affected.

The abundance of atomic hydrogen in the gas phase is quite high at late times as seen from Fig. 5.1, which seems to be at odds with the usual results. In many gas phase chemical models, the abundance of atomic hydrogen in the gas phase is determined by the balance between its adsorption onto the dust grains and the dissociation of H_2 molecules by cosmic rays. The adsorption process is thought to have a sticking coefficient close to unity, and evaporation is assumed not to occur (which is appropriate at low temperatures). In such a framework it can be found that the gas phase atomic hydrogen will always have a fixed density on the order of 1 cm^{-3}. However, in our case with a temperature of 21 K, evaporation is very fast and cannot be neglected. Furthermore, the dissociation of ice mantle by cosmic-ray induced photons generates atomic hydrogen, which enhances its gas phase abundance significantly in the late stage.

We note that, at a time of about 5×10^4 years, the abundances of several species change very quickly, and the abundances of some other species show a spike-like feature. At first sight this may resemble an erroneous behavior caused by the differential equation solver, so we ran the model with the same parameters using a Monte Carlo code (also used for benchmark purpose in Du & Parise 2011), which is free of such problems, and it turns out that these features are genuine. A semi-quantitative explanation of this feature is in appendix 5.A.

5.3.2 Chemical age versus dynamical time scale

As noted before, the time of the closest agreement between our modeling results and the observational results of Bergman et al. (2011a,b) is at $\sim6\times10^5$ year. Interestingly, this time scale is quite close to those derived in André et al. (2007) (their Table 7). For example, the evolution time scale for ρ Oph A as estimated to be three times the free-fall time is $(0.5 - 2)\times10^5$ years, which is close to the statistically estimated age, while the collisional time scale of 5.5×10^5 years and the cross time scale of 8×10^5 years are also within the same order of magnitude.

It is important to define the starting point when talking about age. In the chemical evolution model described above, the whole system starts to evolve from a simple initial state where all the elements except for hydrogen are in atomic form, and the grains are bare. How relevant is such an initial condition when we talk about the dynamical evolution of a cloud condensation? At a density of $\sim 10^3$ cm^{-3}, a temperature of $\sim$20 K, and a visual extinction of 2, which are typical of diffuse or translucent molecular clouds, a chemical model starting from an atomic initial condition (except for H_2) reaches steady state for most of the species in several 10^3 years. Because such a time scale is much shorter than the dynamical time scale of a cloud, it should not make much difference for a time-dependent model (i.e. one in which temperature and density etc. vary with time) to use either atomic or molecular initial conditions. For a time-independent cloud model (such as the one we are using) with constant physical conditions, adopting an atomic initial condition and a high density is equivalent to assuming that the cloud was compressed from the diffuse ISM very quickly. Converging flows in the ISM might play such a role, although this seems unlikely in ρ Oph A because only a very small velocity gradient was observed (André et al. 2007).

However, the time of best match and the predicted abundances may also be very dependent on the value adopted for some of the modeling parameters that are not very well constrained. It is necessary to see how the results would be changed if these parameters are varied.

5.3.3 Effects of changing the energy barrier of the surface reaction $H + O_2 \rightarrow HO_2$

The activation barrier of reaction (5.3) was set to 1200 K in Tielens & Hagen (1982), which was taken from the theoretical calculation by Melius & Blint (1979) for the gas phase case. Cuppen et al. (2010) conclude that this reaction has a negligible barrier. We choose to use an intermediate value for the energy barrier of reaction (5.3), namely, 600 K for the modeling. Here we study how the uncertainties in this parameter would affect the abundances of several species of interest.

In Fig. 5.2 the abundances of several species at the best-match time (6×10^5 yr) are plotted as a function of the activation energy barrier of reaction (5.3). The temperature and density are fixed at 21 K and 6×10^5 cm^{-3}, and the ratio between the diffusion energy barrier and the binding energy is set to 0.77.

The abundance of gas phase O_2 is not affected by changing the energy barrier of reaction (5.3) because its abundance is mainly determined by the gas phase production process $O + OH \rightarrow O_2 + H$ and adsorption. However, the abundance of grain surface O_2 increases by five orders of magnitude as the barrier changes from 0 to 1200 K, because reaction (5.3) is one of the main reactions for the consumption of grain O_2. However, even with a barrier of 1200 K for reaction (5.3), the abundance of O_2 on the grain at a late stage is too low to be detected. Although the rate coefficient of reaction (5.3) is reduced by six orders of magnitude when its barrier changes from 0 to 1200K, the abundance of O_2H on the grain does not change significantly. The reason is that when reaction (5.3) becomes slower, more O_2 will build up on the grain, compensating for the effect of increasing the barrier of reaction (5.3). The abundance of gas phase H_2O_2 does not change much either, as its abundance is mainly determined by accretion onto the grain, and production by

hydrogenation of O_2H followed by partial chemical desorption.

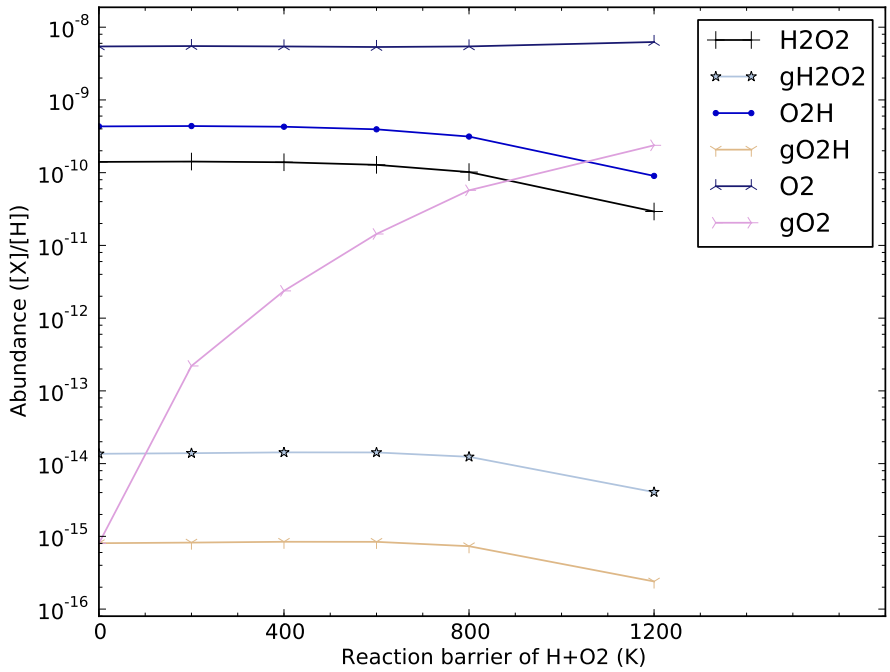

Figure 5.2: Dependence of the abundances of several species at the best-match time (6×10^5 yr) on the reaction barrier of reaction (5.3), with density fixed to 6×10^5 cm^{-3} and temperature fixed to 21 K.

5.3.4 Effects of changing the diffusion energy barriers

The diffusion energy barrier of a species on the grain determines how fast it can migrate on the grain, so it basically determines the pace of the grain chemistry. Usually it is set to a fixed fraction (here we denote it by η) of the binding energy of each species. The latter determines how fast a species evaporates into the gas phase. However, this parameter might depend on the material and morphology of the dust grain, as well as on the property of the adsorbate itself, so it is very uncertain. Values in the range of 0.3 – 0.77 have been adopted in the literature. We mainly used 0.77 for our modeling. Here we investigate how different values of η would affect the abundances of several species of interest.

In Fig. 5.3 we plot the abundances of several species at the time of best match (6×10^5 yr) as a function of the ratio between the diffusion barrier and binding energy (η). Changing this parameter has a strong effect on the abundances of some species. For example, the abundance of CO_2 ice is reduced with a higher η. This is because at the time of concern it mainly forms through the reaction OH + CO $\rightarrow$ CO_2 + H, which requires the migration of two relatively heavy species. With a low diffusion energy and a moderate temperature ($\sim$20 K), OH and CO can thermally hop quite fast, leading to a high abundance of CO_2,

which is not observed. However, if a lower temperature (∼10 K) is adopted, the problem becomes the opposite: the mobilities of OH and CO are so low that it is difficult for them to meet each other to form enough CO_2 ice, and some intricate mechanisms (e.g. three body reaction) have to be introduced to account for this (Garrod & Pauly 2011).

The abundance of H_2O ice increases as η increases. At this stage it is mainly formed by hydrogenation of OH. As the mobility of atomic hydrogen on the grain is not greatly affected by the value of the diffusion energy barrier because it is allowed to migrate through quantum tunneling, the reaction rate of $H + OH \rightarrow H_2O$ is not significantly affected by η; however, a larger η leaves more OH available for water because a lower amount of it is consumed in forming CO_2. This is also the reason for a higher CO (and species dependent on it such as H_2CO and CH_3OH) ice abundance when η is larger. The abundances of gas phase H_2O_2 and O_2H also increase for larger η, albeit only mildly.

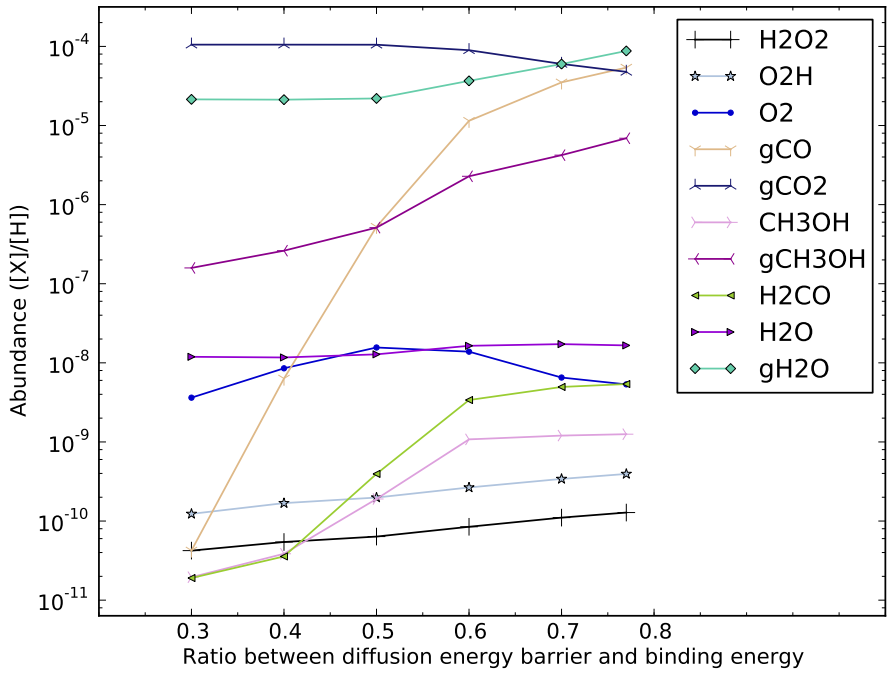

Figure 5.3: Dependence of the abundances of several species at the best-match time (6×10^5 yr) on the ratio between the diffusion and desorption energy, with density fixed to 6×10^5 cm^{-3} and temperature fixed to 21 K.

5.3.5 Dependence on the temperature and density

The physical conditions (temperature and density) of ρ Oph A are determined by non-LTE radiative transfer modeling (Bergman et al. 2011a), which is usually subject to uncertainties from many aspects, such as the excitation condition, source geometry, beam filling factor, etc. In this section we study how the uncertainties in the temperature and density of the system would affect the abundances of several species in our model. In

Figs. 5.4 and 5.6 we plot the abundances of several species at the time of best match (6×10^5 yr) as a function of temperature and density.

Apparently, temperature plays a much more drastic role than density. This is intuitively easy to understand because temperature enters the calculation of rates exponentially for the surface reactions. The general trend is that when the temperature is either too low or too high, the grain surface chemistry tends to be inactive or unimportant. In the former case the mobilities of species other than atomic hydrogen (which migrates through quantum tunneling in our present model) are low, while in the latter case the surface abundances of many species are low due to elevated evaporation rates.

As can be seen in Fig. 5.4, the abundance of CO ice starts to decrease at a temperature of around 20 K. This value can be estimated as the temperature at which the gas phase and grain surface abundance of CO are equal (see also Tielens & Hagen 1982), when only the adsorption and evaporation processes are taken into account (see also Hollenbach et al. 2009):

$$\begin{aligned} T_{\rm evap} &= E_{\rm D}/\ln\left[\frac{\nu}{n_{\rm H}\,R_{\rm G,n}}\frac{1}{\pi r^2}\frac{1}{\sqrt{8kT_{\rm gas}/\pi m}}\right] \\ &\simeq E_{\rm D}/\left\{60+\ln\left[\left(\frac{10^5\ {\rm cm}^{-3}}{n_{\rm H}}\right)\left(\frac{20\ {\rm K}}{T_{\rm gas}}\right)^{1/2}\left(\frac{m}{28\ {\rm au}}\right)^{1/2}\right]\right\}, \end{aligned} \tag{5.6}$$

where $E_{\rm D}$ is the evaporation energy barrier of a species on the grain surface, ν the vibrational frequency of a species on the grain, $R_{\rm G,n}$ the dust-to-gas number ratio, r the grain radius, while m is the molecular mass of the species being considered. A typical value of 10^{12} s^{-1} for ν, a dust grain radius of 0.1 μm, and a dust-to-gas ratio of 2.8×10^{-12} have been adopted in deriving the number 60. Since the logarithmic part in this equation is usually small for a typical gas density and temperature, the evaporation temperature can be approximated simply by $T_{\rm evap}\simeq E_{\rm D}/60$. For CO, a canonical value of $E_{\rm D}$ is 1210 K (Allen & Robinson 1977), which gives an evaporation temperature of 20 K, while for water, an $E_{\rm D}$ of 1860 K (Hasegawa & Herbst 1993a) on bare graphite grains gives an evaporation temperature of ∼30 K. In Garrod & Herbst (2006) a much higher desorption energy of 5700 K for water is used (appropriate for water ice), which gives a evaporation temperature of ∼95 K, close to the observed evaporation temperature of water in envelopes surrounding protostars (Maret et al. 2002). The evaporation temperature of CH_4 ice is close to that of CO ice. The evaporation time scale at the evaporation temperature can be estimated to be roughly $\nu^{-1}\exp(E_{\rm D}/T_{\rm evap})\simeq 10^{-12}e^{60}$ s $\simeq 3.6\times10^6$ yr. For higher temperature, the evaporation will be much faster.

The abundance of CO_2 ice initially increases with increasing temperature. This is because it mainly forms from the reaction CO + OH → CO_2 + H with a barrier of 80 K, and an increase in temperature greatly enhances the mobility of the reacting species, as well as the probability of overcoming the reaction barrier. But when temperature increases more, the abundance of CO ice becomes so low that the CO_2 abundance also drops. The evaporation temperature of CO_2 is about 40 K, so evaporation is not responsible for the decline in CO_2 ice abundance seen in Fig. 5.4. A similar trend is seen in other species, such as H_2CO ice, CH_3OH ice, as well as gas phase H_2O_2, CH_3OH, H_2CO, and H_2O. On the other hand, for species efficiently produced in the gas phase, e.g. O_2, its abundance increases with temperature owing to the faster evaporation at a higher temperature.

The abundances of gas phase H_2O_2, CH_3OH, CO, and O_2 have a sensitive dependence on temperature at around 21 – 24 K as seen from Fig. 5.4. For example, changing the temperature from 20 K to 22 K increases the abundance of H_2O_2 at a given time (6×10^5 yr) by about one order of magnitude. This rather small change of 2 K in temperature is normally below the accuracy of the kinetic temperature as determined from observational data. The dependence of the evolution curves of H_2O_2 and CH_3OH on temperature can be seen more clearly in Fig. 5.5. Changing the temperature not only shifts the evolution curves horizontally, it also changes their shapes significantly. We can see that, although for CH_3OH it is possible to match the observed abundance at multiple stages, for H_2O_2 the best match is only possible at 3×10^5 – 10^6 yr (if we ignore the match in the very early stage).

Regarding the density dependence, Fig. 5.6 shows that the abundances of the gas phase species at 6×10^5 yr generally decrease with increasing density, because the accretion of molecules onto the dust grains is faster for a higher density. This does not necessarily mean that the abundances of the surface species always increase with density. For example, the abundances of CH_4 ice and CH_3OH ice decrease with higher density, while the abundance of H_2CO ice has the opposite trend. One important factor is the time when we look at the system. In Fig. 5.7 we plot the abundances of H_2CO ice and CH_3OH ice as a function of time for different densities, while the temperature is fixed at 21 K. It can be seen that at a given time, the abundances of H_2CO ice or CH_3OH ice can either increase or decrease when the density is increased. We note that the evolution curves of these species have a quasi-oscillatory feature. For the same species, the evolution curves have a similar shape for different densities, except that with a lower density the evolution is slower and thus the curves are shifted toward the right.

5.3.6 Discussions and limits of the model

It can be seen from Figs. 5.1, 5.6, and 5.5 that H_2O_2 can be produced with a rather high abundance at certain evolutionary stages or with certain physical parameters, which is frequently higher than the currently observed value (Bergman et al. 2011b), especially in the early-to-intermediate times ($\sim10^3$ – 10^5 yr). One natural question to ask is why H_2O_2 has not been commonly detected in the ISM. One possibility is that its spectral lines have been overlooked in the past. Another simple explanation would be that it is overproduced in our model, because in the past the chemistry of H_2O_2 (as well as O_2H and O_3, etc.) may not have been studied in detail in the astrochemistry context (especially the destruction reactions in the gas phase), so that its destruction routes might be incomplete. For example, there is no reaction in which H_2O_2 is destroyed by reacting with H_3^+ in the current mainstream gas phase chemical networks. As a rough estimate, if we take the rate of destruction by such a reaction to be the same as the rate of the reaction $H_3^+ + H_2O \rightarrow H_3O^+ + H_2$, then the abundance of gas phase H_2O_2 can be reduced by about one order of magnitude. Further theoretical/experimental studies of the H_2O_2 chemistry would thus be very helpful, given that it has been detected recently and it plays a potentially important role in the grain chemistry of water. A third possibility is that the rarity of H_2O_2 might be an age effect. From Fig. 5.5 we notice that the abundance of H_2O_2 is only very high in a relatively early stage (before $\sim5\times10^5$ yr). If for certain reasons most of these cloud cores that are being observationally studied are older than this (due

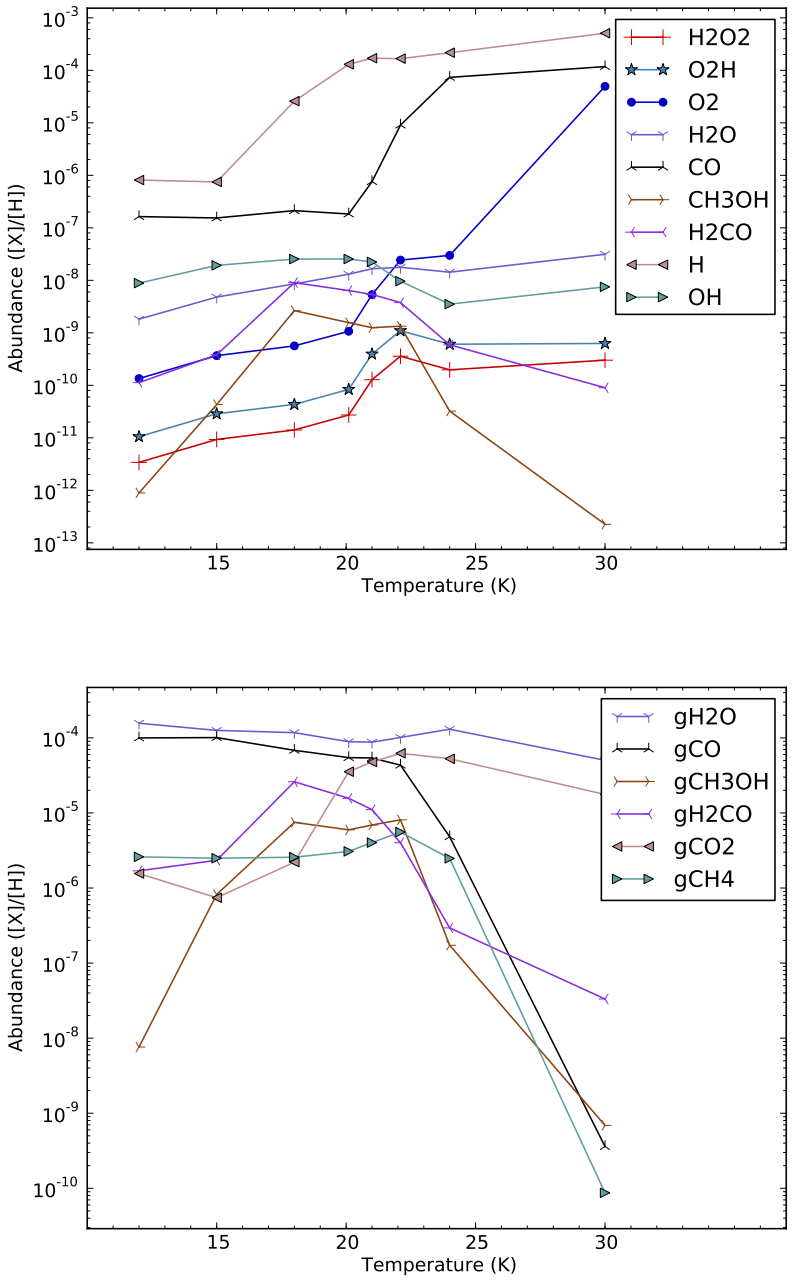

Figure 5.4: Dependence of the abundances of several species at the time of best match (6×10^5 yr) on temperature, with density fixed to 6×10^5 cm^{-3}. Top panel: gas phase species; bottom panel: surface species.

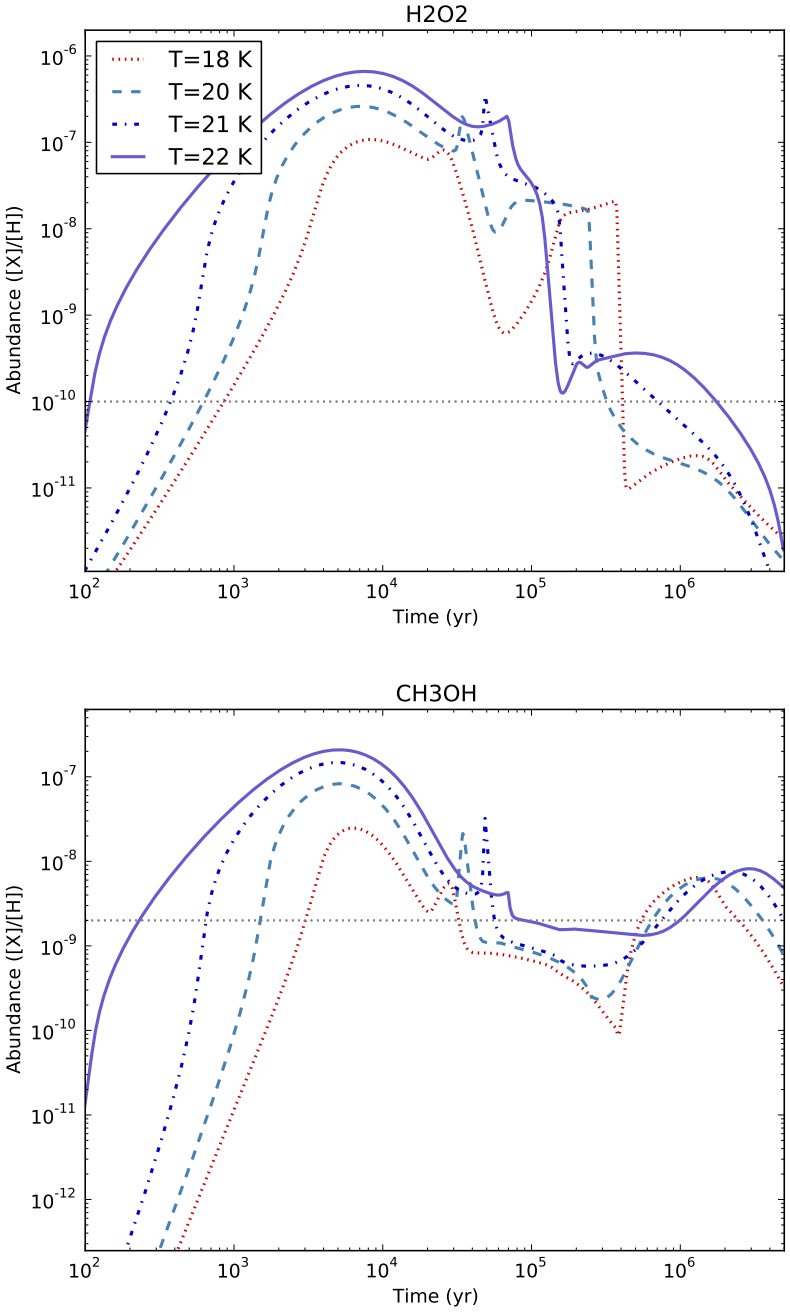

Figure 5.5: The abundances of gas phase H_2O_2 and CH_3OH as a function of time for different temperatures. The density is fixed to $6{\times}10^5$ cm^{-3}. The horizontal dotted lines mark the observed abundances of the corresponding species.

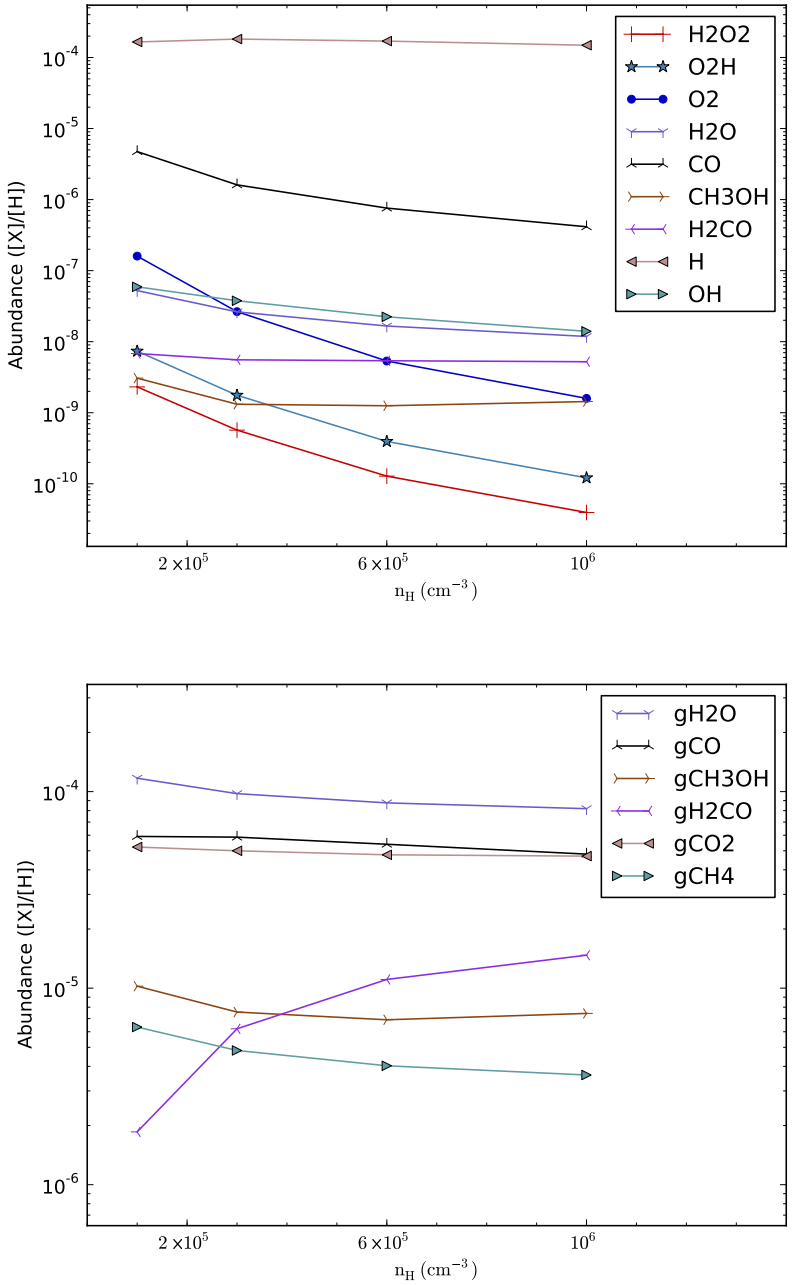

Figure 5.6: Dependence of the abundances of several species at the time of best match (6×10^5 yr) on n_H, with temperature fixed to 21 K. Top panel: gas phase species; bottom panel: surface species.

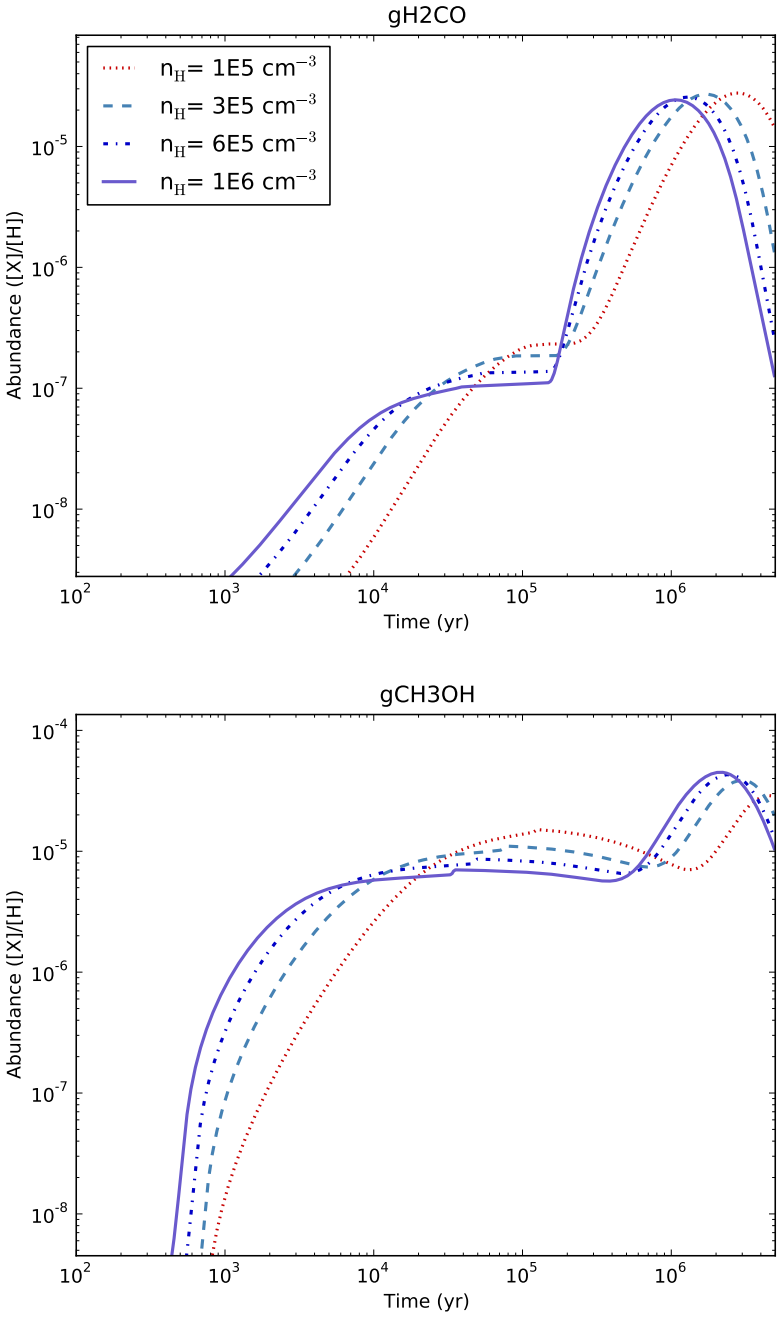

Figure 5.7: The abundances of H_2CO and CH_3OH ice as a function of time for different densities. The temperature is fixed to 21 K.

to some selection effects), then the H_2O_2 abundance in these objects would be too low to detect. Basically, at least three physical parameters are relevant, namely age, density, and temperature. A probability distribution of these three parameters of the cloud cores would help to give the detection probability of H_2O_2 (and any other molecules). Thus ρ Oph A may be considered special in the sense that it has a relatively high density ($\sim 10^6$ cm^{-3}) and temperature (20 – 30 K), while most dark clouds with a high density ($\gtrsim 10^4$ cm^{-3}) tend to be very cold ($\lesssim$15 K) (Bergin & Tafalla 2007). An inhomogeneous physical condition would make the situation more complex, which may require a self-consistent dynamical-chemical model. However, a thorough study of these possibilities has to be left to future work.

On the other hand, although CH_3OH has been studied quite extensively in the past, we notice that the gas phase reactions associated with it contain some important (although not decisive) differences between the OSU09 network and the UMIST RATE06 network. For example, the reaction between CH and CH_3OH to form CH_3 and H_2CO has a rate $2.49\times10^{-10}(T/300)^{-1.93}$ in the UMIST RATE06 network, but it does not exist in the OSU09 network. One possible problem is that the temperature of cold ISM (at most several tens of Kelvins) is out of the indicated valid range for many reactions in RATE06, and it is not clear how to extrapolate these reaction rates correctly, although we have closely followed the instructions in Woodall et al. (2007). In our modeling we have been using the RATE06 network.

The energy barriers for the hydrogenation of CO and H_2CO on the grain are both taken to be 2500 K. Woon (2002) calculated the barrier heights of these two reactions, giving a value of ∼2740 K and 3100 K in the case three water molecules are present, with zero-point energy corrections added. If these values are adopted, then the observed abundances of H_2CO and CH_3OH can only be reproduced within one order of magnitude at best. However, Goumans (2011) gives a lower barrier height (∼2200 K) for the hydrogenation of H_2CO, which would give better agreement with the observational results than if Woon (2002) were used in our model.

The chemical desorption is very important for the abundances of the gas phase H_2O_2 and CH_3OH. However, the efficiency of this mechanism (the "a" parameter in Garrod et al. 2007) is uncertain. Garrod & Pauly (2011) adopt a low value of 0.01 for it, to avoid overproduction of some gas phase species (Garrod et al. 2007). We use a value of 0.1 in our study, and the abundances of H_2CO and CH_3OH are not overproduced, except possibly in the early stages of the evolution. We note that the temperature and density of major concern in our study is around 20 K and 6×10^5 cm^{-3}, while in Garrod et al. (2007) the temperature is set to 10 K and density to 2×10^4 cm^{-3}. As a test we ran our model with the latter physical condition, and in this case CH_3OH and H_2CO are indeed overproduced by about one order of magnitude. Thus it seems that the efficiency of chemical desorption depends on the temperature of the dust grain, in the sense that at higher temperature the probability that the product of a surface exothermic reaction gets ejected to the gas phase is higher. However, a detailed study of this possibility is beyond the scope of the present paper.

Regarding the formation of water ice, Bergin et al. (1998) propose an interesting mechanism in which water is first formed in the high-temperature shocked gas, and then gets adsorbed onto the dust grains in the post-shock phase. This mechanism may act as an alternative or supplement to the grain chemistry route. It is not our aim here to

discuss to what extent this mechanism contributes to the water ice budget. However, we point out that even with a temperature 1000 – 2000 K, the amount of H_2O_2 produced in a pure gas phase chemistry (using the UMIST RATE06 network) is still much lower than the detected level.

5.4 Conclusions

- With a gas-grain chemical model that properly takes the desorption of grain surface species by the heat released by chemical reactions into account, we reproduced the observed abundances of H_2O_2 in ρ Oph A at a time of $\sim 6\times10^5$ yr. The solid phase H_2O_2 abundance is very low at this stage. However, a H_2O_2 to H_2O ratio of a few percent might be obtained in the solid phase if the layered structure of grain mantle is considered.

- The abundances of other species such as H_2CO, CH_3OH, and O_2 detected in the same object can also be reasonably reproduced at a time of $\sim 6\times10^5$ yr. Such a time scale is consistent with the evolution time scale estimated through dynamical considerations.

- The O_2H radical is a precursor of H_2O_2 on the dust grain, and we predict that it has a gas-phase abundance with the same order-of-magnitude of H_2O_2 and should thus be detectable. Observational searches for it are under way.

- For physical conditions relevant to ρ Oph A, water is mainly in solid form, being the dominant grain mantle material. Its gas phase abundance is only on the order of 10^{-8} according to our model.

- We note that the abundance of gas-phase H_2O_2 in our model results can be much higher than the current observed level for a range of physical conditions. This may suggest that its gas-phase destroying channels are incomplete. Due to the potentially important role played by H_2O_2 in the formation of water, its reaction network needs to be studied more thoroughly in the future.

  Other uncertainties in our modeling include the ratio between the diffusion energy barrier to the binding energy of a species on the grain surface, the activation energy barriers of certain key reactions, and the efficiency of the chemical desorption mechanism. In the present work we mainly make use of their canonical values or of values that give good matches to the observational results, and we also vary them to see the effects on the resulting abundances, which are significant in many cases.

5.A An explanation of the spike-like features in the evolution curves

In Fig. 5.1 we note that at a time of $\sim 5\times10^4$ yr a spike-like feature appears in the evolution curves of some species (e.g. gas phase H_2O_2 and CH_3OH), while the abundances of some other species (e.g. H_2O_2 and O_2 on the grain) change very rapidly at the same time. These features might appear to be caused by faults in the program for solving the set

of differential equations. However, after solving the same problem with the Monte Carlo method, which is immune to such numerical instabilities, we find that these features are still present, indicating that they are genuine. How could a smooth ordinary differential equation system generate such an almost-singular feature? In Fig. 5.8 we make a zoom-in of Fig. 5.1 (with several species added and several species removed). It can be seen that, although the time scale of the spike-like feature is relatively short, the evolution is always smooth (except the discreteness caused by the finite sampling of the curve). Then what determines the appearance of such a feature?

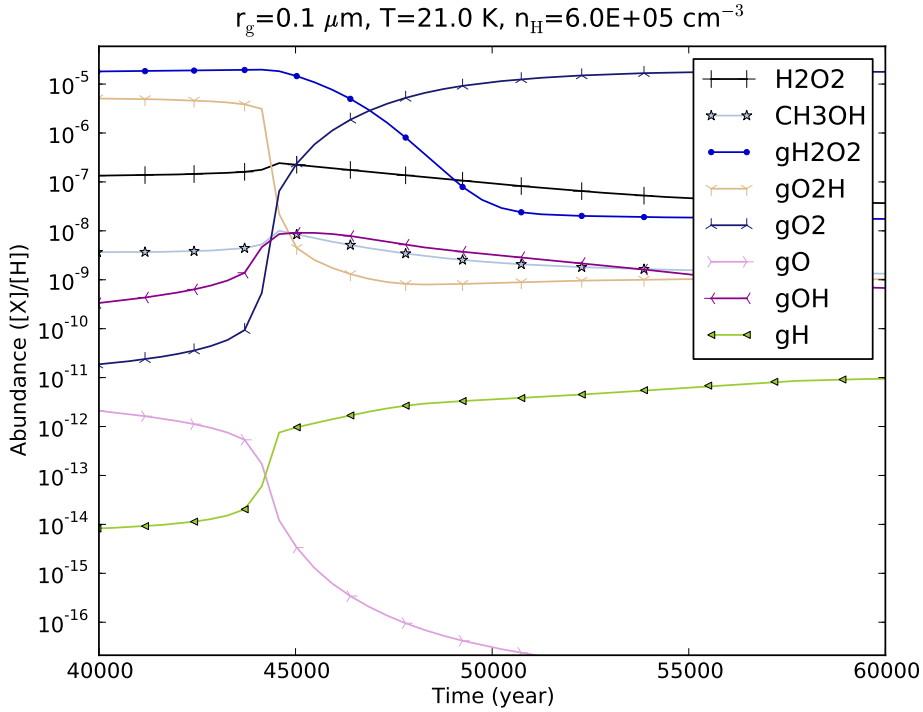

Figure 5.8: A zoom-in plot of Fig. 5.1 (with several species removed and several added), focusing on the spike-like feature (though nothing looks like a spike anymore). The abundance of gH has been multiplied by a factor of 10^{12} (to make the plot look more compact).

Because atomic hydrogen is central to the surface chemistry, we first look at the most important reactions governing its abundance on the grain. The main reactions consuming atomic hydrogen on the grains are (in the following a species name preceded by a "g" means a species on the grain, otherwise it is in the gas phase),

$$\mathrm{gH} + \mathrm{gO_2H} \xrightarrow{k_1} \begin{cases} \mathrm{gOH} + \mathrm{gOH}, \\ \mathrm{gH_2O_2}, \\ \mathrm{OH} + \mathrm{OH}, \\ \mathrm{H_2O_2}, \end{cases} \tag{5.7}$$

$$\mathrm{gH} + \mathrm{gH_2O_2} \xrightarrow{k_2} \begin{cases} \mathrm{gH_2O} + \mathrm{gOH}, \\ \mathrm{H_2O} + \mathrm{OH}, \end{cases} \tag{5.8}$$

while others such as the reactions with $\mathrm{gO_3}$ and $\mathrm{gCH_2OH}$ are relatively unimportant in the early times. It is mainly produced by

$$\mathrm{H} \xrightarrow{\mathrm{k_3}} \mathrm{gH}, \tag{5.9}$$

$$\mathrm{gOH} + \mathrm{gCO} \xrightarrow{\mathrm{k_4}} \mathrm{gCO_2} + \mathrm{gH}, \tag{5.10}$$

$$\mathrm{gH_2O} \xrightarrow{\mathrm{k_5}} \mathrm{gOH} + \mathrm{gH}. \tag{5.11}$$

As the abundance of atomic H in the gas phase and the abundance of gCO and $\mathrm{gH_2O}$ change relatively smoothly, they can be viewed as constant on a short time scale. The main reactions for the consumption and production of gOH are

$$\mathrm{gO} + \mathrm{gOH} \xrightarrow{k_6} \begin{cases} \mathrm{gO_2H}, \\ \mathrm{O_2H}, \end{cases} \tag{5.12}$$

$$\mathrm{gCO} + \mathrm{gOH} \xrightarrow{k_7} \begin{cases} \mathrm{gCO_2} + \mathrm{gH}, \\ \mathrm{CO_2} + \mathrm{H}, \end{cases} \tag{5.13}$$

$$\mathrm{gH} + \mathrm{gO_2H} \xrightarrow{k_8} \mathrm{gOH} + \mathrm{gOH}, \tag{5.14}$$

$$\mathrm{gH} + \mathrm{gH_2O_2} \xrightarrow{k_9} \mathrm{gH_2O} + \mathrm{gOH}, \tag{5.15}$$

$$\mathrm{gH_2O} \xrightarrow{k_{10}} \mathrm{gH} + \mathrm{gOH}. \tag{5.16}$$

From the above reaction list we may write the evolution equation of gH and gOH as[6]

$$\begin{aligned} \partial_t \mathrm{gH} = &- k_1 \mathrm{gH gO_2H} - k_2 \mathrm{gH gH_2O_2} \\ &+ k_3 \mathrm{H} + k_4 \mathrm{gOH gCO} + k_5 \mathrm{gH_2O}, \end{aligned} \tag{5.17}$$

$$\begin{aligned} \partial_t \mathrm{gOH} = &- k_6 \mathrm{gO gOH} - k_7 \mathrm{gCO gOH} \\ &+ 2k_8 \mathrm{gH gO_2H} + k_9 \mathrm{gH gH_2O_2} + k_{10} \mathrm{gH_2O}, \end{aligned} \tag{5.18}$$

or in a more succinct form

$$\begin{aligned} \partial_t \mathrm{gH} =& \kappa_1 \mathrm{gH} + \kappa_2 \mathrm{gOH} + b_1, \\ \partial_t \mathrm{gOH} =& \kappa_3 \mathrm{gH} + \kappa_4 \mathrm{gOH} + b_2, \end{aligned} \tag{5.19}$$

where

$$\begin{aligned} \kappa_1 =& - k_1 \mathrm{gO_2H} - k_2 \mathrm{gH_2O_2}, \\ \kappa_2 =& k_4 \mathrm{gCO}, \\ \kappa_3 =& 2k_8 \mathrm{gO_2H} + k_9 \mathrm{gH_2O_2}, \\ \kappa_4 =& - k_6 \mathrm{gO} - k_7 \mathrm{gCO}, \\ b_1 =& k_3 \mathrm{H} + k_5 \mathrm{gH_2O}, \\ b_2 =& k_{10} \mathrm{gH_2O}. \end{aligned}$$

[6] Here for brevity we use the name of a species to denote its average population on a single grain; for example, if gCO=100, it means on average there are 100 CO molecules on a single grain.

If we view κ_1 – κ_4, as well as b_1 and b_2, as constants (of course they are not), then Eq. (5.19) can be solved exactly; the solution contains an exponential part and a constant part. The amplitude of the exponential part will be inversely proportional to the determinant of the coefficient matrix

$$\det(\kappa) = \begin{pmatrix} \kappa_1 & \kappa_2 \\ \kappa_3 & \kappa_4 \end{pmatrix}.$$

Since κ_1 – κ_4 are not really constant in our problem, we expect that when they become such that $\det(\kappa)$ is close to zero, a spike-like or jump-like behavior would appear. Namely, we require

$$\begin{aligned} \frac{\kappa_1\kappa_4}{\kappa_2\kappa_3} =& \frac{(k_1\mathrm{gO_2H} + k_2\mathrm{gH_2O_2})(k_6\mathrm{gO} + k_7\mathrm{gCO})}{(k_4\mathrm{gCO})(2k_8\mathrm{gO_2H} + k_9\mathrm{gH_2O_2})} \\ \simeq& \frac{\mathrm{gO_2H/gH_2O_2} + 1}{1.2\mathrm{gO_2H/gH_2O_2} + 1} \times \left(2.5 \times 10^8 \mathrm{gO/gCO} + 1\right) \\ \simeq& 1. \end{aligned} \tag{5.20}$$

The actual value of the parameters have been inserted in the second line of the above equation. These parameters depend on the physical conditions.

To satisfy this condition (at least approximately), gO/gCO should be very small. In Fig. 5.9 the ratio $(\kappa_1\kappa_4)/(\kappa_2\kappa_3)$ and the value of 2.5×10^8gO/gCO are plotted as a function of time. The abundances of O, gO, gO_2, gH, and gOH are also plotted for reference (not to scale). It can be seen that the $(\kappa_1\kappa_4)/(\kappa_2\kappa_3)$ ratio does decrease, and it approaches a value of unity before the time of the spike/jump feature, and the gO/gCO ratio drops to a very low value monotonically.

The above mathematical argument can also be understood intuitively. When the gO abundance is so low that reaction (5.12) can be neglected, gOH is only destroyed by reaction (5.13). Each time a gOH radical is consumed, one gH is created (if we neglect the desorption process), and this gH will quickly react with gH_2O_2 or gO_2H to create one or two gOHs. There will then be a net gain in the gOH abundance, leading to its fast growth, and the gH abundance will increase accordingly. Thus we see that reaction (5.14) is crucial in that it produced two gOH radicals by consuming only one gH.

Therefore for such a spike-like feature to occur, the abundance of gO must decrease to a low value such that the reaction between gOH and gO becomes unimportant for consuming gOH. Namely, we require $[\mathrm{gO}] \lesssim [\mathrm{gCO}]\ \mathrm{k_7/k_6} \simeq 5 \times 10^{-13}$. The abundances of atomic oxygen in the gas phase and on the grain surface are related by $\mathrm{O/gO} \simeq k_{\mathrm{evap}}(\mathrm{gO})/k_{\mathrm{ad}}(\mathrm{O}) \simeq 3\times10^6$, so equivalently we require $[\mathrm{O}] < 1.5 \times 10^{-6}$ (i.e., about a factor of 200 less than the initial O abundance) at the time of the spike-like feature. Atomic oxygen is mainly consumed on the grain surface by reacting with another gO to form gO_2 (for $t \lesssim 10^3$ yr) or by reacting with gOH to form gO_2H. Only the latter is relevant here. As the abundance of gOH does not change much before the spike-like feature, the time scale for the consumption of atomic oxygen can be estimated to be $\ln 200 \times (\mathrm{O/gO})/(k_6\mathrm{gOH}) \simeq 10^5$ yr, which is on the same order of magnitude as the time of occurrence of the spike-like feature.

The time scale for the endurance of the spike-like feature itself can be estimated to be the time scale for the exhaustion of gO_2H or gH_2O_2 (so that Eqs. (5.17) and (5.18) do not hold anymore) by reacting with gH, which is

$$1/(k_1\mathrm{gH}) \simeq 10^3 \text{ yr},$$

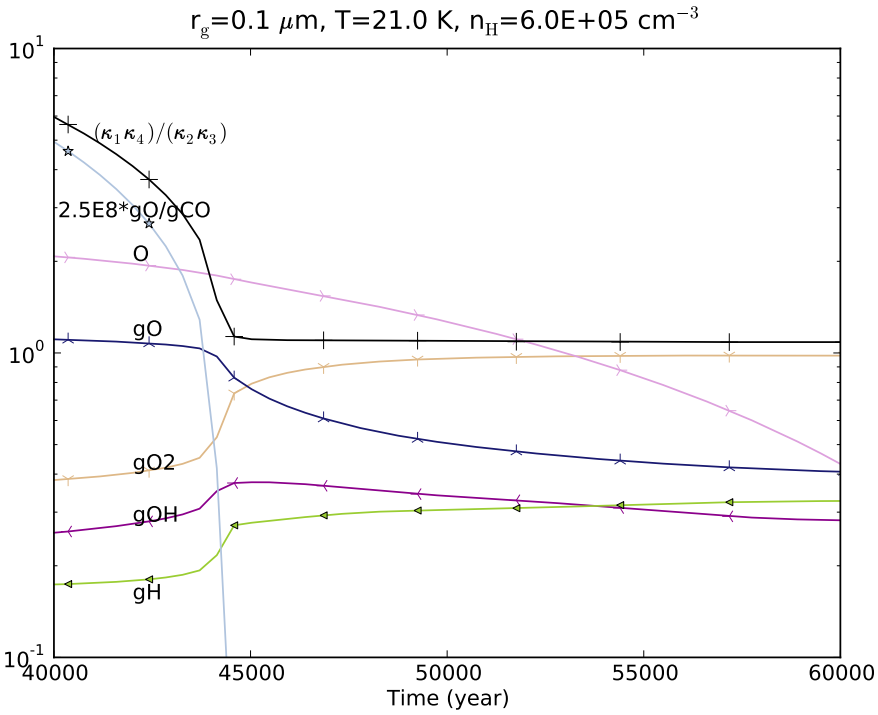

Figure 5.9: The ratio $(\kappa_1\kappa_4)/(\kappa_2\kappa_3)$ and the value of $2.5\times10^8\times$gO/gCO as a function of time. They are to scale. The abundances of several other species are plotted only for reference (not to scale).

where the gH population (the average number of atomic H on a single grain) is taken to be a median value (10^{-14}) during the rapidly varying period. That equation (5.20) seems to hold after this period (see Fig. 5.9) does not mean that gH will keep increasing rapidly, simply because the premise of our argument, namely Eqs. (5.17) and (5.18) are not a good description of the evolution of gH and gOH anymore.

As the abundance of H on the grain increases, almost all the O_3 on the grain are converted into O_2 and OH. O_2 molecules on the grain are then consumed by the slower reaction $gH + gO_2 \rightarrow gO_2H$, with a time scale $\sim10^5$ yr. This explains the prominent peak in the evolution curve of gO_2 (see Fig. 5.1).

Would the spike-like feature have any practical significance (especially observationally)? Ideally, such a short-time feature may be used to constrain the age of a dense cloud, by distinguishing the abundances of certain species between their early-time values (before the spike-like feature) and late-time values (after the spike-like feature). However, due to its dependence on the reaction network being used, which usually contains a lot of uncertainties and is subject to change when new experiments are carried out, the question whether this feature is really relevant for the study of ISM can only be answered by future investigations.

5.B The surface reaction network used in this work

References. HHL92: Hasegawa et al. (1992); ICet10: Ioppolo et al. (2010); CIRL10: Cuppen et al. (2010); ICet08: Ioppolo et al. (2008); G11: Goumans (2011); FCet09: Fuchs et al. (2009) GWH08: Garrod et al. (2008); AR77: Allen & Robinson (1977); TH82: Tielens & Hagen (1982); GMet08: Goumans et al. (2008); ABet04: Atkinson et al. (2004); RH00: Ruffle & Herbst (2000); RH01: Ruffle & Herbst (2001b);

Table 5.1: The surface network used in this work. The photodissociation reactions induced by cosmic rays and the chemical desorption reactions are not included here.

Num	Reaction	Branching ratio	Energy barrier (K)	Reference
1	$H + H \rightarrow H_2$	1.0	0.0	HHL92
2	$H + O \rightarrow OH$	1.0	0.0	ICet10
3	$H + O_2 \rightarrow O_2H$	1.0	600.0	Estimated
4	$H + O_3 \rightarrow O_2 + OH$	1.0	200.0	Estimated
5	$H + OH \rightarrow H_2O$	1.0	0.0	ICet10
6	$H + O_2H \rightarrow H_2O_2$	0.38	0.0	CIRL10
7	$H + O_2H \rightarrow OH + OH$	0.62	0.0	CIRL10
8	$H + H_2O_2 \rightarrow H_2O + OH$	1.0	92.0	ICet08
9	$H + CO \rightarrow HCO$	0.5	2500.0	GWH08
10	$H + HCO \rightarrow H_2CO$	1.0	0.0	FCet09
11	$H + H_2CO \rightarrow CH_3O$	0.5	2500.0	RH00
12	$H + H_2CO \rightarrow HCO + H_2$	0.5	3000.0	G11
13	$H + CH_3O \rightarrow CH_3OH$	1.0	0.0	FCet09
14	$H + CH_2OH \rightarrow CH_3OH$	1.0	0.0	GWH08
15	$H + HCOO \rightarrow HCOOH$	1.0	0.0	AR77
16	$H + C \rightarrow CH$	1.0	0.0	AR77
17	$H + CH \rightarrow CH_2$	1.0	0.0	AR77
18	$H + CH_2 \rightarrow CH_3$	1.0	0.0	AR77
19	$H + CH_3 \rightarrow CH_4$	1.0	0.0	AR77
20	$H + N \rightarrow NH$	1.0	0.0	AR77
21	$H + NH \rightarrow NH_2$	1.0	0.0	AR77
22	$H + NH_2 \rightarrow NH_3$	1.0	0.0	AR77
23	$H + S \rightarrow HS$	1.0	0.0	HHL92
24	$H + HS \rightarrow H_2S$	1.0	0.0	HHL92
25	$H + H_2S \rightarrow HS + H_2$	1.0	860.0	TH82
26	$H + CS \rightarrow HCS$	1.0	0.0	HHL92
27	$C + S \rightarrow CS$	1.0	0.0	HHL92
28	$O + S \rightarrow SO$	1.0	0.0	HHL92
29	$O + SO \rightarrow SO_2$	1.0	0.0	HHL92
30	$O + CS \rightarrow OCS$	1.0	0.0	HHL92
31	$H + CN \rightarrow HCN$	1.0	0.0	AR77
32	$H + NO \rightarrow HNO$	1.0	0.0	AR77
33	$H + NO_2 \rightarrow HNO_2$	1.0	0.0	AR77
34	$H + NO_3 \rightarrow HNO_3$	1.0	0.0	AR77

Table 5.1: continued.

Num	Reaction	Branching ratio	Energy barrier (K)	Reference
35	$H + N_2H \rightarrow N_2H_2$	1.0	0.0	AR77
36	$H + N_2H_2 \rightarrow N_2H + H_2$	1.0	650.0	HHL92
37	$H + NHCO \rightarrow NH_2CO$	1.0	0.0	AR77
38	$H + NH_2CO \rightarrow NH_2CHO$	1.0	0.0	AR77
39	$N + HCO \rightarrow NHCO$	1.0	0.0	AR77
40	$CH + CH \rightarrow C_2H_2$	1.0	0.0	HHL92
41	$O + O \rightarrow O_2$	1.0	0.0	AR77
42	$O + O_2 \rightarrow O_3$	1.0	0.0	ABet04
43	$O + CO \rightarrow CO_2$	1.0	1580.0	GMet08
44	$O + HCO \rightarrow HCOO$	0.5	0.0	GMet08
45	$O + HCO \rightarrow CO_2 + H$	0.5	0.0	GMet08
46	$O + N \rightarrow NO$	1.0	0.0	AR77
47	$O + NO \rightarrow NO_2$	1.0	0.0	AR77
48	$O + NO_2 \rightarrow NO_3$	1.0	0.0	AR77
49	$O + CN \rightarrow OCN$	1.0	0.0	AR77
50	$C + N \rightarrow CN$	1.0	0.0	AR77
51	$N + N \rightarrow N_2$	1.0	0.0	AR77
52	$N + NH \rightarrow N_2H$	1.0	0.0	AR77
53	$H_2 + OH \rightarrow H_2O + H$	1.0	2100.0	ABet04
54	$OH + CO \rightarrow CO_2 + H$	1.0	80.0	RH01
55	$H + C_2 \rightarrow C_2H$	1.0	0.0	HHL92
56	$H + N_2 \rightarrow N_2H$	1.0	1200.0	HHL92
57	$H + C_2H \rightarrow C_2H_2$	1.0	0.0	HHL92
58	$H + HOC \rightarrow CHOH$	1.0	0.0	HHL92
59	$C + OH \rightarrow HOC$	0.5	0.0	HHL92
60	$C + OH \rightarrow CO + H$	0.5	0.0	HHL92
61	$CH + OH \rightarrow CHOH$	1.0	0.0	HHL92
62	$H + CHOH \rightarrow CH_2OH$	1.0	0.0	HHL92
63	$OH + OH \rightarrow H_2O_2$	1.0	0.0	HHL92
64	$OH + CH_2 \rightarrow CH_2OH$	1.0	0.0	HHL92
65	$C + C \rightarrow C_2$	1.0	0.0	HHL92
66	$C + O_2 \rightarrow CO + O$	1.0	0.0	HHL92
67	$O + CH \rightarrow HCO$	1.0	0.0	HHL92
68	$O + OH \rightarrow O_2H$	1.0	0.0	HHL92
69	$O + CH_2 \rightarrow H_2CO$	1.0	0.0	HHL92
70	$O + CH_3 \rightarrow CH_2OH$	1.0	0.0	HHL92
71	$C + O \rightarrow CO$	1.0	0.0	HHL92
72	$C + CH \rightarrow C_2H$	1.0	0.0	HHL92
73	$C + NH \rightarrow HNC$	1.0	0.0	HHL92
74	$C + CH_2 \rightarrow C_2H_2$	1.0	0.0	HHL92
75	$C + NH_2 \rightarrow HNC + H$	1.0	0.0	HHL92
76	$N + CH \rightarrow HCN$	1.0	0.0	HHL92
77	$N + NH_2 \rightarrow N_2H_2$	1.0	0.0	HHL92

Table 5.1: continued.

Num	Reaction	Branching ratio	Energy barrier (K)	Reference
78	O + NH $\rightarrow$ HNO	1.0	0.0	HHL92

5.C Enthalpies of the surface species

References.
BM02: Binnewies & Milke (1999);
NIST Webbook: `http://webbook.nist.gov/chemistry/`;
NCet10: Nagy et al. (2010);
K98: Kaiser et al. (1998);
VS91: Vandooren et al. (1991);
URL1: `http://chem.engr.utc.edu/webres/331f/teams-98/chp/Boiler%20DC/tsld007.htm`

Table 5.2: Enthalpies of the surface species considered in this work that are used to calculate the exoergicities of the surface reactions. The exoergicities are needed to calculate the rate of chemical desorption.

Num	Species	Enthalpy (kJ/mol)	Reference
1	C	716.7	NIST Webbook
2	CH	594.1	BM02, p238
3	CH_2	386.4	BM02, p240
4	CH_3	145.7	BM02, p241
5	CH_3O	17.0	NIST Webbook
6	CH_2OH	−9.0	NIST Webbook
7	CH_3OH	−201.2	BM02, p241
8	CH_4	−74.9	BM02, p241
9	CN	435.1	BM02, p247
10	CO	−110.5	BM02, p251
11	CO_2	−393.5	BM02, p251
12	CS	280.3	BM02, p253
13	H	218.0	BM02, p558
14	H_2	0.0	BM02, p568
15	H_2CO	−115.9	BM02, p240
16	H_2O	−241.8	BM02, p571
17	H_2O_2	−135.8	BM02, p572
18	H_2S	−20.5	BM02, p574
19	HCN	135.1	BM02, p239
20	HNC	135.1	Estimated
21	HCO	43.5	BM02, p239
22	HCOO	−386.8	URL1
23	HCOOH	−378.6	BM02, p240
24	HCS	296.2	K98
25	HNO	99.6	BM02, p563
26	HNO_2	−78.8	BM02, p563
27	HNO_3	−134.3	BM02, p563
28	HS	139.3	BM02, p567
29	N	472.7	BM02, p693
30	N_2	0.0	BM02, p699

Table 5.2: continued.

Num	Species	Enthalpy (kJ/mol)	Reference
31	N_2H	245.2	VS91
32	N_2H_2	213.0	BM02, p570
33	NH	376.6	BM02, p563
34	NH_2	190.4	BM02, p570
35	NH_2CHO	−186.0	NIST Webbook
36	NH_2CO	−13.1	NCet10
37	NH_3	−45.9	BM02, p577
38	NHCO	−101.7	BM02, p239
39	NO	90.3	BM02, p695
40	NO_2	33.1	BM02, p695
41	NO_3	71.1	BM02, p695
42	O	249.2	BM02, p733
43	O_2	0.0	BM02, p741
44	O_2H	2.1	BM02, p567
45	O_3	142.7	BM02, p752
46	OCN	159.4	BM02, p248
47	OCS	−138.4	BM02, p251
48	OH	39.0	BM02, p566
49	S	277.0	BM02, p811
50	SO	5.0	BM02, p736
51	SO_2	−296.8	BM02, p743
52	C_2	837.74	NIST Webbook
53	C_2H	476.98	NIST Webbook
54	C_2H_2	226.73	NIST Webbook

Chapter 6

Deuterium chemistry on dust grain surfaces

Part of the content of this chapter will be submitted to Astronomy & Astrophysics for publication.

Contents

This chapter is about our modeling study on the chemistry of species containing one or more deuterium atoms (we call these species "deuterated"). I begin with a discussion on the uniqueness of deuterium in a general context, followed by a brief review on previous studies on deuterium chemistry. Then I describe how we compile the gas and grain chemical network with deuterium included, and how we implement the "three-phase" gas-grain-mantle prescription. Finally the results and conclusions are presented.

6.1 Why is deuterium special

Besides the major isotope (denoted by ^{1}H and sometimes called protium), hydrogen has two other isotopes: deuterium (^{2}H) and tritium (^{3}H). Deuterium is stable, while tritium is radioactive with a half-life of ∼12.3 yr and decay products $^3_2\mathrm{He}^+ + \mathrm{e}^- + \bar{\nu}_\mathrm{e}$ (Simpson 1987). It is easier for the deuterium and tritium nuclei than the hydrogen nuclei to fuse with other light nuclei, because the presence of more neutrons in the nuclei increases the attractive strong force when they are close by, while the repulsive electrostatic force remains the same. Thus in the stars deuterium is the first to ignite (Clayton 1968). Except for the primordial nucleosynthesis at the beginning of the Universe through the

reaction p+n $\longrightarrow$ D+γ (Weinberg 2008), it is commonly believed that there is no efficient natural process to produce deuterium, so its overall abundance can only decrease with time. However, Mullan & Linsky (1999) challenged this idea by proposing that deuterium can be produced in stellar atmospheres (during a stellar flare for example), which as suggested by these authors might be one reason for the inhomogeneity and enhancement of the deuterium abundance.

The total abundance of deuterium in the early Universe would thus be expected to be higher than its current value if the mainstream assumption about its evolution is correct, i.e. the suggestion of Mullan & Linsky (1999) is disregarded for the moment. Fumagalli et al. (2011) measured the abundance of deuterium using absorption lines towards the sightlines of high-z quasars, obtaining [D/H] $\simeq 2.78\times10^{-5}$, providing a constraint on the baryon density parameter ($\Omega_{\rm b}$) in cosmology, which is consistent with an independent constraint from measurements of the anisotropies in the cosmic microwave background. Linsky et al. (2006) argued that the atomic [D/H] ratio representative of the region within 1 kpc[1] of the Sun $\geq 2.3\times10^{-5}$. By analyzing the solar wind composition, Geiss & Reeves (1972) estimated that the [D/H] ratio $\simeq 2.5\times10^{-5}$ in the proto-solar gas. In Jupiter and Saturn, the [D/H] ratio of H_2 molecules was measured with the Infrared Space Observatory (ISO) by Lellouch et al. (2001) to be $\sim 2.3\times10^{-5}$ and $\sim 1.7\times10^{-5}$, respectively. The [D/H] ratio in comet water was measured to be of the order $(1.5\text{–}3)\times10^{-4}$ (depending on the birth places of these comets) (Hartogh et al. 2011). In Earth's ocean the [D/H] ratio is $\sim 1/6700 \simeq 1.5\times10^{-4}$ (Friedman 1953), and varies slightly from place to place[2]. According to the review of Robert (2003), the overall [D/H] ratio in carbonaceous chondrites lies in the range $(1.2\text{–}3)\times10^{-4}$, and peaks at $\sim 1.5\times10^{-4}$.

Studies on the isotopic ratio of hydrogen and of many other elements in different types of terrestrial and celestial bodies play a vital role in understanding the origin and evolution of objects with vast diversity, from Earth's water, the Earth itself, the origin of biotic matter, to the origin of the solar system, and even to the origin of the Universe. For example, people use tritium (generated by nuclear weapon tests) to trace ocean circulation and ventilation (Jenkins & Smethie 1996); the $^{13}C/^{12}C$ ratio can be used to study the effects of human activities have on the Earth's atmosphere based on the discrimination against ^{13}C in plants (Ghosh & Brand 2003); the organic matter in chondrite meteorites was suggested by Sephton & Gilmour (2000) to have originated in interstellar space because of the ^{13}C and deuterium abundances; finally, the [D/H] ratio at an early cosmological age is a crucial parameter to constrain the baryon density of the Universe (see, e.g., Weinberg 2008).

The observed deuterium enrichment in many species (see the next section) is generally believed to be due to chemical fractionation, in which H and D atoms behave differently in chemical reactions. The effects of chemical fractionation can be distinguished from that of an overall increase in the deuterium abundance due to the mechanisms suggested by Mullan & Linsky (1999). In chemical fractionation, the [D/H] ratio of a species strongly depends on its formation route, while an overall increase in the deuterium abundance would not have such a dependence; thus if the observed deuterium enrichment is chemical in nature, one would expect different species to have different degrees of deuterium

[1] 1 pc $\simeq 3.1\times10^{18}$ cm

[2] In the "Vienna Standard Mean Ocean Water", the [D/H] ratio is 1.5576×10^{-4}; see `http://en.wikipedia.org/wiki/Vienna_Standard_Mean_Ocean_Water`.

enhancement, and the total deuterium abundance would be more or less the same for different regions of the interstellar space (if the consumption of deuterium in the stars is properly accounted for).

The chemical fractionation of the two stable isotopes of hydrogen (H and D) is special when compared to other elements because of their large mass ratio of 2, which is the largest among all elements. Such a large ratio leads to a large difference in the zero-point vibrational energies of deuterium and hydrogen, which is vital at very low temperatures. The difference in mass also causes a difference in their migration and tunneling rates on the dust grain surface, which affects their surface reaction rates. Replacing a hydrogen atom by a deuterium atom in a molecule can also change its energy levels and transition probabilities; for example, H_2 and CH_4 have no electric dipole moment, but HD and CH_3D do.

In this chapter I present a chemical model that takes into account both gas phase processes and reactions occurring on dust grain surfaces. The goal is to investigate to what extent can chemical processes lead to the differentiated distribution of deuterium atoms in various species in the ISM, specifically in dark cloud conditions. Note that the possibility that the atomic deuterium abundance might be enriched by processes in stellar atmosphere (Mullan & Linsky 1999) is not considered in the present work. In Section 6.2 I give a brief overview of previous studies on deuterium fractionation. In Section 6.3 I describe the gas phase reaction network, which is a subset of the UMIST RATE06 network[3] (Woodall et al. 2007) with deuterium added in, then in Section 6.4 I discuss the surface reaction network, especially on the key reactions for formaldehyde, methanol, and water. Our dust grain model takes into account the mantle structure, which is described in detail in Section 6.5. The results and conclusions are presented in Section 6.6.

6.2 Previous studies

Deuterium-containing molecules have been studied in the interstellar space for quite some time. The first one detected beyond our solar system was DCN (Jefferts et al. 1973; Wilson et al. 1973), observed in the Orion molecular cloud. These authors derived a [D/H] ratio of $\sim 6\times10^{-3}$, which they attributed to chemical fractionation. In particular they mentioned that the zero-point vibrational energy of DCN is much lower than that of HCN, which can cause deuterium enrichment, either in the gas phase or on dust grain surfaces, especially at low temperatures. Solomon & Woolf (1973) discussed the deuterium fractionation of HCN with the exchange reactions $\mathrm{HD+HCN} \rightleftharpoons \mathrm{H_2+DCN}$ and $\mathrm{D+HCN} \rightleftharpoons \mathrm{DCN+H}$, based only on energetic considerations. Namely, they claim (for the first reaction)

$$\frac{[\mathrm{DCN}]}{[\mathrm{HCN}]} = \frac{[\mathrm{HD}]}{[\mathrm{H_2}]} \exp\left(\frac{456}{T}\right) = \frac{2[\mathrm{D}]}{[\mathrm{H}]} \exp\left(\frac{456}{T}\right),$$

where the number 456 (K) is the exothermicity of the first reaction. Also based on such an energy argument, they inferred the possible enhancement of the ratio $[\mathrm{HD}]/[\mathrm{H_2}]$ relative to [D]/[H]. However, their arguments have been questioned by Watson (1974) and Brown (1977) due to the presence of activation barriers in those reactions. We may also note that

[3] http://udfa.net/

Watson (1973) proposed another mechanism to enhance the atomic [D/H] ratio (which can then be transferred to HCN and DCN), in which the HD molecule is more likely to be photo-dissociated (into H and D atoms) due to its lower degree of self-shielding than H_2. Such a mechanism may indeed be at work in certain situations. Finally, the lower [DCN/HCN] ratio towards the Galactic center relative to other regions was used by Penzias et al. (1977) to argue against the possibility that the observed deuterium enhancement is due to stellar processes.

DCO^+ was first detected by Hollis et al. (1976) and Guélin et al. (1977) in dark clouds. Watson (1977) and Watson et al. (1978) discussed the possibility of constraining the electron abundance in the ISM by measuring [DCO^+/HCO^+]. This idea is based on the assumption that DCO^+ is formed from $H_2D^+ + CO$, hence the ratio [DCO^+/HCO^+] reflects the ratio [H_2D^+/H_3^+], which is directly related to the electron abundance (hence to the degree of ionization). In this example we can see that the formation route of a specific molecule may provide useful information on certain physical parameters. Dalgarno & Lepp (1984) gave a similar discussion on [DCO^+/HCO^+] and used this ratio to give lower and upper limits on the overall [D/H] ratio.

The HD molecule was first detected by Spitzer et al. (1973) in UV absorption. Deuterated water (HDO) was first detected by Turner et al. (1975) in Orion KL, at an abundance of $\sim 10^{-8}$ relative to H_2, and deuterated ammonia (NH_2D) was first detected by Rodriguez Kuiper et al. (1978) also in this source. The first multiply-deuterated molecule discovered in the ISM is D_2CO, detected by Turner (1990) in the compact ridge component of Orion KL, with a relative abundance of [D_2CO]/[HDCO] $\simeq 0.02$, while [HDCO]/[H_2CO] $\simeq 0.1$. Based on simple equilibrium analysis, Turner concluded that H_2CO and its deuterated counterparts can be formed on dust grain surface. van der Tak et al. (2002) detected triply deuterated ammonia (ND_3) in NGC 1333 with an abundance of 3×10^{-12}–10^{-11}.

In a survey van Dishoeck et al. (1995) detected more than 40 molecules in the low mass proto-binary source IRAS 16293−2422, including many deuterated species, such as DCO^+, DCN, DNC, CCD, HDS, HDO, CH_3OD, etc. This source has a remarkably rich deuterium chemistry. For example, Ceccarelli et al. (1998), Loinard et al. (2000) and Ceccarelli et al. (2001) found high [HDCO/H_2CO] and [D_2CO/HDCO] ratios in it. Parise et al. (2002, 2004) detected doubly and triply deuterated methanol (CHD_2OH and CD_3OH) in this source, with abundances a few to ten percent of the main isotopologue. It has also been found that the D atom has a preference over the CH_3 group than the OH group in this source, so CH_2DOH is much more abundant than CH_3OD. The degree of deuteration of water is relatively low in comparison with methanol and formaldehyde. For example, the [HDO/H_2O] ratio in IRAS 16293−2422 was constrained by Parise et al. (2005) to be 3% in the inner hot region and $\leq$0.2% in the outer envelope, and Liu et al. (2011) found a similar [HDO/H_2O] ratio ($\gtrsim$1%) for the inner region of the low-mass protostar NGC1333-IRAS2A.

Besides the qualitative analysis in the early times, theoretical studies on deuterium chemistry include the gas phase models of Millar et al. (1989), Roberts & Millar (2000b), Roberts & Millar (2000a), Turner (2001), Roberts et al. (2003), Roberts et al. (2004), Roueff et al. (2007), and grain chemical models of Tielens (1983), Brown & Millar (1989), Caselli et al. (2002), Stantcheva & Herbst (2003), and the recent work of Albertsson et al. (2011) and Taquet et al. (2012). The gas phase part of the chemistry is essential, since all

the species on dust grains are from the gas phase, and the "driving force" of deuterium fractionation is in the gas phase. This is because at low temperatures only H and D (and possibly the H_2 isotopologues and light atoms such as C, N, O, though much less mobile than H and D) are mobile on the grain surface, which are the active participants of surface processes. Thus to get a high deuterium fractionation ratio on the grain surface, the [D/H] ratio in the H and D fluxes accreted on the dust grains should not be too low. The gas phase chemistry serves to provide the H and D fluxes in a self-consistent way. This is different from some of the previous studies, e.g. Stantcheva & Herbst (2003) and Caselli et al. (2002), in which the H and D flux ratio was assumed arbitrarily.

D atoms are extracted from HD molecules through cosmic-ray ionization of H_2 and the accompanying ion-neutral and dissociative recombination reactions:

$$H_2 + \mathrm{CRP} \longrightarrow H_2^+ + E^-, \tag{6.1}$$
$$H_2 + H_2^+ \longrightarrow H_3^+ + H, \tag{6.2}$$

$$H_3^+ + HD \longrightarrow H_2D^+ + H_2 + 220\ \mathrm{K}, \tag{6.3}$$
$$H_2D^+ + HD \longrightarrow HD_2^+ + H_2 + 187\ \mathrm{K}, \tag{6.4}$$
$$HD_2^+ + HD \longrightarrow D_3^+ + H_2 + 234\ \mathrm{K}, \tag{6.5}$$

$$H_2D^+ + E^- \longrightarrow D + 2\,H, \tag{6.6}$$
$$HD_2^+ + E^- \longrightarrow 2\,D + H, \tag{6.7}$$
$$D_3^+ + E^- \longrightarrow 3\,D. \tag{6.8}$$

Note that the reactions extracting D from HD by the H_3^+ isotopologues are exothermic by about 200 K, so at low temperatures the reactions in the reverse direction will be very slow. For example, at 10 K an exothermicity of 200 K will render the reverse reaction 10^{-9} times slower than the forward direction. Thus a low temperature tends to enhance the $[H_2D^+/H_3^+]$, $[HD_2^+/H_3^+]$, and $[D_3^+/H_3^+]$ ratios, hence the atomic [D/H] ratio, and the degree of such an enhancement is temperature-sensitive.

Another aspect is, when other abundant heavy molecular species (such as CO and N_2) exist, H_3^+ and its isotopologues are mainly consumed by protonating (or deuterating) them, through reactions such as

$$H_2D^+ + CO \longrightarrow HCO^+ + HD \quad \text{or} \quad DCO^+ + H_2, \tag{6.9}$$

to form species such as HCO^+, DCO^+, N_2H^+, and N_2D^+, returning the deuterium atom back to the HD molecule at the same time. Hence to make the above mechanism for enhancing the atomic [D/H] ratio really work we require the depletion of these heavy molecules from the gas phase. A lower temperature (and a higher density) tends to suppress the evaporation of molecules adsorbed on the dust grains, also pushing the system towards the direction of atomic D enrichment.

Besides the H_3^+ isotopologues, the deuterated isotopologues of CH_3^+ are also believed to play a role in deuterium fractionation at higher temperatures because of the higher exothermicity involved in their deuteration reactions.

These reactions are included in the gas phase part of our network. Our model contains a complete network for species with astrochemical interest, such as H_2O, CH_3OH, and H_2CO, and many others, as well as their deuterated variants, both in the gas phase and on the dust grains. The details of the network are described in the following sections.

6.3 Preparation for the gas phase reaction network

Both gas phase reactions and dust grain surface reactions are included in our model. The coupling between gas phase chemistry and surface chemistry is important, because the latter is driven by the species accreted from the gas phase, and this accretion process can in turn affect the behavior of the gas phase chemistry significantly.

The gas phase chemical networks publicly available usually do not include deuterium[4]. Hence we have to devise an algorithm to add deuterium atom to the network in a "rational" way. One problem is, when deuterium is being added, the number of reactions grows very quickly. This can be understood by a simple example. Given the reaction $H_2 + H_2O^+ \longrightarrow H_3O^+ + H$, its singly deuterated version can be

$$\begin{aligned} &HD + H_2O^+ \longrightarrow H_2DO^+ + H, \\ &HD + H_2O^+ \longrightarrow H_3O^+ + D, \\ &H_2 + HDO^+ \longrightarrow H_2DO^+ + H, \text{ and} \\ &H_2 + HDO^+ \longrightarrow H_3O^+ + D. \end{aligned} \tag{6.10}$$

We can see that even if only one deuterium is included, one single reaction proliferates into $1+4=5$ reactions. Allowing more deuterium atoms will enlarge the network further. For the UMIST RATE06 network, which contains more than 4000 reactions, allowing the simultaneous presence of four deuterium atoms in each reaction will generate a reaction set with ∼27000 reactions. Although a network with such size can still be handled within the rate equation framework, it becomes very slow if the surface reactions are added, and especially if the moment equation approach is adopted.

Thus we need to reduce the size of the gas phase reaction network without sacrificing the accuracy too much. The procedure is described in Section 6.3.1. In Section 6.3.2 we describe the procedure for adding deuterium into the gas phase network.

6.3.1 Reducing the gas phase reaction network

There are several previous papers dedicated to the topic of reducing a chemical network (Rae et al. 2002; Ruffle et al. 2002; Wiebe et al. 2003; Semenov et al. 2004; Grassi et al. 2012). Their motivation is to speed up the chemical evolution code, which may be coupled with a magneto-hydrodynamic code. This purpose leads them to mainly address the ionization degree of the chemical system, and species that are potentially important coolants (such as the CO molecule). This is different from our purpose, namely, to calculate the abundances of a set of molecules of interest that are not necessarily important for the dynamics and energetics of the cloud.

A straightforward approach to reduce the network would be to remove reactions one by one, and if the results obtained with the reduced network deviated too much, to add back the previously removed reaction, and try removing another reaction. Although this seems to be a secure way, it is too time consuming, since the code has to be run as many times as the number of equations in the reaction network, which may take hours to finish.

[4] One exception may be the chemistry file of the Meudon PDR code, available at `http://pdr.obspm.fr/PDRcode_Chemistry.html`. But it is not suitable for our purpose: only one deuterium atom is allowed in each species at most. The format of this network is also different from the one we are usually dealing with.

The reducing methods employed by the authors cited above are based on the so-called "objective" technique, developed by chemists in the field of combustion studies (Tomlin et al. 1992). A species will be considered unimportant if it does not significantly affect the evolving rates of other predefined important species. The method I use below is similar to, but not the same as this "objective" technique.

The guideline for reducing the gas phase network is to exclude those species and reactions that are inessential in the evolution of those important species. One has to make sure that after some reactions have been removed, the abundances of the remaining species should not change too much. Since in our modeling different physical conditions will be used, and the abundances of the important species at different stages are essential in our study, the validity check has to be done for all these situations.

To reduce the reaction network, I first make a list of species "we care about" (Table (6.1); deuterium-containing species are included in this table for later use; see the following). Not all of the species in this list have been detected or have a high abundance, but they are at least related to species we are interested in, or they are known *a priori* to be essential for the chemical evolution; for example, iron (Fe) is included because it is important in charge balancing, though we rarely care about its abundance. Then I run the gas phase model for a given physical condition. At several specified stages in the course of evolution, the reactions that are among the most important for the consumption and production of each species "we care about" are marked to be important. These reactions may contain species not in the original list, hence the important reactions for these newly included species have to be included also, otherwise the abundances of these species may become incorrect and will affect the abundances of the species we care about. This process goes on recursively, until no more species are added. After this, a new set of physical condition will be adopted to get another network, and this new network will be merged with the previous one. This is to make sure that the obtained network will be applicable for a range of physical conditions.

H, D, CO, HCO^+, DCO^+, H_2O, HDO, D_2O, OH, OD, H_2O_2, HDO_2, O_2, CH_3OH, CH_3OD, CH_2DOH, CH_2DOD, CHD_2OH, CHD_2OD, CD_3OH, H_2CO, HDCO, D_2CO, CH_3D, NH_3, NH_2D, NHD_2, ND_3, HCN, DCN, HNC, DNC, HN_2^+, DN_2^+, H_2S, HDS, HCOOH, HCOOD, DCOOH, H_3^+, H_2D^+, HD_2^+, D_3^+, E^-, Fe

Table 6.1: List of species that "we care about". These species are used to reduce the size of the reaction network.

Here I explain the criteria according to which a reaction is considered important or not in the above procedure. For each species in the original list or added in the recursive procedure, two lists of reactions are maintained. One contains all the reactions consuming it, while the other contains all the reactions producing it. Both lists are sorted in descending order based on their absolute rates[5]. For a reaction in each list, it will be considered "important" if the accumulative rate starting from the first (hence the fastest) one is no larger than a certain fraction of the total consumption or production rate. In mathematical terms, let's suppose there are n consumption reactions (the same

[5] For a reaction $A + B \longrightarrow C$ with rate coefficient k, its absolute rate is $kN(A)N(B)$, rather than k. Here N is the concentration or population of a species.

for production reactions) for species A in the unreduced network, and denote the absolute rate of the ith fastest reaction for the consumption of species A by C_i. Note that C_i is a function of the abundances of species in the network, which vary with time; it can also have explicit time dependence. Hence the ordering of the reactions may be different at different times. The jth fastest reaction will be considered important if

$$\sum_{i=1}^{j} C_i \leq f \sum_{i=1}^{n} C_i. \tag{6.11}$$

The f parameter can be tuned, and is taken to be 0.8 for the first iteration (i.e. for the species we care about), and 0.5 for newly added species. These parameters are chosen so that the number of reactions are small while guaranteeing the abundances of the species we care about do not vary by more than a factor of two before and after the reduction. To further limit the number of reactions being added, the f parameter is varied according to the relative importance of the species newly added. New species are added because new reactions are included, which may lead to the inclusion of species that had not been included before. A species being added due to a slower reaction is considered less important than a species being part of a faster reaction.

Furthermore, reactions with a time scale longer than 10^9 yr are excluded, and species with too small abundances and/or too many metal atoms are not included. These numbers can be tuned, balancing between limiting the number of reactions to be included, and keeping the discrepancies in the abundances of the important species small.

By requiring that the resulting network be applicable for a range of temperatures (10–50 K), and a range of densities (10^4–10^6 cm^{-3}), the UMIST RATE06 network is reduced to contain 650 reactions, while abundances of the species we care about do not vary by more than a factor of two for all these physical conditions and for a time range of 10^2–10^7 yr (except for H_2S, which varies by a factor less than three).

6.3.2 Deuterating the gas phase reaction network

By "deuterating" a network, I mean adding deuterium atoms to a reaction network that does not contain deuterium yet. The procedure has two steps, one is to replace the one or more hydrogen atoms in each species by deuterium atoms, based on certain rules, assuming the reactions rates are the same as the undeuterated ones, except for a possible branching ratio based on statistical weights. Another is to include a "driving network", which includes important deuterium transfer reactions, whose inverse reactions usually have a significant endothermicity, and thus are inactive at very low temperatures. Hence these reactions drive the degree of deuteration into one direction, leading to deuterium enhancement in many species.

For the first step, namely, to incorporate deuterium into the gas phase network in an automatic way, I follow the rules listed below:

1. For each reaction, a new reaction obtained by replacing the same number of hydrogen atoms on both sides (reactants and products) by deuterium atoms is always considered viable. Namely, we assume "complete scrambling".

2. For a given set of deuterated reactants, there will likely be several product channels.

Their relative branching ratios are obtained by assuming all the hydrogen atoms in the products have equal probability to be replaced by a deuterium atom.

3. The total reaction rate (summed over all the product branches) is assumed to be the same as for the original reaction.

These rules are not necessarily correct from the point of view of theoretical chemistry. It may be utterly true that in a reaction a deuterium atom in a species could not be transferred from one functional group to another. This depends on our knowledge about the detailed reaction mechanism. The "complete scrambling" assumption is based on a picture that when two reactants collide, they merge to form an activated complex in a chaotic way so that the information on their initial configuration is lost, hence a deuterium atom is able to change its location among functional groups.

Take the dissociative recombination reaction $CH_3OH_2^+ + E^- \longrightarrow CH_3OH + H$ as an example[6] (here E^- means an electron). In one of its singly deuterated versions, the left hand side is $CH_2DOH_2^+ + E^-$. Without the complete scrambling assumption, the products could only be $CH_2DOH + H$. This is based on the picture that an electron is combined with a proton affiliated with the hydroxyl (OH) group of methanol, to neutralize the charge. The attractive force between one hydrogen nucleus of the OH_2 group and the main part of the molecule disappears due to this neutralization, and one hydrogen atom is thus ejected. But assuming complete scrambling, there are several possible product channels, leading to the products:

$$\begin{aligned} &CH_2DOH + H, \\ &CH_3OD + H, \\ &CH_3OH + D. \end{aligned} \tag{6.12}$$

The second and third channel may appear contradictory to our "chemical intuition", but they are nevertheless not impossible. Whether these channels really proceed in reality can only be determined by careful experiments and/or sophisticated theoretical calculations, both of which are out of the scope of our study. So the complete scrambling assumption can be viewed as a "working hypothesis". Another reason to make this assumption is due to a practical challenge in programing: it is not straightforward to determine which part of a sequence of letters such as "CH2DOH2+" can be called a "functional group", and to determine which groups are conserved in a reaction, and which groups have been fragmented or have merged with other reactants. This problem can be illustrated with the reaction $CH_3OH_2^+ + E^- \longrightarrow H_2CO + H_2 + H$. One may imagine that the two hydrogen atoms connected to O are ejected as a H_2 molecule, while one hydrogen atom in the CH_3 group is also ejected. This picture is not necessarily correct. Before this type of pictures are well-justified, it is not urgent to devise an algorithm to implement it.

Regarding the second rule, a deuterium atom may actually prefer to stay in one functional group of a chemical compound than in another (this will be emphasized in Section 6.4 about the surface chemistry network). But since theoretical or experimental studies on most of the deuterated reactions that are needed in our study are not available yet, the best we can do is to assume that all the positions are equally possible. Based

[6] There are another two product channels $CH_3 + OH + H$ and $H_2CO + H_2 + H$, which are neglected here.

on this assumption, the branching ratios can be obtained, depending on how many ways hydrogen atoms can be replaced by deuterium atoms while keeping the products unaltered.

In building the deuterated network, at most 4 deuterium atoms are allowed in the same reaction. If a reaction involves more than 3 metal atoms, then at most one deuterium atom will be included in this reaction. If a reaction involves more than 5 metal atoms, then no deuterium will be included in it. Species containing "rare" elements (such as Si, P) are not deuterated.

For the reduced gas phase network obtained in Section 6.3.1, which contains 650 reactions, the deuteration process yields a network containing ∼4800 reactions. This network is then combined with a "driving network" (see Table (6.2)), taken from Roberts & Millar (2000b) and Roberts et al. (2004). Possible duplicates are handled: if a reaction is included both in the driving network and in the automatically-generated network, the former will be adopted and the latter will be removed.

This deuterated network is then reduced again, using the same procedure and the same criteria as in Section 6.3.1, leading finally to a network containing 2127 reactions[7].

Table 6.2: "Driving" reactions for deuteration in the gas phase network. They are taken from Roberts & Millar (2000b) and Roberts et al. (2004). The parameters A, B, and E_a are used to calculate the rates: $k = A\,(T/300)^B \exp(E_a/T)$. X(Y) means X×10^Y.

Reactions	A	B	E_a
$H_3^+ + HD \longrightarrow H_2D^+ + H_2$	1.7(−9)		—
$H_2D^+ + H_2 \longrightarrow H_3^+ + HD$	1.7(−9)		220.0
$CH_3^+ + HD \longrightarrow CH_2D^+ + H_2$	1.3(−9)		—
$CH_2D^+ + H_2 \longrightarrow CH_3^+ + HD$	8.7(−10)		370.0
$C_2H_2^+ + HD \longrightarrow C_2HD^+ + H_2$	1.0(−9)		—
$C_2HD^+ + H_2 \longrightarrow C_2H_2^+ + HD$	2.5(−9)		550.0
$D^+ + H_2 \longrightarrow H^+ + HD$	2.1(−9)		—
$H^+ + HD \longrightarrow D^+ + H_2$	1.0(−9)		464.0
$D^+ + H \longrightarrow H^+ + D$	1.0(−9)		—
$H^+ + D \longrightarrow D^+ + H$	1.0(−9)		41.0
$H_3^+ + D \longrightarrow H_2D^+ + H$	1.0(−9)		—
$H_2D^+ + H \longrightarrow H_3^+ + D$	1.0(−9)		632.0
$HCO^+ + D \longrightarrow DCO^+ + H$	1.0(−9)		—
$DCO^+ + H \longrightarrow HCO^+ + D$	2.2(−9)		796.0
$N_2H^+ + D \longrightarrow N_2D^+ + H$	1.0(−9)		—
$N_2D^+ + H \longrightarrow N_2H^+ + D$	2.2(−9)		550.0
$OH + D \longrightarrow OD + H$	1.3(−10)		—
$OD + H \longrightarrow OH + D$	1.3(−10)		810.0
$C_2H + D \longrightarrow C_2D + H$	5.0(−11)	0.5	250.0
$C_2D + H \longrightarrow C_2H + D$	5.0(−11)	0.5	832.0

. . . continued on the next page

[7] Three of them are the formation reactions of H_2, HD and D_2 molecules on the dust grains, which will be removed when "genuine" grain chemistry is included (see the later sections).

...continued

Reactions	A	B	E_a
$HCN + D \longrightarrow DCN + H$	1.0(−10)	0.5	500.0
$DCN + H \longrightarrow HCN + D$	1.0(−10)	0.5	500.0
$H_3^+ + D_2 \longrightarrow H_2D^+ + HD$	3.5(−10)		—
$H_2D^+ + HD \longrightarrow H_3^+ + D_2$	3.5(−10)		63.0
$H_3^+ + D_2 \longrightarrow HD_2^+ + H_2$	1.1(−9)		—
$HD_2^+ + H_2 \longrightarrow H_3^+ + D_2$	1.1(−9)		251.0
$H_2D^+ + HD \longrightarrow HD_2^+ + H_2$	8.1(−10)		—
$HD_2^+ + H_2 \longrightarrow H_2D^+ + HD$	8.1(−10)		187.0
$H_2D^+ + D_2 \longrightarrow HD_2^+ + HD$	7.0(−10)		—
$HD_2^+ + HD \longrightarrow H_2D^+ + D_2$	7.0(−10)		107.0
$H_2D^+ + D_2 \longrightarrow D_3^+ + H_2$	7.0(−10)		—
$D_3^+ + H_2 \longrightarrow H_2D^+ + D_2$	7.0(−10)		341.0
$HD_2^+ + HD \longrightarrow D_3^+ + H_2$	6.4(−10)		—
$D_3^+ + H_2 \longrightarrow HD_2^+ + HD$	6.4(−10)		234.0
$HD_2^+ + D_2 \longrightarrow D_3^+ + HD$	8.7(−10)		—
$D_3^+ + HD \longrightarrow HD_2^+ + D_2$	8.7(−10)		159.0
$CH_2D^+ + HD \longrightarrow CHD_2^+ + H_2$	1.6(−9)		—
$CHD_2^+ + H_2 \longrightarrow CH_2D^+ + HD$	1.6(−9)		370.0
$CHD_2^+ + HD \longrightarrow CD_3^+ + H_2$	1.5(−9)		—
$CD_3^+ + H_2 \longrightarrow CHD_2^+ + HD$	1.5(−9)		370.0
$CH_3^+ + D_2 \longrightarrow CH_2D^+ + HD$	4.4(−10)		—
$CH_2D^+ + HD \longrightarrow CH_3^+ + D_2$	4.4(−10)		400.0
$CH_3^+ + D_2 \longrightarrow CHD_2^+ + H_2$	6.6(−10)		—
$CHD_2^+ + H_2 \longrightarrow CH_3^+ + D_2$	6.6(−10)		400.0
$CH_2D^+ + D_2 \longrightarrow CHD_2^+ + HD$	1.2(−9)		—
$CHD_2^+ + HD \longrightarrow CH_2D^+ + D_2$	1.2(−9)		400.0
$H_2D^+ + D \longrightarrow HD_2^+ + H$	2.0(−9)		—
$HD_2^+ + H \longrightarrow H_2D^+ + D$	2.0(−9)		550.0
$HD_2^+ + D \longrightarrow D_3^+ + H$	2.0(−9)		—
$D_3^+ + H \longrightarrow HD_2^+ + D$	2.0(−9)		655.0
$H_3^+ + E^- \longrightarrow H_2 + H$	1.36(−8)	−0.5	—
$H_3^+ + E^- \longrightarrow H + H + H$	5.44(−8)	−0.5	—
$H_2D^+ + E^- \longrightarrow HD + H$	1.20(−8)	−0.5	—
$H_2D^+ + E^- \longrightarrow H_2 + D$	4.20(−9)	−0.5	—
$H_2D^+ + E^- \longrightarrow D + H + H$	4.38(−8)	−0.5	—
$HD_2^+ + E^- \longrightarrow HD + D$	4.20(−9)	−0.5	—
$HD_2^+ + E^- \longrightarrow D_2 + H$	1.20(−8)	−0.5	—
$HD_2^+ + E^- \longrightarrow D + D + H$	4.38(−8)	−0.5	—
$D_3^+ + E^- \longrightarrow D_2 + D$	5.40(−9)	−0.5	—
$D_3^+ + E^- \longrightarrow D + D + D$	2.16(−8)	−0.5	—
$CH_3^+ + H_2 \longrightarrow CH_5^+$	1.3(−14)	−1.0	—
$CH_3^+ + HD \longrightarrow CH_4D^+$	—		—

... continued on the next page

...continued

Reactions	A	B	E_a
$CH_3^+ + D_2 \longrightarrow CH_3D_2^+$	3.5(−14)	−1.0	—
$CH_2D^+ + H_2 \longrightarrow CH_4D^+$	2.0(−14)	−1.0	—
$CH_2D^+ + HD \longrightarrow CH_3D_2^+$	3.5(−14)	−1.0	—
$CH_2D^+ + D_2 \longrightarrow CH_2D_3^+$	—		—
$CHD_2^+ + H_2 \longrightarrow CH_3D_2^+$	3.5(−14)	−1.0	—
$CHD_2^+ + HD \longrightarrow CH_2D_3^+$	—		—
$CD_3^+ + H_2 \longrightarrow CH_2D_3^+$	6.3(−14)	−1.0	—
$C_2H_2^+ + H_2 \longrightarrow C_2H_4^+$	2.3(−14)	−1.5	—
$C_2H_2^+ + HD \longrightarrow C_2H_3D^+$	—		—
$C_2HD^+ + H_2 \longrightarrow C_2H_3D^+$	3.39(−14)	−1.5	—
$CH_3^+ + H_2O \longrightarrow CH_3OH_2^+$	5.5(−12)	−1.7	—
$CH_3^+ + HDO \longrightarrow CH_3OHD^+$	1.1(−11)	−1.7	—
$CH_3^+ + D_2O \longrightarrow CH_3OD_2^+$	1.65(−11)	−1.7	—
$CH_2D^+ + H_2O \longrightarrow CH_2DOH_2^+$	1.1(−11)	−1.7	—
$CH_2D^+ + HDO \longrightarrow CH_2DOHD^+$	1.65(−11)	−1.7	—
$CH_2D^+ + D_2O \longrightarrow CH_2DOD_2^+$	2.2(−11)	−1.7	—
$CHD_2^+ + H_2O \longrightarrow CHD_2OH_2^+$	1.65(−11)	−1.7	—
$CHD_2^+ + HDO \longrightarrow CHD_2OHD^+$	2.2(−11)	−1.7	—
$CHD_2^+ + D_2O \longrightarrow CHD_2OD_2^+$	2.75(−11)	−1.7	—
$CD_3^+ + H_2O \longrightarrow CD_3OH_2^+$	2.2(−11)	−1.7	—
$CD_3^+ + HDO \longrightarrow CD_3OHD^+$	2.75(−11)	−1.7	—
$CD_3^+ + D_2O \longrightarrow CD_3OD_2^+$	2.75(−11)	−1.7	—

6.4 The grain surface chemistry

Adding deuterium to the network complicates things. The size of the network is enlarged by a factor of a few. Abstraction reactions will have to be included, due to difference in the strength of bonds involving H or D, caused by their different zero-point energies. The exact numerical values of these zero-point energies, as well as the heights and widths of the activation barriers associated with those abstraction reactions, can only be obtained by careful analysis of experimental results, or by theoretical computations.

However, up to now it is still not straightforward to extract parameters we need from experimental results. Since the absolute concentration of the reactants and products are not easy to measure, the experimental setups are usually unable to measure the absolute rate of a reaction, and only relative rates can be derived, which are not very accurate by themselves. Nevertheless the experimental results that have been obtained provide important constraints and insights into what is going on in a chemical system, and when combined with "educated" guesses for some of the parameters, the remaining parameters can be reasonably derived.

In this section I will first describe the mobility of hydrogen and deuterium atoms on a surface (which can be the surface of interstellar dust grain, or the surface used in experiments). Their mobilities (surface diffusion rates) will then be used to calculate their surface coverages, mainly in the context of lab experiments, where the surface coverage

of hydrogen and deuterium is much higher than on interstellar dust grains under normal conditions (though still much less than 100%). After this I describe how information on the activation barrier for abstraction reactions of formaldehyde and methanol can be obtained by considering the experimental results and theoretical calculations simultaneously. The surface formation routes for water are also discussed. Finally, I give a brief overview of other reactions in the surface network.

6.4.1 Coverage of H and D on the surface

In lab experiments H or D atoms are injected onto layers of deposited species, to investigate the reaction mechanism and to measure (if possible) the rates of the key reactions. The reactions determining the pace of the process usually have a barrier (that is the very reason that these reactions are of interest to the experimentalists), hence they are slow. The incoming H or D atoms are mainly consumed by recombination with themselves, to form H_2 or D_2 molecules. Their surface coverage can be determined by the balance between the influx and recombination process.

Mobilities of hydrogen and deuterium atoms

At low temperatures, essentially only atomic and molecular hydrogen and deuterium on the dust grain surface are able to migrate across the surface sites. Their mobilities are thus a very important controlling parameter of surface chemistry.

With TPD (Time-Programed Desorption) experiments and rate equation modeling, Katz et al. (1999) obtained the binding energies of H atoms on olivine and amorphous carbon dust, being 370 and 660 K, respectively. The diffusion barriers are 290 and 510 K. The binding energies for H_2 molecule are 310 and 540 K, respectively. Quantum tunneling is not included in their modeling.

Using a similar method, Perets et al. (2005) obtained the binding energy and diffusion energy barriers of H on low density water ice, ∼610 K and 520 K, respectively, and ∼720 and 640 K for high density water ices (the two types of ice are prepared by different methods). The D atoms are assumed to have the same binding energy and barrier as H. The binding sites for HD and D_2 molecules on low density ice are modeled to have three types with different depths, which are in the range 470–760 K. Only one binding energy is assumed for high density ice, 800 K for HD and 835 K for D_2.

Matar et al. (2008) studied the mobility of D atoms on porous amorphous water ice surfaces. O_2 molecules (to be used as an auxiliary tracer) are deposited on a porous amorphous water ice substrate, then D atoms are deposited onto the surface at 10 K. The diffusion energy barrier of D is found to be ∼260 K. They suggest the discrepancy with the Perets et al. (2005) result may be related to the assumed surface coverage of D.

Using classical trajectory methods, Al-Halabi & van Dishoeck (2007) calculated the sticking coefficient, η, and the binding energy, E_b, for H atoms hitting amorphous solid water ice (ASW). The sticking coefficient is shown to be a function of the incident energy $\eta = \exp(-E_i/300)$. The binding energies E_b for H atoms on ASW and on crystalline ice are shown to have an average of ∼650 K and ∼400 K, respectively, with a dispersion of 195 and 111 K, respectively (i.e. in their model E_b does not assume a single value). The H atoms with an initial energy of 100 K landing on the ice surface can travel a distance

of 30 Å before being thermalized. The diffusion coefficient, d, of H atoms for a surface temperature of 10 K is found to be $\sim 10^{-5}$ cm^2 s^{-1}.

The diffusion coefficient, d, is not what we usually need in modeling surface chemistry. What we need are the barrier height and width against surface diffusion. So it would be interesting to see what can be inferred about these parameters from the calculation of Al-Halabi & van Dishoeck (2007). The d parameter is defined to be[8] $d \equiv (\mathbf{r}_f - \mathbf{r}_0)^2/3t$ in their paper, where $\mathbf{r}_0$ and $\mathbf{r}_f$ are the initial and final position of a diffusing particle, and t is the time needed for such a trajectory. For a discrete random walk with step length L (i.e. the distance between successive jumps), $(\mathbf{r}_f - \mathbf{r}_0)^2 = NL^2$, and $t = N\Delta t$, where N is the number of steps in such a trajectory, and Δt is the time interval between each step. Thus $d = L^2/3\Delta t$. Since Δt is related to the characteristic frequency ν and barrier height against diffusion $E_{\rm diff}$ by $\Delta t = 1/[\nu \exp(-E_{\rm diff}/T)]$, assuming no quantum tunneling, we have

$$d = L^2 \nu \exp(-E_{\rm diff}/T)/3, \tag{6.13}$$

With $L = 1$ Å and $E_{\rm diff} = 100$ K, we have $\nu \simeq 6 \times 10^{15}$ s^{-1}. However, using formula (3) of Hasegawa et al. (1992), namely, $\nu = (2\rho_{\rm S} E_{\rm bind}/\pi^2 m)^{1/2}$ (see also Eq. (3.10)), where $\rho_{\rm S}$ is the number density of surface sites, $E_{\rm bind}$ is the binding energy, and m is the mass of the surface species being considered, we have only $\nu \simeq 2 \times 10^{12}$ s^{-1}, lower by three orders of magnitude. If we instead assume quantum tunneling for surface diffusion (Hasegawa et al. 1992), then

$$d = L^2 \nu \exp[-2(a/\hbar)(2mE_{\rm diff})^{1/2}]/3. \tag{6.14}$$

Assuming $a = L = 1$ Å and $E_{\rm diff} = 100$ K, we have $\nu \simeq 2 \times 10^{13}$ s^{-1}, which agrees better with the value calculated from the formula in Hasegawa et al. (1992), although it is still too high. However, Al-Halabi & van Dishoeck (2007) used classical trajectory methods, which by itself should not have quantum tunneling inside. Thus it seems that the effective energy barrier against diffusion has to be very low ($\lesssim$50 K) in this scenario, which is very uncommon.

The diffusion coefficient d can be related to the two-body surface reaction rate. Take the formation of H_2 molecule as an example. Let $\theta_{\rm H}$ be the surface coverage of H atoms (i.e. the area covered by H atoms divided by the total area). Its evolution equation (derived later in this section; see Eq. (6.18)) is

$$\partial_t \theta_{\rm H} = F_{\rm H}/\rho_{\rm S} - 2k_{\rm H,H}\theta_{\rm H}^2 - k_{\rm eva,H}\theta_{\rm H},$$

where $F_{\rm H}$ is the influx of H, $\rho_{\rm S}$ is the surface sites density, and $k_{\rm eva,H}$ is the evaporation rate of H. The parameter $k_{\rm H,H}$ is related to the diffusion coefficient d by

$$k_{\rm H,H} \simeq 3\rho_{\rm S} d. \tag{6.15}$$

With $\rho_{\rm S} = 10^{15}$ cm^{-2}, and $d \simeq 10^{-5}$ cm^2 s^{-1} from Al-Halabi & van Dishoeck (2007), we have $k_{\rm H,H} \simeq 3 \times 10^{10}$ s^{-1}. This is close to the commonly used value ($\sim 10^{10}$ s^{-1}).

In summary, the diffusion energy barriers obtained with the TPD method tend to be quite high. If quantum tunneling is not included, then no active surface reaction can happen at 10 K. The time scale for a hydrogen atom to cover the whole grain surface

[8] This definition is slightly different from that in Chandrasekhar (1943), where the definition of d is equivalent to $d \equiv (\mathbf{r}_f - \mathbf{r}_0)^2/6t$.

through migration would be of the order one month up to millions of years, if the energy barrier against diffusion were as high as 300–500 K. The fact that these values give good fits to the experimental data might indicate some intrinsic shortcomings in the TPD method, in that this method may not be very sensitive to the low temperature behavior of the surface species. The diffusion coefficient obtained by Al-Halabi & van Dishoeck (2007) is consistent with the two-body reaction rate calculated with the formulae in Hasegawa et al. (1992). However, for a reasonable characteristic frequency and energy barrier against surface diffusion, quantum tunneling must be assumed in the calculations.

Surface coverage of H and D

In dark clouds the density of hydrogen atoms is usually $\sim$1 cm^{-3}, determined by the balance between cosmic-ray ionization of H_2 and adsorption onto the dust grains to form H_2. At a kinetic temperature of 10 K, the influx of hydrogen atoms onto the dust grain surface is $\sim 10^4$ cm^{-2} s^{-1}. On the contrary, in experiments the flux are usually in the range 10^{12}–10^{15} cm^{-2} s^{-1}. Considering the small size of the interstellar dust grains, the average number of hydrogen atoms on a dust grain is usually much smaller than one (meaning that most of the time the dust grain contains no free hydrogen atom). This is different from the situation in typical lab experiments, where the surface coverage can be much higher (though still considerably smaller than 100%), otherwise the experiments would take too long a time to finish.

Suppose the total number of adsorption/reaction sites on the experimental surface is N_S, the total number of H atoms on the surface is N_H, the reaction rate coefficient for H recombination is $k_{H,H}$, the evaporation rate of H is $k_{eva,\,H}$, then the evolution equation for the number of H atoms on the surface due to adsorption, recombination, and evaporation is

$$\partial_t N_H = \alpha n(H) v(H) \sigma - 2k_{H,H} N_H (N_H - 1)/N_S - k_{eva,\,H} N_H, \tag{6.16}$$

where α is a coefficient $\lesssim 1$, $n(H)$ and $v(H)$ are the gas phase density and velocity of the H atoms, and σ is the surface area in the experimental setup. The factor 2 is due to the fact that each $H + H \longrightarrow H_2$ reaction consumes two H atoms, and the "-1" in the $(N_H - 1)$ term accounts for the fact that each H atom has $N_H - 1$ potential reaction partners. In the laboratory $N_H \gg 1$, so the "-1" can be neglected in the above equation. Note that in the experiments we are going to consider, H and D atoms are never injected simultaneously in the same setup, so we don't have to include both H and D in the same equation. The coverage of H atoms is mainly determined by the recombination (to form H_2) and evaporation processes, because the coverages of other reactants are low and/or the reaction rates with these other species are low.

Define the surface coverage of H by

$$\theta_H = N_H/N_S, \tag{6.17}$$

which is the fraction of surface sites that are covered by H atoms. Then we have for the evolution of θ_H,

$$\partial_t \theta_H = F_H/\rho_S - 2k_{H,H}\theta_H^2 - k_{eva,H}\theta_H, \tag{6.18}$$

where we have replaced $\alpha n(H) v(H)$ with F_H (the incoming flux of H atoms); ρ_S is the surface density of the reaction sites: $\rho_S \equiv N_S/\sigma$. From equation (6.18) we get the steady

state coverage for H

$$\theta_{\rm H} = \frac{2F_{\rm H}/\rho_{\rm S}}{k_{\rm eva} + \sqrt{k_{\rm eva}^2 + 8k_{\rm H,H}F_{\rm H}/\rho_{\rm S}}}. \tag{6.19}$$

For the coverage of D the formula is the same.

The coverages of H and D will be used in the next section to calculate the barrier parameters for the addition and abstraction reactions of formaldehyde by combining theoretical and experimental results in the literature. The parameters needed for calculating the coverages are either taken from the experimental settings as reported in the corresponding literature, or, for parameters not determinable in those experiments, taken to be their canonical values used in astrochemical modeling.

To get a feeling of the typical H and D coverage in experiments, we may assume their binding energy $E_{\rm bind}$ to be 350 K. The diffusion barrier, $E_{\rm diff}$, is usually taken to be a fixed fraction of $E_{\rm bind}$ in the range 100 – 270 K. Such values are canonically used and are in the lower range of the experimental results described in Section 6.4.1. Since the combination reaction of H atoms has no barrier, $k_{\rm H,H}$ is equal to the migration rate of hydrogen atom, $k_{\rm mig,H}$. In the case of quantum tunneling (Hasegawa et al. 1992) it is

$$k_{\rm H,H} = k_{\rm mig,H} = \nu_{\rm H} e^{-2a/\hbar\sqrt{2m_{\rm H}E_{\rm diff,H}}} = \nu_{\rm H} 10^{-1.8\left(\frac{a}{1\ \text{Å}}\right)\left(\frac{E_{\rm diff,H}}{100\ \rm K}\right)^{1/2}}, \tag{6.20}$$

where $\nu_{\rm H}$ is the vibration frequency of H, while a and $E_{\rm diff,H}$ are the barrier width and height for surface diffusion. The characteristic frequency $\nu_{\rm H}$ can be calculated with Eq. (3.10) on page 32 to be 2.4×10^{12} s^{-1}, which is independent of temperature. Hence we have

$$k_{\rm H,H} = (0.3\text{–}4) \times 10^{10}\ \text{s}^{-1}.$$

The evaporation rate of H atoms is

$$k_{\rm eva,H} = \nu_{\rm H} e^{-E_{\rm bind,H}/T}.$$

For a temperature of 15 K, the evaporation rate is $k_{\rm eva,H} = 176$ s^{-1}. Thus evaporation is unimportant in consuming the surface H atoms unless $\theta_{\rm H}$ is less than $\sim10^{-9}$. Take $\rho_{\rm S}$=10^{15} cm^{-2}, $F_{\rm H}$=2×10^{14} cm^{-2} s^{-1} (Hidaka et al. 2009), we have for the surface coverage of atomic hydrogen

$$\theta_{\rm H} = (0.2\text{–}0.6) \times 10^{-5}.$$

The coverage of D can be estimated in a similar way. The typical values are:

$$\begin{aligned} \nu_{\rm D} &= 1.7 \times 10^{12}\ \text{s}^{-1}, \\ k_{\rm D,D} = k_{\rm mig,D} &= (0.1\text{–}5.3) \times 10^{9}\ \text{s}^{-1}, \\ \theta_{\rm D} &= \sqrt{F_{\rm D}/\rho_{\rm S}/2/k_{\rm D,D}} = (0.6\text{–}4.5) \times 10^{-5}. \end{aligned}$$

The surface coverage of D is higher than that of H due to its lower surface mobility.

6.4.2 Addition and abstraction reactions of formaldehyde

The pathways leading to the formation and deuteration of formaldehyde and methanol on the dust grain surface starting from CO are shown in Fig. (6.26) on page 170. The

addition and abstraction reactions[9] for formaldehyde and its deuterated counterparts have been studied extensively by Goumans (2011). His results are listed in Table (6.3). He considered two cases: one for gas phase reactions, another also for gas phase reactions but with the presence of two water molecules, to mimic the effect of an ice surface. Only the latter is relevant for our purpose. Unfortunately the barrier widths are not calculated in his work. Woon (2002) also studied the hydrogenation and deuteration of H_2CO and the abstraction of H_2CO by H theoretically. The barrier heights obtained by Woon (2002) are similar to those of Goumans (2011).

With lab experiments, Hidaka et al. (2009) measured the relative rates of a subset of these reactions; see Table (6.4). Here we try to combine their experimental results with the theoretical results of Goumans (2011) to get the barrier widths of these reactions.

Reactions	E_a	m_{eff}	E_a	m_{eff}	a (Å)
	Without H_2O		With H_2O		
Addition reactions					
$H + H_2CO \longrightarrow CH_3O$	2318	1.01	2104	1.01	0.89
$H + HDCO \longrightarrow CH_2DO$	2283	1.01	2081	1.01	0.89
$H + D_2CO \longrightarrow CHD_2O$	2254	1.01	2063	1.01	0.89
$D + H_2CO \longrightarrow CH_2DO$	2204	2.01	1980	2.01	0.89
$D + HDCO \longrightarrow CHD_2O$	2163	2.01	1954	2.01	0.89
$D + D_2CO \longrightarrow CD_3O$	2128	2.01	1933	2.01	0.89
Abstraction reactions					
$H + H_2CO \longrightarrow H_2 + HCO$	2234	1.01	2959	1.01	0.60
$H + HDCO \longrightarrow H_2 + DCO$	2274	1.01	3019	1.01	0.60
$H + HDCO \longrightarrow HD + HCO$	2693	1.41	3455	1.45	0.60
$H + D_2CO \longrightarrow HD + DCO$	2742	1.41	3520	1.45	0.60
$D + H_2CO \longrightarrow HD + HCO$	1935	1.15	2628	1.13	0.68
$D + HDCO \longrightarrow HD + DCO$	1973	1.15	2687	1.13	0.68
$D + HDCO \longrightarrow D_2 + HCO$	2400	2.01	3129	2.01	0.68
$D + D_2CO \longrightarrow D_2 + DCO$	2447	2.01	3192	2.01	0.68

Table 6.3: Addition and abstraction reactions of formaldehyde and its deuterated counterparts. The activation barrier heights (in Kelvin) and the effective masses (in m_{proton}) for quantum tunneling are listed. Two cases have been considered: with or without the presence of two additional water molecules. The presence of water molecules is used to imitate the situation on ice surface. We do not make use of the "Without H_2O" (in gray) case. The a parameter is the barrier widths calculated by combining with the experimental results of Hidaka et al. (2009) (see text). Courtesy: All the data in this table except for the last column are from T.P.M. Goumans (private communication); see also Goumans (2011).

Take the reaction between D_2CO and H as an example. The consumption rate of

[9] An addition reaction is something like $H + CO \longrightarrow HCO$, and an abstraction reaction is something like $H + H_2CO \longrightarrow H_2 + CO$.

D_2CO by reacting with atomic hydrogen is

$$\begin{aligned}\partial_t N_{D_2CO} &= -k_{H+D_2CO} N_{D_2CO} N_H / N_S \\ &= -(k_{H+D_2CO}\theta_H) N_{D_2CO},\end{aligned} \tag{6.21}$$

where N_X is the total number of species X on the surface, and N_S is the number of surface sites. In the above expression the reaction can be either an addition or an abstraction reaction. The solution to this equation has the form

$$N_{D_2CO}(t) = N_{D_2CO}|_{t=0} \exp\left(-k_{H+D_2CO}\theta_H t\right). \tag{6.22}$$

The coefficient $k_{H+D_2CO}\theta_H$ is called *effective rate*. The migration rate of D_2CO is much slower than that of H and can be neglected. Hence

$$k_{H+D_2CO} = k_{mig,H} e^{-2a/\hbar\sqrt{2m_{eff}E_{H+D_2CO}}}, \tag{6.23}$$

where m_{eff} is the effective tunneling mass of a reaction, which depends on the detailed reaction mechanism. For other reactions similar expressions can be obtained. Hidaka et al. (2009) fitted the effective rates for three reactions, which are listed in Table (6.4).

With the above formulae, we can calculate the barrier widths from the effective rates obtained by Hidaka et al. (2009), given the barrier heights and the effective masses calculated by Goumans (2011). We also need the surface coverages of H and D, which unfortunately cannot be directly measured in the experiments, so they have to be calculated based on their nominal fluxes used in the experiments (2×10^{14} cm^{-2} s^{-1}) and assumed values for their binding and diffusion energies, as described in the previous section.

Note that in Table (6.4) the effective rates are different at different temperatures. This may be attributed to the temperature dependence of the surface coverage of hydrogen and deuterium atoms, since the evaporation rate always depends on temperature (quantum tunneling does not help in evaporation).

	Effective rates (min^{-1})		
Reaction	$T = 10$ K	$T = 15$ K	$T = 20$ K
$D + H_2CO \longrightarrow HCO + HD$	0.064	0.22	0.12
$H + D_2CO \longrightarrow DCO + HD$	0.026	0.085	0.047
$H + D_2CO \longrightarrow CHD_2O$	0.1	0.15	0.072

Table 6.4: Effective rates for two abstraction reactions and one addition reaction of formaldehyde, taken from Table 3 of Hidaka et al. (2009).

To illustrate how the assumed binding and diffusion energies of H and D atoms affect these species' surface coverages, in Fig. (6.1) I plot their surface coverage as a function of the diffusion energy, with the ratio of diffusion to binding energy fixed to 0.5. The barrier widths calculated for the three reactions in Table (6.4) as a function of the assumed diffusion and binding energy are shown in Fig. (6.2). For the same reaction, the effective rates measured at different temperatures lead to slightly different barrier widths. Since we don't expect the barrier widths to depend on temperature, we take the average value over different temperatures as the true width; each of the three reactions in Table (6.4) has its own average barrier; in Fig. (6.2) these average values are plotted.

With the barrier widths for the three reactions in Table (6.4) obtained, we can check whether the effective rates of Hidaka et al. (2009) can be reproduced. Fig. (6.3) shows the effective rates calculated using the average barrier widths for the three reactions as a function of the assumed diffusion energy of H, together with the measured values. It can be seen that the measured rates can be reasonably matched within a factor of two when the diffusion energy barrier $E_{\rm diff}$∼200 K, and it seems that the best choice for $E_{\rm diff}$ is in the range 150–200 K. This helps us to resolve the ambiguity on the choice of the diffusion and binding energies of H and D. It turns out that adopting a value of 175 K for the diffusion energy and 350 K for the binding energy of H and D seem to be a rational choice. In principle one could let $E_{\rm diff}$ and $E_{\rm bind}$ vary independently to get a best fit to the experimental results, but the meaning of this would be limited by the uncertainties in the experimental results.

Note that for the abstraction reaction $\mathrm{D+H_2CO \longrightarrow HD+HCO}$, Hidaka et al. (2009) claimed that the tunneling mass is not the mass of a D atom, but only 0.5 $m_{\rm H}$. This follows from approximating the abstraction process as an internal motion of a linear molecule composed of three parts. In our calculation we use the effective masses obtained by T.P.M. Goumans (see Table (6.3)), which are based on a different prescription[10]. This does not cause a problem, since the experimental results in Hidaka et al. (2009) do not depend on the assumed effective masses (which are only used for interpretation).

To each of the reactions included in Table (6.3) but not in Table (6.4), namely, the addition and abstraction reactions of formaldehyde that are not constrained or too slow to be detected by Hidaka et al. (2009), we assign a barrier width taken from a "similar" reaction for which we have calculated barrier widths. They are listed in the last column of Table (6.3).

[10] The method used by Hidaka et al. (2009) to calculate the effective mass can be briefly described as follows. Imagine an abstraction reaction $\mathrm{A+XB \longrightarrow AXB^* \longrightarrow AX+B}$, in which the X part of molecule XB is abstracted by an A. The effective mass is then

$$m_{\rm eff} = \frac{m_{\rm A}m_{\rm B}(1+c)^2 + m_{\rm B}m_{\rm X}c^2 + m_{\rm A}m_{\rm X}}{(1+c^2)(m_{\rm A}+m_{\rm B}+m_{\rm X})},$$

where the parameter c is defined to be $\mathrm{d}R_{\rm X-B}/\mathrm{d}R_{\rm A-X}$. The exact value of c depends on the energy surface. If assume $c=-1$, then

$$m_{\rm eff} = \frac{m_{\rm X}(m_{\rm A}+m_{\rm B})}{2(m_{\rm A}+m_{\rm B}+m_{\rm X})} \simeq \frac{m_{\rm X}}{2}.$$

The last approximation is based on the fact that usually $m_{\rm X} \ll m_{\rm B}$.

As noted in Hidaka et al. (2009), this approach to calculate the effective mass depends on the assumption that the intermediate state AXB can be treated as a linear molecule. This may not be the case in reality. The exact value of c is also basically unknown. We didn't use this formulation in our calculation.

The effective tunneling masses in Table (6.3) are calculated with quantum chemical methods by Goumans.

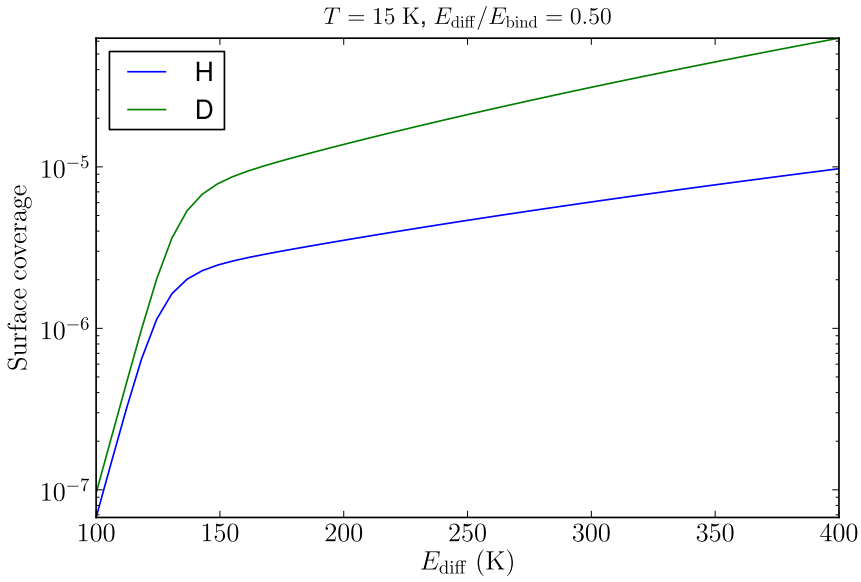

Figure 6.1: The surface coverage of H (blue) and D (green) as a function of $E_{\rm diff}$, with a surface temperature of 15 K. Quantum tunneling is assumed for surface migration. The ratio between the diffusion and binding energies is set to be $E_{\rm diff}/E_{\rm bind} = 0.5$.

6.4.3 Abstraction reactions of methanol

The abstraction reactions of methanol and its deuterated counterparts are important for studying their fractionation behaviors. T.P.M. Goumans also calculated the barrier heights for three of them; see Table (6.5). Since this list is incomplete, we have to find a way to obtain the barrier heights for the remaining reactions. One choice would be to look for clues from the formaldehyde reactions, about which we have more information.

Reaction	$E_{\rm a}$	$m_{\rm eff}$
$H + CH_3OH \longrightarrow H_2 + CH_2OH$	3224	1.01
$H + CD_3OH \longrightarrow HD + CD_2OH$	4219	1.59
$D + CH_3OH \longrightarrow HD + CH_2OH$	3253	1.08

Table 6.5: Barrier heights and effective masses for three (deuterated) methanol abstraction reactions, calculated by T.P.M. Goumans (private communication; see also Goumans & Kastner (2011)).

From the list of barriers for the abstraction reactions of formaldehyde in the presence of two water molecules in Table (6.3), we can deduce the following empirical rules:

1. A deuterium atom is deeper in the barrier (for abstraction) than a hydrogen atom by ∼400 K.

2. Replacing one hydrogen atom in the CH_2 group of H_2CO by deuterium can deepen the overall barrier by ∼60 K. For example, the H atom in HDCO is more difficult to abstract (by either H or D) than the H atom in H_2CO by about 60 K.

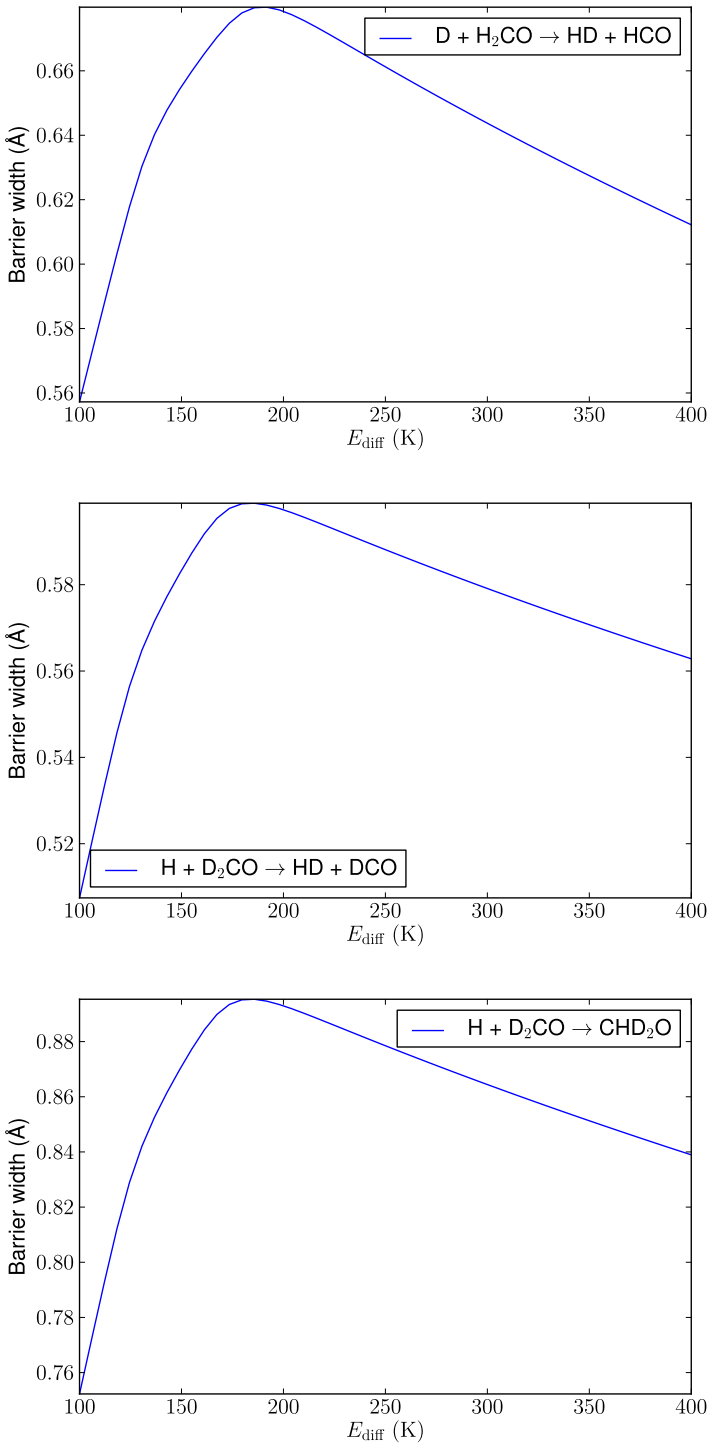

Figure 6.2: Calculated barrier widths for the three reactions listed in Table (6.4) as a function of $E_{\rm diff}$, assuming $E_{\rm diff}/E_{\rm bind} = 0.5$, averaged over the three temperatures (10 K, 15 K, 20 K).

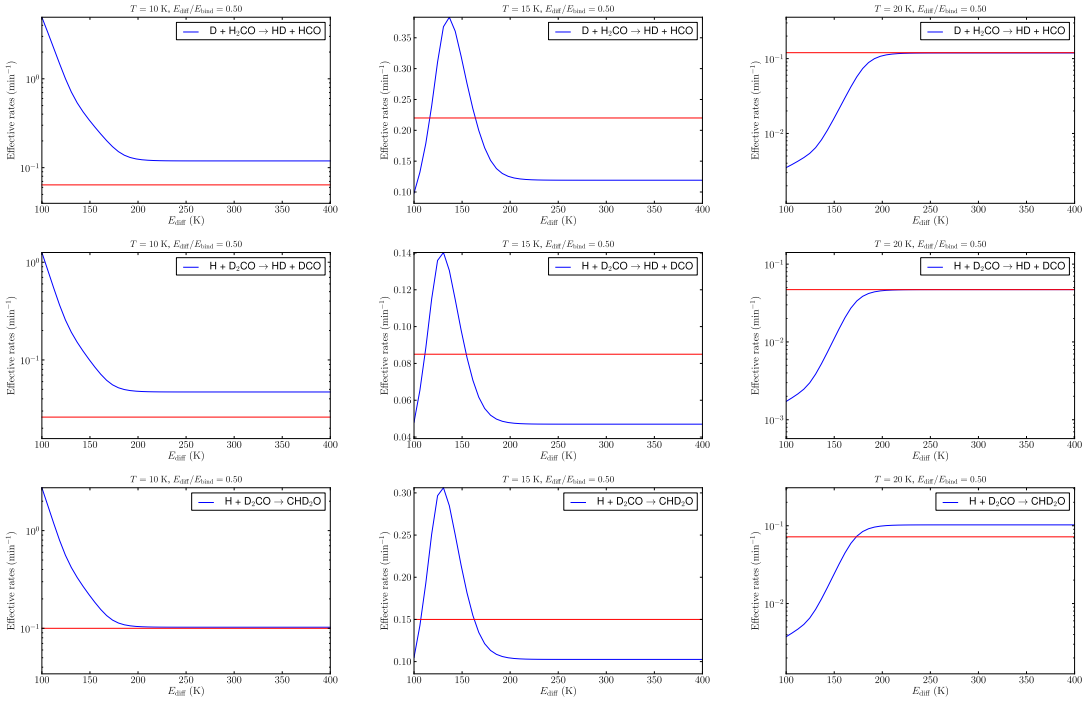

Figure 6.3: Calculated effective rates for abstraction and addition reactions of (deuterated) formaldehyde by H and D as a function of $E_{\rm diff}$, with surface temperature being 10 K (left), 15 K (middle), and 20 K (right). The red lines mark the measured values.

3. An incoming abstracting hydrogen atom experiences a barrier ∼300 K higher than an abstracting deuterium atom.

If the barrier height of only one abstraction reaction of formaldehyde is known, these rules enable us to obtain the approximate barrier heights of all the other possible abstraction reactions. Let's first test whether these rules really work for formaldehyde.

For example, suppose we are only given the barrier of the reaction $H_2CO + H \longrightarrow H_2 + HCO$, being 2960 K, we can get the barrier of other abstraction reactions of H_2CO step by step in the following way (the numbers in parenthesis are the exact theoretical values from Goumans, and the middle column shows the detailed addition and subtraction operations involved):

Reaction	Calculation step	Estimated E_a (exact E_a)
$H_2CO + H \longrightarrow H_2 + HCO$	—	2960 K
$H_2CO + D \longrightarrow HD + HCO$	2960 K − 300 K	2660 K (2628 K)
$HDCO + H \longrightarrow H_2 + DCO$	2960 K + 60 K	3020 K (3019 K)
$HDCO + H \longrightarrow HD + HCO$	3020 K + 400 K	3420 K (3455 K)
$HDCO + D \longrightarrow HD + DCO$	3020 K − 300 K	2720 K (2687 K)
$HDCO + D \longrightarrow D_2 + HCO$	2720 K + 400 K	3120 K (3129 K)
$D_2CO + H \longrightarrow HD + DCO$	3420 K + 60 K	3480 K (3520 K)
$D_2CO + D \longrightarrow D_2 + DCO$	3480 K − 300 K	3180 K (3192 K)

The rules for the effective masses (in unit of m_{proton}) in these abstraction reactions are:

- H abstracting H: 1.01;
- H abstracting D: 1.45;
- D abstracting H: 1.13;
- D abstracting D: 2.01.

We can see that the barriers obtained with the three rules approximate the exact values quite well. Thus we may apply the same rules to the abstraction of methanol and its isotopologues, since not all of them have been calculated by Goumans. However, from the known barriers of three abstraction reactions (Table 6.5) of the methanol isotopologues, it seems that the third rule in the case of formaldehyde does not hold anymore. Namely, an incoming H or D atom experiences very similar barrier heights (the E_a for the first and third reaction in Table (6.5) are almost the same).

Moreover, since the barrier height of $H + CD_3OH \longrightarrow HD + CD_2OH$ is 995 K higher than that of $H + CH_3OH \longrightarrow H_2 + CH_2OH$, in contrast to the case of formaldehyde, where the barrier height of $H + D_2CO \longrightarrow HD + DCO$ is higher than that of $H + H_2CO \longrightarrow H_2 + HCO$ by 561 K, for the methanol abstraction reactions we have to scale up the parameters compared to the formaldehyde abstraction reactions to account for such a difference. Denote by x the increase in barrier height due to replacing one H in the CH_3 group by D, and by y the difference in the zero point energies of H and D in the same group. Then we have

$$3x + y = 4219 - 3224 = 995,$$
$$x : y = 60 : 400,$$

where the ratio 60 : 400 results from rule 1 and 2 for formaldehyde. Hence x=103, and y=686.

Hence we may have the following two rules for the barrier heights of the methanol abstraction reactions:

1. A deuterium atom is ∼686 K deeper in the barrier than a hydrogen atom in the CH_3 group of methanol.
2. Replacing one hydrogen atom in the CH_3 group by a deuterium atom can deepen the overall barrier in the same group by 103 K.

And for the effective tunneling masses:

1. H abstracting H: 1.01;
2. H abstracting D: 1.59;
3. D abstracting H: 1.08;
4. D abstracting D: 2.01.

The first three are taken from Table (6.5), while the fourth one is taken from Table (6.3).

From these rules we can derive the barrier heights and effective masses for abstracting methanol and its isotopologues by H and D. We assume that the methyl group (CH_3) is not affected should the hydroxyl group (OH) be deuterated, though this is not well-studied. The parameters for the abstraction of methanol and its deuterated counterparts are listed in Table (6.6). The barrier widths are taken to be the same as the barrier widths for the abstraction reactions of formaldehyde by H and by D (0.6 and 0.68 Å in Table 6.3).

Nagaoka et al. (2007) measured the relative rates for three of the methanol abstraction reactions $D + CH_3OH \longrightarrow HD + CH_2OH$, $D + CH_2DOH \longrightarrow HD + CHDOH$, and $D + CHD_2OH \longrightarrow HD + CD_2OH$, which are

$$1 : 0.69 : 0.52. \tag{6.24}$$

Using the barrier parameters in Table (6.6), we can calculate these relative rates (since only D atoms are involved, the absolute coverage of D atoms on the surface is not needed for the calculation), which are:

$$1 : 0.77 : 0.59. \tag{6.25}$$

The agreement is not bad.

6.4.4 Hydrogenation/deuteration of CO

The reactions we consider here are $H + CO \longrightarrow HCO$ and $D + CO \longrightarrow DCO$. They have been studied theoretically by Woon (2002) with ab initio quantum mechanical calculations. In the presence of three water molecules (to simulate the effect of an ice surface), the former has a barrier height of 5.45 kcal mol^{-1} = 2740 K, in which 0.68 kcal mol^{-1} is contributed by zero-point energy (thus the potential part of the barrier is 4.77 kcal mol^{-1}). For the latter reaction the total barrier height is 5.13 kcal mol^{-1} = 2579 K in Woon (2002), however, in the presence of only two water molecules.

Reactions	E_a	m_{eff}	a
$H + CH_3OH \longrightarrow H_2 + CH_2OH$	3224.0	1.01	0.60
$H + CH_2DOH \longrightarrow H_2 + CHDOH$	3327.0	1.01	0.60
$H + CH_2DOH \longrightarrow HD + CH_2OH$	4013.0	1.59	0.60
$H + CHD_2OH \longrightarrow H_2 + CD_2OH$	3430.0	1.01	0.60
$H + CHD_2OH \longrightarrow HD + CHDOH$	4116.0	1.59	0.60
$H + CD_3OH \longrightarrow HD + CD_2OH$	4219.0	1.59	0.60
$D + CH_3OH \longrightarrow HD + CH_2OH$	3224.0	1.08	0.68
$D + CH_2DOH \longrightarrow HD + CHDOH$	3327.0	1.08	0.68
$D + CH_2DOH \longrightarrow D_2 + CH_2OH$	4013.0	2.01	0.68
$D + CHD_2OH \longrightarrow HD + CD_2OH$	3430.0	1.08	0.68
$D + CHD_2OH \longrightarrow D_2 + CHDOH$	4116.0	2.01	0.68
$D + CD_3OH \longrightarrow D_2 + CD_2OH$	4219.0	2.01	0.68

Table 6.6: Abstraction reactions for methanol and its deuterated counterparts, obtained with the rules described in Section 6.4.3. The parameters are assumed to be unchanged if the H atom in the OH group is replaced by D.

Hiraoka et al. (2002) and Watanabe et al. (2003) studied the hydrogenation route from CO to CH_3OH. Their results are not completely consistent with each other, possibly due to differences in experimental setup. Hidaka et al. (2004) and Hidaka et al. (2007) studied this route in more detail. The quantitative results for the rate coefficients that are essential for our purpose are:

(1) $k_{H+CO\longrightarrow HCO} = 2k_{H+H_2CO\longrightarrow CH_3O}$ at 15 K, and possibly
$k_{H+CO\longrightarrow HCO} > 2k_{H+H_2CO\longrightarrow CH_3O}$ at 10 K.

(2) $k_{D+CO\longrightarrow DCO} = 0.08k_{H+CO\longrightarrow HCO}$, assuming the surface coverage of H and D are the same, which may not be true.

Note that the rate coefficients do not depend on the surface coverage of H or D, unlike the effective rates; see Section 6.4.2. However, assumptions have to be made to derive the ratio between the rate coefficients from the effective rates measured in experiments.

Using the first point listed above, and adopting the barrier parameters in Table (6.3) for the reaction $H + H_2CO \longrightarrow CH_3O$, we have for the reaction $H + CO \longrightarrow HCO$

$$2a/\hbar\sqrt{2m_{eff}E_a} = -\ln 2 + 2a'/\hbar\sqrt{2m'_{eff}E'_a} \simeq 16, \tag{6.26}$$

where the a, m_{eff}, and E_a without $'$ are for $H + CO \longrightarrow HCO$, and those with $'$ are for $H + H_2CO \longrightarrow CH_3O$. Take $E_a = 2740$ K as calculated by Woon (2002), and $m_{eff} = m_H$, we have $a = 0.75$ Å.

However, with this barrier width, the ratio between the rate coefficients of $D + CO \longrightarrow DCO$ and $H + CO \longrightarrow HCO$ is 1.4×10^{-4}, much lower than the value 0.08 as indicated by Hidaka et al. (2007). To get the latter ratio, the barrier width has to be very small, ∼0.02 Å, which is unphysical. Note that in the calculation we have taken into account the fact that H and D atoms migrate on the surface with different speeds.

Hidaka et al. (2007) also tried to obtain the barrier width of $H + CO \longrightarrow HCO$ and $D + CO \longrightarrow DCO$. They used the Eckart potential for the barrier, which is different from

the usually assumed rectangular form, though this should not make a big difference. Their results (for the tunneling length) lie in the range 0.5–1.3 Å, depending on which barrier height is used. However, in their calculation they implicitly assumed that the mobilities of H and D are the same, which may not be the case. Using the formulae in Section 6.4.1, one can find that the ratio of the migration rate of D and H is $k_{\rm mig,D}/k_{\rm mig,H} \simeq 0.08$ (which is close to the ratio between the effective rates of the two reactions), and the coverage ratio $\theta_{\rm D}/\theta_{\rm H} \simeq 1.2$. Thus the coverages of H and D are indeed very similar, as assumed by Hidaka et al. (2007), but their mobilities are quite different. However, if only thermal hopping is allowed for surface diffusion, then the mobilities of H and D will be the same again. So here we face the dilemma that we may assume equal reaction probability for the two reactions and attribute their different effective rates to the different mobilities of H and D and, or, we may assume H and D diffuse on the surface only through thermal hopping to arrive at a "normal" barrier width.

For the following I assume a barrier width of 0.75 Å obtained with the first approach. If quantum tunneling does not play a role in surface migration (but still works for surface reactions), then the ratio between the effective rates of the two reactions D + CO and H + CO is consistent with a barrier width of 0.3 Å. This value is different from the value obtained by Hidaka et al. (2007) because they used a different formalism. The effect of disallowing quantum tunneling for surface migration (even if the tunneling rate calculated with the usual formula is higher than the thermal hopping rate) may be investigated later.

6.4.5 The formation of water

There are mainly three different routes to surface water formation:

1. Starting from O: $\rm O + H \longrightarrow OH$, $\rm OH + H \longrightarrow H_2O$;
2. Starting from $\rm O_2$: $\rm O_2 + H \longrightarrow O_2H$, $\rm O_2H + H \longrightarrow H_2O_2$, $\rm H_2O_2 + H \longrightarrow H_2O + OH$;
3. Starting from O and $\rm O_2$: $\rm O + O_2 \longrightarrow O_3$, $\rm O_3 + H \longrightarrow O_2 + OH$, $\rm OH + H \longrightarrow H_2O$.

Besides the reaction $\rm OH + H \longrightarrow H_2O$, OH can also be hydrogenated into $\rm H_2O$ through $\rm OH + H_2 \longrightarrow H_2O + H$.

The first reaction chain is barrierless, hence needs not to be discussed. The remaining routes do possibly have a barrier. But they are still potentially important since large abundances of $\rm O_2$ and $\rm H_2$ might be accumulated on the dust grain surface, at least in some situations. They will be discussed in the following.

The $\rm O_2$ route

Miyauchi et al. (2008) exposed solid $\rm O_2$ (with a thickness of 8 monolayers) to H and D atoms, and fitted the effective reaction rate constants for the reactions $\rm O_2 + H \longrightarrow O_2H$, $\rm H + H_2O_2 \longrightarrow H_2O + OH$, $\rm O_2 + D \longrightarrow O_2D$, and $\rm D + D_2O_2 \longrightarrow D_2O + OD$, for temperatures of 10 K and 15 K. They compared these rate constants to those of the two reactions H + CO $\longrightarrow$ HCO and D + CO $\longrightarrow$ DCO. The experimental conditions of this experiment were quite different from those of the investigation by Hidaka et al. (2009), so a direct quantitative comparison is not possible. It seems that surface migration is not important in the study of Miyauchi et al. (2008), because the surface is completely covered by the

deposited O_2 molecules. Rather the penetration of H and D atoms deep into the ice interior might be more important (the authors divide the ice mantle into three parts: the deepest part containing only O_2 and having no reaction, the middle part where only hydrogenation of O_2 into H_2O_2 is possible, and the topmost part where the conversion of H_2O_2 into H_2O also occurs).

Information about the reaction barriers can still be obtained from the ratio between the rates of hydrogenation and deuteration reactions. The effective rate constants for $O_2 + H \longrightarrow O_2H$ and $O_2 + D \longrightarrow O_2D$ are almost the same ($\sim$12 min^{-1}), indicating both reactions have negligible barriers. On the other hand, $H + H_2O_2 \longrightarrow H_2O + OH$ is about one order of magnitude faster than $D + D_2O_2 \longrightarrow D_2O + OD$ (3.9 versus 0.49 min^{-1}), thus they are mediated by an activation barrier. Miyauchi et al. concluded that an activation energy of 3.6–4.3 kcal/mol (=1800–2200 K) from calculation for the gas phase (Koussa et al. 2006) is consistent with such a ratio. But if a typical barrier width of 0.6–1 Å is assumed, then the barrier height should more likely lie in the range 200–500 K.

The ratio between the rates of $H + H_2O_2 \longrightarrow H_2O + OH$ and $H + O_2H \longrightarrow H_2O_2$ is about 0.05 in Cuppen et al. (2010). Taking into account the fact that the latter has another branch, $H + O_2H \longrightarrow 2\,OH$, the ratio between the reaction rates of $H + H_2O_2$ and $H + O_2H$ is about 0.02. As the latter reaction has no barrier, their ratio can be used to estimate the reaction barrier of the former. Combining the results of the two studies (Miyauchi et al. 2008; Cuppen et al. 2010), one gets

$$\begin{aligned} \exp[-\frac{2a}{\hbar}\sqrt{2m_{\rm H}E_{\rm a}}] &= 0.02, \\ \exp[-\frac{2a}{\hbar}\sqrt{2E_{\rm a}}(\sqrt{m_{\rm D}} - \sqrt{m_{\rm H}})] &= 0.13. \end{aligned} \tag{6.27}$$

The value 0.13 (=0.49/3.9) in the above equation is the ratio between the effective reaction rates of $D + D_2O_2$ and $H + H_2O_2$. The tunneling masses are taken to be the mass of either H or D, and the barrier heights is taken to be the same for H and D.

Unfortunately, the above two equations cannot be used to solve for a and $E_{\rm a}$, the barrier width and activation energy, respectively, of the reaction $H + H_2O_2 \longrightarrow H_2O + OH$; but both of the two equations are consistent with

$$\left(\frac{a}{0.68\ \text{Å}}\right)\left(\frac{E_{\rm a}}{200\ \text{K}}\right)^{1/2} \simeq 1. \tag{6.28}$$

Since the $O_2 + H \longrightarrow O_2H$ reaction is also likely barrierless in addition to the reaction $H + O_2H \longrightarrow H_2O_2$, we can get another constraint based on the relative rate between $H + H_2O_2 \longrightarrow H_2O + H$ and $O_2 + H \longrightarrow O_2H$, which is $3.9/12.8 = 0.3$ in Miyauchi et al. (2008). This leads to

$$\exp[-\frac{2a}{\hbar}\sqrt{2m_{\rm H}E_{\rm a}}] = 0.3, \tag{6.29}$$

which is equivalent to

$$\left(\frac{a}{0.21\ \text{Å}}\right)\left(\frac{E_{\rm a}}{200\ \text{K}}\right)^{1/2} \simeq 1. \tag{6.30}$$

This is quite different from Eq. (6.28).

The main assumption used in the above calculation is that the two reactions $H + O_2 \longrightarrow O_2H$ and $H + O_2H \longrightarrow H_2O_2$ are barrierless. Although this may be true, the

uncertainties in these experiments might have caused the above apparent contradiction. To resolve this, I simply set the barrier height to a value of 200 K, and the barrier width to the average of Eq. (6.28) and Eq. (6.30), namely, 0.5 Å.

The O_3 route

The reaction $H + O_3 \longrightarrow O_2 + OH$ was assumed to have a barrier of 450 K in Tielens & Hagen (1982). Romanzin et al. (2011) experimentally studied this reaction with solid O_3 ice and concluded that it does play a role in water formation, although detailed information regarding the activation barrier cannot be extracted from this study. Mokrane et al. (2009) studied the reaction $D + O_3 \longrightarrow O_2 + OD$, with O_3 deposited on non-porous amorphous water ice and arrived at a similar conclusion; a barrier of 450 K is consistent with their results. Due to the limited information on this reaction, I take as a working assumption that this reaction has a barrier of 450 K with a width of 0.5Å.

The $OH + H_2 \longrightarrow H_2O + H$ reaction

This reaction received more study than the previous one. In the gas phase it has a barrier of ∼2100 K (Atkinson et al. 2004) or higher (Nguyen et al. 2011). Oba et al. (2012) studied this reaction and its deuterated counterparts, finding that it does possess a barrier, as evidenced by the isotopic effect on the relative reactions rates. Since the theoretical study about the barrier heights has not converged, here I will take the canonic value 2100 K.

To estimate the barrier width, as before, we may make use of the relative reaction efficiency roughly obtained by Oba et al. (2012). In their Table (2) it is shown that the rate of $OH + D_2 \longrightarrow HDO + D$ is 10% that of $OH + H_2 \longrightarrow H_2O + H$. Taking the tunneling mass of the two reactions to be the mass of a deuterium atom and a hydrogen atom, we have

$$\exp[-\frac{2a}{\hbar}\sqrt{2E_\mathrm{a}}(\sqrt{m_\mathrm{D}} - \sqrt{m_\mathrm{H}})] = 0.1, \tag{6.31}$$

which is equivalent to

$$\left(\frac{a}{0.3\ \text{Å}}\right)\left(\frac{E_\mathrm{a}}{2100\ \mathrm{K}}\right)^{1/2} \simeq 1. \tag{6.32}$$

So a barrier width of 0.3 Å will be adopted. If we assume the effective mass formula used by these authors (or Hidaka et al. 2009; see page 119), then a slightly larger width will result[11].

The full set of reactions and their parameters for the formation of water and its deuterated counterparts are listed in Table (6.7).

6.4.6 The formation of CO_2 through OH + CO

For the formation of CO_2, Garrod & Pauly (2011) implemented a three-body mechanism, $H + O + CO \longrightarrow CO_2 + H$, which is inspired by the two-body reaction OH + CO (which by itself does not occur at low temperatures because both OH and CO are immobile).

[11] We may note that the implicit "mental picture" based on which to calculate the effective mass with this formula is, for reaction $OH + H_2 \longrightarrow H_2O + H$, an H atom in H_2 is abstracted ("grabbed") by an OH radical. Whether this is true depends on the detailed energy surface and reaction path, which affect the exact effective mass.

Reactions	E_a	m_{eff}	a
$H + O \longrightarrow OH$			
$D + O \longrightarrow OD$			
$H + OH \longrightarrow H_2O$			
$D + OH \longrightarrow HDO$			
$H + OD \longrightarrow HDO$			
$D + OD \longrightarrow D_2O$			
$H + O_2 \longrightarrow O_2H$			
$D + O_2 \longrightarrow O_2D$			
$H + O_2H \longrightarrow H_2O_2$			
$D + O_2H \longrightarrow HDO_2$			
$H + O_2D \longrightarrow HDO_2$			
$H + O_3 \longrightarrow O_2 + OH$	450	1	0.5
$D + O_3 \longrightarrow O_2 + OD$	450	2	0.5
$H + H_2O_2 \longrightarrow H_2O + OH$	200	1	0.5
$D + H_2O_2 \longrightarrow HDO + OH$	200	2	0.5
$D + H_2O_2 \longrightarrow H_2O + OD$	200	2	0.5
$H + HDO_2 \longrightarrow HDO + OH$	200	1	0.5
$H + HDO_2 \longrightarrow H_2O + OD$	200	1	0.5
$H_2 + OH \longrightarrow H_2O + H$	2100	1	0.3
$HD + OH \longrightarrow H_2O + D$	2100	1	0.3
$HD + OH \longrightarrow HDO + H$	2100	2	0.3
$D_2 + OH \longrightarrow HDO + D$	2100	2	0.3
$H_2 + OD \longrightarrow HDO + H$	2100	1	0.3
$HD + OD \longrightarrow HDO + D$	2100	1	0.3
$HD + OD \longrightarrow D_2O + H$	2100	2	0.3
$D_2 + OD \longrightarrow D_2O + D$	2100	2	0.3

Table 6.7: Key reactions and their parameters for surface water formation and deuteration.

Namely, when an H atom arrives at a surface site occupied by an O atom, and if this O atom is on top of a CO molecule, then a CO_2 molecules is assumed to be formed. This is similar to the Eley-Rideal mechanism, in which a gas phase molecule reaching the surface directly react with a molecule attached to the surface.

Since the adsorption energy of OH is 2850 K, much higher than the barrier height (80 K) of the reaction $OH + CO \longrightarrow CO_2 + H$, it is reasonable to assume that the newly adsorbed OH can overcome such a barrier and react with CO to form CO_2. Note that the adsorption energy of OH quoted here is for amorphous water ice, while we are talking about an OH arriving on top of a CO molecule. But even if the adsorption energy of OH on CO ice is lower, it should still be larger than the small barrier of 80 K.

Besides the adsorption process, we may assume that, in general, each time an OH radical is formed, and if it is on top of a CO molecule, a CO_2 molecule will be immediately formed. This is because all the surface reactions that are of interest at the low temperature of dark clouds are exothermic, and the energy released in each reaction should be much higher than the small activation barrier.

Mathematically, this amounts to taking away a fraction of the surface OH formation rate and adding it to the formation rate of CO_2. Namely,

$$\begin{aligned} \partial_t N(\mathrm{OH}) &= P(\mathrm{OH})\left[1-\theta(\mathrm{CO})\right] - \cdots, \\ \partial_t N(\mathrm{CO}) &= -P(\mathrm{OH})\theta(\mathrm{CO}) + \cdots, \\ \partial_t N(\mathrm{CO_2}) &= P(\mathrm{OH})\theta(\mathrm{CO}) + \cdots, \\ \partial_t N(\mathrm{H}) &= P(\mathrm{OH})\theta(\mathrm{CO}) + \cdots, \end{aligned} \tag{6.33}$$

where $P(\mathrm{OH})$ is the production rate of OH, and $\theta(\mathrm{CO})$ is the surface coverage of CO,

$$\theta(\mathrm{CO}) \equiv N(\mathrm{CO})/N_\mathrm{S}, \tag{6.34}$$

where N_S is the total number of surface sites, and $N(\mathrm{CO})$ is the number of CO molecules on the surface of single dust grain.

The production rate of OH contains terms like $N(\mathrm{H})N(\mathrm{O})$, so the term $P(\mathrm{OH})\theta(\mathrm{CO})$ contains a product of the abundances of three species, hence we are practically considering three-body reactions.

However, the above prescription is susceptible to numerical instabilities. This is because, in the first line of Eq. (6.33), the negative term for OH is not proportional to $N(\mathrm{OH})$, which causes the loss of self-correction in the numeric evolution. Hence the $\theta(\mathrm{CO})$ term in these equations should be replaced by $\min(1, \theta(\mathrm{CO}))$.

In coding this mechanism, to be "fair", the two reactants will be treated the same way. That is to say, not only $P(\mathrm{OH})\theta(\mathrm{CO})$, but also $P(\mathrm{CO})\theta(\mathrm{OH})$ will be added to the formation rate of CO_2, even if the latter is not as important.

To allow more flexibility, a "pre-factor" is also included. So the actual contribution added to the CO_2 formation rate is $f_\mathrm{pre}P(\mathrm{OH})\theta(\mathrm{CO})$. Such a pre-factor is in principle a free parameter. It may be used to account for the possibility that an OH radical sitting on a CO molecule may evaporate or hop away before the reaction occurs. In this case, we have

$$f_\mathrm{pre} = \frac{k_\mathrm{reac}}{k_\mathrm{reac} + k_\mathrm{hop} + k_\mathrm{eva}}. \tag{6.35}$$

Here $k_{\rm reac}$ is $\nu \exp[-E_{\rm a}/T]$, where ν is the characteristic frequency. The exponential part may be replaced by a quantum tunneling version, depending on whichever is faster. Note that the above form is similar to, but not the same as equation (6) in Garrod & Pauly (2011), which was used to enhance the reaction rate by considering the competition between reaction, hopping, and evaporation processes. We don't include such an enhancement for normal surface reactions.

6.4.7 Other reactions in the surface reaction network

Other reactions included in our model are basically the same as those used in our previous study on the formation of H_2O_2, except that deuterium is included. Basically, besides formaldehyde, methanol, and water that have been described in the previous sections, we include the formation of methane (CH_4), ammonia (NH_3), H_2S, HCOOH, HCN, HNC, etc., and their deuterated counterparts (if applicable). They are listed in Table (6.8); deuterated reactions are not included for simplicity.

6.4.8 The zero-point energy issue for the evaporation and surface migration rates

For an oscillatory system, quantum mechanics predicts that the energy of its lowest energy state is not zero, but has a finite value $h\nu/2$, where h is Planck's constant, and ν is the frequency of the system. If the system has more than one independent vibrational modes, then the total zero-point energy is the sum of the zero-point energy of all these modes. We note that in classical physics (with the exception of general relativity) only the differences between energies really enter the dynamical equations.

In surface evaporation processes, the rate is determined by $\nu \exp\left[-E_{\rm bind}/T\right]$, where ν is the characteristic frequency for the vibration of a species on the surface. If the same amount is subtracted from the binding energies $E_{\rm bind}$ of all the species, then their relative evaporation rates won't change. However, all the rates would have to be scaled by a common factor, which has an observable consequence (in principle), because it would lead to a different absolute time scale. Furthermore, since different species have different characteristic vibrational frequencies, they also have different zero-point energies. Hence including the zero-point energy also has a measurable change to the relative evaporation rates.

The effect due to difference in vibrational frequencies is most obvious between different isotopologues of the same species. Since the electronic structure of two isotopologues should be very similar, they experience very similar energy potentials[12]. For example, the zero point energy corresponding to the characteristic frequency of H ($\sim 2.4\times10^{12}$ Hz) is $\sim$58 K, while for D ($\sim 1.7\times10^{12}$ Hz) is $\sim$41 K; together with the difference in vibrational frequencies (a factor of 1.4), H evaporates about 7 times faster than D at 10 K. The characteristic frequency of H_2 molecule is $\sim 1.94\times10^{12}$ Hz, for HD molecule it is $\sim 1.58\times10^{12}$ Hz, while for D_2 it is $\sim 1.37\times10^{12}$ Hz (calculated with Eq. (3.10)). The

[12] In principle, the differences in the dipole moments of different isotopologues can also contribute to the variation in binding energy by changing the bond strength.

(1)	$H + H \longrightarrow H_2$	(25)	$O + CH_2 \longrightarrow H_2CO$
(2)	$H + C \longrightarrow CH$	(26)	$O + N \longrightarrow NO$
(3)	$H + CH \longrightarrow CH_2$	(27)	$O + NO \longrightarrow NO_2$
(4)	$H + CH_2 \longrightarrow CH_3$	(28)	$O + CN \longrightarrow OCN$
(5)	$H + CH_3 \longrightarrow CH_4$	(29)	$O + NH \longrightarrow HNO$
(6)	$H + N \longrightarrow NH$	(30)	$C + OH \longrightarrow HOC$
(7)	$H + NH \longrightarrow NH_2$	(31)	$C + OH \longrightarrow CO + H$
(8)	$H + NH_2 \longrightarrow NH_3$	(32)	$H + HOC \longrightarrow CHOH$
(9)	$H + HCOO \longrightarrow HCOOH$	(33)	$H + CHOH \longrightarrow CH_2OH$
(10)	$H + S \longrightarrow HS$	(34)	$C + O_2 \longrightarrow CO + O$
(11)	$H + HS \longrightarrow H_2S$	(35)	$CH + OH \longrightarrow CHOH$
(12)	$H + H_2S \longrightarrow HS + H_2$	(36)	$C + N \longrightarrow CN$
(13)	$H + CN \longrightarrow HCN$	(37)	$C + NH \longrightarrow HNC$
(14)	$H + NO \longrightarrow HNO$	(38)	$C + NH_2 \longrightarrow HNC + H$
(15)	$OH + CO \longrightarrow CO_2 + H$	(39)	$C + CH \longrightarrow C_2H$
(16)	$O + CO \longrightarrow CO_2$	(40)	$C + CH_2 \longrightarrow C_2H_2$
(17)	$O + O \longrightarrow O_2$	(41)	$H + C_2H \longrightarrow C_2H_2$
(18)	$O + O_2 \longrightarrow O_3$	(42)	$N + N \longrightarrow N_2$
(19)	$O + OH \longrightarrow O_2H$	(43)	$N + CH \longrightarrow HCN$
(20)	$OH + OH \longrightarrow H_2O_2$	(44)	$N + NH \longrightarrow N_2H$
(21)	$O + HCO \longrightarrow HCOO$	(45)	$N + NH_2 \longrightarrow N_2H_2$
(22)	$O + HCO \longrightarrow CO_2 + H$	(46)	$H + N_2H \longrightarrow N_2H_2$
(23)	$O + C \longrightarrow CO$	(47)	$H + N_2H_2 \longrightarrow N_2H + H_2$
(24)	$O + CH \longrightarrow HCO$		

Table 6.8: Surface reactions other than those directly related to the formation of formaldehyde, methanol, and water. The deuterated counterparts are not shown for simplicity.

differences in zero-point energies are

$$E_{\rm ZPE}({\rm H_2}) - E_{\rm ZPE}({\rm HD}) \simeq 8 \text{ K},$$
$$E_{\rm ZPE}({\rm H_2}) - E_{\rm ZPE}({\rm D_2}) \simeq 14 \text{ K}.$$

At 10 K the evaporation rate of D_2 will be $e^{-1.4} \simeq 0.25$ time slower than that of H_2. This can enhance the surface abundance of D_2 relative to H_2, which might play a role in determining the deuteration of water through the reaction channel $H_2 + OH \longrightarrow H_2O + H$.

In our code, the zero-point energy of each surface species is subtracted from its "pure" potential energy. The zero-point energy itself is calculated with the characteristic frequency of each species. Then the total energy is used to calculate the evaporation rate, and a fraction (a free parameter of the code, usually taken to be in the range of 0.3–0.8) of it is used to calculate the surface diffusion rate. Such a treatment is subject to uncertainties. Moreover, the evaporation of a species corresponds to the vertical vibrational mode of its motion on the surface, which may have a different frequency from the horizontal modes. Calculating the vibrational frequencies is a highly nontrivial task by itself (Groß 2009, page 243), since in principle the details of the potential energy surface should be known for such a calculation. Hence our implementation of the zero-point energy should be only viewed as a hypothetical trial.

6.5 The three-phase gas-surface-mantle model

In our previous treatment of grain chemistry, all the species on the grain are allowed to participate in chemical reactions. In reality, one may imagine that species on the surface layer can be covered by incoming molecules and become inert to chemical changes. In such a manner an ice mantle is formed for each grain, which serves as a reservoir for the products of gas phase and surface chemistry. When the temperature of the dust grain rises, the mantle material evaporates and returns to the gas phase, liberating their rotational motions so that they may be observed at radio and (sub)millimeter wavelengths.

There are several types of chemical models for dust grains, depending on to what extent the details of the grain structure are captured. Models with the least details do not distinguish between surface and mantle layers, and only a distinction between the gas phase and grain surface is made—these are called "two phase" models. The so-called "three-phase" models distinguish between the surface and mantle layers; see Fig. (6.4) for a schematic view. All the layers below the surface layer and above the dust core are called mantle, and are treated as a whole. Thus we see that such a "three-phase" model still cannot describe the detailed distribution of different species inside the grain mantle[13]. Only models in the style of Chang et al. (2005) and Cuppen & Herbst (2007) maintain these details. However, for a reaction network large enough for astrochemical study, such an approach is too demanding in computational resources and impractical, since one has to keep track of the position of each species in the grain mantle and the chemical reactions have to be simulated one by one.

Here we adopt the "three-phase" model of grain structure. We neglect the possibility that an incoming atom (such as H or D) may penetrate into the mantle layers and react

[13] In this sense the "three-phase model" should not be called a "multi-layer" model, since essentially only two layers are considered on the grain.

with the inside species. H atom, H_2 molecule, and their isotopologues are not allowed to form an ice mantle; they are not allowed to cover other species either (even if the surface coverage of H_2 can be appreciable sometimes), since they are very mobile relative to other heavier species. The mobilities of C, N, O atoms are low, so they are allowed to cover others. In the following I describe the mathematics related with such a model, which is slightly different from the prescription of Hasegawa & Herbst (1993b) and Garrod & Pauly (2011).

The roles played by adsorption and evaporation processes are two-folds in the context of "three-phase" models. The abundance of a surface species can increase because of the supply from the gas phase, but can also decrease since it can be covered by the incoming molecules. On the other hand, although evaporation consumes the surface species, removing the upper covering layers reveals the underneath layers, which may actually increase the abundance of certain species in the surface layer.

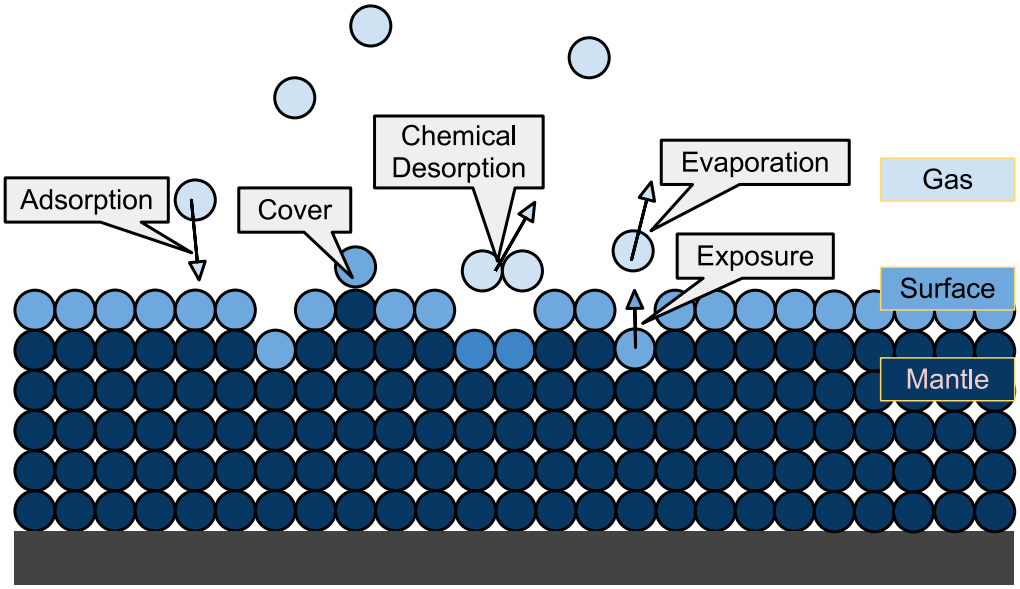

Figure 6.4: A schematic view of the three-phase model.

6.5.1 Accretion onto the dust grain

Denote the number of species i on the surface of a single grain by $n_{\rm S}(i)$, in the mantle of a dust grain by $n_{\rm M}(i)$, and in the gas phase inside a space volume containing one dust grain by $n_{\rm G}(i)$. Define $n_{\rm S} \equiv \sum_i n_{\rm S}(i)$, and $n_{\rm M} \equiv \sum_i n_{\rm M}(i)$. The total number of surface sites is denoted by $N_{\rm S}$. In principle all these numbers should only take non-negative integer values, although in practice they are allowed to take fraction values, even if they are close to zero.

Considering accretion processes only, we have

$$\partial_t n_{\rm S}(i) = k_{\rm acc}(i) n_{\rm G}(i) - k_{\rm acc} n_{\rm S}(i)/N_{\rm S}, \tag{6.36}$$

where $k_{\rm acc} \equiv \sum_i k_{\rm acc}(i) n_{\rm G}(i)$ is the total accretion rate, that is, the total number of particles arriving on the surface of a dust grain in unit time. The first term is the number

of species i arriving on a dust grain in unit time, and the second term accounts for the fact that each surface site has a probability of $k_{\rm acc}/N_{\rm S}$ to be covered by an incoming particle in unit time.

If the gas phase concentration of species i can be approximated to be constant, then the solution of Eq. (6.36) can be written as

$$n_{\rm S}(i,t) = N_{\rm S}\frac{k_{\rm acc}(i)n_{\rm G}(i)}{\sum_j k_{\rm acc}(j)n_{\rm G}(i)}\left[1-e^{-k_{\rm acc}t/N_{\rm S}}\right], \tag{6.37}$$

which is proportional to the accretion rate of species i, and never becomes greater than $N_{\rm S}$, which is expected.

The total number of particles in the surface layer as a function of time is

$$n_{\rm S} = N_{\rm S}\left[1-e^{-k_{\rm acc}t/N_{\rm S}}\right], \tag{6.38}$$

which is essentially a constant ($=N_{\rm S}$) at a late stage. This is trivially correct, of course.

For the mantle component, we have

$$\partial_t n_{\rm M}(i) = k_{\rm acc}n_{\rm S}(i)/N_{\rm S}, \tag{6.39}$$

which is simply a result of conservation of material. Its time evolution can also be obtained if the gas phase concentration of species i is fixed:

$$n_{\rm M}(i,t) = k_{\rm acc}(i)n_{\rm G}(i)\,t - n_{\rm S}(i)|_{t\to\infty}\left[1-e^{-k_{\rm acc}t/N_{\rm S}}\right]. \tag{6.40}$$

In the limit $t\to+\infty$, $n_{\rm M}(i,t)\to k_{\rm acc}(i)n_{\rm G}(i)\,t - n_{\rm S}(i)|_{t\to\infty}$, which is intuitively obtainable by simple counting.

6.5.2 Evaporation of grain material

Consider evaporation process only, we have

$$\partial_t n_{\rm S}(i) = -k_{\rm eva}(i)n_{\rm S}(i) + k_{\rm eva}n_{\rm M}(i)/\max(n_{\rm M},n_{\rm S}), \tag{6.41}$$

where $k_{\rm eva}\equiv\sum_i k_{\rm eva}(i)n_{\rm S}(i)$ is the total evaporation rate, namely, the total number of particles that are evaporated from a dust grain in unit time. The max() function in the denominator accounts for the fact that, when the number of mantle species is less than the number of surface sites, removing a surface particle does not necessarily reveal a mantle particle, since the particle being removed may be located on top of the dust core material, rather than on mantle material. In contrast, when the number of mantle species is greater than the number of surface sites, removing a surface particle *must* lead to the exposure of one mantle particle, due to our simplified assumption that all the mantle material is uniformly distributed over the dust grain core (hence presenting only one "phase").

It is evident that the mantle material is considered as a whole in this treatment of the evaporation process. Each species in the grain mantle has equal probability to be exposed to external space when a surface molecule is removed, regardless of its depth in the dust grain. The mantle composition is uniform, regardless of depth. Such a description is an approximation to the real situation, where molecules buried deep in the mantle are

evaporated later than those in shallower layers. Nevertheless it is arguably better than the two-phase model.

For the mantle component, we have

$$\partial_t n_{\rm M}(i) = -k_{\rm eva} n_{\rm M}(i) / \max(n_{\rm M}, n_{\rm S}), \tag{6.42}$$

which is simply a result of conservation of material.

Suppose there is only one single species on the dust grain, then $n_{\rm M}$=$n_{\rm M}(i)$, and suppose there are many layers on the dust grain initially, we have

$$n_{\rm M}(t) = \begin{cases} n_{\rm M}|_{t=0} - k_{\rm eva}\, t, & \text{when } t < t_0, \\ N_{\rm S} e^{-k_{\rm eva}(i)(t-t_0)}, & \text{when } t \geq t_0; \end{cases} \tag{6.43}$$

$$n_{\rm S}(t) = \begin{cases} N_{\rm S}, & \text{when } t < t_0, \\ N_{\rm S} e^{-k_{\rm eva}(i)(t-t_0)} \left[k_{\rm eva}(i)(t-t_0) + 1\right], & \text{when } t \geq t_0. \end{cases} \tag{6.44}$$

In the above equation $t_0 \equiv (n_{\rm M}|_{t=0} - N_{\rm S})/k_{\rm eva}$.

6.5.3 The complete set of equations

The full set of equations describing the evolution of surface and mantle species can be written as

$$\begin{aligned} \partial_t n_{\rm S}(i) =& \sum_{j,k} k_{jk} n_{\rm S}(j) n_{\rm S}(k) - \sum_j k_{ij} n_{\rm S}(i) n_{\rm S}(j) \\ &+ k_{\rm acc}(i) n_{\rm G}(i) - k_{\rm acc} n_{\rm S}(i)/N_{\rm S} \\ &+ k_{\rm eva} n_{\rm M}(i) / \max(n_{\rm M}, n_{\rm S}) - k_{\rm eva}(i) n_{\rm S}(i), \end{aligned} \tag{6.45}$$

$$\partial_t n_{\rm M}(i) = k_{\rm acc} n_{\rm S}(i)/N_{\rm S} - k_{\rm eva} n_{\rm M}(i) / \max(n_{\rm M}, n_{\rm S}). \tag{6.46}$$

The first two terms in Eq. (6.45) are the direct contribution from chemical reactions. The total accretion rate $k_{\rm acc}$ and evaporation rate $k_{\rm eva}$ include contributions from surface reactions.

Ordinary differential equations of the above form are stable by themselves (as far as a good implicit solver is used). This can be inferred from the exact solutions for the simple cases in Section 6.5.1 and Section 6.5.2, which involve only exponential and linear functions. The stability is also confirmed in practical model runs.

Besides adsorption and evaporation, in principle surface reactions can also alter the surface coverage and mantle composition. For example, each time the reaction A+B $\longrightarrow$ C occurs, the number of surface particles decreases by one, thus one surface site will become empty, and one mantle particle is exposed to the gas phase. The chemical desorption (see Chapter 5) of surface particle also leaves at least one surface site empty, thus liberating one mantle particles.

To take this effect into account, I divide the surface reactions into two types: those leading to the decrease in total surface population, and those leading to the increase of the surface coverage. The former are treated as if they were evaporation reactions (only in calculating the surface-mantle transfer, of course), and the latter is treated as if they were adsorption reactions. Surface reactions involving no mantle species (such as H+H $\longrightarrow$ H_2)

are not considered. Only the total absolute rates of these two types of reactions enter the equations governing the transfer between surface and mantle populations. Including such an effect is optional.

Another issue is whether to allow the interconversion between surface mantle species even when the mantle is still growing. Such a situation is possible when the concentration of a species inside the mantle is higher than in the surface layer. This can be seen from equation Eq. (6.46): even if the total accretion rate is higher than the evaporation rate ($k_{\rm acc}$>$k_{\rm eva}$), in case

$$\frac{n_{\rm S}(i)}{N_{\rm S}} < \frac{k_{\rm eva}}{k_{\rm acc}} \frac{n_{\rm M}(i)}{n_{\rm M}},$$

$\partial_t n_{\rm M}(i)$ can be negative. It is not clear whether such a scenario is realistic. One option is to disallow the conversion of mantle species into surface species when $k_{\rm acc}$>$k_{\rm eva}$. This can be done by redefining $k'_{\rm acc} = k_{\rm acc} - k_{\rm eva}$, and $k'_{\rm eva} = 0$.

In grain chemistry models the radius of a grain particle is canonically taken to be 0.1 μm. It will gain in size by adsorbing gas phase particles. With the usual gas-to-dust mass ratio of 100, and an estimated metal-to-gas mass ratio[14] of ∼0.006, the mass of a typical dust grain can increase by about 60% at most, and the increase in radius can be 20% at most (assuming uniform density), if all the metals are assimilated into the dust grains. If the mass density of the mantle layer is assumed to be lower, then the increase in radius can be ∼60% (Walmsley et al. 2004). Hence the accretion rate can increase by a factor of 1.4–2.5. Such a change in accretion rate is insignificant and will not be included in our model.

6.6 Results and discussions

As can be seen from previous sections, the model contains a lot of parameters. Some of them may be considered free, while others are not completely free but are not well constrained either. Table (6.9) is a list of parameters that we vary during the modeling in a reasonable interval to see how the behavior of the model changes. For a specific source, some of the parameters (mainly temperature and density) can usually be constrained relatively well observationally. Table (6.10) is a list of parameters that are fixed during the modeling.

(1)	Gas density $n_{\rm H}$;
(2)	Gas temperature $T_{\rm gas}$ and dust temperature $T_{\rm dust}$: we always assume $T_{\rm dust} = T_{\rm gas}$;
(3)	The binding energies of H and D;
(4)	We tested whether to include the $H_2 + OH$ channel for water formation, and whether to allow the abstraction reactions of CH_3OH and H_2CO.

Table 6.9: List of parameters that are varied in our model.

[14] Based on the elemental abundance of the metals usually assumed in the initial conditions of chemical models. Here all the elements heavier than helium are called metal.

(1)	Elemental abundances; mainly taken from Garrod & Pauly (2011); included in table Table (6.11) for reference;
(2)	Initial condition; we always use the abundances obtained with a gas phase chemistry at $t = 10^7$ yr with all the grain reactions turned off except for the formation of H_2 isotopologues;
(3)	The rate parameters of many reactions are not known for sure; here we take their canonical values, or constrain them with experimental and theoretical results;
(4)	We allow CO_2 formation through the three-body reaction H + O + CO, though this mechanism is still largely hypothetical;
(5)	Dust-to-gas mass ratio: $\eta_{\rm m} = 0.01$;
(6)	Dust material density $\rho_{\rm G} = 2$ g cm^{-3};
(7)	Dust grain radius $r_{\rm grain} = 0.1$ μm;
(8)	Cosmic-ray ionization rate: $\zeta = 1.36 \times 10^{-17}$ s^{-1};
(9)	Cosmic-ray desorption rate: 3.16×10^{-19} s^{-1}; assume a cosmic-ray can heat the dust grain to 70 K; cf. Page 33;
(10)	Chemical desorption efficiency is fixed to 0.01 except for one case; unlike the previous chapter on H_2O_2 formation, for the present study we are not very concerned with the release of surface species into the gas phase;
(11)	We disallow dissociation by cosmic-ray-induced photons; this is allowed in the previous chapter;
(12)	Albedo of dust grains: 0.6;
(13)	Density of surface sites: 10^{15} cm^{-2};
(14)	Width of barriers against surface diffusion: 1 Å;
(15)	Height of barriers against surface diffusion: $E_{\rm diff} = 0.5 E_{\rm bind}$;
(16)	Binding energy of each species ($E_{\rm bind}$): taken from literature and fixed (except for H and D); cf. Page 33.
(17)	We always include the contribution of zero-point energies to the desorption and surface migration processes;
(18)	We disallow exposure of mantle species if the accretion rate is higher than the evaporation rate.

Table 6.10: List of parameters that are fixed in our model.

Element	Abundance
H	1
D	2.00(−5)
He	0.09
C	1.40(−4)
N	7.50(−5)
O	3.20(−4)
S	8.00(−8)
Si	8.00(−9)
Na	2.00(−8)
Mg	7.00(−9)
Fe	3.00(−9)
P	3.00(−9)
F	2.00(−8)
Cl	4.00(−9)

Table 6.11: Elemental abundances assumed in our model; taken from Garrod & Pauly (2011), except D and F. The F abundance is taken from Woodall et al. (2007). The D abundance is based on the value for proto-solar gas; see Section 6.1. X(Y) means $\mathrm{X} \times 10^{\mathrm{Y}}$.

6.6.1 Ice mantle composition

Similar to previous chapters, in the following a species name with prefix "g" means a surface species, while a prefix "m" means a mantle species. These prefixes are not always included for brevity when writing the name of a species, and the meaning should always be clear from the context.

We first run a set of reference models, the results of which will be described in the following. For a given set of physical parameters (temperature and density, grain radius, etc.), the initial abundances of the gas phase species are taken to be the state at $t = 10^7$ yr of a pure gas phase model (with accretion and evaporation of H and D atoms and the surface formation of H_2 isotopologues included) starting from atomic initial condition (except that H is in the form of H_2 while D is in the form of HD). For the reference models, the binding energies of H and D atoms are taken to be 350 K subtracted by their respective zero-point energies; hence $E_{\mathrm{bind}}(\mathrm{H}) = 292$ K, and $E_{\mathrm{bind}}(\mathrm{D}) = 309$ K.

Fig. (6.5) shows the fractional ice mantle composition in each mantle layer for $T = 10$ K and 15 K, $n_{\mathrm{H}} = 10^3$–10^6 cm^{-3}. A possibly more intuitive view may be seen in Fig. (6.6). The abundances of the major mantle species as a function of time are shown in Fig. (6.7) (relative to H_2O) and Fig. (6.8) (relative to H_2), and the growth of the number of mantle layers is shown in Fig. (6.9).

For most of the physical conditions considered here, the ice mantle is dominated by H_2O, which can be clearly seen in Fig. (6.6) and Fig. (6.7). The [mCO/mH_2O] ratio generally increases with density, while the [mCH_3OH/mH_2CO] ratio decreases with density, as can be seen in Fig. (6.10), especially when $T = 10$ K; at $T = 15$ K the trend is not as obvious. For $T = 10$ K and $n_{\mathrm{H}} = 10^6$ cm^{-3}, the mantle is dominated by CO and O_3, with a $\mathrm{CO} : \mathrm{O_3} : \mathrm{H_2O}$ ratio of about $9 : 3 : 1$.

The reason for the decrease in water and methanol abundances as density increases is

because a higher gas density (for $T = 10$ K) means a lower atomic hydrogen abundance in the gas phase (see the following), while the abundance of CO in the gas phase (when accretion has not started) does not have a strong dependence on density. This can be seen in Fig. (6.11) for the $T = 10$ K case, where the initial abundances of H, D, and CO (obtained from a pure gas phase chemistry) are plotted as a function of gas density. As the [H/CO] ratio becomes lower at higher density, there will not be enough H atoms available to produce water, or to hydrogenate CO into CH_3OH, which leads to the higher $[CO/H_2O]$ and $[H_2CO/CH_3OH]$ ratios at a higher density.

The reason for the abundance of gas phase atomic hydrogen to decrease with density is explained in the following. The gas phase density of H, $n(H)$, is usually $\sim$1 cm^{-3} independent of temperature and the overall gas density in dark clouds. Hence its abundance, [H], which is defined to be the ratio between its density and the total density[15] of hydrogen nuclei n_H, varies with n_H as $[H] \propto n_H^{-1}$. The fact that $n(H)$ is constant is based on the assumption that the gas phase atomic hydrogen is mainly produced by cosmic-ray ionization of H_2 molecules, and mainly consumed by adsorption onto the dust grains. Namely, we may assume H is mainly formed in the following reaction chain

$$\begin{aligned} H_2 + \mathrm{CRP} &\xrightarrow{k_{\cos}} H_2^+ + E^-, \\ H_2^+ + H_2 &\xrightarrow{k_1} H_3^+ + H, \\ H_3^+ + E^- &\xrightarrow{k_2} 3\,H, \\ gH &\xrightarrow{k_{\mathrm{eva}}} H, \end{aligned} \tag{6.47}$$

and consumed through

$$H \xrightarrow{k_{\mathrm{acc}}} gH. \tag{6.48}$$

These yield the following equations

$$\begin{aligned} \partial_t n(H_2^+) &= k_{\cos} n(H_2) - k_1 n(H_2) n(H_2^+), \\ \partial_t n(H_3^+) &= k_1 n(H_2) n(H_2^+) - k_2 n(H_3^+) n(E^-), \\ \partial_t n(H) &= k_1 n(H_2) n(H_2^+) + 3k_2 n(H_3^+) n(E^-) + k_{\mathrm{eva}} n(gH) - k_{\mathrm{acc}} n(H), \end{aligned} \tag{6.49}$$

where the density of H_2 is assumed to be constant. Using Eq. (3.4) on page 31, which indicates that

$$k_{\mathrm{acc}} = \eta v(H) \sigma n_H R_{G,n}, \tag{6.50}$$

where η is the sticking coefficient (we assume $\eta = 1$), σ is the dust grain cross section, and $R_{G,n}$ is the dust-to-gas number ratio, we have for the steady-state (i.e. $\partial_t n(X) = 0$) solution

$$n(H) = \frac{k_{\cos} 4 n(H_2) + k_{\mathrm{eva}} n(gH)}{k_{\mathrm{acc}}} \simeq \frac{2k_{\cos}}{v(H)\sigma R_{G,n}}, \tag{6.51}$$

where in the last step the evaporation of surface H has been neglected. The above expression does not depend on the total gas density, and indeed has a typical value of $\sim$1 cm^{-3}.

[15] For molecular clouds the total density of hydrogen nuclei can be approximated very well by two times the density of H_2 molecule.

Why is the steady-state abundance of CO in gas phase chemistry roughly independent of gas density? This is simply because practically all the carbon atoms have been converted into CO molecules (note that the abundance of oxygen is about two times the abundance of C) in steady state, so the abundance of CO is just the elemental abundance of carbon, which is widely considered constant.

Then, can we say that it is impossible to form a large amount of water and methanol ice at very high gas density ($\gtrsim 10^6$ cm^{-3}, for example) because in these cases the [H/CO] ratio will be low? Seemingly not, since it can be clearly seen in Fig. (6.5)–Fig. (6.8) that in the $T = 15$ K case the water and methanol ice can still be present with a high abundance at $n_{\rm H} = 10^6$ cm^{-3}.

The fact is that at $T = 15$ K the evaporation of surface H atoms becomes important. Note that for a binding energy of 300 K for H, the evaporation rate at 15 K is about $e^{10} \simeq 2{\times}10^4$ times faster than at 10 K. This is a significant difference. As can be seen in the right panel of Fig. (6.11), the initial abundances of gas phase H and D for $T = 15$ K are much higher than for $T = 10$ K, especially when $n_{\rm H} > 10^3$ cm^{-3}, and they are almost independent of density at 15 K.

This independence on density is due to the fact that we set the initial abundances of the gas-grain model to be the abundances of a gas phase model at $t = 10^7$ yr, and when the surface evaporation rate of H is too high, the steady state has not been reached at this time. This is because a high evaporation rate means H_2 cannot be efficiently formed on the grain, and the H_2 molecules will be continuously converted into H atoms by cosmic-ray ionization. The latter process is quite slow, with a time scale of $\sim 2.6{\times}10^9$ yr.

Hence the apparently very different results at $T = 10$ K and 15 K for $n_{\rm H} = 10^6$ cm^{-3} are due to our way of setting the initial abundances, and to the low binding energies of H and D atoms. To confirm this, we tried higher values for the binding energies for H and D, 618 K for H and 642 K for D, which are obtained from a common value of 700 K subtracted by their corresponding zero-point energies. In this case their evaporation rates become negligible (the evaporation time scales are hundreds of years). The resulting ice mantle compositions are shown in Fig. (6.12). Now the differences between the $T = 10$ K and 15 K case are much smaller than before, though still noticeable.

On the other hand, the presence of "dry" CO ice (i.e. not mixed with water ice) in our reference model and in the one with higher binding energies for H and D at $n_{\rm H} = 10^6$ cm^{-3} is consistent with the existence of non-polar CO ice suggested by observations. By observing the absorption band of solid CO toward 18 protostars, Tielens et al. (1991) discovered that at least two independent grain mantle compositions are needed to explain the spectra: a polar mixture component rich in H_2O and a nonpolar component dominated by CO. Our modeling results suggest that in cold dense ($\gtrsim 10^6$ cm^{-3}) environments nonpolar grain mantles tend to be formed, while at lower densities or higher temperatures (which, however, must still be lower than the evaporation temperature of the heavy species) water-rich ice mantles tend to be formed. This is similar to the suggestion of Pontoppidan et al. (2008).

We may note that, accompanying the formation of CO-dominated ice, a relatively high abundance of O_3 can also be accumulated on the grain mantle, which may serve as a test of our model. However, the formation of O_3 is subject to uncertainties, since it is sensitive to the surface mobility of O atoms (while the water formation is not). If O is immobile, then O_3 cannot be formed, at least in the Langmuir-Hinshelwood mechanism.

One may also invoke the Eley-Rideal mechanism to form O_3, in which an O atom from the gas phase hitting a surface O_2 molecule can directly react with it to form O_3, similar to the formation of CO_2 through a three-body reaction mechanism.

Our modeling results may be compared with the observational results, as compiled in Table (6.12), where the abundances of a few major ice species expressed relative to H_2O are listed. Due to the intrinsic complexity of the ISM, where the dust can be processed by various processes, such as shock sputtering and heating, radiative evaporation and dissociation, collision with high-energy particles, etc., one should not expect that a single model can reproduce all the observational results. Furthermore, we should not expect that the dust is formed in the environments where it is currently observed either; evolution in time, as well as transportation in space are likely to be common for the interstellar matter. Observationally, the abundance ratios of those major ice species can vary from source to source significantly, even for sources within the same class. However, our modeling results can already match the observed abundances of most of them reasonably well, if different physical conditions for the formation of grain mantles are assumed.

The CO abundance is the easiest to match, which is typically 10%–50% with respect to water except for the extreme case of $T = 10$ K and $n_{\rm H} = 10^6$ cm^{-3}, where little water ice is present; see Fig. (6.7) and Fig. (6.10). For CO_2, the $[CO_2/H_2O]$ ratio is around 10%–30% at $T = 10$ K and $n_{\rm H} = 10^4$ cm^{-3}, which are also consistent with the observational results in Table (6.12). In the nonpolar case where water is deficient the $[CO_2/H_2O]$ ratio can be up to 40%.

The CH_3OH and H_2CO abundances seem to be more challenging. For $T = 10$ K, only with a low density (10^3 cm^{-3}) can the $[CH_3OH/H_2O]$ ratio be higher than 20%, and for $n_{\rm H} = 10^4$ cm^{-3} the ratio is a few percent. Similar for the $[H_2CO/H_2O]$ ratio, though it is typically higher by a factor of a few to ten than the $[CH_3OH/H_2O]$ ratio at higher densities. The $[CH_4/H_2O]$ ratio can be about 1%–2% at most in our reference model, while the $[NH_3/H_2O]$ ratio is normally a few percent, and can be up to 10%. Our model produces CH_4 and NH_3 at lower quantities than observed. This is understandable, since in the initial conditions of our model practically all the carbon is in CO and all the nitrogen is in N_2.

From Figs. (6.5), (6.6) and (6.9) we may notice that the number of mantle layers at steady state is different for different physical conditions, and it seems to be larger at a higher temperature, and that for $T = 10$ K, the number of layers at $n_{\rm H} = 10^6$ cm^{-3} is smaller than at 10^5 cm^{-3}. Though apparently counterintuitive, since we might think that at lower temperature or higher density more species can be adsorbed, the reason also lies in the abundance of H atoms. A higher flux of H atoms injected on the dust grain tends to hydrogenate the heavy molecules (atoms) on the surface, instead of letting them combine with each other. For example, on the surface oxygen atoms can combine to form O_2 and O_3 molecules, which will be stored in the mantle layer and become unavailable for hydrogenation. If the hydrogen flux is high, they may be converted into water ice before being covered. Note that one layer of O_3, if completely converted into H_2O, will be counted as three layers. The same holds for CO_2, where one layer of CO_2, if divided into O and CO, will be counted as two layers. When the hydrogen flux is high, the probability for the three-body reaction $H + O + CO \longrightarrow CO_2$ becomes lower, because O and CO will most likely directly react with an incoming H atom; but when the hydrogen flux is low, the accumulation of surface O and CO makes this reaction much more likely.

The total number of layers can be estimated by assuming all the oxygen and carbon atoms have been converted into H_2O and CO ices. The elemental abundance of O is adopted to be 3.2×10^{-4} relative to H. With a dust-to-gas number ratio of 2.8×10^{-12}, the number of O atoms that can accumulate on one dust grain is $3.2\times10^{-4}/(2.8\times10^{-12}) \simeq 10^8$, which gives a total layer number of $\sim$100, since the number of surface sites on a dust grain is $\sim10^6$. The elemental abundance of nitrogen is about 1/4 that of oxygen, and if it is mainly in the form of N_2, it constitutes only about 1/8 of the mantle volume.

Reference	CO	CO_2	CH_3OH	H_2CO	CH_4	NH_3	HCOOH	$HCOO^-$	XCN	Source
Skinner et al. (1992)			10% (or >0.5?)							LM
Schutte et al. (1996)			4%	6%						LM
Chiar et al. (1994)	40%									DC
Chiar et al. (2000)	<12%	14%	<4%		2%	20–30%	6%			GC
Gibb et al. (2000)	8%	13%	18%	6%	1.5%	15%	7%		3.5%	LM
Thi et al. (2006)			10%							LM
Boogert et al. (2008)			1%–30%	6%		3%–8%	1%–5%	0.3%		LM
Pontoppidan et al. (2008)		32%								LM
Öberg et al. (2008)					2%–8%					LM
Bottinelli et al. (2010)						2%–15%				LM
Öberg et al. (2011)	29%	29%	3%		5%	5%			0.3%	LM
Öberg et al. (2011)	13%	13%	4%		2%	5%			0.6%	HM
Öberg et al. (2011)	31%	38%	4%							CC
Boogert et al. (2011)			11%							CC
Chiar et al. (2011)			2%			5%				DC

Table 6.12: Observed composition of dust grain mantles. The abundances are relative to water ice. LM: Low mass young stellar objects; HM: High mass protostars; DC: Dark clouds; CC: cloud cores. GC: Galactic center; Sgr A*.

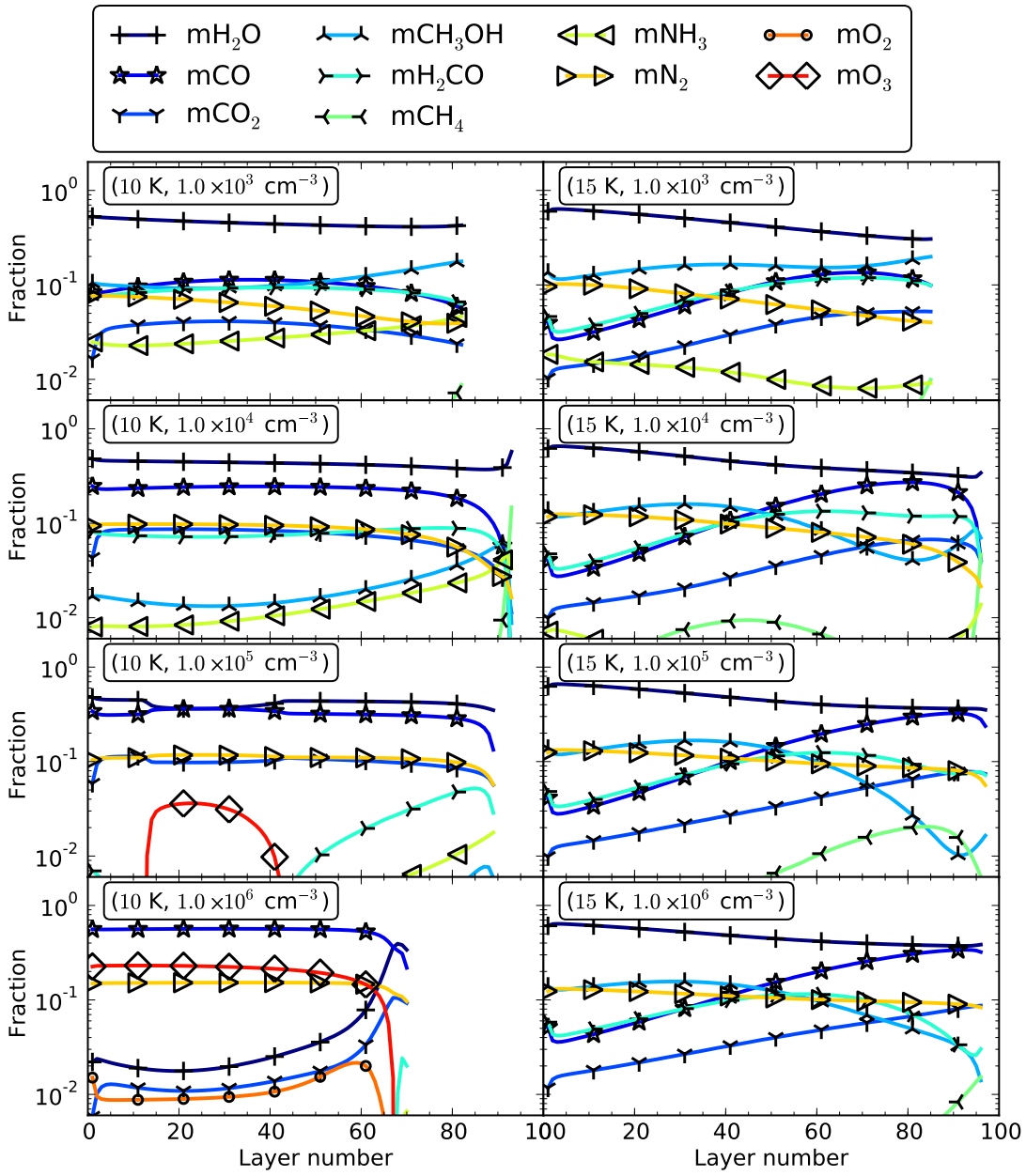

Figure 6.5: Fractional composition of ice mantle by layer. The fractional abundance of a species is defined as its number in a layer divided by the total number of all the species in that layer. Different panels correspond to a different combination of temperature and density. Note that in this and all the subsequent figures of this chapter each curve has a unique marker, which is useful for distinguishing one curve from the others.

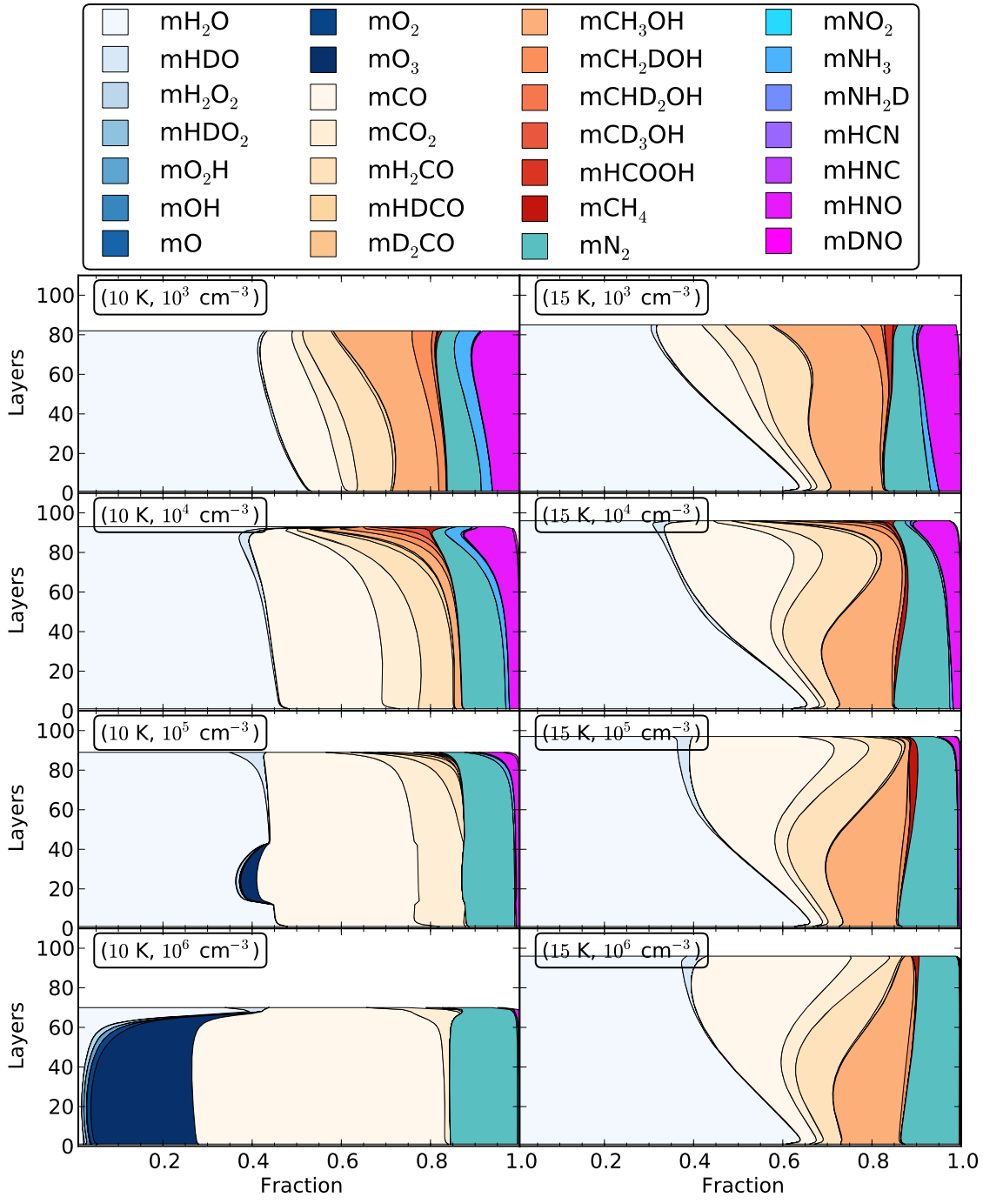

Figure 6.6: Distribution of a selection of ice species in the mantle layers. The fractional abundance of a species in a layer is proportional to the width of the corresponding region at that layer. Note that the left-to-right order of species in the sub-figures corresponds to the top-to-bottom-then-left-to-right order in the legend. The C, N, O based molecules are color-coded differently. In principle the color-filled region in all the sub-figures should be a perfect rectangle; the fact that some are not perfectly rectangular is due to the omission of certain minor species (such as mDCOOH, mCH_3D, etc.). The abundance of HNO may be unreliable due to the possible incompleteness of the surface nitrogen chemistry.

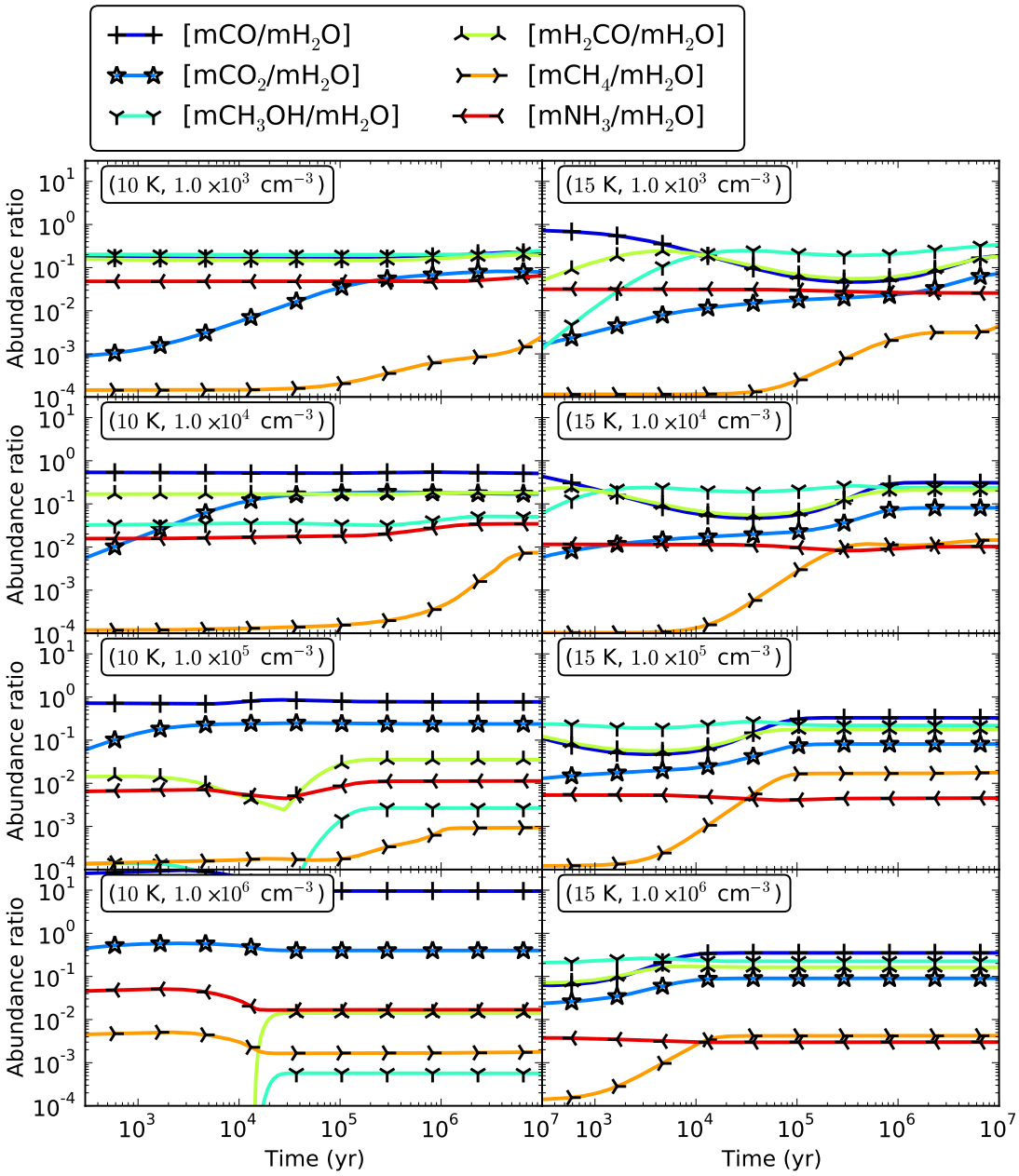

Figure 6.7: Abundances (relative to H_2O) of major ice mantle species as a function of time. Different panels corresponds to a different combination of temperature and density.

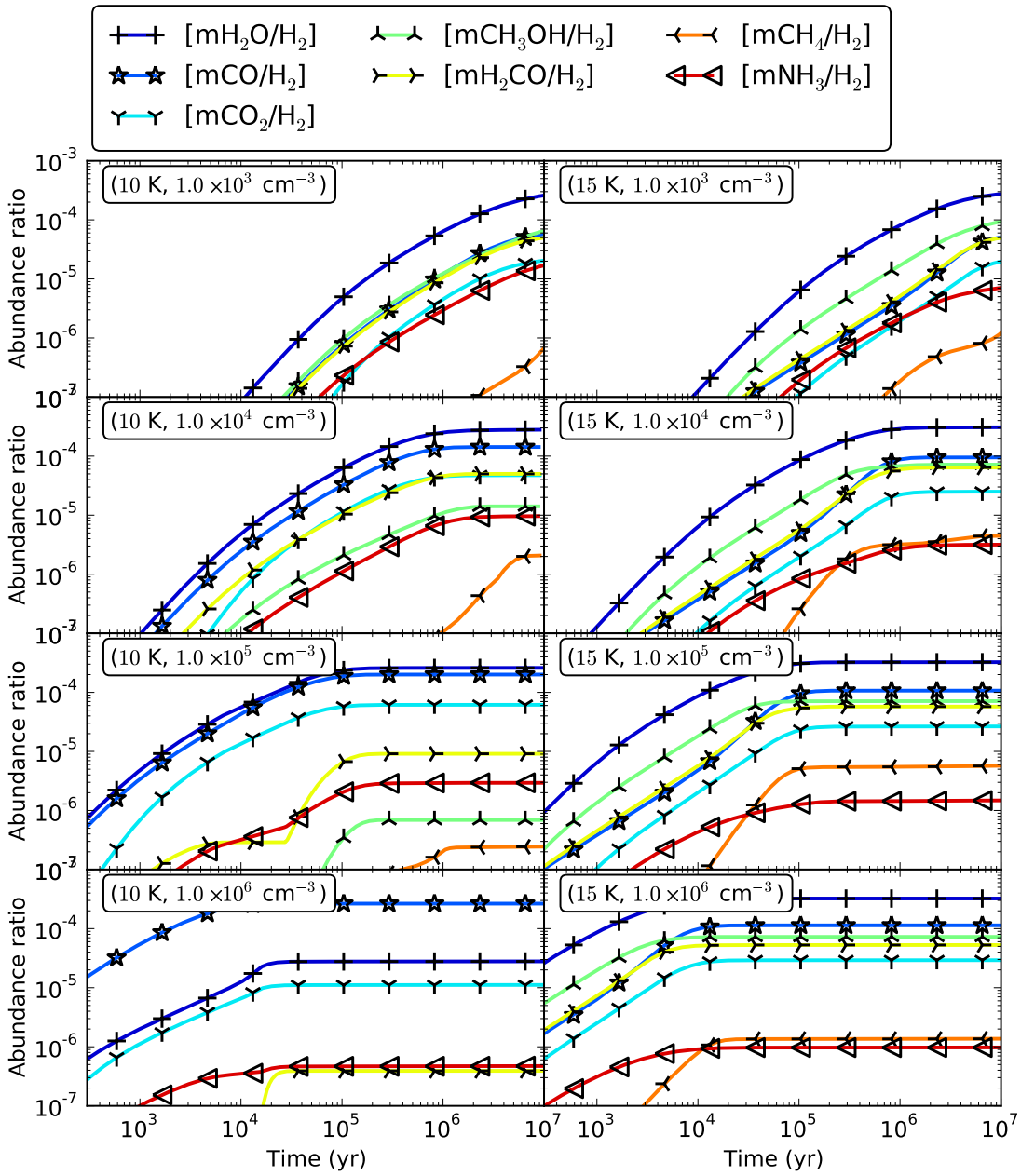

Figure 6.8: Abundances (relative to H_2) of major ice mantle species as a function of time. Different panels corresponds to a different combination of temperature and density.

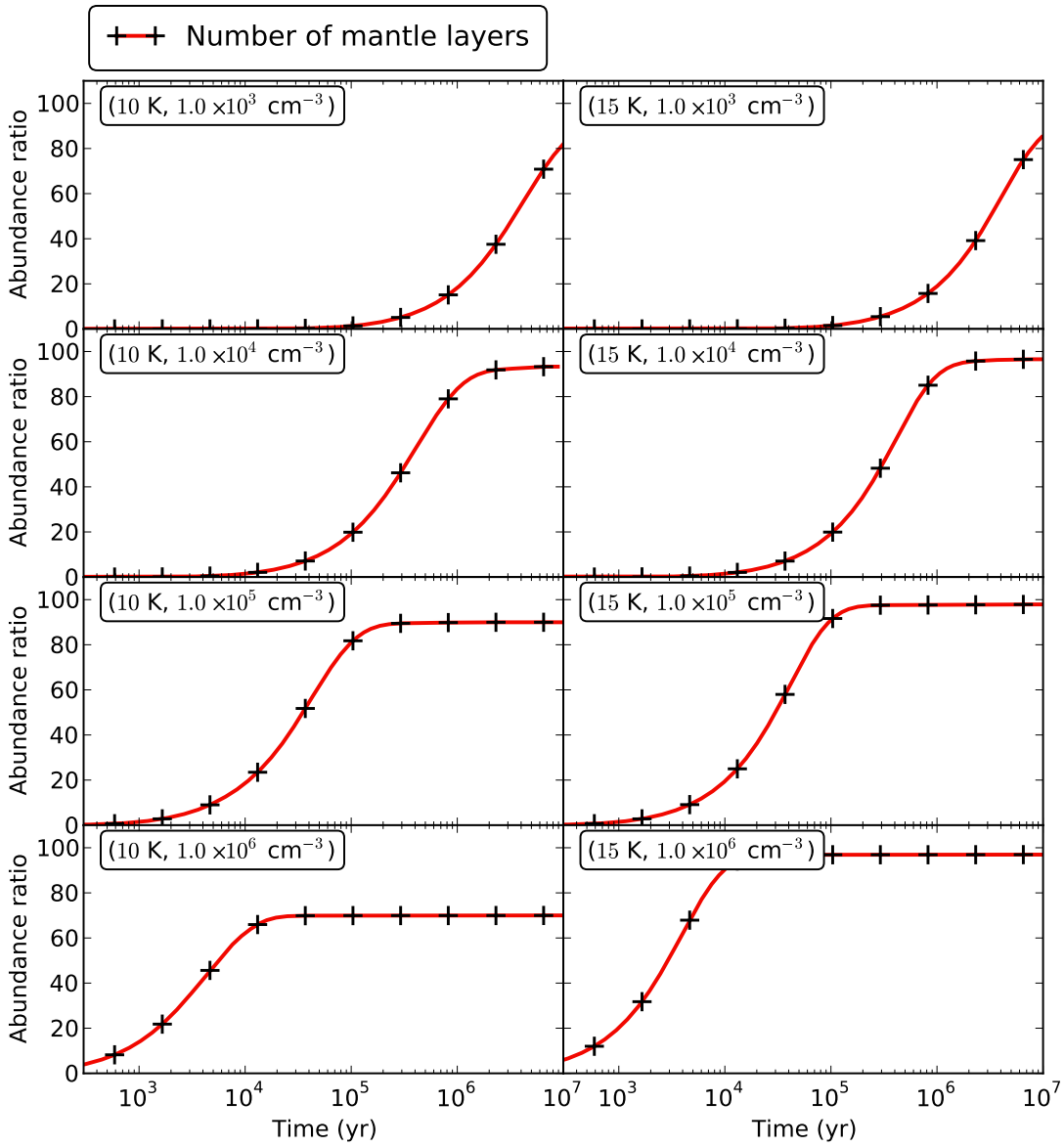

Figure 6.9: Number of mantle layers as a function of time. Different panels corresponds to a different combination of temperature and density.

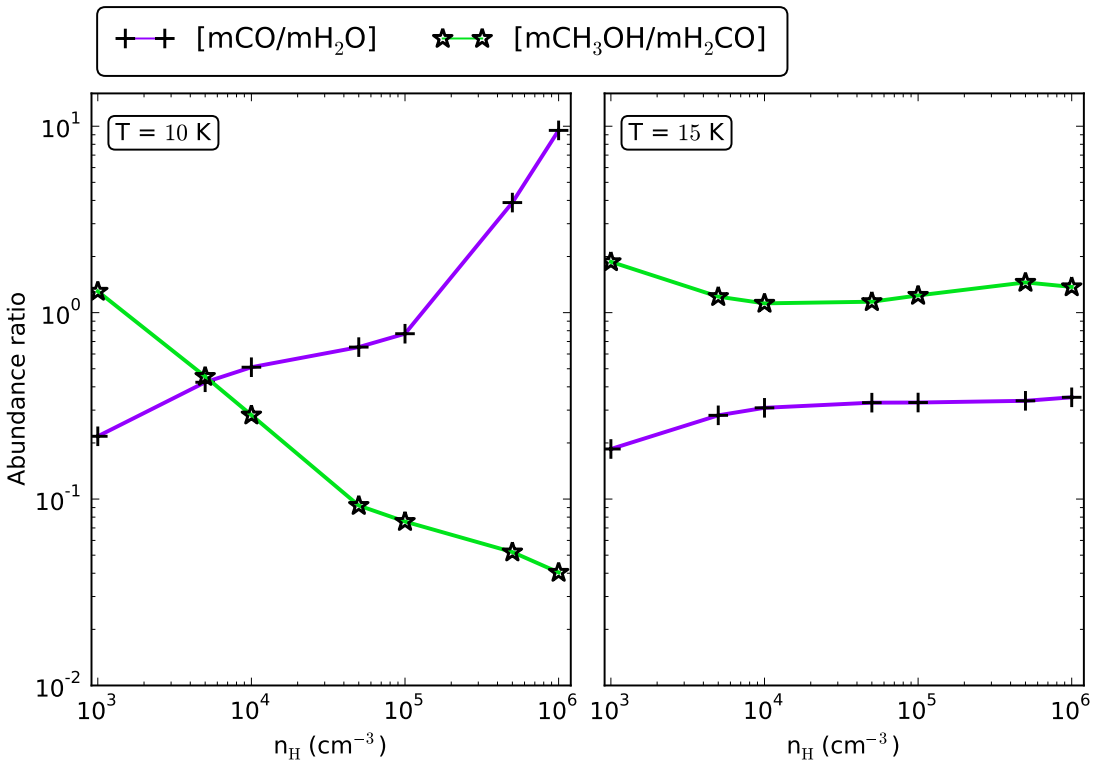

Figure 6.10: The ratios between the abundances of CO ice and water ice, and between the abundances of CH_3OH ice and H_2CO ice at $t = 10^7$ yr, as a function of gas density, for $T = 10$ K and 15 K.

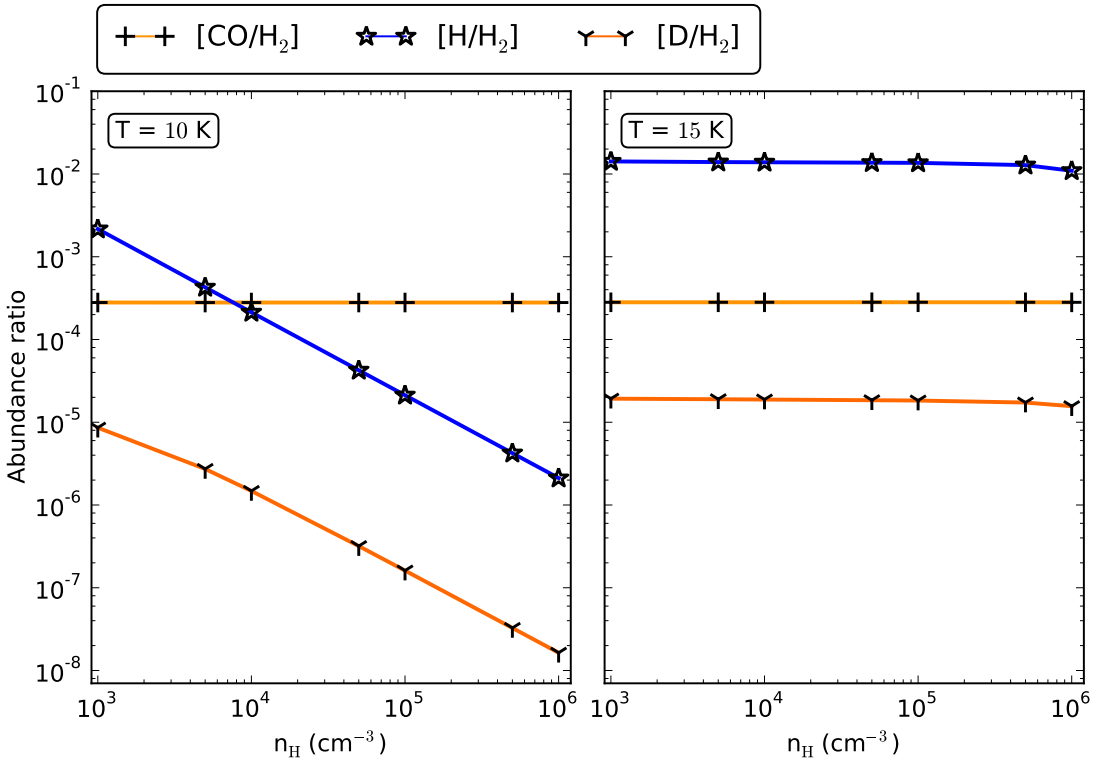

Figure 6.11: Initial abundances of CO, H, and D as a function of density for $T = 10$ K and 15 K. The initial conditions are taken as the steady-state abundances of a gas phase chemical model, with only surface formation of the H_2 isotopologues included.

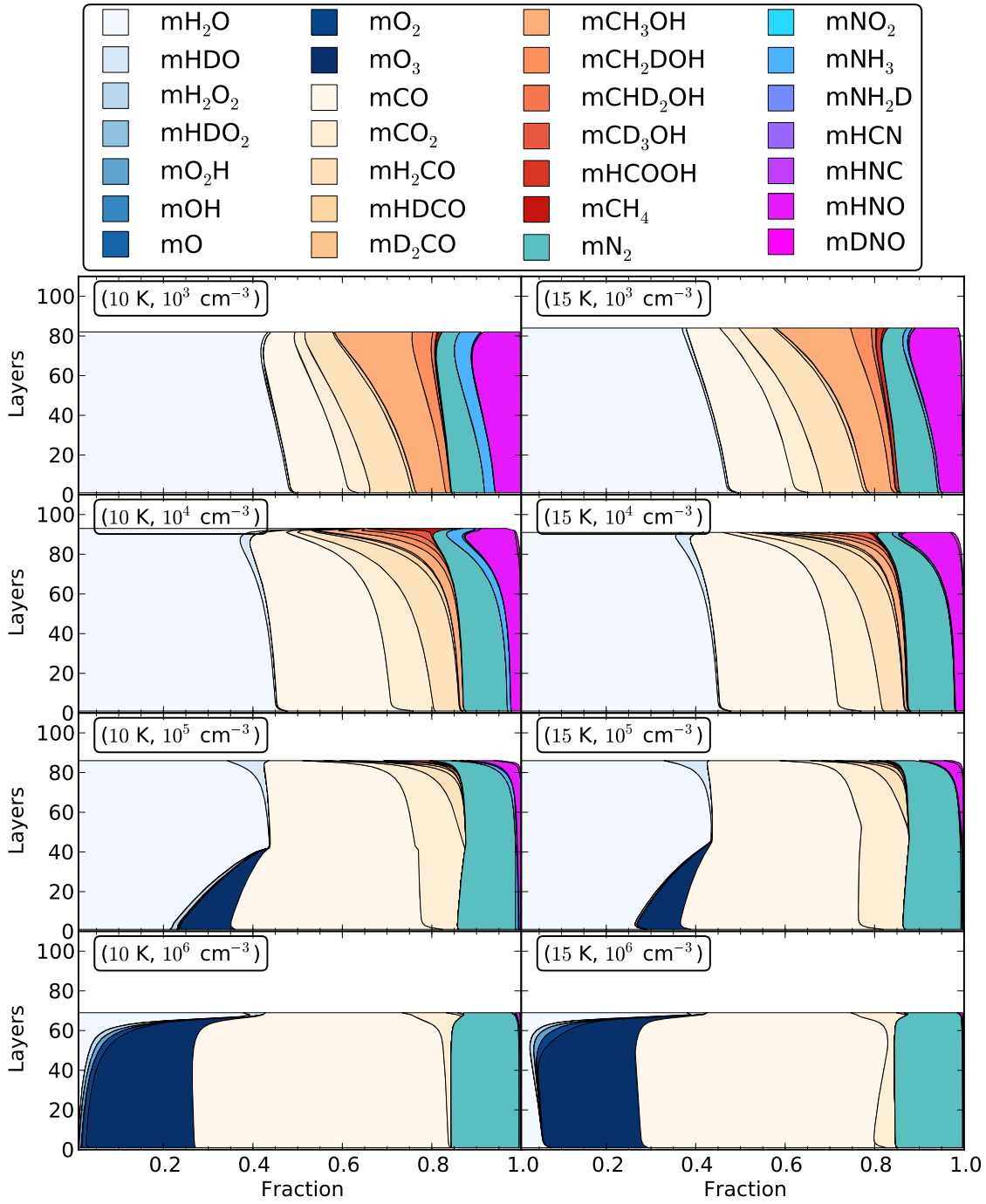

Figure 6.12: Distribution of a selection of ice species in the mantle layers. Obtained with the same parameters as in Fig. (6.6) except that higher values (700 K) have been adopted for the binding energies of H and D atoms on the surface.

6.6.2 Deuterium fractionation

In the previous section we discussed the general ice mantle composition obtained from a set of models. In this section our emphasis will switch to the deuterium fractionation in ice mantles for the same set of models.

Fig. (6.13) shows the abundance ratios between the singly deuterated species and the main isotopologues of water, methanol, and formaldehyde as a function of time, for temperatures of 10 K and 15 K, and densities of 10^3–10^6 cm^{-3}. Fig. (6.14) is for doubly deuterated species.

Obviously, the methyl (CH_3) group of methanol has the highest degree of deuteration, while the degree of deuteration for water is always much lower, and formaldehyde lies in between. CH_2DOH can be as abundant as CH_3OH, while the [HDO/H_2O] ratio is mostly only a few percent, and never exceeds 0.1. The [$HDCO/H_2CO$] ratio is between a few percent to a few 10%.

The situation is similar for doubly deuterated species. In the extreme case ($T = 10$ K, $n_H = 10^5$–10^6 cm^{-3}), the abundances of CHD_2OH and D_2CO can even be comparable to those of their main isotopologues, while for water, the [D_2O/H_2O] ratio never exceeds 10^{-4}. However, we have to note that at high densities the absolute abundances of these species (whether deuterated or not) tend to be low, especially for methanol, as discussed in the previous section.

The D atoms in the hydroxyl (OH) group of CH_3OH are special, in the sense that the [CH_3OD/CH_3OH] ratio has a large variance with respect to the deuteration ratio of other species. For $T = 10$ K and $n_H = 10^3$ and 10^4 cm^{-3}, it is almost identical to the [HDO/H_2O] ratio, while for the same temperature but higher densities it becomes a few times larger than the [HDO/H_2O] ratio. For $T = 15$ K and $n_H = 10^3$–10^6 cm^{-3} it is about one order of magnitude lower than the [HDO/H_2O] ratio.

As the mantle grows with time, the degree of deuteration also increases. This is due to the increase in the [D/H] ratio caused by the adsorption of molecules such as CO and N_2 to the dust grains (see Section 6.2), as can be clearly seen in Fig. (6.15).

Dependence on density and temperature

Fig. (6.16) plots the deuteration ratios of the singly deuterated species at $t = 10^7$ yr as a function of density for $T = 10$ K and 15 K. At $T = 10$ K, the deuteration ratios increase with density, as one might expect. But at $T = 15$ K the behavior becomes different: the deuteration ratios are not very sensitive to density, and may in fact decrease with density. What causes this behavior? The situation may be more clearly seen in Fig. (6.17), where the deuteration ratios are plotted versus the gas phase [D/H] ratio for each evolution track. Its right panel (the $T = 15$ K case) shows that the deuterium fractionation ratios of mantle CH_3OH, H_2CO, and H_2O are rather insensitive to the atomic [D/H] ratio; they are almost constant along the full evolution tracks.

The reason is still related with the way we set the initial abundances and the binding energies of H and D on the grain surface. As discussed in the previous section, when the binding energies of H and D are low, their initial gas phase abundances will be very high regardless of the gas density, since they cannot be efficiently converted into H_2 (and its isotopologues) on the grain surface. When the accretion process has started, molecules such as CO accumulate on the grains, which then act as an efficient sink for the injected

H and D atoms, and the gas phase abundance of H and D will start to decline. The time scales for the consumption of H and D are their accretion time scale, which are within one order of magnitude of the accretion time scales of heavier species such as CO and O_2. Over such an period, the [D/H] ratio in the H and D fluxes injected on the dust grains have essentially the ratio set by the initial conditions. This explains why the resulting deuteration ratios of H_2O, H_2CO, and CH_3OH are seemingly independent of density.

This explanation is confirmed by using higher binding energies for H and D on the surface. Fig. (6.18) shows the evolution of the abundances of several deuterated species for $T = 15$ K, $n_H = 10^6$ cm^{-3}, for two different values of the binding energies (350 K and 700 K) of H and D. For the low-binding-energy case, the abundances of gas phase H and D decreases with time, while for the high-binding-energy case, the H abundance keeps roughly constant, while the D abundance increases with time, due to the accretion of heavy molecules such as CO and N_2, just as expected (see Section 6.2), as can be clearly seen in Fig. (6.19)[16]. The resulting deuteration degrees as a function of gas density for $T = 10$ K and 15 K are shown in Fig. (6.20). Now, in contrast to Fig. (6.16), the curves for the two different temperatures are nearly identical.

Hence we have seen that the assumed binding energies of H and D, as well as the way to assign the initial abundances, have a significant effect on the deuterium fractionation ratios.

Fractionation of fractionation

The differences in the deuterium concentrations of different species can be informally described as "fractionation of fractionation". The reason lies in the formation paths of different species. The mantle species X (denoted by mX) is formed from surface X (denoted by gX) through the surface-mantle conversion process due to continuous accretion of materials onto the grain surface. Since there is no evaporation at low temperatures, essentially

$$n(\mathrm{mX}, t) = \int_0^t \frac{k_{\mathrm{acc}}}{N_S} n(\mathrm{gX}, t')\mathrm{d}t', \tag{6.52}$$

where N_S is the number of surface sites, and k_{acc} is the total accretion rate. So to understand the deuterium fractionation of mantle species, we need to look at the evolution history of surface species.

In our model HDO is mainly formed through H_2+OD $\longrightarrow$ HDO+H, and H_2O is mainly formed through $H_2 + OH \longrightarrow H_2O + H$. Other channels, such as $H + HDO_2 \longrightarrow HDO + OH$ and $D + H_2O_2 \longrightarrow HDO + OH$ only play a minor role. The addition channels $H + OD \longrightarrow HDO$ and $D + OH \longrightarrow HDO$ contribute even less to the HDO formation, except for $n_H = 10^3$ cm^{-3} and for low binding energies of H and D, leading to high fluxes of H and D injected onto the dust, but even in this case these two channels are still unimportant.

The reaction H_2+OH $\longrightarrow$ H_2O+H has a relatively high barrier of 2100 K, and we have been using a barrier width of 0.3 Å for it. Assuming quantum tunneling, the probability

[16] The reason that the evolution of H_2D^+ isotopologues in Fig. (6.19) has a peak, instead of approaching a certain limit asymptotically, is due to the increase in the abundances of electrons, which is a consumer of the H_2D^+ isotopologues. The increase in electron abundance is also caused by the depletion of CO, O_2, etc., because electrons are mainly consumed by reacting with HCO^+, H_3O^+, ..., if they are abundantly present.

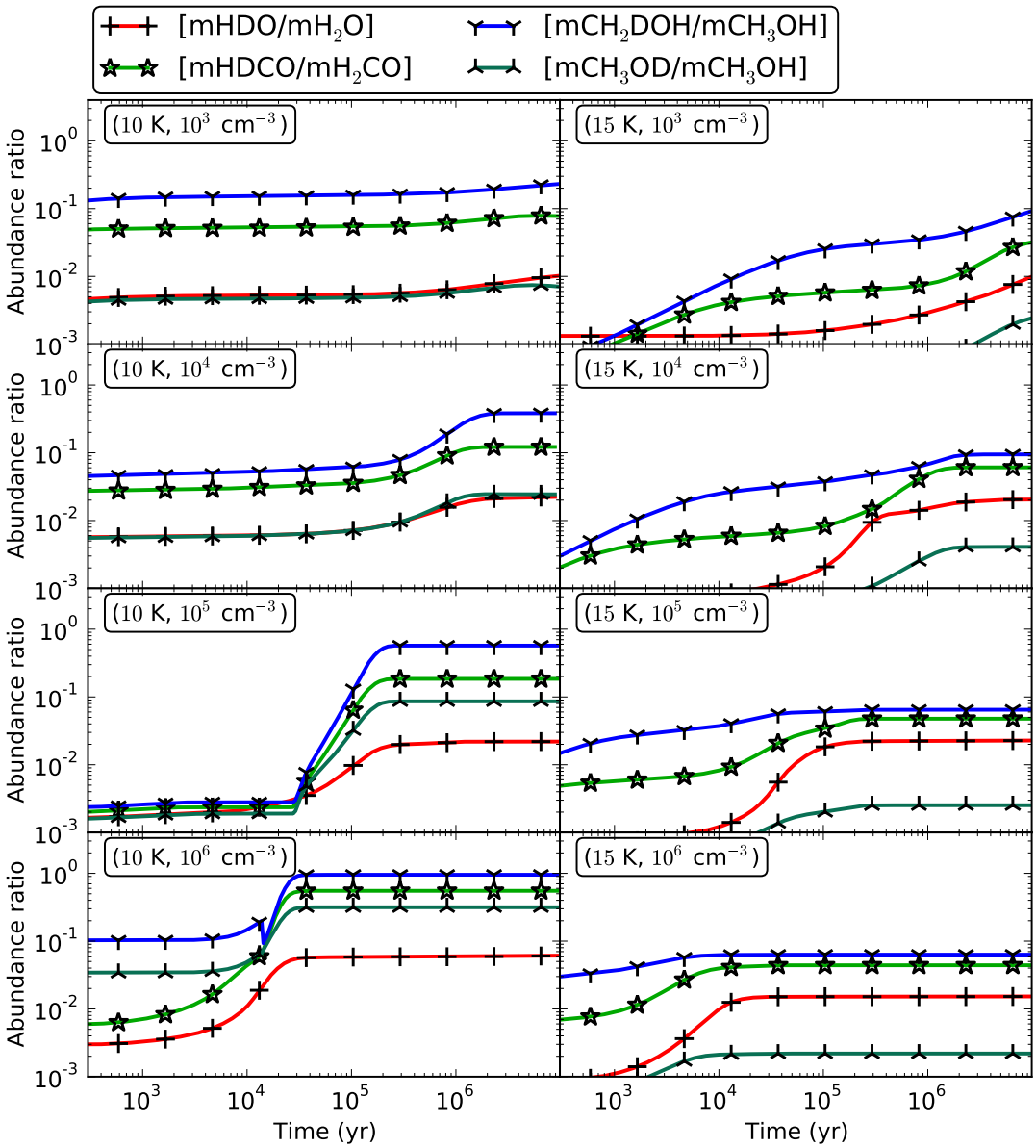

Figure 6.13: Abundances of singly deuterated water, methanol, and formaldehyde relative to their main isotopologues under different physical conditions. Different species are marked with different markers. All the panels share the same X- and Y- axis scale.

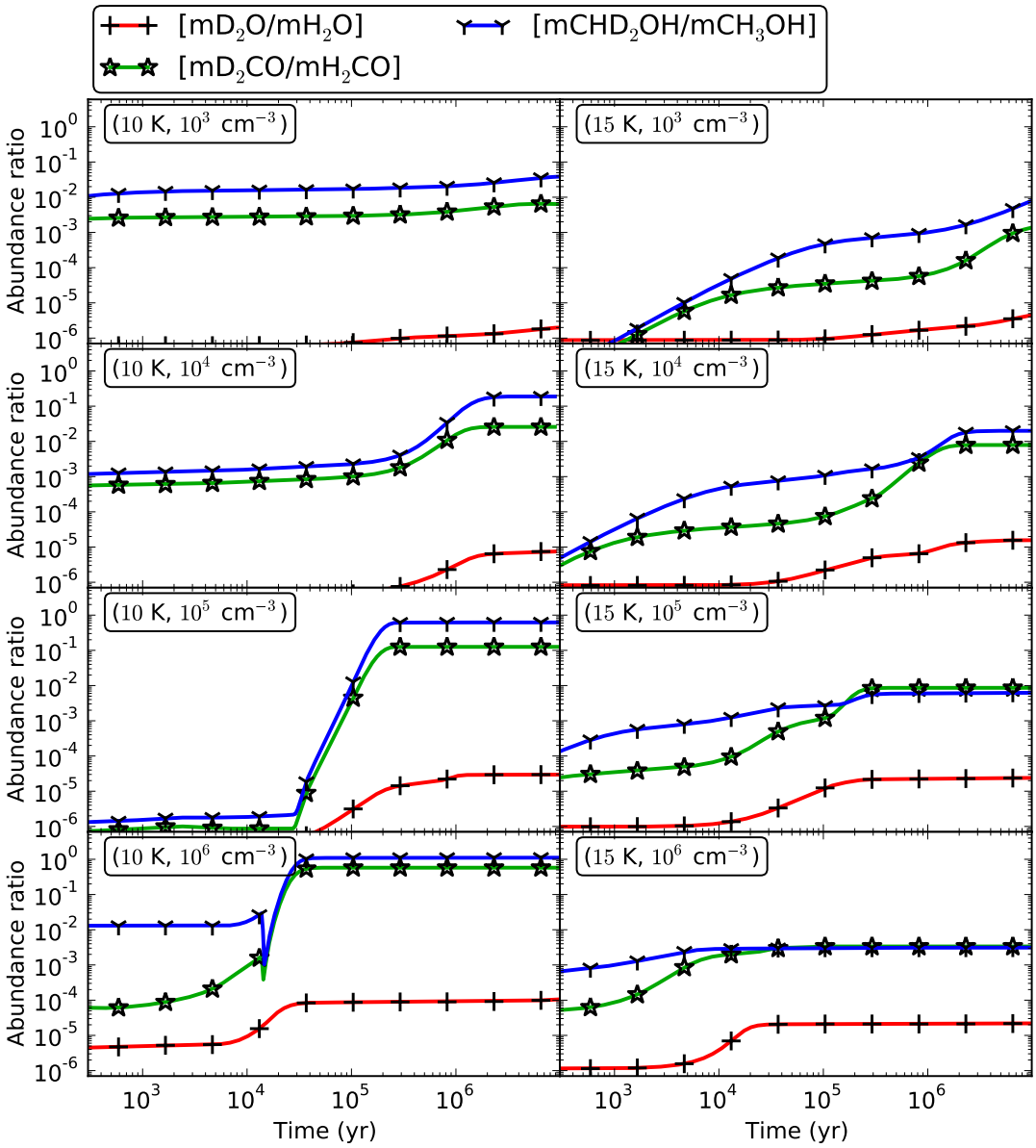

Figure 6.14: The same as Fig. (6.13), except for doubly deuterated species.

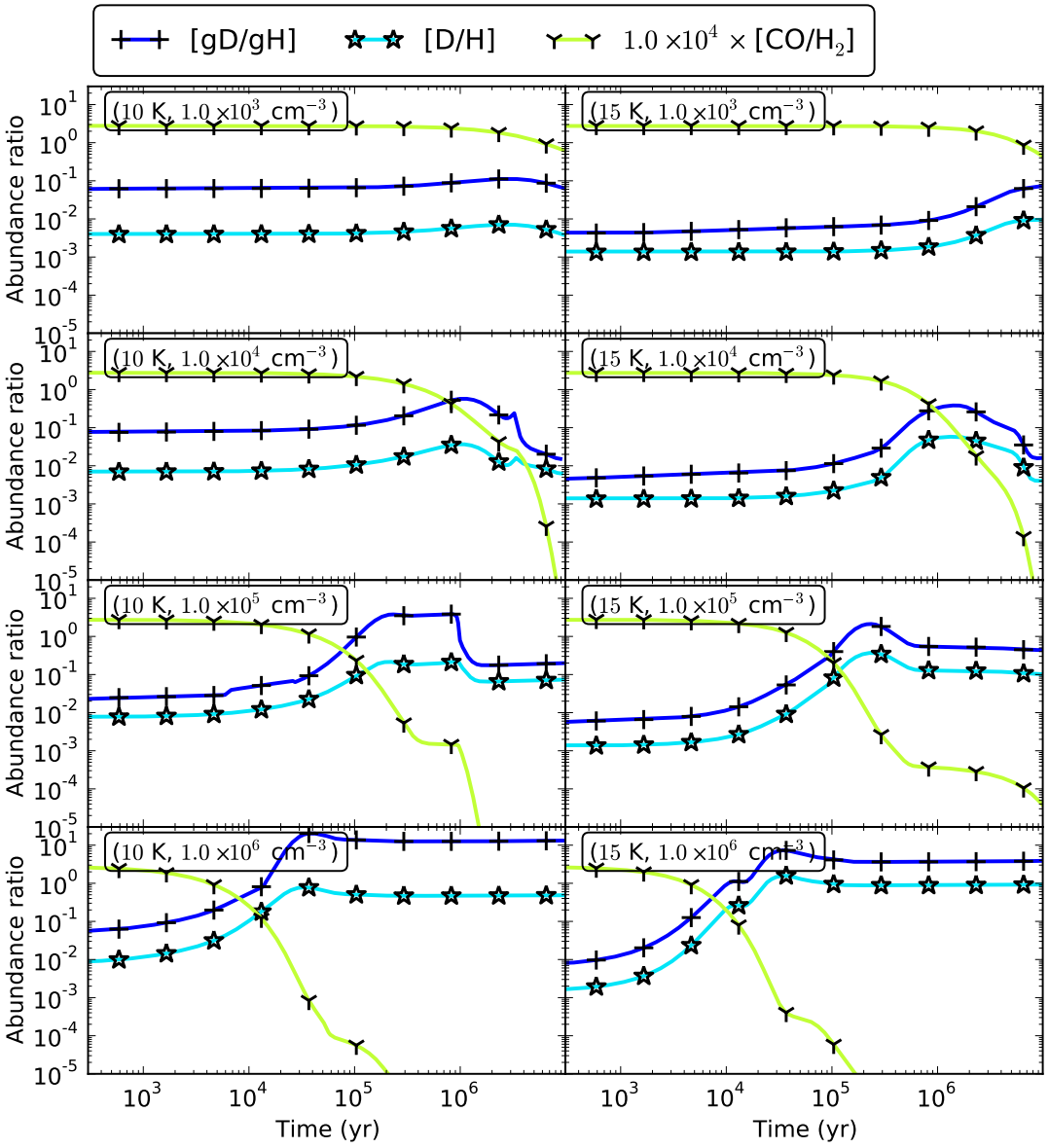

Figure 6.15: The gas phase [D/H] ratio and the surface [gD/gH] ratio as a function of time for different physical conditions. The evolution of the gas phase CO abundance (multiplied by a factor of 10^4) is also plotted for comparison.

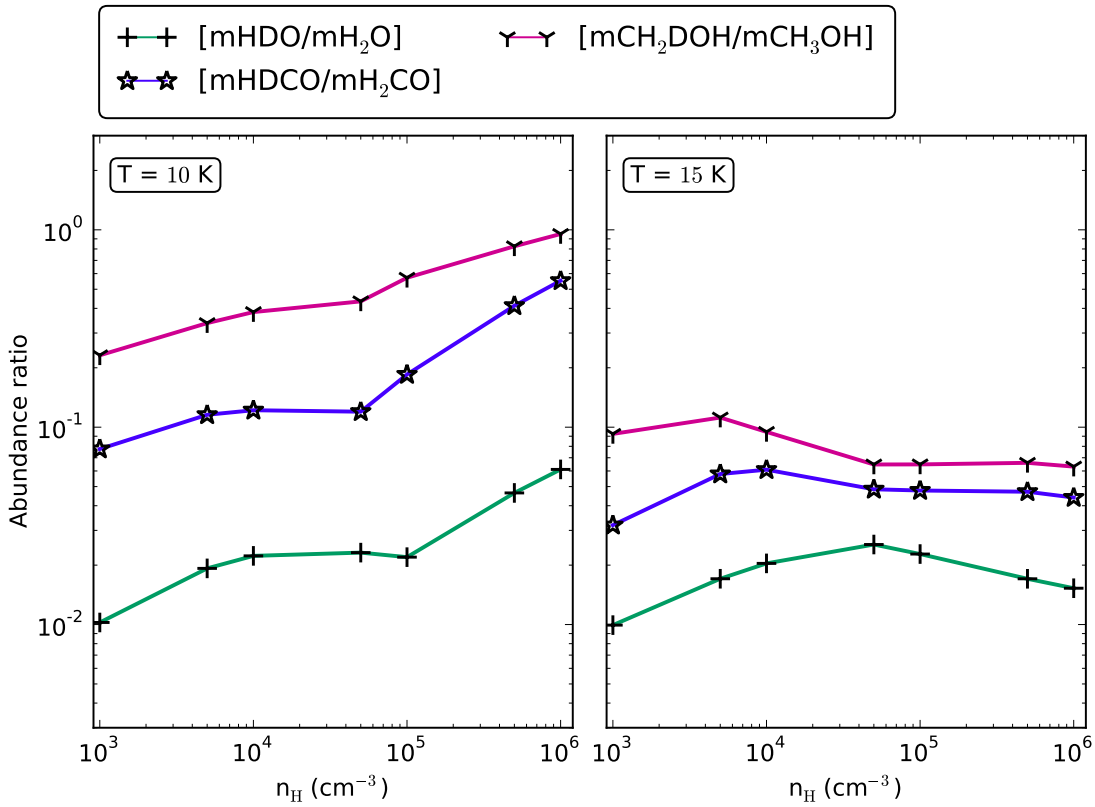

Figure 6.16: Degree of deuterium fractionation of water, methanol, and formaldehyde at $t = 10^7$ yr as a function of density for $T = 10$ K and 15 K.

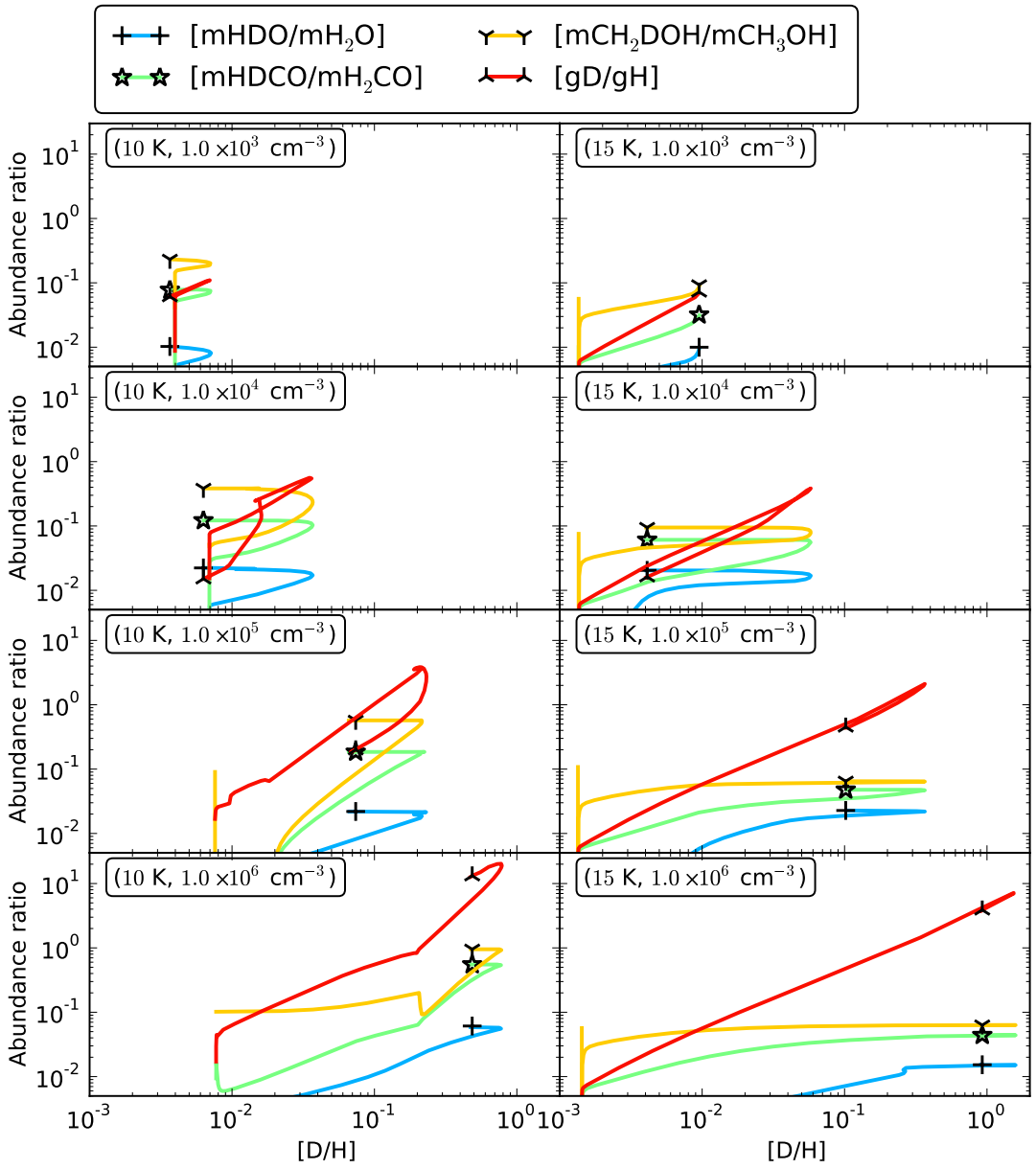

Figure 6.17: The mantle deuterium fractionation ratios versus the gas phase [D/H] ratio through the whole evolution track. The marked point on each curve is the end point of evolution (i.e. at $t = 10^7$ yr).

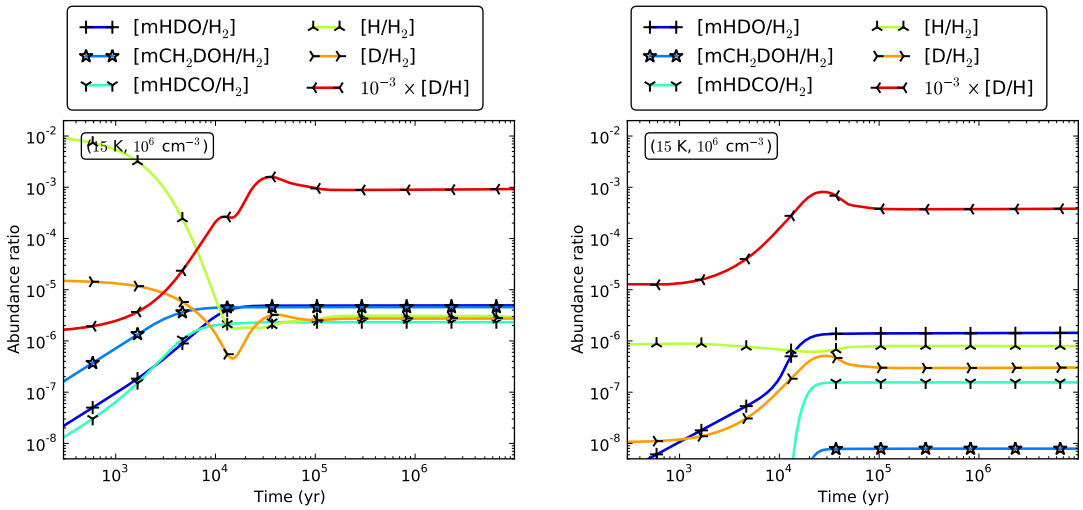

Figure 6.18: The time evolution of a few deuterated species at $T = 15$ K and $n_{\rm H} = 10^6$ cm^{-3}, for low (left) and high (right) binding energies of H and D on the surface.

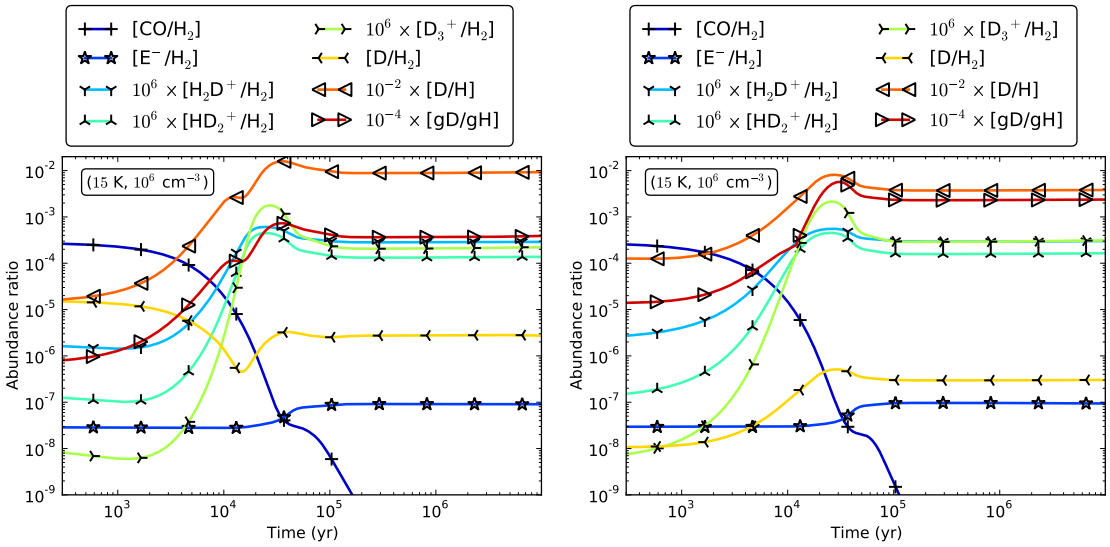

Figure 6.19: The time-evolution of species that play a key role in gas-phase deuterium fractionation, for low (left) and high (right) binding energies of H and D.

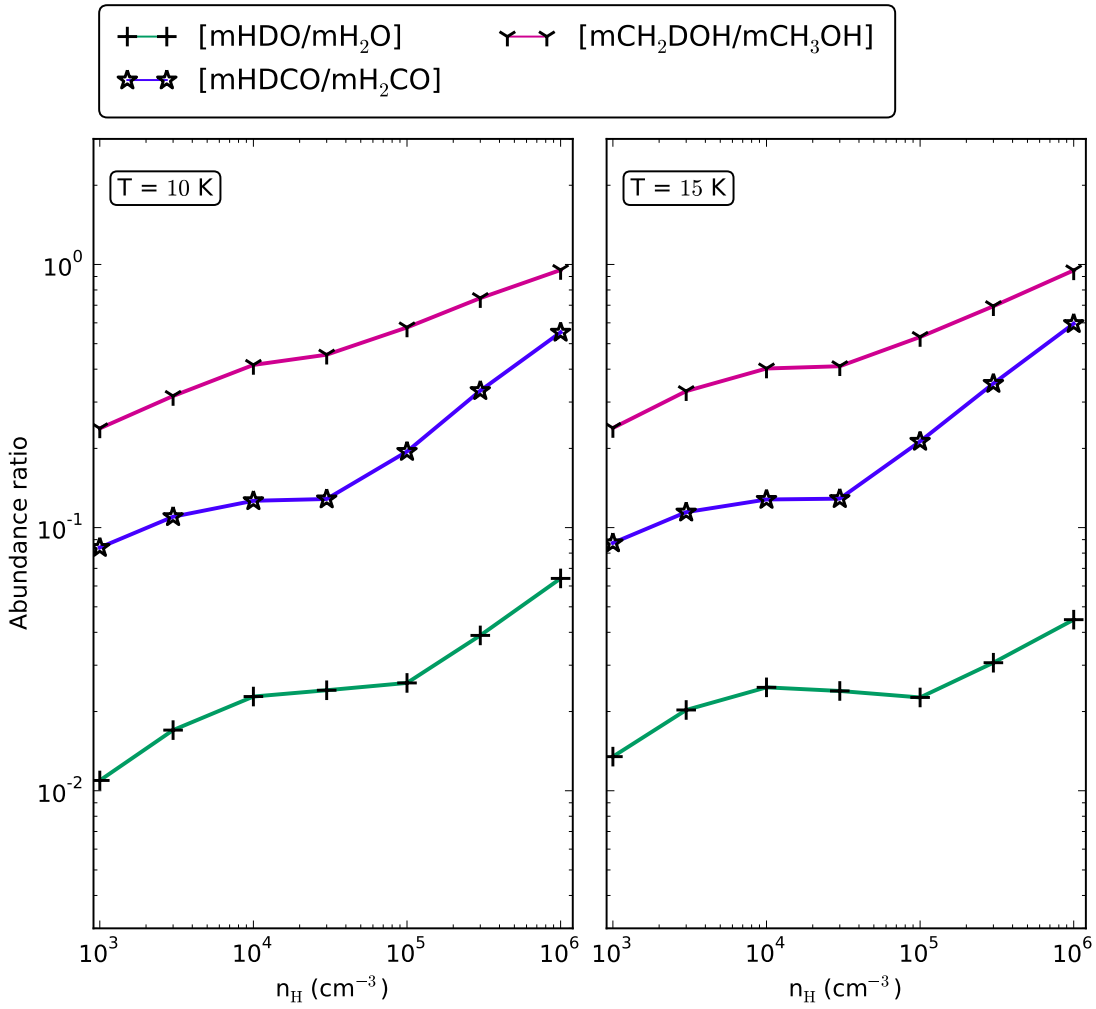

Figure 6.20: The same as Fig. (6.16), except higher values (700 K) for the binding energies of H and D on the surface are assumed.

for an H_2 (HD) and an OH (OD) molecule to react upon meeting is 10^{-4}–10^{-3}, depending on whether an H or D atom is being transferred. Due to its higher mass, the mobility of H_2 on a grain surface is about 30 times lower than that of H. Considering the high population of H_2 on the surface, which can be up to a few 10%, and the extremely low coverage of atomic H, which is around ten orders of magnitude lower than that of H_2, the dominance of the $H_2 + OH$ reaction over the $H + OH$ reaction is thus understandable.

The surface [HDO/H_2O] ratio is approximately equal to the surface [OD/OH] ratio at the time when H_2O and HDO are being formed. See Fig. (6.21) for an example. The surface [OD/OH] ratio is roughly proportional to the surface [D/H] ratio, the former being lower by a factor of around ten. So even if the surface [D/H] ratio can become quite high (which can be higher than one in Fig. (6.21)), the [HDO/H_2O] ratio cannot be very high. Another fact is, the surface [D/H] ratio (hence the [OD/OH] ratio) only becomes very high at a late stage when most of the H_2O ice has already formed; this can be seen from the vertical line in Fig. (6.21), which marks the time when 90% of water ice has formed (and it is about the same time when 90% of the gas phase CO, O_2, etc., have been adsorbed onto the dust grains). So a late-time high surface [D/H] ratio cannot be transferred to water.

Since both the $H + OH \longrightarrow H_2O$ channel and the $H_2 + OH \longrightarrow H_2O + H$ channel involve OH as an intermediate, and since the [HDO/H_2O] ratio is determined by the surface [OD/OH] ratio in the formation stage of water ice, would it make a difference in the deuteration ratio of water if OH is turned into water by reacting with H instead of H_2? To address this, I switch off the reaction $H_2 + OH \longrightarrow H_2O + H$ and its deuterated counterparts completely, while other parameters are unchanged. The resulting ice mantle composition is shown in Fig. (6.22), where evidently water is still the dominant species except for $T = 10$ K and $n_H = 10^6$ cm^{-3}; the reason for this has been explained before. Hence a model without the $H_2 + OH$ reaction seems to be viable, at least in the sense of being able to produce enough water ice. Here our focus is on deuteration ratios, which for the singly deuterated species are shown in Fig. (6.23). Clearly H_2O is still the least-deuterated species, which never has a fractionation ratio higher than 10% except for the cases when it is not abundant (for $T = 10$ K, $n_H = 10^5$ and 10^6 cm^{-3}), while CH_3OH has the highest deuteration ratio, which can be up to order unity, and H_2CO is still in the intermediate.

A comparison between Fig. (6.13) and Fig. (6.23) indicates that excluding the H_2+OH channel can indeed increase the deuteration degree of H_2O by a factor of about two (more at higher densities). The reason is that, with the H+OH channel, HDO can be formed via two reactions, $H + OD \longrightarrow HDO$ or $D + OH \longrightarrow HDO$, while with the $H_2 + OH$ channel, only the $H_2 + OD \longrightarrow HDO + H$ reaction works efficiently; the $HD + OH \longrightarrow HDO + H$ channel is much less efficient due to its higher tunneling mass and the lower mobility of HD compared to H_2 (and the [HD/H_2] ratio is much lower than [OD/OH] anyway).

To see the difference in the surface [HDO/H_2O] ratio caused by the two routes more quantitatively, in the following we list the relevant reactions (again, a prefix "g" is included for the surface species to distinguish them from the gas phase species)

$$\begin{aligned} gH_2 + gOH &\xrightarrow{k_1} gH_2O + gH, \\ gH_2 + gOD &\xrightarrow{k_1} gHDO + gH, \end{aligned} \tag{6.53}$$

and

$$\begin{aligned} \mathrm{gH} + \mathrm{gOH} &\xrightarrow{k_2} \mathrm{gH_2O}, \\ \mathrm{gH} + \mathrm{gOD} &\xrightarrow{k_2} \mathrm{gHDO}, \\ \mathrm{gD} + \mathrm{gOH} &\xrightarrow{k_3} \mathrm{gHDO}. \end{aligned} \tag{6.54}$$

Hence we have for the $H_2 + OH$ channel (neglecting the term for converting surface species into mantle species):

$$\begin{aligned} \partial_t n(\mathrm{gH_2O}) &= k_1 n(\mathrm{gH_2}) n(\mathrm{gOH}), \\ \partial_t n(\mathrm{gHDO}) &= k_1 n(\mathrm{gH_2}) n(\mathrm{gOD}), \end{aligned} \tag{6.55}$$

which leads to

$$\frac{n(\mathrm{gHDO})}{n(\mathrm{gH_2O})} = \frac{n(\mathrm{gOD})}{n(\mathrm{gOH})}. \tag{6.56}$$

For the H + OH channel,

$$\begin{aligned} \partial_t n(\mathrm{gH_2O}) &= k_2 n(\mathrm{gH}) n(\mathrm{gOH}), \\ \partial_t n(\mathrm{gHDO}) &= k_2 n(\mathrm{gH}) n(\mathrm{gOD}) + k_3 n(\mathrm{gD}) n(\mathrm{gOH}), \end{aligned} \tag{6.57}$$

which gives

$$\frac{n(\mathrm{gHDO})}{n(\mathrm{gH_2O})} = \frac{n(\mathrm{gOD})}{n(\mathrm{gOH})} + \frac{k_3}{k_2}\frac{n(\mathrm{gD})}{n(\mathrm{gH})}. \tag{6.58}$$

The last term in the last equation is roughly the ratio between the consumption rate of surface D and H, which can be estimated to be the ratio between their accretion fluxes (under the quasi-steady-state approximation), namely,

$$\frac{k_3}{k_2}\frac{n(\mathrm{gD})}{n(\mathrm{gH})} \simeq \frac{1}{\sqrt{2}}\frac{n(\mathrm{D})}{n(\mathrm{H})}, \tag{6.59}$$

where the factor $\frac{1}{\sqrt{2}}$ accounts for the mass ratio between D and H, and $\frac{n(\mathrm{D})}{n(\mathrm{H})}$ is the abundance ratio of gas phase D and H. So we finally get

$$\frac{n(\mathrm{gHDO})}{n(\mathrm{gH_2O})} \simeq \frac{n(\mathrm{gOD})}{n(\mathrm{gOH})} + \frac{1}{\sqrt{2}}\frac{n(\mathrm{D})}{n(\mathrm{H})}. \tag{6.60}$$

Thus it is clear that the H + OH channel gives a higher deuteration ratio for water than the H_2 + OH channel.

Note that the mantle abundance of any species is an integral over time of its surface abundance weighted by the accretion flux of heavy mantle-making species (cf. Eq. (6.52)), so the final [mHDO/mH_2O] ratio will lie somewhere in between the maximum and minimum of the [gHDO/gH_2O] ratio.

In contrast to singly deuterated water, a vast change in the abundance of doubly deuterated water can be seen by comparing Fig. (6.24) with Fig. (6.14). When the H_2+OH channel is turned off, the [D_2O/H_2O] ratio increases by 2–3 orders of magnitude relative to the case when the $H_2 + OH$ channel is on. The reason is easily understood: on the dust grain surface the reactions forming D_2O are D + OD $\longrightarrow$ D_2O, HD + OD $\longrightarrow$ D_2O + H,

$D_2 + OD \longrightarrow D_2O + D$, and $D_2 + OH \longrightarrow D_2O + H$; the latter ones cannot give a high fractionation ratio for D_2O because the $[HD/H_2]$ and $[D_2/H_2]$ ratios never get very high. So we may consider the $D + OD \longrightarrow D_2O$ reaction only. When the $H_2 + OH$ channel is allowed, a D atom has to compete with the very abundant H_2 molecules to react with OD, which renders the D + OD reaction practically impossible; in fact, in this case the surface D_2O molecules are mainly from the gas phase. Without the $H_2 + OH$ channel, the competitor of D is mainly atomic H, which is much less abundant than H_2, hence the D + OD reaction can proceed to produce much more D_2O than the previous case. We remark that a low $[D_2O/H_2O]$ ratio ($\sim 10^{-5}$) when water is mainly formed through the $H_2 + OH$ channel is consistent with the value obtained by Butner et al. (2007) in the low mass protostar IRAS 16293-2422 (and it seems up to now D_2O is only detected in this source).

By comparing Figs. (6.6) and (6.22) one may also note that, for $T = 10$ K and $n_H = 10^5$ cm^{-3}, when the $H_2 + OH$ channel is removed, the O_3 abundance (occupying $\sim$10% of the mantle volume) in the ice mantle is much higher than when the $H_2 + OH$ channel is included, where O_3 only occupies about 1% of the mantle volume. This is due to the fact that removing the $H_2 + OH$ channel means a higher consumption rate of surface H, which leaves more O and O_2 on the surface free to form O_3 to be stored in the mantle.

Since $H_2 + OH \longrightarrow H_2O + H$ being the major channel to produce water in our previous models seems not to be the main reason for the lower deuterium fractionation ratio of water in comparison to formaldehyde and methanol, then the question becomes why the latter two species are more prone to deuterium enhancement. One apparent reason is their abstraction and the associated addition reactions, which do not exist for water. So I made a test by turning off all the abstraction reactions related to H_2CO and CH_3OH, and the results are shown in Fig. (6.25). Now the prevalence of CH_3OH and H_2CO in deuteration have disappeared. In most cases the fractionation ratios of H_2CO and CH_3OH are almost the same, and can be either greater than or lower than that of H_2O. Hence we may conclude that the existence of differentiating abstraction reactions for H_2CO and CH_3OH, in which the efficiencies to abstract H and D are different due to the different tunneling masses and barrier heights, is the main reason for their higher deuterium fractionation ratios. The reason for CH_3OH to have a higher deuteration ratio than H_2CO is that CH_3OH has more such abstraction channels. The addition and abstraction pathways related to them are shown in Fig. (6.26).

Why do abstraction reactions such as $H + H_2O \longrightarrow OH + H_2$ not exist for water? The very fact that one major formation channel of H_2O is $OH + H_2 \longrightarrow H + H_2O$ means that the abstraction reaction $H + H_2O \longrightarrow OH + H_2$ must be endothermic. A search in the NIST database[17] indicates that the endothermicity of this reaction is around 1 eV. This can also be verified by calculating the enthalpy change of this reaction using Table (5.2) on page 99. We find that the total enthalpy of the products is higher than that of the reactants, indicating the reaction is endothermic. Hence it cannot occur on cold dust grain surfaces. Neither can it for its deuterated counterparts, because the differences in the zero-point energies of H and D won't be able to compensate for such a big endothermicity. Enthalpy calculations using Table (5.2) also confirm that the abstraction of the H atoms

[17] `http://kinetics.nist.gov/kinetics/rpSearch?cas=7732185`. Look for "`H + H2O`" within this page.

attached to the carbon atoms of H_2CO and CH_3OH are exothermic, while abstracting the H atom of the OH radical in CH_3OH is close to thermally neutral (i.e. the total enthalpies of the reactants and products of the reaction $H + CH_3OH \longrightarrow CH_3O + H_2$ are very close to each other).

A comparison between Fig. (6.13) and Fig. (6.25) shows that the deuteration ratio in water is higher when the abstraction reactions of methanol and formaldehyde are included. This is because these abstraction reactions act as an efficient absorber for H atoms, while for D atoms this effect is less dramatic due to the generally larger barrier widths and effective masses for abstraction reactions involving D as a reactant (cf. Table (6.3) and Table (6.6)). Hence H atoms are more likely to be consumed by these abstraction reactions than D, leading to a higher atomic [D/H] ratio on the surface.

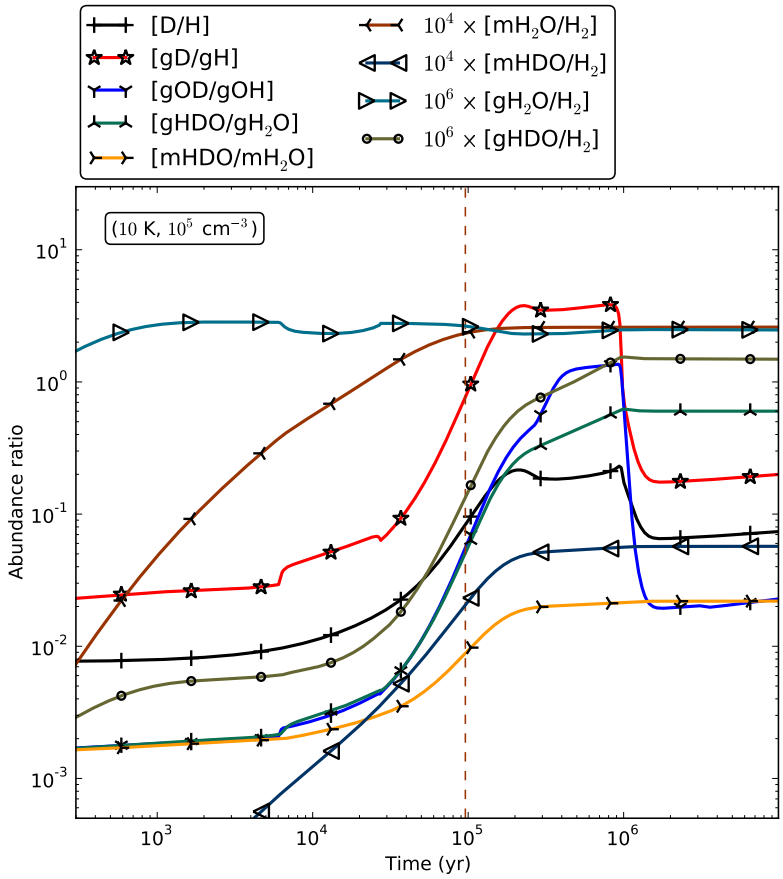

Figure 6.21: A comparative view of the deuterium fractionation ratio in H_2O, OH, and H as a function of time, for $T = 10$ K and $n_H = 10^5$ cm^{-3}. The absolute abundances of surface and mantle H_2O and HDO are also plotted. The vertical line marks the time when 90% of the mantle H_2O has formed.

We note from Fig. (6.17) that a very high gas phase [D/H] ratio is not necessary to get a high deuterium fractionation ratio in CH_3OH and H_2CO. For example, for the $T = 10$ K, $n_H = 10^4$ cm^{-3} case, the [CH_2DOH/CH_3OH] ratio can be up to 0.4, while the highest gas phase [D/H] ratio is only 0.04. The [gD/gH] ratio on the surface is indeed

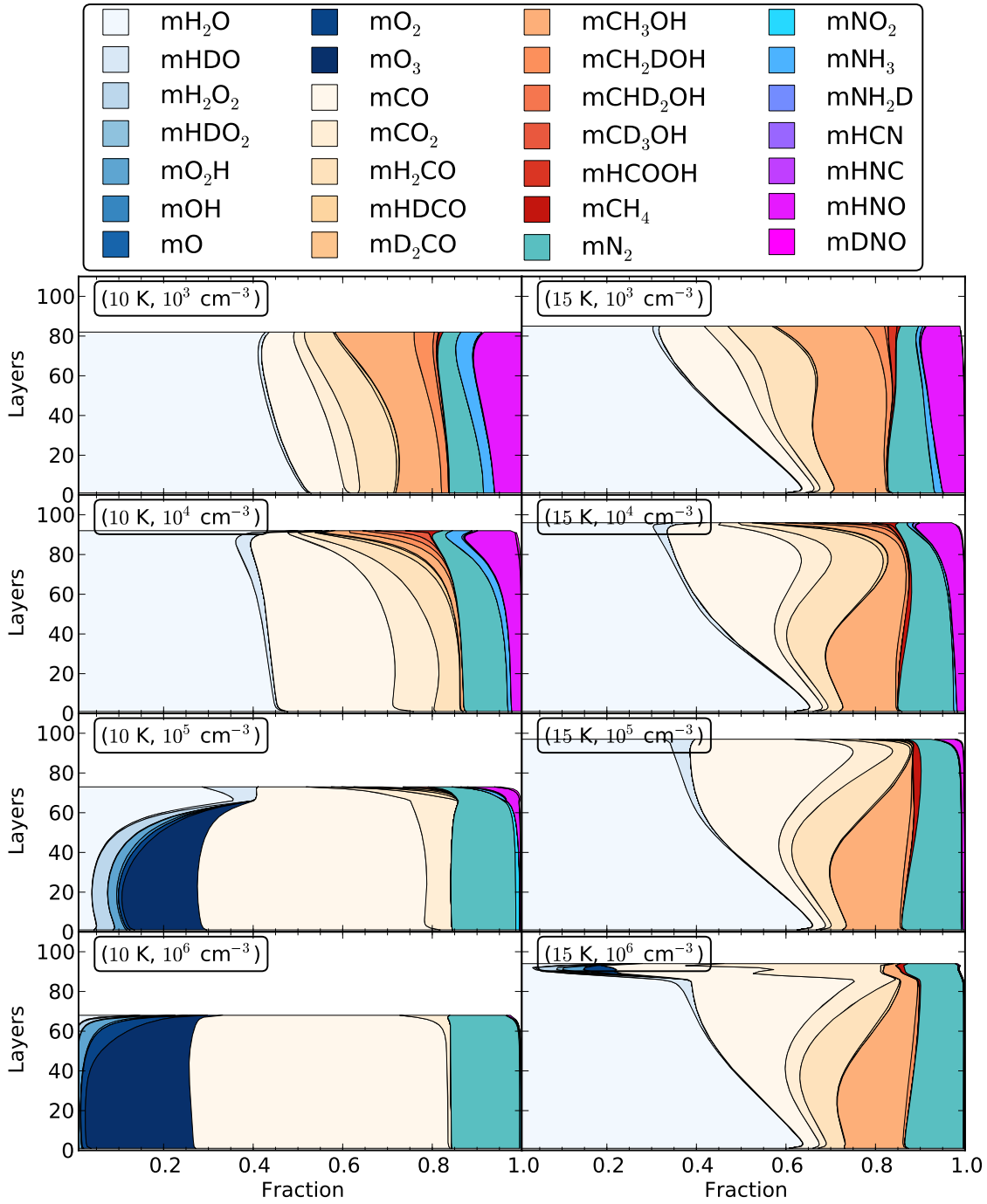

Figure 6.22: Ice mantle composition by layer. Obtained with the same parameters as in Fig. (6.6) except the $H_2 + OH \longrightarrow H_2O + H$ reaction and its deuterated counterparts are turned off.

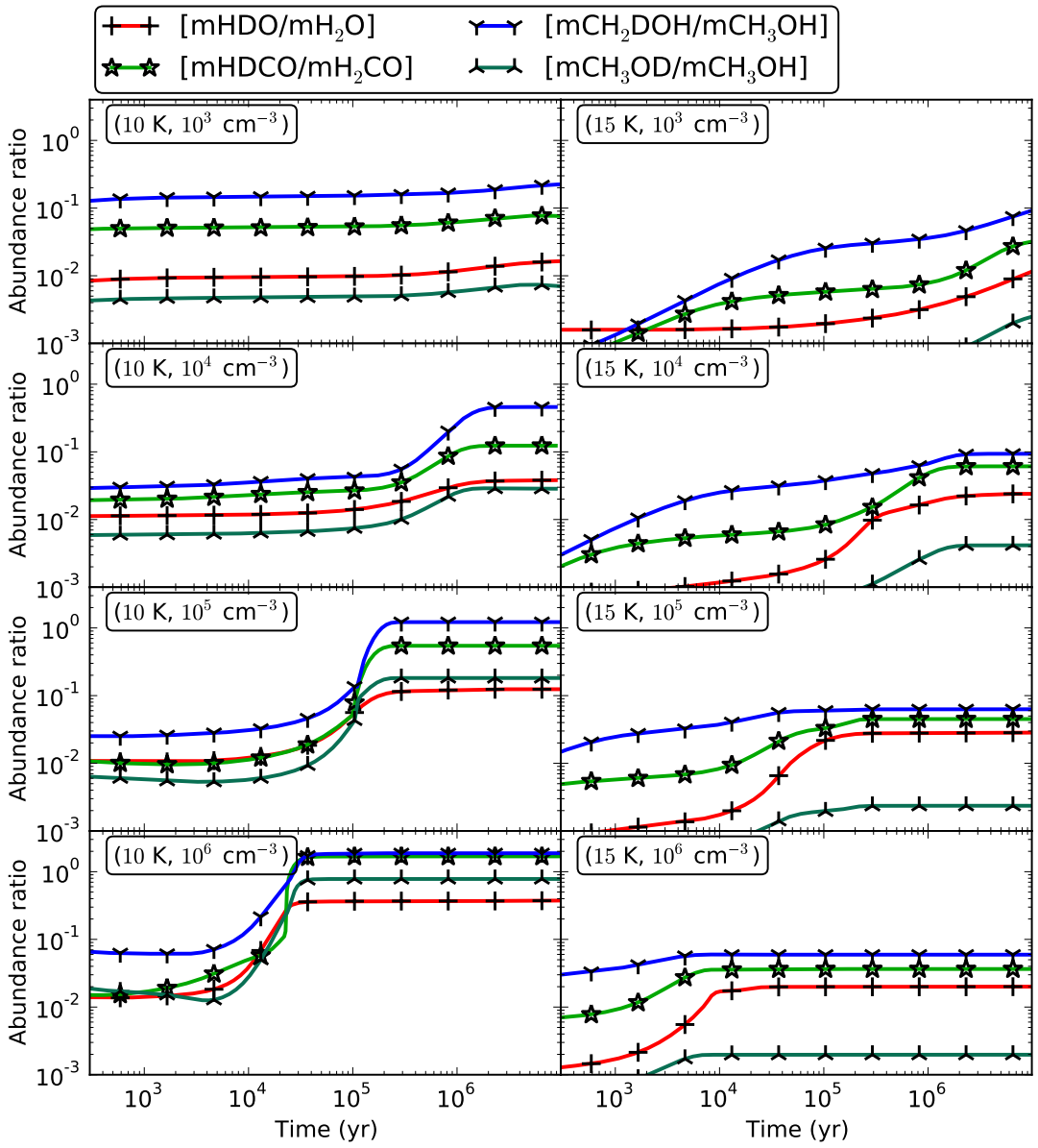

Figure 6.23: Deuterium fractionation ratio of major H-containing species. The same as in Fig. (6.13), except the $H_2 + OH \longrightarrow H_2O + H$ reaction and its deuterated counterparts are turned off.

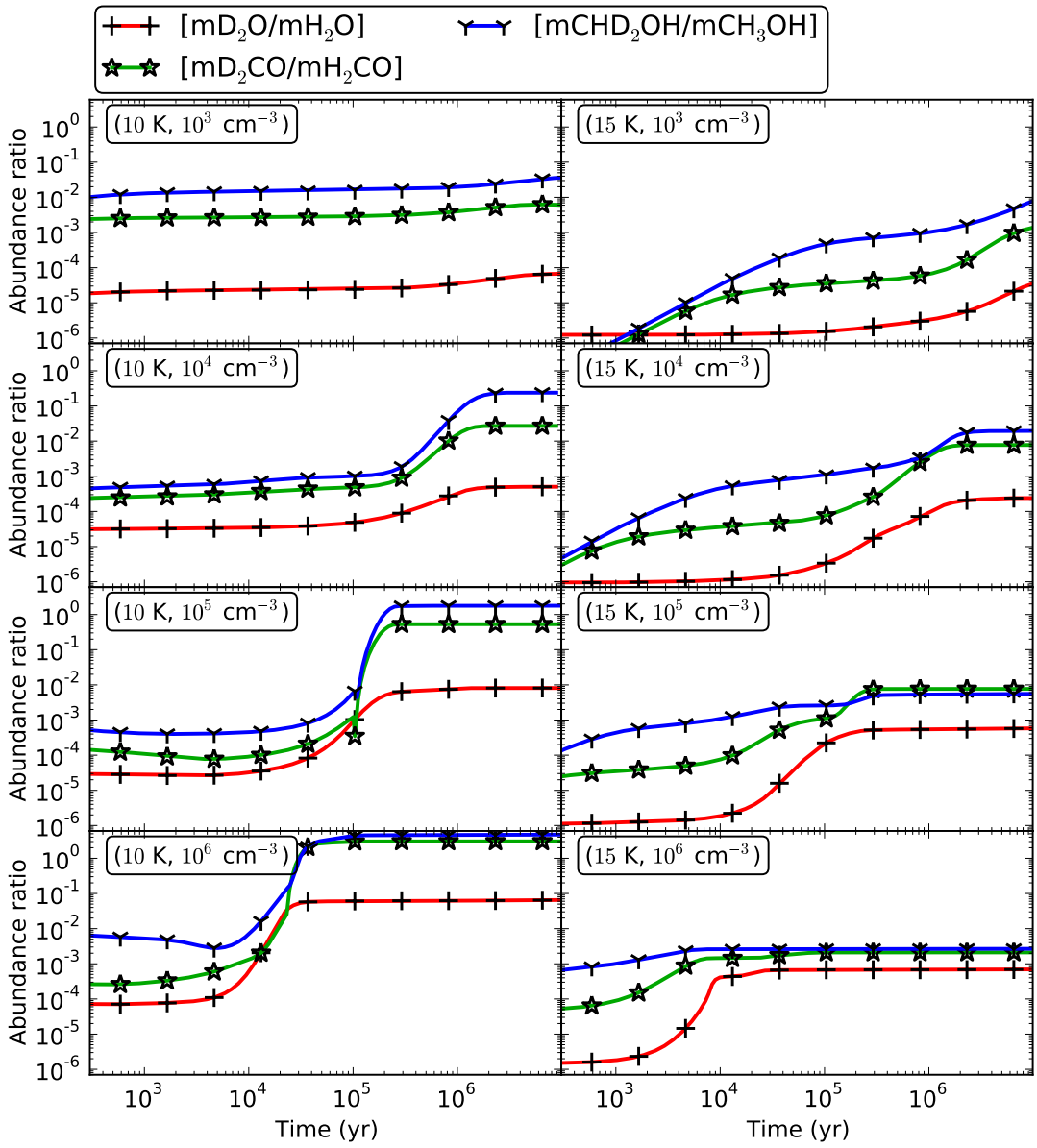

Figure 6.24: Deuterium fractionation ratio of doubly deuterated species. The same as in Fig. (6.14), except the $H_2 + OH \longrightarrow H_2O + H$ reaction and its deuterated counterparts are turned off.

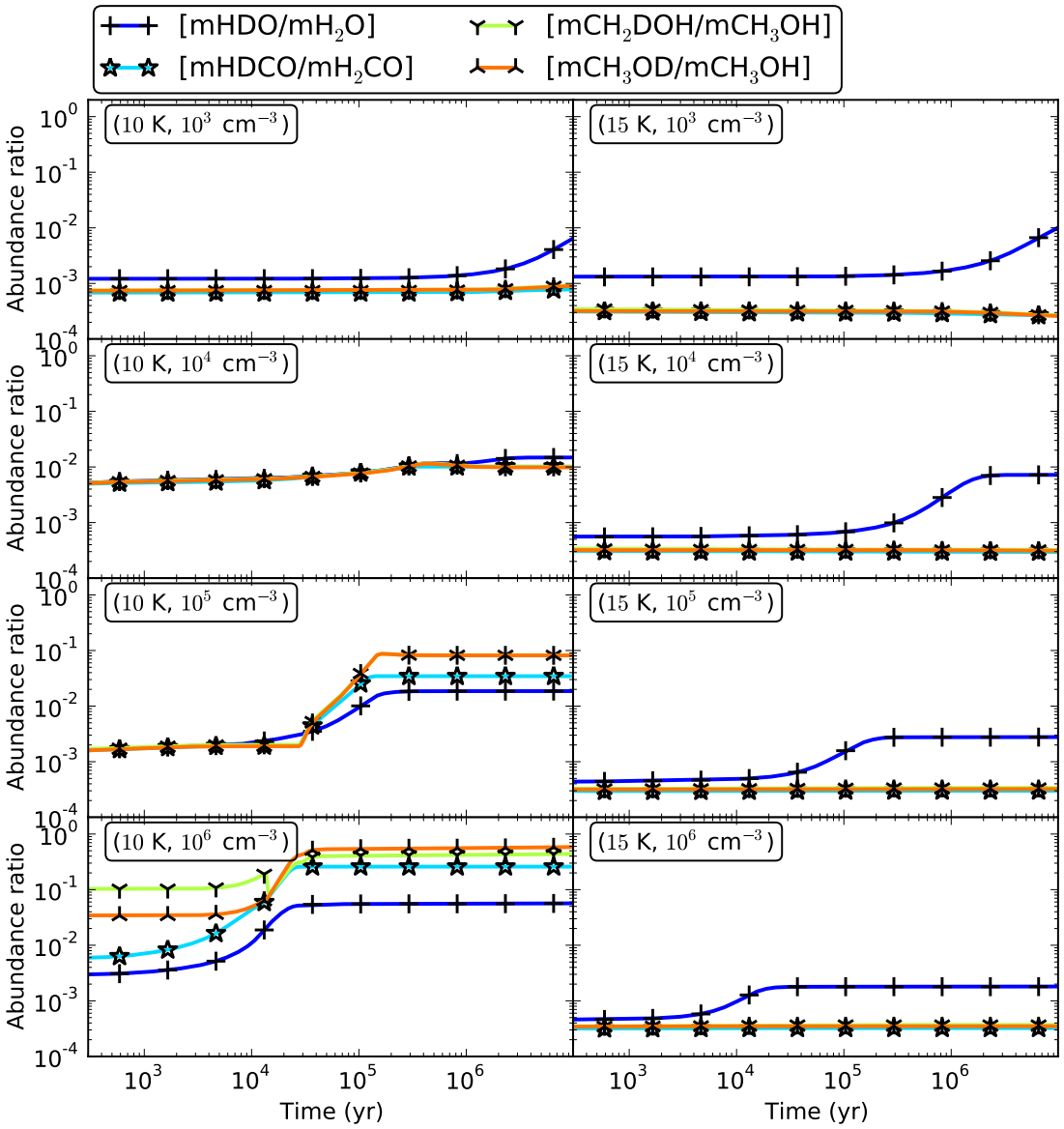

Figure 6.25: Deuterium fractionation ratio of major H-containing species. The same as in Fig. (6.13), except the abstractions related to H_2CO and CH_3OH are turned off.

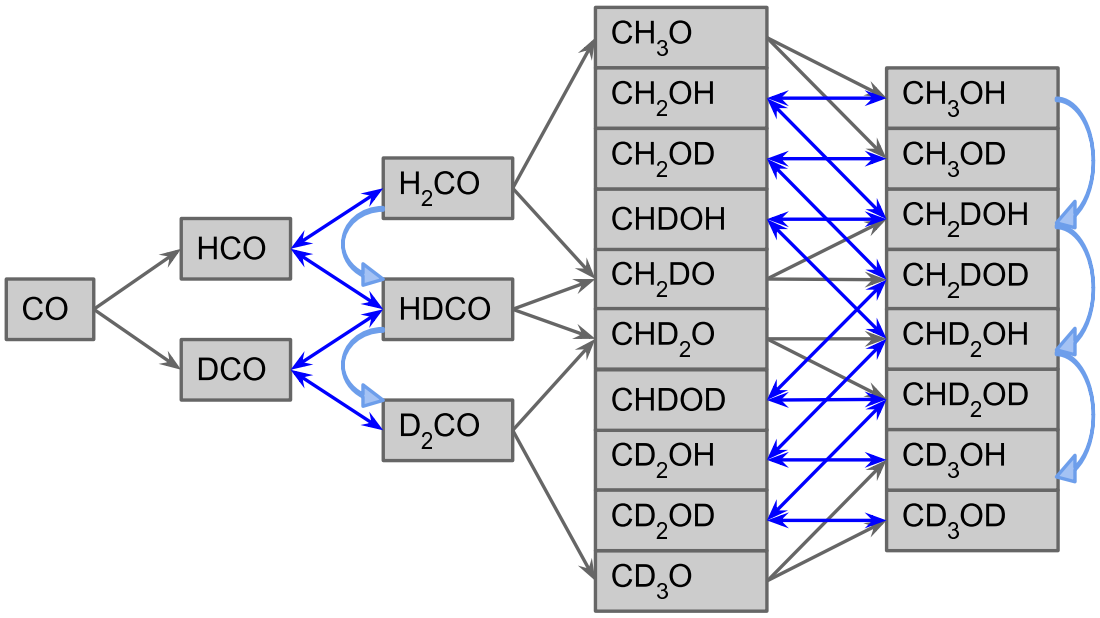

Figure 6.26: Formation and deuteration pathways of the CO-H_2CO-CH_3OH system. Gray arrows mark the H and D addition reactions that have no abstraction counterparts, and blue bi-directional arrows mark the abstraction and addition reactions that can proceed in both directions. Note that abstractions by H and by D are not distinguished. The curved arrows show the direction of deuterium transfer, caused by the abstraction and the followed addition reactions.

high, due to the slower evaporation and reaction rate of surface D caused by its higher mass and lower zero-point energy in comparison with H.

6.6.3 Comparison with observations

Table (6.13) lists the deuterium fractionation ratio for methanol, formaldehyde, and water, observed for different sources. In general, low mass and cold sources have higher deuterium fractionation ratios than the hot high mass sources, and methanol and formaldehyde have higher deuterium fractionation ratios than water, which are qualitatively in agreement with our modeling results as has been discussed in previous sections. A quantitative match is more challenging because, after all, the observational results usually have large uncertainties, and vary from one source to another considerably. Each source is unique, with its own environment and evolution, and detailed modeling following the time evolution is necessary, though the initial condition and external action are usually unknown.

In the next two small sections a more detailed analysis of two recent observational results is presented in the context of our modeling results.

Ref.	$\frac{CH_2DOH}{CH_3OH}$	$\frac{CHD_2OH}{CH_3OH}$	$\frac{CD_3OH}{CH_3OH}$	$\frac{CH_3OD}{CH_3OH}$	$\frac{HDCO}{H_2CO}$	$\frac{D_2CO}{H_2CO}$	$\frac{HDO}{H_2O}$	$\frac{D_2O}{H_2O}$
Low mass protostars, dark clouds								
(1)					0.01–0.1	0.007–0.14		
(2,3,4,5)	0.1–0.5	0.01–0.1	0.002–0.03	0.02	0.13–0.16	0.04–0.06	0.002–0.03	5×10^{-5}
(6)						0.03		
(7)	<0.03							
(8)					0.02–0.2	0.01–0.16		
(9)							<0.005–0.02	
(10)	0.4–0.6	0.1–0.25		0.02–0.05	0.1–1.7	0.05–0.44		
(11)							0.01–0.07	
High mass star forming regions, hot cores								
(12,13,14)	<0.01–0.06			0.01–0.06	0.14	0.003	0.02	
(15)							$0.8–3\times10^{-3}$	
(16)							$3–6\times10^{-4}$	
(17)							8×10^{-4}–0.01	
(18)							$\lesssim$0.01	
(19)		≤0.03	<0.01					
(20)							0.001	
(21,22)					0.01–0.03		0.001	
(23)	0.01–0.09							
Other								
(24)							4×10^{-4}	
(25)							$<6\times10^{-4}$	

Table 6.13: Deuterium fractionation ratio for a selection of species. Literature and targets: (1). Bergman et al. (2011a); ρ Oph A. (2,3,4,5). Parise et al. (2004); Loinard et al. (2000); Parise et al. (2005); Butner et al. (2007); IRAS 16293−2422. (6). Ceccarelli et al. (2002); L1689N, a small cloud in ρ Oph. (7). Sakai et al. (2009); L1527. (8). Roberts & Millar (2007); Low-mass proto-stellar cores. (9). Parise et al. (2003); low-mass protostars; for solid water. (10). Parise et al. (2006); Low-mass protostars. (11). Liu et al. (2011); NGC 1333-IRAS2A. (12,13,14). Bergin et al. (2010); Mauersberger et al. (1988); Turner (1990); Orion KL. (15). Knacke et al. (1988); Orion BN object (an intermediate-mass protostar). (16). Jacq et al. (1990); Galactic hot cores. (17). Teixeira et al. (1999); W33A and NGC7538 IRS9. (18). Dartois et al. (2003); high- and intermediate-mass protostars; for solid water. (19). Roberts & Millar (2007); Hot molecular cores. (20). van der Tak et al. (2006); high-mass-star formation regions. (21,22). Petuchowski & Bennett (1988); Loren & Wootten (1985); OMC-1. (23). Jacq et al. (1993); Orion-IRc2; (24). Villanueva et al. (2009); comet 8P/Tuttle. (25). Jørgensen & van Dishoeck (2010); Inner region of a low-mass protostar.

The D_2CO/HDCO ratio

Bergman et al. (2011a) found a [D_2CO/HDCO] ratio larger than one in one position of ρ Ophiuchus A cloud core, where the gas density and temperature is 6×10^5 cm^{-3} and 24 K, respectively. The H_2CO abundance relative to H_2 was found to be a few 10^{-9}.

The modeling results for the deuterium fractionation ratio of formaldehyde as a function of time with density and temperature constrained by Bergman et al. (2011a) are shown in Fig. (6.27), where two values for the binding energies of H and D have been assumed, 350 K for the top panels and 700 K for the bottom panels.

It can be seen that the observed absolute abundance of gas phase H_2CO can be reasonably reproduced in both cases. For the low binding energy case the [HDCO/H_2CO] ratio is only around 0.01; but for the higher binding energies this ratio can be close to the observed value of ∼0.1 at the time when the H_2CO abundance matches the observation. However, the [D_2CO/H_2CO] ratio is always in the range 0.001–0.01, and it never becomes comparable to the [HDCO/H_2CO] ratio.

The mantle deuteration ratio of H_2CO is lower than in the gas phase. This is because the H_2CO in the mantle is formed in an early stage, so it is not affected by the later increase in the gas phase atomic [D/H] ratio.

Since the model with $T = 24$ K cannot produce a high enough [D_2CO/H_2CO] ratio, we look again at the low temperature models we have been using in the previous sections. Fig. (6.28) shows the gas phase deuteration ratio of H_2CO as a function of time for $T = 10$ K and $n_{\rm H} = 10^5$ and 10^6 cm^{-3}. The binding energies of H and D are taken as 350 K, and the chemical desorption efficiency as 0.01. Again in this case the absolute abundance of H_2CO can match the observed value at certain stages. But now the problem is that the [HDCO/H_2CO] and [D_2CO/H_2CO] ratios become too high, especially for the $n_{\rm H} = 10^6$ cm^{-3} case. Next we look at the mantle species.

Fig. (6.29) shows the deuterium fractionation ratio of multiply-deuterated mantle formaldehyde and methanol as a function of time, with the same physical parameters as in Fig. (6.28). We can see that both the [HDCO/H_2CO] ratio and the [D_2CO/H_2CO] ratio can be higher than 0.1 for the two physical conditions, and are indeed close to each other. The absolute abundances (with respect to H_2) of H_2CO and CH_3OH in the ice mantle are in the range 10^{-7}–10^{-5} and 10^{-8}–10^{-6}, respectively, much higher than the detected abundances of $\sim 10^{-9}$.

Hence if the observed H_2CO isotopologues are formed on the surface at the observed temperature of ∼24 K and directly released into the gas phase through chemical desorption, then the observed high [D_2CO/H_2CO] ratio cannot be reproduced. If they are formed at low temperatures and released by chemical desorption, then they will be "overdeuterated". If they are released by an unknown mechanism from the dust grain mantles, and these mantles are formed at a low temperature and high density, then the two observed ratios [HDCO/H_2CO] and [D_2CO/H_2CO] can be matched.

Fig. (6.29) shows that the abundances of triply-deuterated methanol, CD_3OH, can even be a factor of a few higher than that of the main isotopologue, CH_3OH, which is most obvious for $n_{\rm H} = 10^6$ cm^{-3}. This is due to the very high atomic [D/H] ratio on the surface and in the gas phase (cf. Fig. 6.17), driven by the fast depletion of gas phase species (CO, N_2, ...), as discussed before. One may ask why a higher density tends to give a higher atomic [D/H] ratio. Atomic D in the gas phase is mainly formed via

dissociative recombination reactions, such as $H_2D^+ + E^- \longrightarrow 2\,H + D$, while H_2D^+ itself results from $H_3^+ + HD \longrightarrow H_2D^+ + H_2$. At late times, when abundant molecules such as CO and N_2 have depleted, H_2D^+ is mainly consumed[18] by reacting with E^-. Hence the ratio $[H_2D^+/H_3^+]$ is proportional to $[HD/E^-]$. Assuming HD has not been exhausted, then $[H_2D^+/H_3^+] \propto 1/[E^-]$. The electron abundance decreases with density, simply because at higher density the neutralization processes are faster. Thus the $[H_2D^+/H_3^+]$ is higher at higher density, leading to a higher [D/H] ratio.

The deuteration ratios in other positions of ρ Ophiuchus A found by Bergman et al. (2011a) are much lower. The $[HDCO/H_2CO]$ ratios are around 1%, and the $[D_2CO/H_2CO]$ ratios are less than 1%. However, our modeling results illustrated by Figs. (6.13) and (6.14), indicate that the $[HDCO/H_2CO]$ and $[D_2CO/H_2CO]$ ratios never gets much lower than 10% and 1%, respectively. Note that the temperatures of these ρ Oph A points determined by radiative transfer modeling are in the range 20–30 K, higher than the low temperatures we adopted in the models represented by Figs. (6.13) and (6.14), and we have seen that for higher temperatures our models indeed produce very low values for these two ratios (for low binding energies of H and D; see Fig. 6.27). This suggests that: (1) the dust grain material is inhomogeneous, particularly in the sense of having different binding energies for H and D; sites of different binding energies may be on the same grain, or on different grains; (2) small scale cool and dense region may exist, which produces high deuteration ratio in certain species; and (3) certain mixing mechanism may be responsible for transferring these species to regions with higher temperature. But a comprehensive model is beyond our scope.

The OD/HDO ratio

Recently, the deuterated hydroxyl radical, OD, has been detected (in the gas phase) towards the low-mass protostar IRAS 16293−2422 by Parise et al. (2012b), using the *GREAT* receiver on board *SOFIA* (Stratospheric Observatory for Infrared Astronomy)[19]. The inferred [OD/HDO] ratio is in the range 17–90. In that paper this ratio was compared with modeling results on the gas phase $[OH/H_2O]$ ratio. Here with a more complete model containing gas-grain deuterium chemistry, the [OD/HDO] ratio is plotted in Fig. (6.30), along with [OD/OH], $[OH/H_2O]$, as well as the absolute abundances of HDO and OD. It can be seen that for almost all the physical conditions we have considered, the [OD/HDO] ratio can indeed be around 20–40 at $t \gtrsim 3\times10^4$–10^6 yr (depending on density), at the same time OD and HDO are still abundant enough to be detectable.

In the models the [OD/HDO] ratio is in the range 10^{-3} to a few initially, set by the gas phase chemistry. OD is mainly formed from the exchange reaction $OH + D \longrightarrow OD + H$, with an exothermicity of 810 K, and is mainly destructed by reacting with O to form O_2, with N to form NO, and also destroyed by ions such as HCO^+ and H_3^+. When adsorption has started, its abundance first tends to increase, because the abundances of species destroying it are decreasing. But at last the abundance of OD itself will also decrease due to accretion. HDO is formed by $H_2DO^+ + E^-$, and destroyed by reacting

[18] We assume low temperature of 10–15 K, hence the reverse reaction $H_2D^+ + H_2 \longrightarrow H_3^+ + HD$ can be neglected. But at slightly higher temperature of ∼20 K this reaction cannot be neglected anymore. This is because the high abundance of H_2 in comparison with HD compensates for its slowness.

[19] `http://www.sofia.usra.edu/`

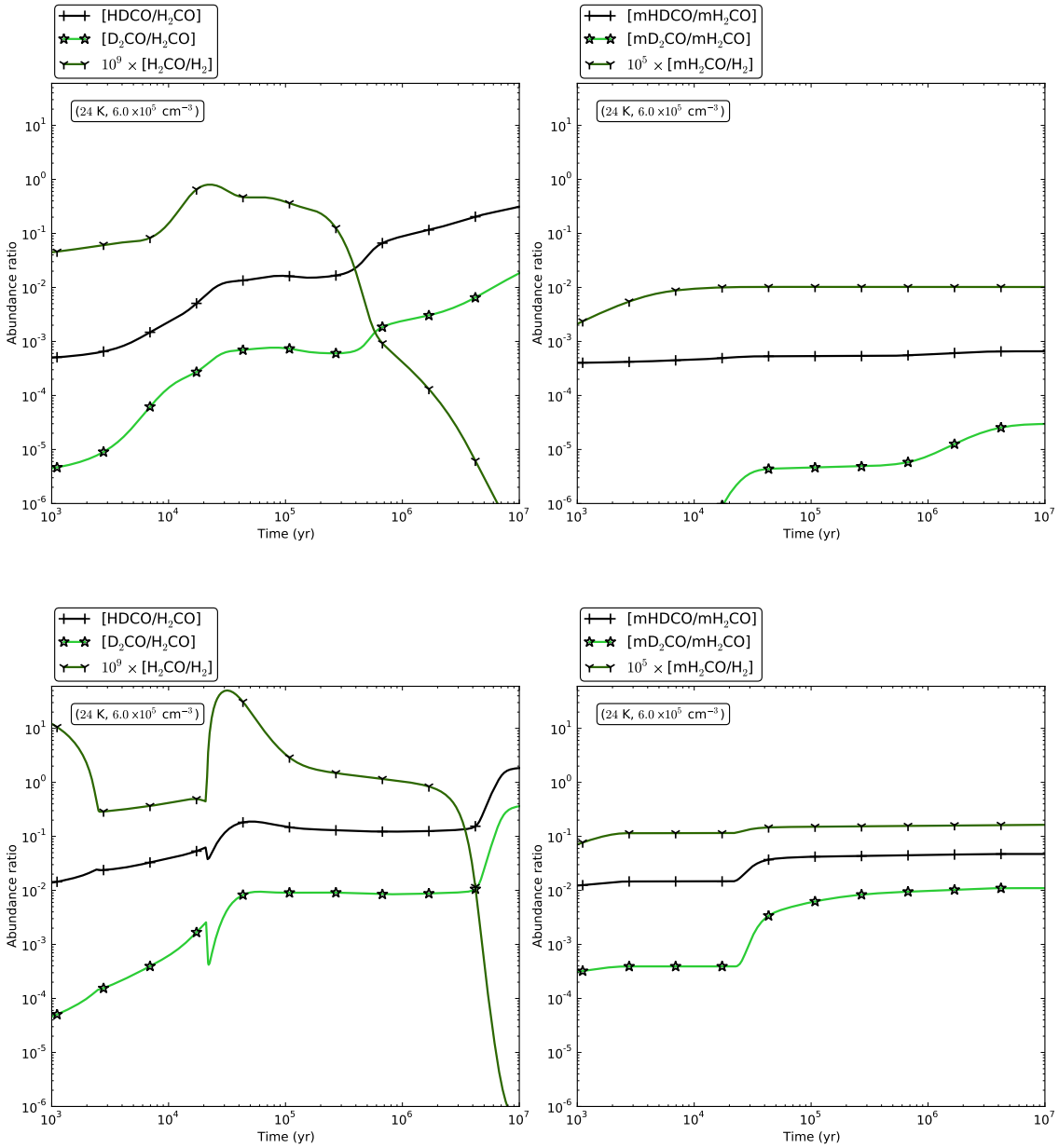

Figure 6.27: Deuterium fractionation ratio of formaldehyde as a function of time, with T = 24 K and $n_{\rm H}$ = 6×10^5 cm^{-3}, which is relevant for ρ Ophiuchus A. The chemical desorption efficiency is set to 0.1. Left: gas phase; right: mantle. Top: the binding energies of H and D are set to a low value of 350 K; Bottom: the binding energies of H and D are set to a high value of 700 K.

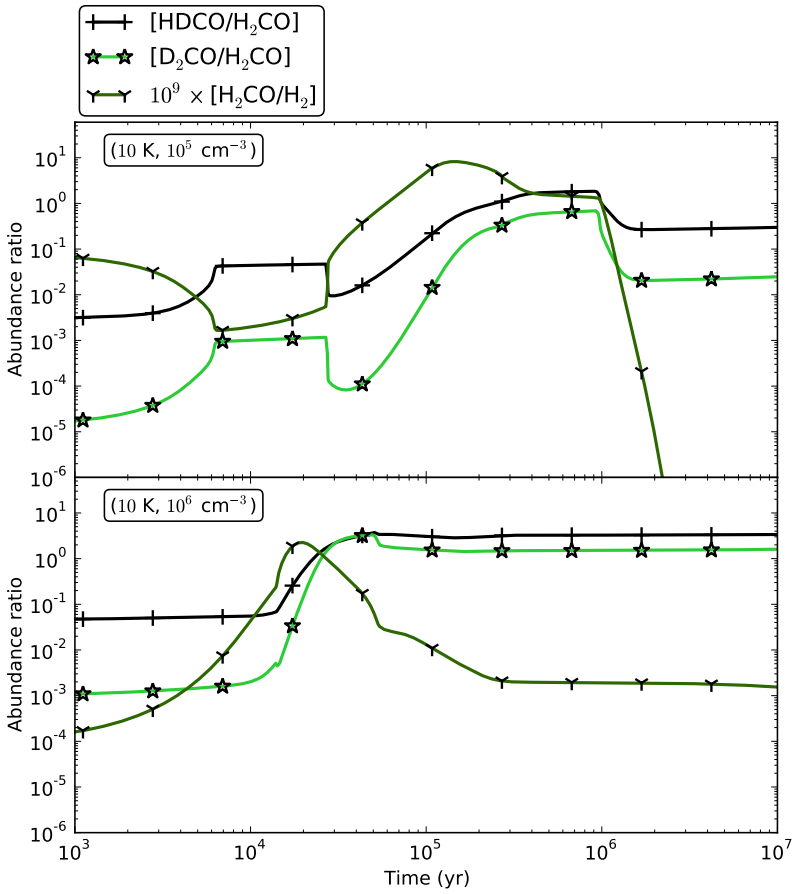

Figure 6.28: The deuterium fractionation ratio of H_2CO in the gas phase as a function of time for $T = 10$ K and $n_H = 10^5$ and 10^6 cm^{-3}. The binding energies of H and D are assumed to be 350 K, and the chemical desorption efficiency is taken as 0.01.

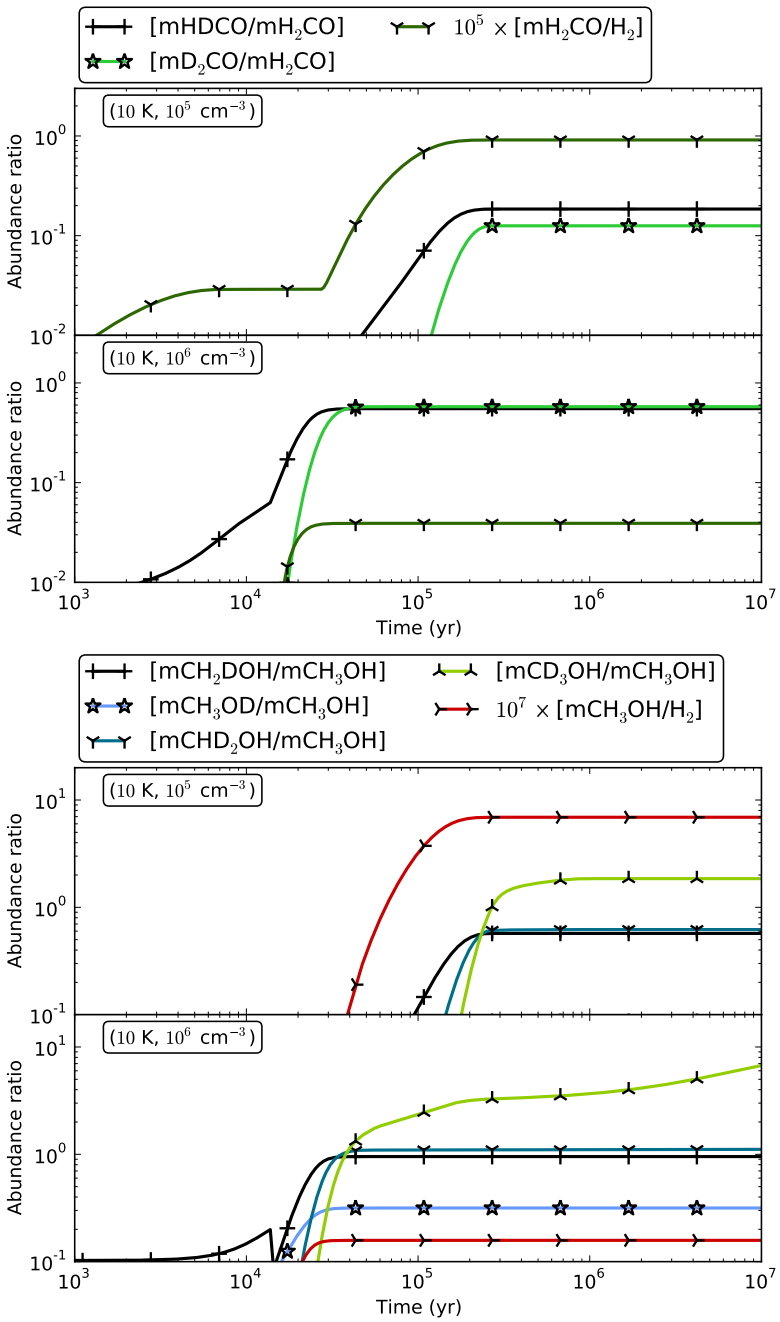

Figure 6.29: Relative abundance of multiply-deuterated formaldehyde and methanol in the ice mantle. The absolute abundances of formaldehyde and methanol are also plotted. The physical parameters are the same as in Fig. (6.28).

with ions. To understand why the [OD/HDO] ratio increases with time, we may write (based on quasi-steady state approximation)

$$n(\mathrm{OD}) \propto \frac{n(\mathrm{OH})n(\mathrm{D})}{\sum_i k_i \mathrm{M}_i}, \tag{6.61}$$

where M_i are the metal-containing species and ions reacting with OD. Note that OH is mainly formed from $\mathrm{H_3O^+ + E^-}$, which is similar to the formation reaction of HDO, and OH and HDO are also destroyed by similar reactions, we have roughly $n(\mathrm{OH}) \propto n(\mathrm{HDO})$, and

$$\frac{n(\mathrm{OD})}{n(\mathrm{HDO})} \propto \frac{n(\mathrm{OD})}{n(\mathrm{OH})} \propto \frac{n(\mathrm{D})}{\sum_i k_i M_i}. \tag{6.62}$$

Since initially n(D) increases with time (for T =10 K), and the terms in the denominator generally decrease with time due to adsorption, the [OD/HDO] ratio will increase with time.

Simply put, the gas phase [OD/HDO] ratio can be much higher than the [OH/$\mathrm{H_2O}$] ratio (which is equivalent to saying that the [OD/OH] ratio can be much higher than the [HDO/$\mathrm{H_2O}$] ratio) because a D-enhancement reaction exists for OH (D+OH $\longrightarrow$ OD+H), but not for $\mathrm{H_2O}$.

6.7 Conclusions

In the study presented in this chapter, we have built up a three-phase gas-grain-mantle chemical network containing deuterium fractionation reactions. Experimental results on the key reactions have been taken into account.

The resulting ice mantle composition can roughly match that derived from observations, if we assume different physical conditions are responsible for the formation of interstellar dust grain mantles in different regions of the sky.

The deuterium fractionation ratios of methanol, formaldehyde, and water from our model also agree with observations of cold regions (envelope of low mass protostar, dark cloud) reasonably well; in particular the model reproduces the general trend that methanol and formaldehyde tend to have a higher deuteration ratio than water.

The degree of deuterium fractionation is higher at higher densities, due to the fast depletion of gas phase molecules that consume deuterated $\mathrm{H_3^+}$ ($\mathrm{H_2D^+}$, ...). A lower temperature also gives a higher deuteration ratio, because the reactions driving the deuterated $\mathrm{H_3^+}$ back to $\mathrm{H_3^+}$ are suppressed. Note that for a high density and low temperature, the ice mantle is usually dominated by CO and $\mathrm{O_3}$ ice in our model.

$\mathrm{H_2O}$ and HDO ice are mainly formed through $\mathrm{H_2}$+OH $\longrightarrow$ $\mathrm{H_2O}$+H and its deuterated counterparts. The dominance of this channel over the H + OH $\longrightarrow$ $\mathrm{H_2O}$ channel tends to give a lower [HDO/$\mathrm{H_2O}$] ratio, but this is not the main reason for the generally lower deuterium fractionation ratio in water than in methanol and formaldehyde.

The existence of abstraction and addition reactions for the H atoms attached to the carbon atoms of $\mathrm{H_2CO}$ and $\mathrm{CH_3OH}$ is the main reason for these two species to have higher deuteration ratios than $\mathrm{H_2O}$. The fact that [$\mathrm{CH_3OD/CH_2DOH}$] is usually found to be smaller than 1/3 observationally (as expected from statistical arguments) is due to the same reason.

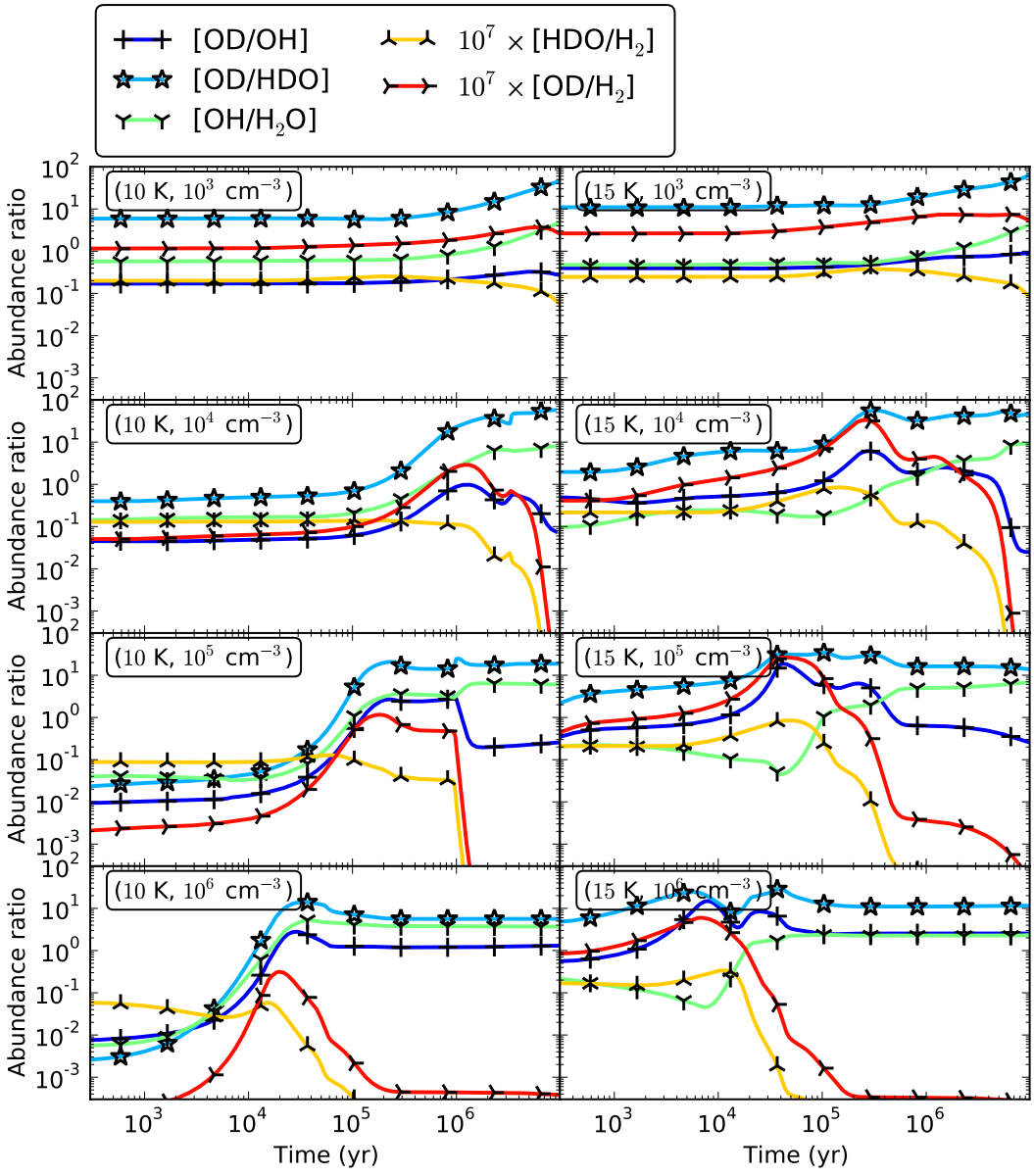

Figure 6.30: The [OD/OH] ratio and [OD/HDO] ratio as a function of time for different density and temperatures. The absolute abundances of HDO and OD (scaled by a factor of 10^7) are also shown for reference.

The $[D_2O/H_2O]$ ratio is very sensitive to whether water is formed through the $H + OH$ channel or the $H_2 + OH$ channel. The former channel gives a $[D_2O/H_2O]$ ratio 2–3 orders of magnitude higher than the latter channel. The low observed $[D_2O/H_2O]$ ratio supports the $H_2 + OH$ channel for water formation on dust grains.

There are a few caveats (the generic ones will be listed in the next chapter) we need to be aware of.

We found that the way we set the initial abundances and the binding energies of H and D on the grain surface affect the overall behavior of the system abruptly, by changing the fluxes of H and D injected onto the dust grains. It is not clear to what extent our initial setting approximates the real conditions of interstellar molecular clouds.

The zero-point energies of H and D affect their relative surface coverage. We calculated the zero-point energies by simply using their characteristic vibrational frequency on the surface, which is not guaranteed to be accurate.

We take single values for the binding and diffusion energies of each surface species. A real dust grain surface may actually contain sites with different characteristics. This may specifically be important for the surface binding and migration of H_2, which is responsible for water formation.

The high coverage of H_2 at low temperatures may alter the binding energy of other species, an effect that has not been included in our models.

There are uncertainties in the surface reaction network. Many of the reaction parameters are not well-constrained. Even for those we have discussed in detail, the experimental results should be considered semi-quantitative at best. Further input from the chemical community would be very helpful.

Chapter 7

Summary and outlook

7.1 Summary

This thesis contains the major part of the work I have done during my doctoral studies. I first wrote a code for solving the time-evolution of a gas phase chemical system under interstellar conditions, which has been applied to the study of the ortho and para forms of deuterated H_3^+, where the interaction between gas phase and dust grain surface processes can be simplified. This is described in Chapter 2. Common types of reactions are also described there.

Then I studied the grain surface chemistry by first looking at the necessity of incorporating it, identifying the basic processes that are involved, and then digging into its mathematical formulation based on the master equation. Following this, I wrote a Monte Carlo code, which is based on the stochastic simulation approach proposed by Gillespie (1976). All this is discussed in Chapter 3. The Monte Carlo code mainly serves as a benchmark, and is not used for studying astrochemical problems.

Grain surface chemistry is stochastic in nature due to the small sizes of dust grains and the discreteness of the surface reactions. This renders the rate equation approach usually adopted for gas phase chemistry inaccurate in some cases. The master equation prescription is accurate but difficult to solve. The Monte Carlo approach is easy to implement but it is slow. Hence we developed a new method to solve the coupled gas-grain chemistry, named the "hybrid moment equation" approach that is based on the moment equations that are derivable from the master equation. By benchmarking with the Monte Carlo method, we demonstrated that this HME approach is superior to the rate equation approach in the sense of producing accurate results. The main drawback of the HME approach is that for very large surface networks its speed degrades significantly. This is the topic of Chapter 4.

Inspired by the recent detection of hydrogen peroxide (H_2O_2) in the interstellar medium by Bergman et al. (2011b), we modeled its formation through gas-grain chemistry. It is found that the resulting gas phase H_2O_2 abundance, together with the abundances of H_2CO and CH_3OH, can match the observed values at a certain stage, which agrees with the dynamical time scale of the source constrained observationally. This is the content of Chapter 5. The O_2H molecule predicted by our model has actually been detected very recently in the same source.

Finally we build up a gas-grain-mantle model to study the deuterium fractionation

processes. Our model can produce a range of ice mantle compositions that are consistent with observations of different regions in space. The general trend that methanol and formaldehyde have a higher deuterium fractionation ratio than water is also reproduced. The abstraction reactions of methanol and formaldehyde are vital in differentiating them from water in their deuterium enhancement, while the dominance of the $H_2 + OH \longrightarrow H_2O + H$ channel over the $H + OH \longrightarrow H_2O$ channel plays only a minor role in lowering the [HDO/H_2O] ratio. On the other hand, the [D_2O/H_2O] ratio is sensitive to the route through which water is formed, and the observed low value for this ratio strongly suggests that water is mainly formed through $H_2 + OH \longrightarrow H_2O + H$. All this is discussed in Chapter 6.

7.2 Outlook

There are several aspects of our work that can be continued or improved.

One feature that is obviously missing from the modeling work presented here is that the time evolution of the physical parameters is not included. An explicitly time-dependent density and temperature is relatively straightforward to implement, and has actually been used in a small study contained in Parise et al. (2012b).

What is more challenging is to couple the chemical and physical evolution. The abundances of gas phase species such as CO and H_2O can alter the cooling efficiency, which in turn affects the dynamical evolution of the cloud. The ionization degree is also related to the chemical processes, hence the coupling between matter and magnetic field can also be affected by chemistry.

For the surface chemistry, we have assumed that the surface sites are homogeneous, meaning that all the sites have the same characteristics. A more realistic treatment may assume a distribution for certain parameters describing surface sites. An even more detailed approach would take into account the micro-physics of dust grain surface (and possibly the mantle layers), using a Monte Carlo method. It is still not clear how to couple such an approach to a large gas phase network.

Our modeling of H_2O_2 formation can explain the abundances of H_2O_2 and other species in the source where H_2O_2 is detected. The time-evolution of the H_2O_2 abundance shows that it can be very abundant at an early stage. However, at present it has only been detected in a single source, namely, ρ Ophiuchus A, by Bergman et al. (2011b). We note that the position in ρ Oph A, toward which H_2O_2 was detected has a very high H_2 column density of $3{\times}10^{22}$ cm^{-2}, which is 3 times higher than the value in the canonical dark cloud TMC-1 (Frerking et al. 1982). Given the H_2O_2 abundance determined by Bergman et al. (2011b), these authors would not have detected H_2O_2 were the H_2 column density a few times lower. Alternatively, limitations of our modeling and/or the natural evolution of interstellar clouds combined with certain observational selection effects may also be responsible for the rarity of H_2O_2 detections, and more work will be needed to investigate this.

Regarding deuterium chemistry in the gas phase, it is not completely clear whether including the ortho/para discrimination of species such as the H_2 and H_3^+ isotopologues can alter the degree of deuteration appreciably. This is an issue because the different spin states have different rotational energy levels, which may be high enough to overcome the barriers of certain reactions that act in the reverse direction of deuterium enhancement

in some species.

The surface chemistry involving deuterium also has large room of improvement. Many (if not most) of the parameters of the reactions related to water, formaldehyde, and methanol are not well-constrained, and certain "educated guesses" had to be made. After the arrival of new quantitative experimental results, it may be necessary to check how the deuterium fractionation for the species of interest is affected.

Finally some technical remarks on the code. Generally speaking, prospective improvements should be in the software side, rather than in the hardware side. Parallelization of the code is not an urgent requirement for astrochemical studies, unless, of course, the chemistry is to be coupled with a parallelized hydrodynamical code. Usually a "poor man's parallelization" would suffice, in which the code is arranged to run on different computers at the same time using different physical parameters.

Our hybrid moment equation (HME) approach is faster than the Monte Carlo method for a medium-to-large-sized system. But for a system involving many surface reactions that need to be treated stochastically, especially when the number of surface reactions approaches 1000, it also becomes very slow or even stops integration if its internal iteration does not converge. Including the three-phase gas-surface-mantle structure can further degrade its behavior. On the other hand, the Monte Carlo method, no matter how slow it may be, never gets stuck, because by design it does not involve solving any equations, and only simple algebraic operations (plus evaluation of exponential functions) are needed[1].

There are two possibilities to mitigate this situation. With the moment equation, many terms involving the second-order (or higher order depending on the accuracy required) moments have to be taken as indeterminate variables and need to be solved, which increases the size of the differential equation system significantly and slows down the code. Hence reducing the size of the system by eliminating some of the high order terms can increase the speed. This requires some "moment closure" method, namely, a systematic way to express the higher order moments in terms of lower order ones.

The next possibility is related to the solver for the differential equations. I use the `DLSODES` solver taken from the *ODEPACK* package, which is implicit in nature. The general consensus on solving a stiff system (a generic chemical system is stiff) of differential equations is that an implicit method must be used to guarantee stability. An implicit method involves solving a set of nonlinear algebraic equations, which is done with the Newton iteration method by linearization. The iteration process does not necessarily converge to the correct solution due to the potential sensitivity on the starting point, and this is the most time-consuming part of the code. Recently Guidry et al. (2011) claimed that an explicit method can actually be used for stiff systems, specifically for reaction network problems (chemical or nuclear), by stabilizing the integration with certain algebraic methods. Though this approach is still preliminary, it may turn out to be useful for solving a large system of equations as in the case of our HME approach, or for a large chemical network coupled with dynamics.

Another technical issue is related to the fact that a chemical model usually involves many parameters, some of which are free while others are not. A thorough and quick understanding of how the system behavior depends on these parameters requires novel analysis and visualization methods.

[1] Unfortunately, the Monte Carlo method cannot be parallelized to boost its speed, at least in its present form, because the evolution of a chemical system has to be followed step by step.

Appendix A

A comparison of different approaches for surface chemistry — the case of H_2 formation on dust grain surfaces

As a concrete demonstration of the utility of grain surface chemistry, here I show two different approaches to the formation of H_2, including a description of how this process is implemented in usual gas phase chemistry. The first one is based on the rate equation, and the second is based on the master equation.

In many purely gas phase chemical models, no surface processes are included, but the formation of H_2 is nevertheless accounted for, in a somewhat "handwaving" way, although for normal dark cloud conditions, the efficiency of H_2 formation is actually unimportant. This is because most of the hydrogen is usually assumed to be in molecular form in the initial condition. The destruction of H_2 by cosmic rays is very slow, with a typical time scale of 10^9 yr. Even if no formation channel for H_2 is included, the gas phase chemistry will not be affected much, since the H_2 abundance is essentially constant for time spans of astrochemical interest. Even the surface chemistry will not be affected much by neglecting the surface formation of H_2 either, due to the presence of a lot of heavy molecules (such as CO and O_2) on the surface. An H atom landing on the dust grain surface will almost always combine with one of these heavy molecules, with an extremely low chance to keep free before evaporation and react with another incoming H atom to form an H_2 molecule. Thus the H_2 formation is not competitive with other hydrogenation reactions. However, when the active surface reactions have ceased, and when a long time scale is of interest, the surface formation of H_2 becomes important.

Only three reactions will be involved in the following discussion:

$$\mathrm{H} \xrightarrow{k_{\mathrm{acc}}} \mathrm{gH}, \tag{A.1}$$

$$\mathrm{gH} \xrightarrow{k_{\mathrm{eva}}} \mathrm{H}, \text{ and} \tag{A.2}$$

$$\mathrm{gH} + \mathrm{gH} \xrightarrow{k_{\mathrm{H,H}}} \mathrm{gH_2}. \tag{A.3}$$

Here the "g" in gH means that the atomic H is on the grain surface. Such a distinction

between the symbols for gas phase and grain surface species is not always necessary, since the meaning can be easily judged from the context.

A.1 With the rate equation approach

Usually we are interested in the production rate of H_2 in terms of the change rate of its gas phase density $n(H_2)$. With the rate equation, the production rate of H_2 is

$$R(H_2) \equiv \partial_t n(H_2)|_{\rm prod} = \frac{k_{\rm H,H}}{N_{\rm S}V} N_{\rm H}^2, \tag{A.4}$$

where $N_{\rm H}$ is the number of H atoms on the surface of *one* dust grain, $N_{\rm S}$ is the number of reaction sites on the surface of this dust grain, $k_{\rm H,H}$ is the surface reaction rate of H atoms, and V is the gas volume containing *one* dust grain (see Eq. (3.5) on page 31; not to be confused with the volume of a dust grain).

The evolution equation of $N_{\rm H}$ is (cf. Eq. (6.16))

$$\partial_t N_{\rm H} = \alpha n({\rm H}) v({\rm H}) \sigma - 2k_{\rm H,H} N_{\rm H}^2 / N_{\rm S} - k_{\rm eva,\ H} N_{\rm H},$$

where $\alpha n({\rm H}) v({\rm H})$ is the flux of H atoms accreted onto the grain surface, the α factor being related to the surface shape and sticking coefficient, σ is the surface area of a dust grain, and $k_{\rm eva,H}$ is the evaporation rate of surface H atoms. With a Maxwell distribution for the gas phase velocity, we have $\alpha = 1/4$ (assuming unity sticking coefficient), and $v({\rm H}) = (8{\rm k}T/\pi m_{\rm H})^{1/2}$.

Assuming steady state has been reached, then $N_{\rm H}$ can be solved for from the above equation (cf. Eq. (6.19)):

$$N_{\rm H} = \frac{2\alpha n({\rm H}) v({\rm H}) \sigma}{k_{\rm eva} + \sqrt{k_{\rm eva}^2 + 8k_{\rm H,H}\alpha n({\rm H}) v({\rm H}) \sigma / N_{\rm S}}}. \tag{A.5}$$

In gas phase chemical models, the formation rate of H_2 on the dust grains is usually expressed as (Le Petit et al. 2009)

$$R(H_2) = \beta(H_2) n({\rm H}) n_{\rm H}. \tag{A.6}$$

The parameter $\beta(H_2)$ may be called formation rate coefficient. We have

$$\begin{aligned} \beta(H_2) =& \frac{k_{\rm H,H}}{N_{\rm S}V} N_{\rm H}^2 / \left[n({\rm H}) n_{\rm H} \right] \\ =& \frac{k_{\rm H,H}}{N_{\rm S} V n_{\rm H}} \frac{4\alpha^2 n({\rm H}) v^2({\rm H}) \sigma^2}{\left(k_{\rm eva} + \sqrt{k_{\rm eva}^2 + 8k_{\rm H,H}\alpha n({\rm H}) v({\rm H}) \sigma / N_{\rm S}} \right)^2}. \end{aligned} \tag{A.7}$$

If $k_{\rm eva}$ is so small that it can be neglected (so that all the H atoms arriving on the dust grain surface recombine to form H_2 molecules), then

$$\begin{aligned} \beta(H_2) \simeq& \frac{\alpha v({\rm H}) \sigma}{2V n_{\rm H}} = \frac{1}{2} \alpha v({\rm H}) \sigma R_{\rm G,n} \\ =& 1.44 \times 10^{-17}\ {\rm cm^3\ s^{-1}} \\ & \times \left(\frac{T}{10\ {\rm K}} \right)^{1/2} \left(\frac{R_{\rm G,m}}{0.01} \right) \left(\frac{0.1\ \mu{\rm m}}{r_{\rm grain}} \right) \left(\frac{2\ {\rm g\ cm^{-3}}}{\rho_{\rm G}} \right), \end{aligned} \tag{A.8}$$

where α has been assigned 1/4. The above value is typically adopted in pure gas phase chemical models.

When the temperature is not extremely low, the evaporation rate should not be neglected. Fig. (A.1) shows the production rate coefficient of H_2 on dust grains as a function of temperature. Two cases for surface diffusion of H atoms have been plotted: thermal hopping or quantum tunneling. At very low temperatures the thermal accretion rate becomes very low, and the formation rate of H_2 also decreases, even if the H atoms on the grain surface are allowed to diffuse through quantum tunneling. At high temperatures the evaporation rate is too high to allow any H atoms on the grain surface to stay long enough to meet another H atom to form an H_2 molecule. Physically this is completely understandable; however, mathematically, one may notice that according to Eq. (A.7) the production rate coefficient of H_2 actually increases with temperature when the temperature is very high. This is because at high temperatures both the evaporation and surface diffusion rate approach the characteristic frequency ν_0 (taken to be a constant), so the rate coefficient is only controlled by the thermal accretion velocity, which increases with temperature. Of course this has no relevance since the absolute value of the formation rates of H_2 at these high temperatures is very low.

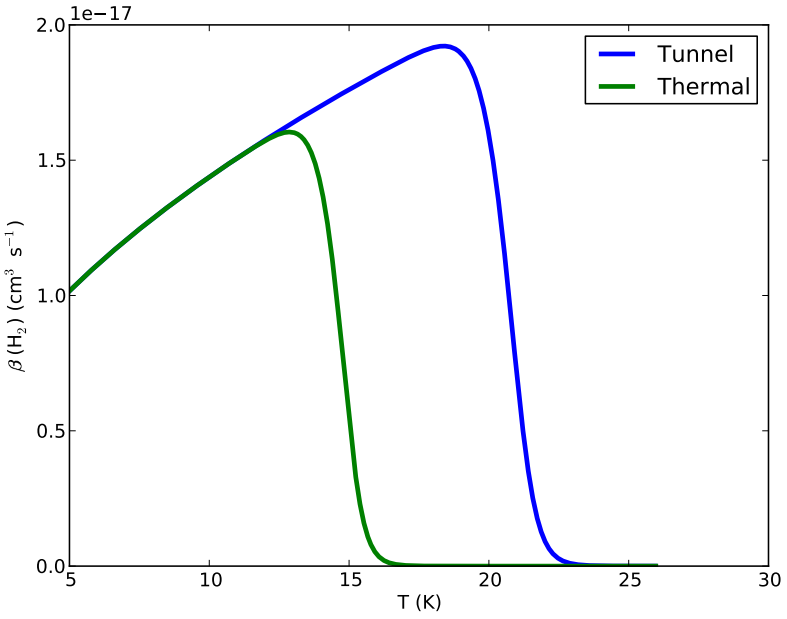

Figure A.1: Production rate coefficient of H_2 as a function of temperature in the case of quantum tunneling and thermal hopping. The barrier against diffusion is taken to be 510 K, and the binding energy is taken to be 650 K (Katz et al. 1999)

A.2 The master equation approach

This section is mainly of mathematical interest only. It deals with one of the simplest systems, namely, the formation of H_2 molecules on the dust grain surface, for which the

(steady-state) master equation can be solved analytically.

For the master equation, we let the probability distribution function $P(n,t)$ describe the probability that there are n H atoms on the surface of one specific dust grain at time t. For brevity I denote it by $P(n)$. Its evolution equation (the master equation) is

$$\begin{aligned}\partial_t P(n) = {} & k_{\rm acc}[P(n-1) - P(n)] \\ & + k_{\rm eva}[P(n+1)(n+1) - P(n)n] \\ & + k_{\rm H,H}[P(n+1)(n+2)(n+1) - P(n)n(n-1)],\end{aligned} \tag{A.9}$$

where $k_{\rm acc}$, $k_{\rm eva}$, and $k_{\rm H,H}$ are the accretion rate, evaporation rate, and surface reaction rate, respectively.

The corresponding generating function (see Section 4.A on Page 66) is

$$f(x) = \sum_{n=0}^{\infty} P(n) x^n. \tag{A.10}$$

Since the probability must sum up to unity, we have $f(1) = 1$; and $f(0) = P(0)$; in general,

$$P(n) = f^{(n)}(0)/n!. \tag{A.11}$$

The evolution equation of $f(x)$ is

$$\begin{aligned}\partial_t f(x) = {} & \sum_{n=0}^{\infty} \partial_t P(n) x^n \\ = {} & k_{\rm acc} \sum_{n=0}^{\infty} [P(n-1) - P(n)] x^n \\ & + k_{\rm eva} \sum [P(n+1)(n+1) - P(n)n] x^n \\ & + k_{\rm H,H} \sum [P(n+1)(n+2)(n+1) - P(n)n(n-1)] x^n,\end{aligned} \tag{A.12}$$

which can be simplified into

$$\partial_t f(x) = (x-1)\left[k_{\rm acc} f - k_{\rm eva} \partial_x f - k_{\rm H,H}(x+1)\partial_{xx} f\right]. \tag{A.13}$$

At steady state, $\partial_t f(x) = 0$, hence

$$k_{\rm acc} f - k_{\rm eva} \partial_x f - k_{\rm H,H}(x+1)\partial_{xx} f = 0. \tag{A.14}$$

If $k_{\rm H,H} = 0$, i.e. there is no surface reaction, then

$$f(x) = \exp\left[\frac{k_{\rm acc}}{k_{\rm eva}}(x-1)\right], \tag{A.15}$$

where the condition $f(1) = 1$ has been used. In this case the probability that there are n H atoms on the grain surface is

$$P(n) = \frac{\exp\left[-k_{\rm acc}/k_{\rm eva}\right]}{n!}\left(\frac{k_{\rm acc}}{k_{\rm eva}}\right)^n, \tag{A.16}$$

which is simply the Poisson distribution, with average number $k_{\rm acc}/k_{\rm eva}$. It is interesting to see that the Poisson distribution can be derived this way.

Eq. (A.14) has a closed-form solution (Green et al. 2001), though it is somewhat complicated. Define $a{\equiv}k_{\rm acc}/k_{\rm H,H}$, $b{\equiv}k_{\rm eva}/k_{\rm H,H}$, then

$$f(x) = \frac{2^{-(1-b)/2}}{\mathrm{I}[-(1-b), 2\sqrt{2a}]}(1+x)^{(1-b)/2}\mathrm{I}[-(1-b), 2\sqrt{a(1+x)}], \tag{A.17}$$

where I is the Bessel I-function:

$$\mathrm{I}[\nu, z] = \left(\frac{z}{2}\right)^{\nu}\sum_{k=0}^{\infty}\frac{1}{k!\Gamma(\nu+k+1)}\left(\frac{z^2}{4}\right)^{k}. \tag{A.18}$$

Hence $f(x)$ can also be written as

$$f(x) = \frac{\sum_{k=0}^{\infty}\frac{a^k}{k!}\frac{(1+x)^k}{\Gamma(k+b)}}{\sum_{k=0}^{\infty}\frac{a^k}{k!}\frac{2^k}{\Gamma(k+b)}}. \tag{A.19}$$

From the above equations and using the relation Eq. (A.11), with some algebra we can also have

$$\begin{aligned} P(n) &= \frac{1}{n!}2^{-(1-b)/2}a^{n/2}\frac{\mathrm{I}[-(1-b)+n, 2\sqrt{a}]}{I[-(1-b), 2\sqrt{2a}]} \\ &= \frac{1}{n!}\frac{\sum_{k=n}^{\infty}\frac{a^k}{(k-n)!}\frac{1}{\Gamma(k+b)}}{\sum_{k=0}^{\infty}\frac{a^k}{k!}\frac{2^k}{\Gamma(k+b)}} \\ &= \frac{a^n}{n!}\frac{\sum_{k=0}^{\infty}\frac{a^k}{k!}\frac{1}{\Gamma(k+n+b)}}{\sum_{k=0}^{\infty}\frac{a^k}{k!}\frac{2^k}{\Gamma(k+b)}}. \end{aligned} \tag{A.20}$$

The average occupation number of H atoms on a single grain $\langle n\rangle$ can be calculated by $\partial_x f(x)|_{x=1}$:

$$\begin{aligned} \langle n\rangle &= a\cdot\frac{\sum_{k=0}^{\infty}\frac{1}{k!}\frac{1}{\Gamma(k+b+1)}(2a)^k}{\sum_{k=0}^{\infty}\frac{1}{k!}\frac{1}{\Gamma(k+b)}(2a)^k} \\ &\simeq \begin{cases} \frac{a}{b+2a} = \frac{k_{\rm acc}}{2k_{\rm acc}+k_{\rm eva}}, & \text{when } a\ll 1 \text{ and } b\ll 1, \\ \frac{a}{b} = \frac{k_{\rm acc}}{k_{\rm eva}}, & \text{when } b\gg 1, \\ \sqrt{\frac{a}{2}} = \sqrt{\frac{k_{\rm acc}}{2k_{\rm H,H}}}, & \text{when } a\gg 1 \text{ and } b\ll 1. \end{cases} \end{aligned} \tag{A.21}$$

and $\langle n(n-1)\rangle$ can be calculated by $\partial_x^2 f(x)|_{x=1}$:

$$\begin{aligned} \langle n(n-1)\rangle &= a^2\cdot\frac{\sum_{k=0}^{\infty}\frac{1}{k!}\frac{1}{\Gamma(k+b+2)}(2a)^k}{\sum_{k=0}^{\infty}\frac{1}{k!}\frac{1}{\Gamma(k+b)}(2a)^k} \\ &\simeq \begin{cases} \frac{a^2}{b+2a} = \frac{k_{\rm acc}^2}{k_{\rm H,H}(2k_{\rm acc}+k_{\rm eva})}, & \text{when } a\ll 1 \text{ and } b\ll 1, \\ \frac{a^2}{b^2} = \frac{k_{\rm acc}^2}{k_{\rm eva}^2}, & \text{when } b\gg 1, \\ \frac{a}{2} = \frac{k_{\rm acc}}{2k_{\rm H,H}}, & \text{when } a\gg 1 \text{ and } b\ll 1. \end{cases} \end{aligned} \tag{A.22}$$

The results at the limits when a or b are much greater or smaller than 1 are easy to interpret. When $b{=}k_{\rm eva}/k_{\rm H,H} \gg 1$, the evaporation rate is much faster than the reaction rate, hence the surface average population $\langle n\rangle$ is determined by the ratio between the accretion rate $k_{\rm acc}$ and evaporation rate $k_{\rm eva}$. When $a \gg 1$ and $b \ll 1$, the surface population is determined by the surface reaction rate, and can be calculated with the usual rate equation formula. When $a \ll 1$ and $b \ll 1$, the situation is a bit more complex. If furthermore $b \ll a$, then $\langle n\rangle{\simeq}1/2$; this simply means that half of the time the surface empty, and half of them time only one hydrogen atom is on the surface; when two hydrogen atoms are on the surface at the same time, they immediately react and the surface becomes empty again.

The H_2 formation rate is $R(H_2) = k_{\rm H,H}\langle n(n-1)\rangle$. In the rate equation approach it is set to $k_{\rm H,H}\langle n\rangle^2$, while in the modified rate equation approach of Garrod (2008) (see his equation (16) and (17)) it is set to

$$R(H_2) = k_{\rm H,H} \cdot \frac{k_{\rm acc}\langle n\rangle}{k_{\rm eva} + k_{\rm H,H}}. \tag{A.23}$$

What about our moment equation approach? As noted in Chapter 4, our hybrid moment equation approach at second order is partially equivalent to the modified equation approach of Garrod (2008), and they give the same steady-state results. However, if the third-order moments are included, then we may have the following set of equations

$$\begin{aligned}\partial_t\langle n(n-1)\rangle = {} & 2k_{\rm acc}\langle n\rangle - 2k_{\rm eva}\langle n(n-1)\rangle \\ & - 2k_{\rm H,H}\langle n(n-1)\rangle - 4k_{\rm H,H}\langle n(n-1)(n-2)\rangle,\end{aligned} \tag{A.24}$$

and

$$\begin{aligned}\partial_t\langle n(n-1)(n-2)\rangle = {} & 3k_{\rm acc}\langle n(n-1)\rangle - 3k_{\rm eva}\langle n(n-1)(n-2)\rangle \\ & - 6k_{\rm H,H}\langle n(n-1)(n-2)\rangle - \cdots,\end{aligned} \tag{A.25}$$

where the fourth-order term is neglected. At steady-state we can solve the above equations and get

$$\begin{aligned}k_{\rm H,H}\langle n(n-1)\rangle &= k_{\rm H,H} \cdot \frac{k_{\rm acc}\langle n\rangle}{k_{\rm eva} + k_{\rm H,H} + 2k_{\rm acc}k_{\rm H,H}/(k_{\rm eva} + 2k_{\rm H,H})} \\ &= k_{\rm H,H} \cdot \frac{a\langle n\rangle}{1 + b + 2a/(2+b)}.\end{aligned} \tag{A.26}$$

We can see that Eq. (A.23) is an approximation to the above equation.

Fig. (A.2) visualizes the differences among these approaches (the master equation result is considered to be the most correct), for a grid of rate parameters. It can be seen that for a very high accretion or evaporation rate (with respect to the reaction rate), the rate equation works quite well. For very low accretion rate or very high evaporation rate, the modified rate equation works fine. In a intermediate parameter space, where the accretion rate is neither very low nor very high, both the rate equation and modified rate equation fail to reproduce the master equation results. The region for which the third-order moment equation works fine is similar to, and slightly larger than that of the modified rate equation, which demonstrates that including higher order moments can indeed improve the accuracy.

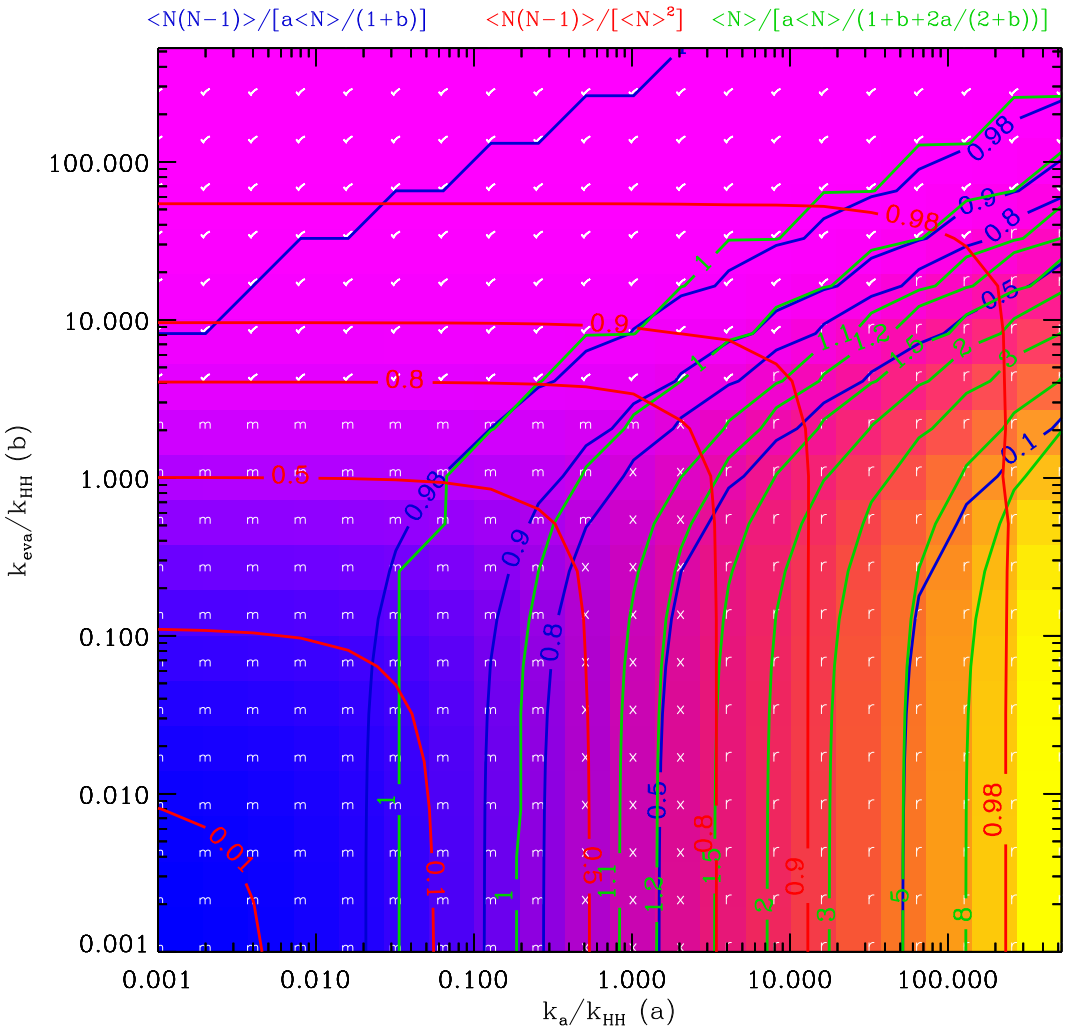

Figure A.2: Comparison among different formulations for the H_2 formation rate. The X- (Y-) axis are the ratio between the accretion (evaporation) rates and reaction rates. The red contours are the ratio between the master equation rates and the rate equation rates, the blue contours are the ratio between the master equation rates and the modified rate equation rates, and the green contours are the ratio between the master equation rates and the rates from third order moment equations. The rate equation tends to work fine in the right region (marked "r"), while the modified rate equation tends to work fine in the left region (marked "m"), and both work fine in the upper region (marked "✓"). Both fail in a small region in the mid bottom part (marked "x"), where $k_{\rm acc}/k_{\rm H,H}\simeq 1$, where the third order moment equation still works reasonably well.

Finally, we remark that the master equation Eq. (A.9) in the steady-state case can also be solved with continued fractions (Biham & Lipshtat 2002). The starting point is a recurrence relation that can be derived from Eq. (A.9)

$$P(n) = \frac{n+1}{a} P(n+1) \left[(n+b) + (n+2) \frac{P(n+2)}{P(n+1)} \right]. \tag{A.27}$$

The derivation involves summing over n from 1 to N (such a procedure is commonly used in reducing a set of linear equations) to get

$$\begin{aligned} -aP(0) + aP(N) + bP(1) - b(N+1)P(N+1) + 2P(2) \\ - N(N+1)P(N+1) - (N+1)(N+2)P(N+2) = 0, \end{aligned} \tag{A.28}$$

and making use of the relation

$$2P(2) = aP(0) - bP(1), \tag{A.29}$$

which is obtained by setting $n = 1$ in Eq. (A.9).

Define

$$q(n) \equiv \frac{aP(n)}{(n+1)P(n+1)},$$

then Eq. (A.27) becomes

$$q(n) = n + b + \frac{a}{q(n+1)}, \tag{A.30}$$

which can be solved using continued fraction

$$q(n) = n + b + \cfrac{a}{n+1+b+\cfrac{a}{n+2+b+\cfrac{a}{n+3+b+\cdots}}}, \tag{A.31}$$

and $P(n)$ can be expressed as

$$P(n) = \frac{a}{nq(n-1)} P(n-1) = \frac{a^n}{n!} \frac{1}{q(n-1)\cdots q(0)} P(0), \tag{A.32}$$

which is indeed related to the continued fraction expansion of the ratio between two Bessel I-functions (Biham & Lipshtat 2002)[1].

[1] See also `http://people.math.sfu.ca/~cbm/aands/page_363.htm`.

Appendix B

Formal solution to the master equation

We introduced the chemical master equation in Section 3.4.2 on page 40. The master equation can rarely be solved analytically due to its complex structure and large size. One known exception is the H_2 formation problem in the steady-state case; see Appendix A. Here we discuss if the master equation is analytically solvable in principle, what form would the solution take. Note that the following investigation is mainly out of mathematical curiosity, and it does not seem to ease the difficulties in numerically solving the real-life stochastic problem underlying the master equation.

Symbolically, the solution to Eq. (3.32) can be written as

$$\mathbf{p}(t) = \exp\left[\mathsf{T}t\right]\mathbf{p}|_{t=0}, \tag{B.1}$$

where $\exp\left[\mathsf{T}t\right]$ is to be understood as

$$\exp\left[\mathsf{T}t\right] \equiv \sum_{n=1}^{\infty} \frac{t^n}{n!}\mathsf{T}^n.$$

If one can somehow obtain the spectrum of matrix T, namely, all the eigenvectors and their corresponding eigenvalues, and if these eigenvectors form a complete system, then one may decompose the initial vector $\mathbf{p}_0 \equiv \mathbf{p}|_{t=0}$ into a superposition of the eigenvectors, and the solution of the master equation would be obtained immediately. That is, if we have $\mathsf{T}\mathbf{v}_i = \lambda_i \mathbf{v}_i$, and $\mathbf{v}_i$ (i=1, 2, ..., $N_{\mathbf{p}}$, $N_{\mathbf{p}}$ being the dimension of $\mathbf{p}$) form a complete set, then the initial probability distribution vector can be expressed as $\mathbf{p}|_{t=0} = \sum_i^{N_{\mathbf{p}}} c_i \mathbf{v}_i$. Putting this expansion into Eq. (B.1), we have

$$\begin{aligned} \mathbf{p}(t) &= \sum_{n=1}^{\infty} \frac{t^n}{n!}\mathsf{T}^n \sum_{i=1}^{N_{\mathbf{p}}} c_i \mathbf{v}_i = \sum_{n=1}^{\infty}\sum_{i=1}^{N_{\mathbf{p}}} \frac{t^n}{n!} c_i \lambda_i^n \mathbf{v}_i \\ &= \sum_{i=1}^{N_{\mathbf{p}}} c_i \exp\left(t\lambda_i\right)\mathbf{v}_i. \end{aligned} \tag{B.2}$$

However, the eigensystem of the matrix operator T is not always complete, that is to say, the number of linearly independent eigenvectors of T may be smaller than its

dimension, so there may exist an $N_{\mathbf{p}}$-dimensional vector $\mathbf{v}_0$ that cannot be expressed as a linear combination of the eigenvectors of T. In this case the solution with initial condition $\mathbf{v}_0$ cannot be written in the form of Eq. (B.2).

However, the formal solution in Eq. (B.1) always holds, and we can still get a clue of how the solution of Eq. (3.32) looks like with the help of the Jordan normal form of T. The matrix T can be transformed into its Jordan normal form via a similarity transformation:

$$\mathsf{O}^{-1}\mathsf{T}\mathsf{O} = \begin{pmatrix} J_1(\lambda_1) & & \\ & \ddots & \\ & & J_p(\lambda_p) \end{pmatrix}, \tag{B.3}$$

where each Jordan block $J_i(\lambda_i)$ has the form

$$J_i(\lambda_i) = \begin{pmatrix} \lambda_i & 1 & & \\ & \lambda_i & \ddots & \\ & & \ddots & 1 \\ & & & \lambda_i \end{pmatrix}. \tag{B.4}$$

Note that in Eq. (B.3) the same eigenvalue can have multiple entries (Lancaster & Tismenetsky 1985, page 237); namely, more than one $J_i(\lambda_i)$ may correspond to the same λ; the same Jordan block J with the same λ can also appear multiple times in the Jordan normal form.

Each Jordan block $J(\lambda)$ can be written as a sum of a diagonal part (denoted by Λ) and a super-diagonal part (denoted by S):

$$J(\lambda) = \begin{pmatrix} \lambda & & \\ & \ddots & \\ & & \lambda \end{pmatrix} + \begin{pmatrix} & 1 & \\ & \ddots & 1 \\ & & \end{pmatrix}. \tag{B.5}$$

It can be readily verified that the diagonal part and the super-diagonal part commute with each other. Hence the exponential function of $J(\lambda)t$ is

$$\exp\left[J(\lambda)t\right] = \exp\left[(\Lambda + S)t\right] = \exp\left[\Lambda t\right]\exp\left[St\right]. \tag{B.6}$$

The super-diagonal part S is a nilpotent matrix, meaning that there is an integer k such that $S^k = 0$, i.e., S multiplies itself by k times yields a zero matrix. Thus $\exp\left[St\right]$ is actually a polynomial in t, with the coefficients being matrices. The $\exp\left[\Lambda t\right]$ part is a diagonal matrix with entries equal $\exp\left[\lambda t\right]$, so

$$\exp\left[\Lambda t\right]\exp\left[St\right] = e^{\lambda t}\exp\left[St\right] = e^{\lambda t}\sum_{i=1}^{n} A_i t^i, \tag{B.7}$$

where each A_i is a matrix, and n is a finite number.

We finally have

$$\begin{aligned} \exp\left[\mathsf{T}t\right] &= \mathsf{O}\exp\left[\mathsf{O}^{-1}\mathsf{T}\mathsf{O}t\right]\mathsf{O}^{-1} \\ &= \mathsf{O}\begin{pmatrix} e^{\lambda_1 t}\sum_{i=1}^{n_1} A_{1,i}t^i & & \\ & \ddots & \\ & & e^{\lambda_p t}\sum_{i=1}^{n_p} A_{p,i}t^i \end{pmatrix}\mathsf{O}^{-1}, \end{aligned} \tag{B.8}$$

where O is a constant invertible matrix, and each $A_{j,i}$ is a matrix.

Thus the general solution of the master equation is no more than a superposition of many simple exponential functions (if the corresponding eigenvalue is an imaginary number, then the exponential function becomes a trigonometric function) multiplied by polynomials in t. Such a solution describes the evolution of the probability distribution function. What we usually care about is the abundance (or population) of each species in a system, which can be obtained by taking the moments of the probability distribution (see Chapter 4). Since the operation of taking moments is also a linear operation (with constant coefficients), the abundance of each species as a function of time is also in principle a superposition of many functions of the form $t^n e^{\lambda t}$. This might seem to be a surprise at first glance, since the evolution curve of a species can be quite complex; the truth is that a linear superposition of many simple exponential functions of the form $e^{-\lambda t}$ can indeed appear very complex.

The formal solution presented in Eq. (B.2) or Eq. (B.8) indicates that the eigenvalues of the stochastic matrix T must have certain special properties. For example, none of them can be positive, otherwise the solution $\mathbf{p}(t)$ would grow without limit. They cannot be all negative either, otherwise $\mathbf{p}(t)$ would vanish as time goes by. So the largest of the λ_is should be zero. Another strong constraint is that the sum of all the components of $\mathbf{p}(t)$ should always equal one because of probability conservation.

Unfortunately, the above derivation only has theoretical value. In practice, the dimension of the state vector $N_{\mathbf{p}}$ is extremely large and impossible to enumerate (even calculating the value of $N_{\mathbf{p}}$ is quite non-trivial), let alone to solve the eigenvalue problem associated with T (which is a matrix of dimension $N_{\mathbf{p}} \times N_{\mathbf{p}}$).

Bibliography

Agúndez, M., Cernicharo, J., Guélin, M., et al. 2008, A&A, 478, L19

Aikawa, Y., Umebayashi, T., Nakano, T., & Miyama, S. M. 1997, ApJ, 486, L51

Al-Halabi, A., & van Dishoeck, E. F. 2007, MNRAS, 382, 1648

Albertsson, T., Semenov, D. A., & Henning, T. 2011, ArXiv e-prints

Allen, M., & Robinson, G. W. 1977, ApJ, 212, 396

Amiaud, L., Fillion, J. H., Baouche, S., et al. 2006, The Journal of Chemical Physics, 124, 094702

An, D., Ramírez, S. V., Sellgren, K., et al. 2011, ApJ, 736, 133

André, P., Belloche, A., Motte, F., & Peretto, N. 2007, A&A, 472, 519

Asplund, M., Grevesse, N., Sauval, A. J., & Scott, P. 2009, ARA&A, 47, 481

Atkinson, R., Baulch, D. L., Cox, R. A., et al. 2004, Atmospheric Chemistry & Physics, 4, 1461

Awad, Z., Chigai, T., Kimura, Y., Shalabiea, O. M., & Yamamoto, T. 2005, ApJ, 626, 262

Bacmann, A., Lefloch, B., Ceccarelli, C., et al. 2002, A&A, 389, L6

Barzel, B., & Biham, O. 2007a, ApJ, 658, L37

—. 2007b, J. Chem. Phys., 127, 144703

—. 2011, Physical Review Letters, 106, 150602

Bates, D. R. 1951, MNRAS, 111, 303

—. 1983, ApJ, 270, 564

Bates, D. R., & Spitzer, Jr., L. 1951, ApJ, 113, 441

Belloche, A., Garrod, R. T., Müller, H. S. P., et al. 2009, A&A, 499, 215

Belloche, A., Menten, K. M., Comito, C., et al. 2008, A&A, 482, 179

Bergin, E. A., Neufeld, D. A., & Melnick, G. J. 1998, ApJ, 499, 777

Bergin, E. A., & Tafalla, M. 2007, ARA&A, 45, 339

Bergin, E. A., Melnick, G. J., Stauffer, J. R., et al. 2000, ApJ, 539, L129

Bergin, E. A., Phillips, T. G., Comito, C., et al. 2010, A&A, 521, L20

Bergman, P., Parise, B., Liseau, R., & Larsson, B. 2011a, A&A, 527, A39+

Bergman, P., Parise, B., Liseau, R., et al. 2011b, A&A, 531, L8+

Biham, O., Furman, I., Pirronello, V., & Vidali, G. 2001, ApJ, 553, 595

Biham, O., & Lipshtat, A. 2002, Phys. Rev. E, 66, 056103

Binnewies, M., & Milke, E. 1999, Thermochemical data of elements and compounds (Wiley-VCH)

Boger, G. I., & Sternberg, A. 2006, ApJ, 645, 314

Boogert, A. C. A., Pontoppidan, K. M., Knez, C., et al. 2008, ApJ, 678, 985

Boogert, A. C. A., Huard, T. L., Cook, A. M., et al. 2011, ApJ, 729, 92

Bottinelli, S., Boogert, A. C. A., Bouwman, J., et al. 2010, ApJ, 718, 1100

Boudin, N., Schutte, W. A., & Greenberg, J. M. 1998, A&A, 331, 749

Bradley, J. P., Humecki, H. J., & Germani, M. S. 1992, ApJ, 394, 643

Brown, P. D., & Millar, T. J. 1989, MNRAS, 240, 25P

Brown, R. D. 1977, Nature, 270, 39

Butner, H. M., Charnley, S. B., Ceccarelli, C., et al. 2007, ApJ, 659, L137

Caselli, P., Hasegawa, T.I., & Herbst, E. 1998, ApJ, 495, 309

Caselli, P., Stantcheva, T., Shalabiea, O., Shematovich, V. I., & Herbst, E. 2002, Planet. Space Sci., 50, 1257

Caselli, P., Walmsley, C. M., Tafalla, M., Dore, L., & Myers, P. C. 1999, ApJ, 523, L165

Cazaux, S., Cobut, V., Marseille, M., Spaans, M., & Caselli, P. 2010, A&A, 522, A74+

Ceccarelli, C., Castets, A., Loinard, L., Caux, E., & Tielens, A. G. G. M. 1998, A&A, 338, L43

Ceccarelli, C., Loinard, L., Castets, A., et al. 2001, A&A, 372, 998

Ceccarelli, C., Vastel, C., Tielens, A. G. G. M., et al. 2002, A&A, 381, L17

Cernicharo, J., Guélin, M., Agündez, M., et al. 2007, A&A, 467, L37

Chandrasekhar, S. 1943, Reviews of Modern Physics, 15, 1

Chang, Q., Cuppen, H., & Herbst, E. 2005, A&A, 434, 599

Chang, Q., Cuppen, H. M., & Herbst, E. 2007, A&A, 469, 973

Charnley, S. B. 1998, ApJ, 509, L121

—. 2001, ApJ, 562, L99

—. 2005, Adv. Space Res., 36, 132

Charnley, S. B., & Markwick, A. J. 2003, A&A, 399, 583

Charnley, S. B., & Rodgers, S. B. 2009, in ASP Conf. Ser., ed. K. J. Meech, J. V. Keane, M. J. Mumma, J. L. Siefert, & D. J. Werthimer, Vol. 420, 29

Charnley, S. B., Tielens, A. G. G. M., & Millar, T. J. 1992, ApJ, 399, L71

Charnley, S. B., Tielens, A. G. G. M., & Rodgers, S. D. 1997, ApJ, 482, L203

Chiar, J. E., Adamson, A. J., Kerr, T. H., & Whittet, D. C. B. 1994, ApJ, 426, 240

Chiar, J. E., Tielens, A. G. G. M., Whittet, D. C. B., et al. 2000, ApJ, 537, 749

Chiar, J. E., Pendleton, Y. J., Allamandola, L. J., et al. 2011, ApJ, 731, 9

Clancy, R. T., Sandor, B. J., & Moriarty-Schieven, G. H. 2004, Icarus, 168, 116

Clayton, D. 1968, Principles of Stellar Evolution and Nucleosynthesis: With a New Preface (University of Chicago Press)

Cuppen, H., & Herbst, E. 2007, ApJ, 668, 294

Cuppen, H. M., Ioppolo, S., Romanzin, C., & Linnartz, H. 2010, Physical Chemistry Chemical Physics (Incorporating Faraday Transactions), 12, 12077

Dalgarno, A., & Lepp, S. 1984, ApJ, 287, L47

Dalgarno, A., & McCray, R. A. 1973, ApJ, 181, 95

Dalgarno, A., Oppenheimer, M., & Berry, R. S. 1973, ApJ, 183, L21

Dartois, E., Thi, W.-F., Geballe, T. R., et al. 2003, A&A, 399, 1009

Dash, J. G. 1968, J. Chem. Phys., 48, 2820

Davis, Jr., L., & Greenstein, J. L. 1951, ApJ, 114, 206

de Jong, T. 1972, A&A, 20, 263

Draine, B. T. 1979, ApJ, 230, 106

—. 2003, ARA&A, 41, 241

Draine, B. T., & Salpeter, E. E. 1979, ApJ, 231, 77

Du, F., & Parise, B. 2011, A&A, 530, A131+

Du, F., Parise, B., & Bergman, P. 2012, A&A, 538, A91

Duley, W., & Williams, D. 1984, Interstellar chemistry (Academic Press)

Duley, W. W. 1970, JRASC, 64, 331

Dvoretzky, A., & Erdős, P. 1951, in Second Berkeley Symposium on Mathematical Statistics and Probability, ed. J. Neyman, 353–367

Eisberg, R. 1961, Fundamentals of modern physics (Wiley)

Flower, D. R., Pineau des Forêts, G., & Walmsley, C. M. 2004, A&A, 427, 887

Frerking, M. A., Langer, W. D., & Wilson, R. W. 1982, ApJ, 262, 590

Friberg, P., Hjalmarson, A., Madden, S. C., & Irvine, W. M. 1988, A&A, 195, 281

Friedman, I. 1953, Geochim. Cosmochim. Acta, 4, 89

Fuchs, G. W., Cuppen, H. M., Ioppolo, S., et al. 2009, A&A, 505, 629

Fumagalli, M., O'Meara, J. M., & Prochaska, J. X. 2011, Science, 334, 1245

Garrod, R. 2008, A&A, 491, 239

Garrod, R., Park, I. H., Caselli, P., & Herbst, E. 2006, Faraday Discussions, 133, 51

Garrod, R., Vasyunin, A., Semenov, D., Wiebe, D., & Henning, T. 2009, ApJ, 700, L43

Garrod, R., Wakelam, V., & Herbst, E. 2007, A&A, 467, 1103

Garrod, R. T., & Herbst, E. 2006, A&A, 457, 927

Garrod, R. T., & Pauly, T. 2011, ApJ, 735, 15

Garrod, R. T., Weaver, S. L. W., & Herbst, E. 2008, ApJ, 682, 283

Geiss, J., & Reeves, H. 1972, A&A, 18, 126

Geppert, W. D., Hamberg, M., Thomas, R. D., et al. 2006, Faraday Discussions, 133, 177

Ghosh, P., & Brand, W. A. 2003, International Journal of Mass Spectrometry, 228, 1

Gibb, E. L., Whittet, D. C. B., Boogert, A. C. A., & Tielens, A. G. G. M. 2004, ApJS, 151, 35

Gibb, E. L., Whittet, D. C. B., Schutte, W. A., et al. 2000, ApJ, 536, 347

Gillespie, D. 1976, J. Comp. Phys., 22, 403

—. 1977, J. Phys. Chem, 81, 25

—. 2007, Annu. Rev. Phys. Chem., 58, 35

Gillespie, D. T. 2000, J. Chem. Phys., 113, 297

Glassgold, A. E. 1996, ARA&A, 34, 241

Goicoechea, J. R., Cernicharo, J., Lerate, M. R., et al. 2006, ApJ, 641, L49

Goldsmith, P. F., Liseau, R., Bell, T. A., et al. 2011, ApJ, 737, 96

Gómez, L., Wyrowski, F., Pillai, T., Leurini, S., & Menten, K. M. 2011, A&A, 529, A161

Gomis, O., Leto, G., & Strazzulla, G. 2004, A&A, 420, 405

Gould, R. J., & Salpeter, E. E. 1963, ApJ, 138, 393

Goumans, T. P. M. 2011, MNRAS, 413, 2615

Goumans, T. P. M., & Bromley, S. T. 2012, Monthly Notices of the Royal Astronomical Society, no

Goumans, T. P. M., & Kastner, J. 2011, The Journal of Physical Chemistry A, 115, 10767

Goumans, T. P. M., Uppal, M. A., & Brown, W. A. 2008, MNRAS, 384, 1158

Grassi, T., Bovino, S., Gianturco, F. A., Baiocchi, P., & Merlin, E. 2012, ArXiv e-prints

Gredel, R., Lepp, S., Dalgarno, A., & Herbst, E. 1989, ApJ, 347, 289

Green, N., Toniazzo, T., Pilling, M., et al. 2001, A&A, 375, 1111

Greenberg, J. M. 1963, ARA&A, 1, 267

Groß, A. 2009, Theoretical Surface Science: A Microscopic Perspective (Springer)

Guélin, M., Langer, W. D., Snell, R. L., & Wootten, H. A. 1977, ApJ, 217, L165

Guidry, M. W., Budiardja, R., Feger, E., et al. 2011, ArXiv e-prints

Gusdorf, A., Pineau Des Forêts, G., Cabrit, S., & Flower, D. R. 2008, A&A, 490, 695

Harada, N., Herbst, E., & Wakelam, V. 2010, ApJ, 721, 1570

Hartogh, P., Lis, D. C., Bockelée-Morvan, D., et al. 2011, Nature, 478, 218

Hasegawa, T., Herbst, E., & Leung, C. M. 1992, ApJS, 82, 167

Hasegawa, T. I., & Herbst, E. 1993a, MNRAS, 261, 83

—. 1993b, MNRAS, 263, 589

Hassel, G. E., Herbst, E., & Garrod, R. T. 2008, ApJ, 681, 1385

Herbst, E. 1981, Nature, 289, 656

Herbst, E., & Klemperer, W. 1973, ApJ, 185, 505

Herbst, E., & Leung, C. M. 1989, ApJS, 69, 271

Hidaka, H., Kouchi, A., & Watanabe, N. 2007, The Journal of Chemical Physics, 126, 204707

Hidaka, H., Watanabe, M., Kouchi, A., & Watanabe, N. 2009, ApJ, 702, 291

Hidaka, H., Watanabe, N., Shiraki, T., Nagaoka, A., & Kouchi, A. 2004, ApJ, 614, 1124

Hindmarsh, A. C. 1983, IMACS Transactions on Scientific Computation, 1, 55

Hiraoka, K., Sato, T., Sato, S., et al. 2002, ApJ, 577, 265

Hodge, P. 1981, Interplanetary dust (Gordon and Breach Science Publishers)

Hollenbach, D., Kaufman, M. J., Bergin, E. A., & Melnick, G. J. 2009, ApJ, 690, 1497

Hollenbach, D., & Salpeter, E. E. 1970, J. Chem. Phys., 53, 79

—. 1971, ApJ, 163, 155

Hollis, J. M., Snyder, L. E., Lovas, F. J., & Buhl, D. 1976, ApJ, 209, L83

Hoyle, F., & Wickramasinghe, C. 1979, Ap&SS, 66, 77

Hoyle, F., & Wickramasinghe, N. C. 1962, MNRAS, 124, 417

—. 1977, Nature, 266, 241

Hugo, E., Asvany, O., & Schlemmer, S. 2009, J. Chem. Phys., 130, 164302

Indriolo, N., & McCall, B. J. 2012, ApJ, 745, 91

Ioppolo, S., Cuppen, H. M., Romanzin, C., van Dishoeck, E. F., & Linnartz, H. 2008, ApJ, 686, 1474

—. 2010, Physical Chemistry Chemical Physics (Incorporating Faraday Transactions), 12, 12065

Jacq, T., Walmsley, C. M., Henkel, C., et al. 1990, A&A, 228, 447

Jacq, T., Walmsley, C. M., Mauersberger, R., et al. 1993, A&A, 271, 276

Jefferts, K. B., Penzias, A. A., & Wilson, R. W. 1973, ApJ, 179, L57

Jenkins, W. J., & Smethie, W. M. 1996, Oceanus, `http://www.whoi.edu/oceanus/viewArticle.do?id=2330`

Jørgensen, J. K., & van Dishoeck, E. F. 2010, ApJ, 725, L172

Kaiser, R. I., Ochsenfeld, C., Head-Gordon, M., & Lee, Y. T. 1998, Science, 279, 1181

Kalos, M. H., & Whitlock, P. A. 2008, Monte Carlo Methods: Second Revised and Enlarged Edition (Wiley-VCH Verlag)

Katz, N., Furman, I., Biham, O., Pirronello, V., & Vidali, G. 1999, ApJ, 522, 305

Keane, J. 1997, PhD thesis, Rijks Univ., Leiden, (1997)

Knacke, R. F., Larson, H. P., & Noll, K. S. 1988, ApJ, 335, L27

Koussa, H., Bahri, M., Jadane, N., & Lakhdar, Z. B. 2006, Journal of Molecular Structure: THEOCHEM, 770, 149

Kramer, C., Alves, J., Lada, C. J., et al. 1999, A&A, 342, 257

Kristensen, L. E., Amiaud, L., Fillion, J., Dulieu, F., & Lemaire, J. 2011, A&A, 527, A44+

Lancaster, P., & Tismenetsky, M. 1985, The Theory of Matrices: With Applications, Computer Science and Applied Mathematics (Academic Press)

Langmuir, I. 1918, Journal of the American Chemical Society, 40, 1361

Larsson, B., Liseau, R., Pagani, L., et al. 2007, A&A, 466, 999

Le Bourlot, J. 1991, A&A, 242, 235

Le Bourlot, J., Pineau des Forets, G., Roueff, E., & Schilke, P. 1993, ApJ, 416, L87

Le Petit, F., Barzel, B., Biham, O., Roueff, E., & Le Bourlot, J. 2009, A&A, 505, 1153

Le Petit, F., Nehmé, C., Le Bourlot, J., & Roueff, E. 2006, ApJS, 164, 506

Le Teuff, Y. H., Millar, T. J., & Markwick, A. J. 2000, A&AS, 146, 157

Lellouch, E., Bézard, B., Fouchet, T., et al. 2001, A&A, 370, 610

Lequeux, J., Falgarone, E., & Ryter, C. 2005, The Interstellar Medium, Astronomy and Astrophysics Library (Springer)

Leung, C. M., Herbst, E., & Huebner, W. F. 1984, ApJS, 56, 231

Li, A., & Draine, B. T. 2001, ApJ, 554, 778

Linsky, J. L., Draine, B. T., Moos, H. W., et al. 2006, ApJ, 647, 1106

Lipshtat, A., & Biham, O. 2003, A&A, 400, 585

Liu, F.-C., Parise, B., Kristensen, L., et al. 2011, A&A, 527, A19

Loinard, L., Castets, A., Ceccarelli, C., et al. 2000, A&A, 359, 1169

Loren, R. B., & Wootten, A. 1985, ApJ, 299, 947

Maret, S., Ceccarelli, C., Caux, E., Tielens, A. G. G. M., & Castets, A. 2002, A&A, 395, 573

Matar, E., Congiu, E., Dulieu, F., Momeni, A., & Lemaire, J. L. 2008, A&A, 492, L17

Mathis, J. S., Rumpl, W., & Nordsieck, K. H. 1977, ApJ, 217, 425

Mattis, D., & Glasser, M. 1998, Rev. Mod. Phys., 70, 3

Mauersberger, R., Henkel, C., Jacq, T., & Walmsley, C. M. 1988, A&A, 194, L1

McCarthy, M. C., Gottlieb, C. A., Gupta, H., & Thaddeus, P. 2006, ApJ, 652, L141

McQuarrie, D. A. 1967, J. Appl. Probab., 4, 413

Melius, C. F., & Blint, R. J. 1979, Chemical Physics Letters, 64, 183

Menten, K. M., Walmsley, C. M., Henkel, C., & Wilson, T. L. 1988, A&A, 198, 253

Menten, K. M., Walmsley, C. M., Henkel, C., et al. 1986, A&A, 169, 271

Menten, K. M., & Wyrowski, F. 2011, in Interstellar Molecules, ed. Yamada, K. M. T. and Winnewisser, G., 27

Millar, T. J., Bennett, A., & Herbst, E. 1989, ApJ, 340, 906

Millar, T. J., Bennett, A., Rawlings, J. M. C., Brown, P. D., & Charnley, S. B. 1991, A&AS, 87, 585

Millar, T. J., Defrees, D. J., McLean, A. D., & Herbst, E. 1988, A&A, 194, 250

Millar, T. J., Farquhar, P. R. A., & Willacy, K. 1997, A&AS, 121, 139

Millar, T. J., & Herbst, E. 1990, MNRAS, 242, 92

Millar, T. J., & Nejad, L. A. M. 1985, MNRAS, 217, 507

Millar, T. J., & Williams, D. A. 1975, MNRAS, 173, 527

Miyauchi, N., Hidaka, H., Chigai, T., et al. 2008, Chemical Physics Letters, 456, 27

Mokrane, H., Chaabouni, H., Accolla, M., et al. 2009, ApJ, 705, L195

Montroll, E. W. 1969, Journal of Mathematical Physics, 10, 753

Moore, W. 1972, Physical chemistry, Prentice-Hall chemistry series (Prentice-Hall)

Mullan, D. J., & Linsky, J. L. 1999, ApJ, 511, 502

Nagaoka, A., Watanabe, N., & Kouchi, A. 2007, The Journal of Physical Chemistry A, 111, 3016

Nagy, B., Csontos, J., Kallay, M., & Tasi, G. 2010, The Journal of Physical Chemistry A, 114, 13213

Nemirovsky, A. M., Mártin, H. O., & Coutinho-Filho, M. D. 1990, Phys. Rev. A, 41, 761

Neufeld, D. A., Lepp, S., & Melnick, G. J. 1995, ApJS, 100, 132

Nguyen, T. L., Stanton, J. F., & Barker, J. R. 2011, The Journal of Physical Chemistry A, 115, 5118

Oba, Y., Watanabe, N., Hama, T., et al. 2012, ApJ, 749, 67

Öberg, K. I., Boogert, A. C. A., Pontoppidan, K. M., et al. 2008, ApJ, 678, 1032

Öberg, K. I., Boogert, A. C. A., Pontoppidan, K. M., et al. 2011, ArXiv e-prints

Öberg, K. I., Fuchs, G. W., Awad, Z., et al. 2007, ApJ, 662, L23

Ohkubo, J. 2008, J. Chem. Phys., 129, 044108

Padovani, M., Galli, D., & Glassgold, A. E. 2009, A&A, 501, 619

Pagani, L., Steinacker, J., Bacmann, A., Stutz, A., & Henning, T. 2010, Science, 329, 1622

Pagani, L., Vastel, C., Hugo, E., et al. 2009, A&A, 494, 623

Parise, B., Belloche, A., Du, F., Güsten, R., & Menten, K. M. 2011, A&A, 526, A31

Parise, B., Bergman, P., & Du, F. 2012a, A&A, 541, L11

Parise, B., Castets, A., Herbst, E., et al. 2004, A&A, 416, 159

Parise, B., Ceccarelli, C., Tielens, A. G. G. M., et al. 2006, A&A, 453, 949

Parise, B., Simon, T., Caux, E., et al. 2003, A&A, 410, 897

Parise, B., Ceccarelli, C., Tielens, A. G. G. M., et al. 2002, A&A, 393, L49

Parise, B., Caux, E., Castets, A., et al. 2005, A&A, 431, 547

Parise, B., Du, F., Liu, F.-C., et al. 2012b, A&A, 542, L5

Penzias, A. A., Wannier, P. G., Wilson, R. H., & Linke, R. A. 1977, ApJ, 211, 108

Perets, H. B., Biham, O., Manicó, G., et al. 2005, ApJ, 627, 850

Petuchowski, S. J., & Bennett, C. L. 1988, ApJ, 326, 376

Pontoppidan, K. M., van Dishoeck, E. F., & Dartois, E. 2004, A&A, 426, 925

Pontoppidan, K. M., Boogert, A. C. A., Fraser, H. J., et al. 2008, ApJ, 678, 1005

Prasad, S. S., & Tarafdar, S. P. 1983, ApJ, 267, 603

Prölss, G. 2004, Physics Of The Earth's Space Environment: An Introduction (Springer)

Purcell, E. M. 1976, ApJ, 206, 685

Radhakrishnan, K., & Hindmarsh, A. C. 1993, LLNL report UCRL-ID-113855

Rae, J. G. L., Bell, N., Hartquist, T. W., Pilling, M. J., & Ruffle, D. P. 2002, A&A, 383, 738

Rae, J. G. L., Green, N. J. B., Hartquist, T. W., Pilling, M. J., & Toniazzo, T. 2003, A&A, 405, 387

Rammal, R. 1984, Journal of Statistical Physics, 36, 547

Rimmer, P. B., Herbst, E., Morata, O., & Roueff, E. 2012, A&A, 537, A7

Ripley, B. D. 2008, Stochastic Simulation (John Wiley & Sons, Inc.)

Robert, F. 2003, Space Sci. Rev., 106, 87

Roberts, H., & Herbst, E. 2002, A&A, 395, 233

Roberts, H., Herbst, E., & Millar, T. J. 2003, ApJ, 591, L41

—. 2004, A&A, 424, 905

Roberts, H., & Millar, T. J. 2000a, A&A, 364, 780

—. 2000b, A&A, 361, 388

—. 2007, A&A, 471, 849

Rodriguez Kuiper, E. N., Kuiper, T. B. H., & Zuckerman, B. 1978, ApJ, 219, L49

Romanzin, C., Ioppolo, S., Cuppen, H. M., van Dishoeck, E. F., & Linnartz, H. 2011, J. Chem. Phys., 134, 084504

Roueff, E., Parise, B., & Herbst, E. 2007, A&A, 464, 245

Ruffle, D. P., & Herbst, E. 2000, MNRAS, 319, 837

—. 2001a, MNRAS, 322, 770

—. 2001b, MNRAS, 324, 1054

Ruffle, D. P., Rae, J. G. L., Pilling, M. J., Hartquist, T. W., & Herbst, E. 2002, A&A, 381, L13

Sakai, N., Sakai, T., Hirota, T., & Yamamoto, S. 2009, ApJ, 702, 1025

Savage, B. D., & Sembach, K. R. 1996, ARA&A, 34, 279

Schiff, L. I. 1949, American Journal of Physics, 17, 453

Schmidt, R. A., & Keil, K. 1966, Geochimica et Cosmochimica Acta, 30, 471

Schutte, W. A., Gerakines, P. A., Geballe, T. R., van Dishoeck, E. F., & Greenberg, J. M. 1996, A&A, 309, 633

Semenov, D., Wiebe, D., & Henning, T. 2004, A&A, 417, 93

Sephton, M. A., & Gilmour, I. 2000, ApJ, 540, 588

Shi, J., Raut, U., Kim, J.-H., Loeffler, M., & Baragiola, R. A. 2011, ApJ, 738, L3+

Simpson, J. J. 1987, Phys. Rev. C, 35, 752

Skinner, C. J., Tielens, A. G. G. M., Barlow, M. J., & Justtanont, K. 1992, ApJ, 399, L79

Snow, T. P., & McCall, B. J. 2006, ARA&A, 44, 367

Solomon, P. M., & Klemperer, W. 1972, ApJ, 178, 389

Solomon, P. M., & Woolf, N. J. 1973, ApJ, 180, L89

Spitzer, L., Drake, J. F., Jenkins, E. B., et al. 1973, ApJ, 181, L116

Stantcheva, T., Caselli, P., & Herbst, E. 2001, A&A, 375, 673

Stantcheva, T., & Herbst, E. 2003, MNRAS, 340, 983

Stantcheva, T., & Herbst, E. 2004, A&A, 423, 241

Stantcheva, T., Shematovich, V., & Herbst, E. 2002, A&A, 391, 1069

Sternberg, A., Dalgarno, A., & Lepp, S. 1987, ApJ, 320, 676

Stief, L. J., Donn, B., Glicker, S., Gentieu, E. P., & Mentall, J. E. 1972, ApJ, 171, 21

Swings, P. 1942, ApJ, 95, 270

Taquet, V., Ceccarelli, C., & Kahane, C. 2012, ApJ, 748, L3

Tassis, K., Willacy, K., Yorke, H. W., & Turner, N. J. 2011, ArXiv e-prints

Teixeira, T. C., Devlin, J. P., Buch, V., & Emerson, J. P. 1999, A&A, 347, L19

Ter Haar, D. 1944, ApJ, 100, 288

Thi, W.-F., van Dishoeck, E. F., Dartois, E., et al. 2006, A&A, 449, 251

Tielens, A., & Hagen, W. 1982, A&A, 114, 245

Tielens, A. G. G. M. 1983, A&A, 119, 177

—. 2008, ARA&A, 46, 289

Tielens, A. G. G. M., & Charnley, S. B. 1997, OLEB, 27, 23

Tielens, A. G. G. M., & Hollenbach, D. 1985, ApJ, 291, 722

Tielens, A. G. G. M., McKee, C. F., Seab, C. G., & Hollenbach, D. J. 1994, ApJ, 431, 321

Tielens, A. G. G. M., Tokunaga, A. T., Geballe, T. R., & Baas, F. 1991, ApJ, 381, 181

Tomlin, A. S., Pilling, M. J., Turnyi, T., Merkin, J. H., & Brindley, J. 1992, Combustion and Flame, 91, 107

Turner, B. E. 1990, ApJ, 362, L29

—. 2001, ApJS, 136, 579

Turner, B. E., Fourikis, N., Morris, M., Palmer, P., & Zuckerman, B. 1975, ApJ, 198, L125

van der Tak, F. F. S., Schilke, P., Müller, H. S. P., et al. 2002, A&A, 388, L53

van der Tak, F. F. S., Walmsley, C. M., Herpin, F., & Ceccarelli, C. 2006, A&A, 447, 1011

van Dishoeck, E. F. 2004, ARA&A, 42, 119

van Dishoeck, E. F., & Black, J. H. 1986, ApJS, 62, 109

van Dishoeck, E. F., Blake, G. A., Jansen, D. J., & Groesbeck, T. D. 1995, ApJ, 447, 760

van Kampen, N. 2007, Stochastic processes in physics and chemistry, 3rd edn. (North Holland)

Vandooren, J., Sarkisov, O. M., Balakhnin, V. P., & van Tiggelen, P. J. 1991, Chemical Physics Letters, 184, 294

Vasyunin, A., Semenov, D., Henning, T., et al. 2008, ApJ, 672, 629

Vasyunin, A., Semenov, D., Wiebe, D., & Henning, T. 2009, ApJ, 691, 1459

Villanueva, G. L., Mumma, M. J., Bonev, B. P., et al. 2009, ApJ, 690, L5

Wakelam, V., Herbst, E., & Selsis, F. 2006, A&A, 451, 551

Walmsley, C. M., Flower, D. R., & Pineau des Forêts, G. 2004, A&A, 418, 1035

Walsh, C., Harada, N., Herbst, E., & Millar, T. J. 2009, ApJ, 700, 752

Wampfler, S. F., Bruderer, S., Kristensen, L. E., et al. 2011, A&A, 531, L16+

Watanabe, N., Shiraki, T., & Kouchi, A. 2003, ApJ, 588, L121

Watson, W. D. 1973, ApJ, 181, L129

—. 1974, ApJ, 188, 35

—. 1976, Reviews of Modern Physics, 48, 513

Watson, W. D. 1977, in Astrophysics and Space Science Library, Vol. 67, CNO Isotopes in Astrophysics, ed. J. Audouze, 105–114

Watson, W. D., & Salpeter, E. E. 1972, ApJ, 174, 321

Watson, W. D., Snyder, L. E., & Hollis, J. M. 1978, ApJ, 222, L145

Weinberg, S. 2008, Cosmology (Oxford University Press)

Wickramasinghe, N. C. 2011, ArXiv e-prints

Wiebe, D., Semenov, D., & Henning, T. 2003, A&A, 399, 197

Williams, D. A. 1968, ApJ, 151, 935

Wilson, R. W., Penzias, A. A., Jefferts, K. B., & Solomon, P. M. 1973, ApJ, 179, L107

Woodall, J., Agúndez, M., Markwick-Kemper, A., & Millar, T. 2007, A&A, 466, 1197

Woon, D. E. 2002, ApJ, 569, 541

Woon, D. E., & Herbst, E. 2009, ApJS, 185, 273

Acknowledgements

First of all, I owe great thanks to my supervisor, Doctor Bérengère Parise, who offered me the opportunity to study in her new group, from which I have gained immeasurably. I am grateful for her patience in reading my papers and thesis and pointing out many potential problems in the models, and for her concern about her students in various aspects. I also enjoyed the time we spent in her and her husband's house.

I am grateful to Professor Tielens, for the vivid discussions with him and for his support in my application for a postdoc position.

I thank Professor Menten for his suggestions as a thesis committee member of mine, for his support during my postdoc application, and for his careful reading of this thesis.

I also benefit from the suggestions from my other thesis committee members, Arnaud Belloche and Professor Kroupa.

Thanks are also directed to all the referees who will be reading my thesis.

My room mates, the perfect couple Guangxing Li and Xun Shi, have shared with me many interesting stuffs. I would also like to thank my office mates, especially Felipe for his help during my starting days in Bonn, Laura for her knowing practically everything, and Fangchun for her delicious Taiwan food. Regarding food, I must also acknowledge Zhiyu Zhang for his master cooking skills, and another perfect couple, Kejia Li and Yingzheng Li for the nice dinners we had at their home. I have also learnt a lot in discussions with them, and also with Keping Qiu, Yiping Ao, Lijing Shao, Yuanwei Wu, and Jie Gu. I thank Xinzhong Er for his kindness and help during my early days in Germany.

I thank our institute secretaries for their assistance in many respects.

Finally I would like to acknowledge my "tools". They include (probably incomplete) `screen`, `vim`, `gfortran` and the *ODEPACK* package, `python` and its `numpy` and `matplotlib` packages, and of course, LaTeX, especially its `mhchem` package that makes typing chemical formulas much easier. All the flowcharts in this thesis (except the one in the HME chapter, which is made with the `TikZ and PGF` package) are made with the online `Google Document` toolkit, which is very simple to use. During certain period of my study I also used the `GILDAS` package, the `IDL` software, and `Mathematica` (to get the analytical form of certain generating functions). The ADS database, the Google search engine (and Google Scholar), as well as Wikipedia and Scholarpedia are all very helpful for my research.